NASA Tech Briefs

National
Aeronautics and
Space
Administration

Operating just offshore from the St. Louis, Missouri, Gateway Arch is Firefly I — a commercial mobile firefighting module made possible by NASA developments in pumps for rocket engines, lightweight materials, and compact packaging. Completely self-contained, the module is transported by a barge fireboat, as shown here, or by a pickup truck and trailer for fighting fires on land. *[See the bottom of page A1.]*

Vol. 6, No. 3

FALL/WINTER 1981

About the NASA Technology Utilization Program

The National Aeronautics and Space Act of 1958, which established NASA and the United States civilian space program, requires that "The Administration shall provide for the widest practicable and appropriate dissemination of information concerning its activities and the results thereof."

To help carry out this objective, NASA's Technology Utilization (TU) Program was established in 1962. Now, as an element of NASA's Government/Industry Affairs Division, this program offers a variety of valuable services to help transfer aerospace technology to nonaerospace applications, thus assuring American taxpayers maximum return on their investment in space research; thousands of spinoffs of NASA research have already occurred in virtually every area of our economy.

The TU program has worked for engineers, scientists, technicians, and businessmen; and it can work for you.

NASA Tech Briefs

Tech Briefs is published quarterly and is free to engineers in U.S. industry and to other domestic technology transfer agents. It is both a current-awareness medium and a problem-solving tool. Potential products . . . industrial processes . . . basic and applied research . . . shop and lab techniques . . . computer software . . . new sources of technical data . . . concepts . . . can be found here. The short section on New Product Ideas highlights a few of the potential new products contained in this issue. The remainder of the volume is organized by technical category to help you quickly review new developments in your areas of interest. Finally, a subject index makes each issue a convenient reference file.

Further Information on Innovations

Although some new technology announcements are complete in themselves, most are backed up by Technical Support Packages (TSP's). TSP's are available without charge and may be ordered by simply completing a TSP Request Card found at the back of this volume. Further information on some innovations is available for a nominal fee from other sources, as indicated. In addition, Technology Utilization Officers at NASA Field Centers will often be able to lend necessary guidance and assistance.

Patent Licenses

Patents have been issued to NASA on some of the inventions described, and patent applications have been submitted on others. Each announcement indicates patent status and availability of patent licenses if applicable.

Other Technology Utilization Services

To assist engineers, industrial researchers, business executives, Government officials, and other potential users in applying space technology to their problems, NASA sponsors Industrial Applications Centers. Their services are described on page A7. In addition, an extensive library of computer programs is available through COSMIC, the Technology Utilization Program's outlet for NASA-developed software.

Applications Program

NASA conducts applications engineering projects to help solve public-sector problems in such areas as safety, health, transportation, and environmental protection. Two applications teams, staffed by professionals from a variety of disciplines, assist in this effort by working with Federal agencies and health organizations to identify critical problems amenable to solution by the application of existing NASA technology.

Reader Feedback

We hope you find the information in *NASA Tech Briefs* useful. A reader-feedback card has been included because we want your comments and suggestions on how we can further help you apply NASA innovations and technology to your needs. Please use it; or if you need more space, write to the Manager, Technology Transfer Division, P.O. Box 8757, Baltimore/Washington International Airport, Maryland 21240.

National Aeronautics and Space Administration

FALL/WINTER 1981
Volume 6, Number 3

NASA TU Services	A3	Technology Utilization services that can assist you in learning about and applying NASA technology.
New Product Ideas	A9	A summary of selected innovations of value to manufacturers for the development of new products.
Tech Briefs	245	**Electronic Components and Circuits**
	259	**Electronic Systems**
	265	**Physical Sciences**
	275	**Materials**
	289	**Life Sciences**
	293	**Mechanics**
	317	**Machinery**
	331	**Fabrication Technology**
	355	**Mathematics and Information Sciences**
Subject Index	361	Items in this issue are indexed by subject; a cumulative index will be published yearly.

COVERS: The photographs on the front and back covers illustrate developments by NASA that have resulted in commercial and nonaerospace spinoffs. To find out more about the Mobile Firefighting Module, Circle 78 on the TSP Request Card at the back of this issue of NASA Tech Briefs. To find out more about the Improved Seafloor Imaging Techniques, Circle 79.

About This NASA Publication

NASA Tech Briefs, a quarterly publication, is distributed free to qualified U.S. citizens to encourage commercial application of U.S. space technology. For information on publications and services available through the NASA Technology Utilization Program, write to the Manager, Technology Transfer Division, P.O. Box 8757, Baltimore/Washington International Airport, Maryland 21240.

"The Administrator of National Aeronautics and Space Administration has determined that the publication of this periodical is necessary in the transaction of the public business required by law of this Agency. Use of funds for printing this periodical has been approved by the Director of the Office of Management and Budget."

Change of Address

If you wish to have NASA Tech Briefs forwarded to your new address, use the Subscription Card enclosed at the back of this volume of NASA Tech Briefs. Be sure to check the appropriate box indicating change of address, and also fill in your identification number (T number) in the space indicated.

Communications Concerning Editorial Matter

For editorial comments or general communications about NASA Tech Briefs, you may use the Feedback card in the back of NASA Tech Briefs, or write to: The Publications Manager, Technology Utilization Office (LGT-1), NASA Headquarters, Washington, DC 20546. Technical questions concerning specific articles should be directed to the Technology Utilization Officer of the sponsoring NASA Center (addresses listed on page A4).

Acknowledgements

NASA Tech Briefs is published quarterly by the National Aeronautics and Space Administration, Technology Transfer Division, Washington, DC: Administrator: **James E. Beggs;** Director, Government/Industry Affairs Division: **Ronald J. Philips;** Publications Manager: **Leonard A. Ault.** Prepared for the National Aeronautics and Space Administration by **Logical Technical Services Corp.:** Editor-in-Chief: **Jay Kirschenbaum;** Art Director: **Ernest Gillespie;** Managing Editor: **Jerome Rosen;** Chief Copy Editor: **Oden Browne;** Staff Editors: **Donald Blattner, Larry Grunberger, Ted Selinsky, George Watson;** Graphics; **Concetto Auditore, Germaine Keller, Luis Martinez,** Editorial & Production; **Richard Johnson, Jeanne Bonner, Janet McCrie, Frank Ponce, Vincent Susinno, Ernestine Walker.**

NASA TU SERVICES

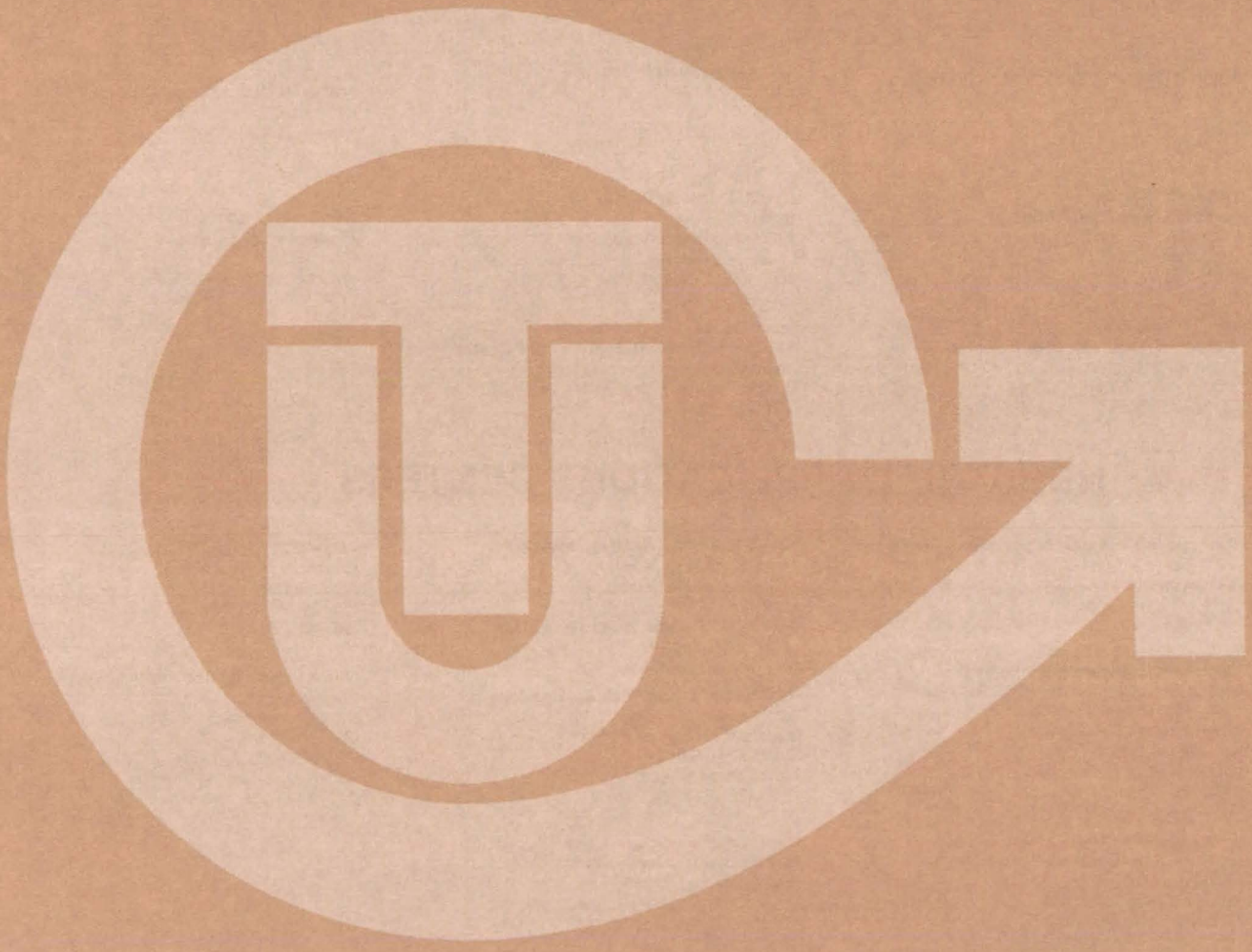

NASA TECHNOLOGY UTILIZATION NETWORK

★ TECHNOLOGY UTILIZATION OFFICERS

Stanley A. Miller
Ames Research Center
Code 240-10
Moffett Field, CA 94035
(415) 965-6471

Stanley A. Miller
Hugh L. Dryden Flight Research Center
Code 240-10
Moffett Field, CA 94035
(415) 965-6471

Donald S. Friedman
Goddard Space Flight Center
Code 702.1
Greenbelt, MD 20771
(301) 344-6242

John T. Wheeler
Lyndon B. Johnson Space Center
Code AT-3
Houston, TX 77058
(713) 483-3809

U. Reed Barnett
John F. Kennedy Space Center
Code PT-SPD
Kennedy Space Center, FL 32899
(305) 867-3017

John Samos
Langley Research Center
Mail Stop 139A
Hampton, VA 23665
(804) 827-3281

Harrison Allen, Jr.
Lewis Research Center
Mail Code 7-3
21000 Brookpark Road
Cleveland, OH 44135
(216) 433-4000, Ext. 6422

Ismail Akbay
George C. Marshall Space Flight Center
Code AT01
Marshall Space Flight Center, AL 35812
(205) 453-2224

Leonard A. Ault
NASA Headquarters
Code ETD-6
Washington, DC 20546
(202) 755-2244

Aubrey Smith
NASA Resident Office-JPL
4800 Oak Grove Drive
Pasadena, CA 91103
(213) 354-4849

Gilmore H. Trafford
Wallops Flight Center
Code OD
Wallops Island, VA 23337
(804) 824-3411, Ext. 201

● INDUSTRIAL APPLICATIONS CENTERS

Aerospace Research Applications Center
1201 East 38th Street
Indianapolis, IN 46205
John M. Ulrich, director
(317) 264-4644

Computer Software Management and Information Center (COSMIC)
Suite 112, Barrow Hall
University of Georgia
Athens, GA 30602
Robert L. Brugh, director
(404) 542-3265

Kerr Industrial Applications Center
Southeastern Oklahoma State University
Durant, OK 74701
James Harmon, director
(405) 924-0121, Ext. 413

NASA Industrial Applications Center
701 LIS Building
University of Pittsburgh
Pittsburgh, PA 15260
Paul A. McWilliams, executive director
(412) 624-5211

New England Research Applications Center
Mansfield Professional Park
Storrs, CT 06268
Daniel Wilde, director
(203) 486-4533

North Carolina Science and Technology Research Center
Post Office Box 12235
Research Triangle Park, NC 27709
James E. Vann, director
(919) 549-0671

Technology Applications Center
University of New Mexico
Albuquerque, NM 87131
Stanley Morain, director
(505) 277-3622

NASA Industrial Applications Center
University of Southern California
Denny Research Building
University Park
Los Angeles, CA 90007
Robert Mixer, acting director
(213) 743-6132

■ STATE TECHNOLOGY APPLICATIONS CENTERS

NASA/University of Florida
State Technology Applications Center
500 Weil Hall
University of Florida
Gainesville, FL 32611
J. Ronald Thornton, director

Gainesville:	(904) 392-6760
Boca Raton:	(305) 395-5100, Ext. 2292
Fort Lauderdale:	(305) 776-6645
Jacksonville:	(904) 646-2478
Orlando:	(305) 275-2706
Pensacola:	(904) 476-9500, Ext. 426
Tampa:	(813) 974-2499

NASA/University of Kentucky
State Technology Applications Program
109 Kinkead Hall
University of Kentucky
Lexington, KY 40508
William R. Strong, manager
(606) 258-4632

◆ PATENT COUNSELS

Robert F. Kempf
Asst. Gen. Counsel for patent matters
NASA Headquarters
Code GP-4
400 Maryland Avenue, SW.
Washington, DC 20546
(202) 755-3954

Darrell G. Brekke
Ames Research Center
Mail Code: 200-11A
Moffett Field, CA 94035
(415) 965-5104

Paul F. McCaul
Hugh L. Dryden Flight Research Center
Code OD/TU Office - Room 2015
Post Office Box 273
Edwards, CA 93523
(213) 354-2734

John O. Tresansky
Goddard Space Flight Center
Mail Code: 204
Greenbelt, MD 20771
(301) 344-7351

Marvin F. Matthews
Lyndon B. Johnson Space Center
Mail Code: AL-3
Houston, TX 77058
(713) 483-4871

James O. Harrell
John F. Kennedy Space Center
Mail Code: SA-PAT
Kennedy Space Center, FL 32899
(305) 867-2544

Howard J. Osborn
Langley Research Center
Mail Code: 279
Hampton, VA 23665
(804) 827-3725

Norman T. Musial
Lewis Research Center
Mail Code: 500-311
21000 Brookpark Road
Cleveland, OH 44135
(216) 433-4000, Ext. 346

Leon D. Wofford, Jr.
George C. Marshall Space Flight Center
Mail Code: CC01
Marshall Space Flight Center, AL 35812
(205) 453-0020

Paul F. McCaul
NASA Resident Office-JPL
Mail Code: 180-601
4800 Oak Grove Drive
Pasadena, CA 91103
(213) 354-2700

▲ APPLICATION TEAMS

Doris Rouse, director
Research Triangle Institute
Post Office Box 12194
Research Triangle Park, NC 27709
(919) 541-6980

James P. Wilhelm, director
SRI International
333 Ravenswood Avenue
Menlo Park, CA 94026
(415) 326-6200, Ext. 3520

TECHNOLOGY UTILIZATION OFFICERS

Technology transfer experts can help you apply the innovations in NASA Tech Briefs.

The Technology Utilization Officer at each NASA Field Center is an applications engineer who can help you make use of new technology developed at his center. He brings you NASA Tech Briefs and other special publications, sponsors conferences, and arranges for expert assistance in solving technical problems.

Technical assistance, in the form of further information about NASA innovations and technology, is one of the services available from the TUO. Together with NASA scientists and engineers, he can often help you find and implement NASA technology to meet your specific needs.

Technical Support Packages (TSP's) are prepared by the center TUO's. They provide further technical details for articles in NASA Tech Briefs. This additional material can help you evaluate and use NASA technology. You may receive most TSP's free of charge by using the TSP Request Card found at the back of this issue.

Technical questions about articles *in NASA Tech Briefs are answered in the TSP's. When no TSP is available, or you have further questions, contact the Technology Utilization Officer at the center that sponsored the research* [see page A4].

NASA INVENTIONS AVAILABLE FOR LICENSING

Over 3,500 NASA inventions are available for licensing in the United States — both exclusive and nonexclusive.

Nonexclusive licenses for commercial use of NASA inventions are encouraged to promote competition and to achieve the widest use of inventions. They must be used by a netotiated target date.

Exclusive licenses may be granted to encourage early commercial development of NASA inventions, especially when considerable private investment is required. These are generally for 5 to 10 years and usually require royalties based on sales or use.

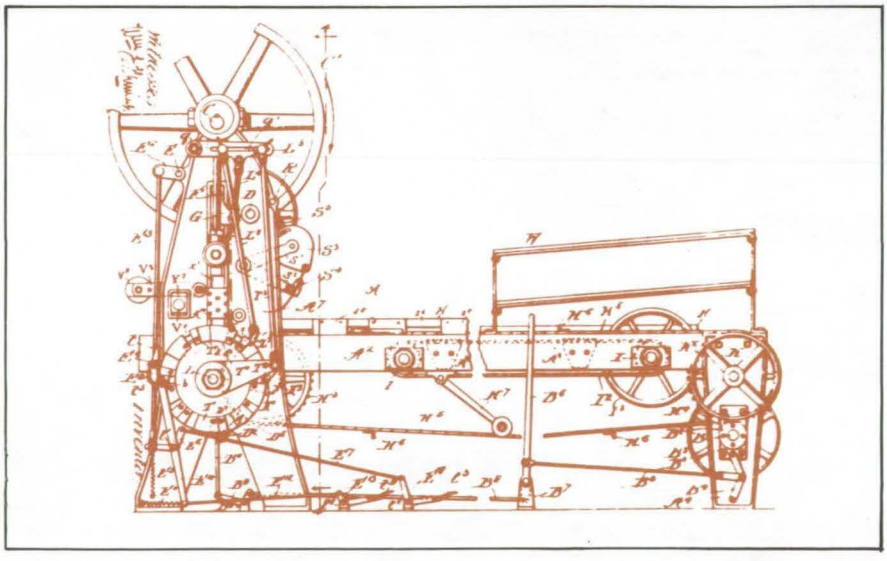

Additional licenses available include those of NASA-owned foreign patents. In addition to inventions described in NASA Tech Briefs, *"NASA Patent Abstract Bibliography"* (PAB), containing abstracts of all NASA inventions, can be purchased from National Technical Information Service, Springfield, VA 22161. The PAB is updated semiannually.

Patent licenses for Tech Briefs *are frequently available. Many of the inventions reported in NASA Tech Briefs are patented or are under consideration for a patent at the time they are published. The current patent status is described at the end of the article; otherwise, there is no statement about patents. If you want to know more about the patent program or are interested in licensing a particular invention, contact the Patent Counsel at the NASA Field Center that sponsored the research* [see page A5]. *Be sure to refer to the NASA reference number at the end of the Tech Brief.*

APPLICATION TEAMS

Technology-matching and problem-solving assistance to public-sector organizations

Application engineering projects are conducted by NASA to help solve public-sector problems in such areas as safety, health, transportation, and environmental protection. Some application teams specialize in biomedical disciplines; others, in engineering and scientific problems. Staffed by professionals from various disciplines, these teams work with other Federal agencies and health organizations to identify critical problems amenable to solution by the application of existing NASA technology.

Public-sector organization *representatives can learn more about application teams by contacting a nearby NASA Field Center Technology Utilization Office* [see page A4].

INDUSTRIAL APPLICATIONS CENTERS

Computerized access to over 10 million documents worldwide

Computerized information retrieval from one of the world's largest banks of technical data is available from NASA's network of industrial Applications Centers (IAC's). The IAC's give you access to 1,800,000 technical reports in the NASA data base and to more than 10 times that many reports and articles found in nearly 200 other computerized data bases.

The major sources include:

- *750,000 NASA Technical Reports*
- *Selected Water Resources Abstracts*
- *NASA Scientific and Technical Aerospace Reports*
- *Air Pollution Technical Information Center*
- *NASA International Aerospace Abstracts*
- *Chem Abstracts Condensates*
- *Engineering Index*
- *Energy Research Abstracts*
- *NASA Tech Briefs*
- *Government Reports Announcements*

and many other specialized files on food technology, textile technology, metallurgy, medicine, business, economics, social sciences, and physical science.

The IAC services range from tailored literature searches through expert technical assistance:

- *Retrospective Searches:* Published or unpublished literature is screened, and documents are identified according to your interest profile. IAC engineers tailor results to your specific needs and furnish abstracts considered the most pertinent. Complete reports are available upon request.
- *Current-Awareness Searches:* IAC engineers will help design a program to suit your needs. You will receive selected monthly or quarterly abstracts on new developments in your area of interest.
- *Technical Assistance:* IAC engineers will help you evaluate the results of your literature searches. They can help find answers to your technical problems and put you in touch with scientists and engineers at appropriate NASA Field Centers.

Prospective clients *can obtain more information about these services by contacting the nearest IAC* [see page A4]. *User fees are charged for IAC information services.*

STATE TECHNOLOGY APPLICATIONS CENTERS

Technical information services for industry and state and local government agencies

Government and private industry in Florida and Kentucky can utilize the services of NASA's State Technology Applications Centers (STAC's). The STAC's differ from the Industrial Applications Centers described on page A7, primarily in that they are integrated into existing state technical assistance programs and serve only the host state, whereas the IAC's serve multistate regions.

Many data bases, including the NASA base and several commercial bases, are available for automatic data retrieval through the STAC's. Other services such as document retrieval and special searches are also provided. (Like the IAC's, the STAC's normally charge a fee for their services.)

To obtain information *about the services offered, write or call the STAC in your state* [*see page A4*].

COSMIC®

An economical source of computer programs developed by NASA and other government agencies

A vast software library is maintained by COSMIC — the Computer Software Management and Information Center. COSMIC gives you access to approximately 1,600 computer programs developed for NASA and the Department of Defense and selected programs for other government agencies. Programs and documentation are available at reasonable cost.

Available programs range from management (PERT scheduling) to information science (retrieval systems) and computer operations (hardware and software). Hundreds of engineering programs perform such tasks as structural analysis, electronic circuit design, chemical analysis, and the design of fluid systems. Others determine building energy requirements and optimize mineral exploration.

COSMIC services go beyond the collection and storage of software packages. Programs are checked for completeness; special announcements and an indexed software catalog are prepared; and programs are reproduced for distribution. Customers are helped to identify their software needs; and COSMIC follows up to determine the successes and problems and to provide updates and error corrections. In some cases, NASA engineers can offer guidance to users in installing or running a program.

Information about programs *described in NASA Tech Briefs articles can be obtained by completing the COSMIC Request Card at the back of this issue. Just circle the letters that correspond to the programs in which you are interested.*

NEW PRODUCT IDEAS

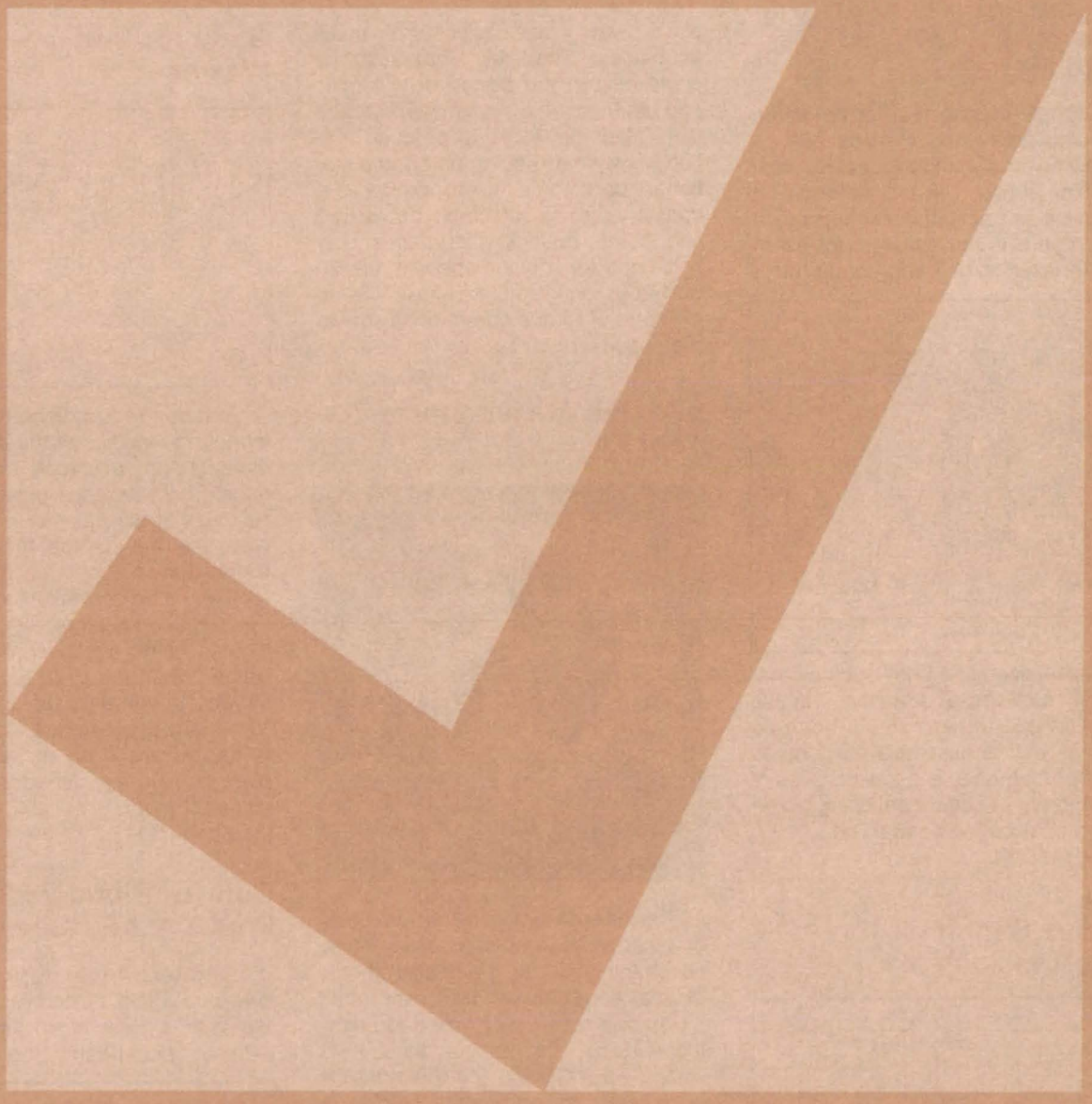

NEW PRODUCT IDEAS are just a few of the many innovations described in this issue of NASA Tech Briefs and having promising commercial applications. Each is discussed further on the referenced page in the appropriate section in this issue. If you are interested in developing a product from these or other NASA innovations, you can receive further technical information by requesting the TSP referenced at the end of the full-length article or by writing the Technology Utilization Office of the sponsoring NASA center (see page A4). NASA's patent-licensing program to encourage commercial development is described on page A6.

Staking Tool for Hard Metals

A simple staking tool for hard-steel parts makes heavy presses unnecessary and would be ideal for small machine shops. The tool deforms the receiving part so that it restrains the inserted part. It can be used, for example, to insert a ball and spring into a

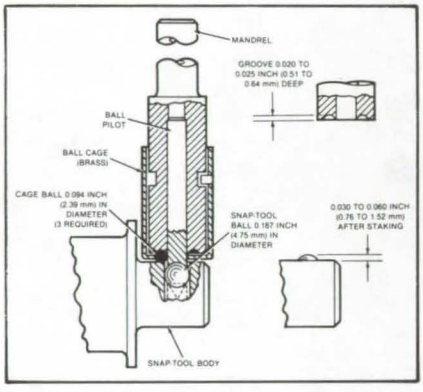

hard-steel snap-tool body such as that used to turn socket wrenches. Its use is not limited to hard steel; it can be used as well to assemble parts made of softer materials. The tool consists of a mandrel, a cage containing three balls, and a sliding central rod.
(See page 328.)

Torque Simulator for Rotating Systems

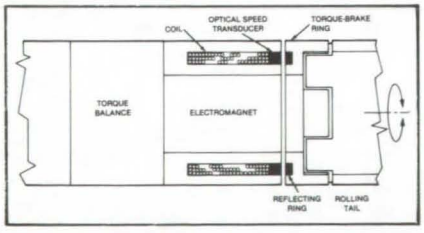

A new torque brake simulates varying levels of friction in the bearings of a rotating body. The new system allows for the first time an in-depth study of the effects of tail-fin spin rates on pitch-, yaw-, and roll-control characteristics. The new torque brake could help in the design of windmills and other rotating systems. The brake uses magnetic force to produce friction between a rotating part and a stationary part. The simulator produces a constant torque, selectable between 0 and 6 inch-pounds, for various flow fields and for rotation speeds from 20 to 1,000 rpm. Output signals give a measure of torque and rotation speed.
(See page 311.)

Tile-Gap Measurement Tool

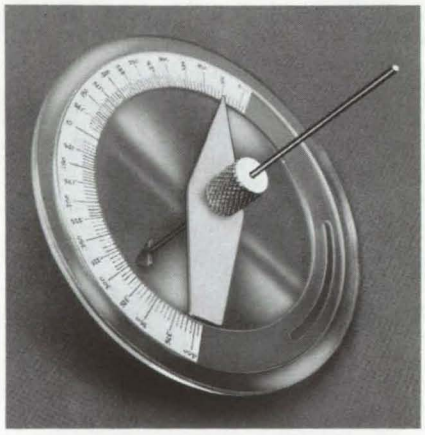

Precise setting of gaps between tiles or other structures is possible with a new hand-held tool. Its measurements of small gaps between tiles, even when the gap is tapered or indented below the surface, are rapid and accurate within ±0.003 inch. The tool consists of a flat blade on a shaft held by a knurled knob on a calibrated disk. The disk indicates the gap dimensions. The depth of the blade can be adjusted to measure progressively smaller or larger depths in the gap; when the knob is loosened, the blade can be moved from the shallow position to the deep one.
(See page 300.)

Gage for Surface Waviness

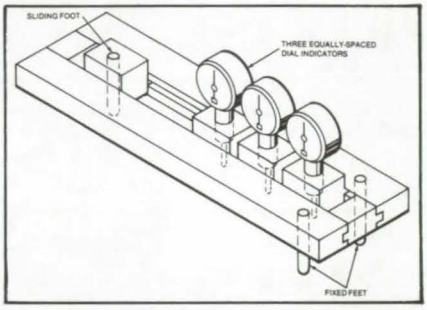

Surface irregularities are measured by noting readings of the three dial indicators on a simple, inexpensive gage. The new gage gives qualitative readings of the flatness, curvature, or waviness of a surface. It consists of a frame that is supported by two fixed feet and one movable foot, plus the three dial indicators, which can be located with various spacings in the frame. When the gage is applied to a surface under test, the dial readings reveal any irregularities. As the device is moved about on the surface, the dials indicate any departure from true planar contour.
(See page 301.)

Cuff for Blood-Vessel Pressure Measurements

Long-term monitoring of the pressure within a blood vessel is possible with a new noninvasive sensor. Without penetrating the vessel or

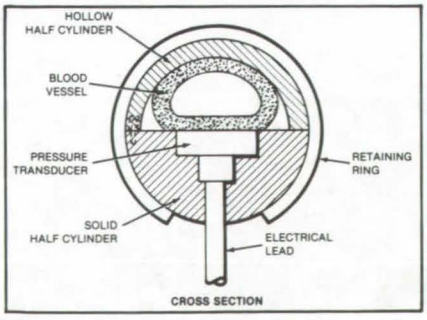

harming it, a cufflike device continuously monitors blood pressure for up to 6 months or longer. The device is used on an exposed vessel that is clamped between a solid half cylinder and a hollow half cylinder held together by retaining rings. It can be adapted for pressure measurements in flexible hoses and other fluid lines. The cuff measures pressure in vessels ranging from 1 to 30 millimeters in diameter. It is equally suitable for the small pressures in veins and the large pressures in arteries.
(See page 291.)

Load-Limiting System Reduces Crash Injuries

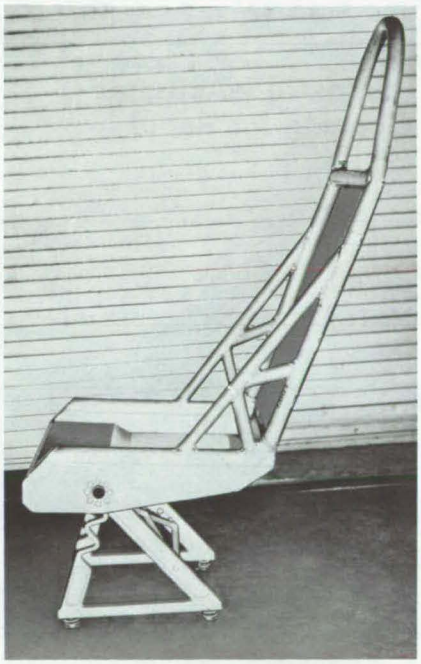

Injuries to crash victims can be reduced by a new yielding torque-tube system that limits the loads transmitted to a seat and its occupant. When properly integrated into the seat structure, the torque tube yields and maintains a relatively constant resistance to applied torque for many degrees of rotation. With proper sizing and selection of material for the system, it is possible to limit the loads to the occupant throughout the allowable movement of the seat. By using the yielding torque tube as a pivot point for the legs of the seat, load response can be controlled in a predictable way.
(See page 350.)

Binders for Thermal-Control Coatings

POLYMER: "LADDERED" METHYL SILICONE

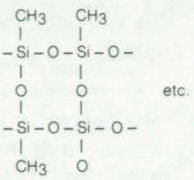

Methyl trialkoxysilane hydrolysates have been found to be superior binders for radiative thermal-control coatings. The improved coatings are tough and abrasion-resistant. In a test preparation, a coating survived a mandrel bend test and thermal cycling from $-160°$ to $+160°$ F with no signifcant damage; also, exposure for 500 hours to ultraviolet radiation resulted in no visible degradation. The binders are made from monomers of trialkoxysilanes or chain-extended alkoxysilanes. The new binders are believed to polymerize to ladder-type structures that reduce the number of Si-CH_3 groups available for damage from ultraviolet radiation.
(See page 287.)

Improved Magnetic-Field-Component Resolvers

New resolvers for vectorially summing the outputs of aircraft-mounted magnetometers are lighter and more economical to fabricate than conventional electromagnetic resolvers. One resolver is based on potentiometric principles, the second uses polarization filters, and the third has a variable-capacitance element. The potentiometric resolver consists of an assembly of inexpensive, easily fabricated components; the polarized-light resolver generates the sine/cosine function by photoresistive elements illuminated by light, the intensity of which is modified by linearly polarized filters; and the printed-circuit capacitive resolver consists of two capacitor plates separated by sheets of dielectric material and a rotatable metallic shield.
(See page 296.)

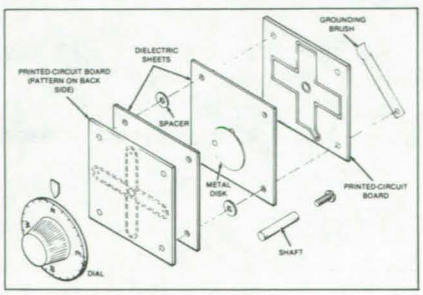

Articulated Vacuum Chuck

A new vacuum chuck conforms to complex surface contours. It can be used for pull-testing contoured surfaces, holding asssemblies together for repairs, or for handling unusually shaped parts. Its gripping surface is a polyurethane panel embedded with links of roller chain. The panel flexes under vacuum to adjust to the surface

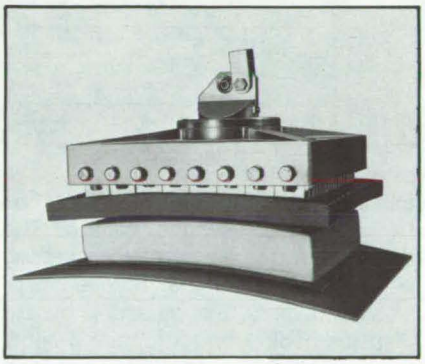

contour, and then drawbolts are tightened to lock an array of slotted plates.
(See page 323.)

Wide-Temperature-Range Torque-Stripe Paint

A "torque-stripe" paint withstands a wide range of temperatures, from $-320°$ to $+180°$ F, and can be used on electrical connectors or machine bolts that are exposed to extremes of heat and cold. The paint, brushed on an electrical connector, serves as both a locking agent and an indicator of a loosened connection. A crack in the paint stripe is readily visible and shows that a torqued connector has loosened. A urethane resin, ensures adhesion, nonflammability, viscosity, and visibility. Silica powder and a bright

(continued on next page)

Component	Units by Weight
Urethane (Uralite 3124, Part A)*	100
Urethane (Uralite 3124, Part B)*	32
Ammonium Phosphate	30
Silica Powder (Cabosil)*	10
Yellow Pigment	1

*Equivalent materials could be substituted.

yellow pigment are added to improve the paint qualities.
(See page 284.)

A Simple Tiltmeter

A bubble vial with external aluminum-foil electrodes is the sensing element for a new tiltmeter. Using no

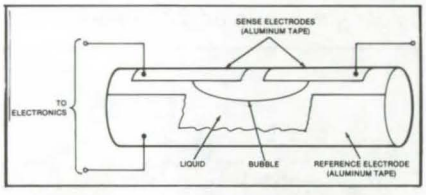

precision electronic circuits, the tiltmeter indicates angular orientation to within 0.05 second of arc. The device can be used remotely; among its uses would be the forecasting of seismic events. To measure bubble displacement, a bridge circuit detects the difference in capacitance between two sensing electrodes and a reference electrode.
(See page 319.)

Universal Assembly for Captive Bolts

Virtually any bolt can be easily converted to a "captive" bolt, using a new technique. A cup-shaped washer that is flattened secures a tab to the bolt, and a wire attached to the tab holds the bolt assembly captive. To assemble a captive bolt, a snugly fitting spacer is slid down the shaft of the bolt, and a tab with an opening slightly larger than the spacer is slipped over the spacer. After this combination is in

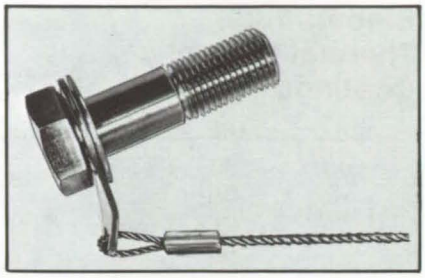

place, the washer is flattened to secure the tab and the spacer to the bolt. The captive bolt when it is not in use can hang loosely from the wire attached to the tab.
(See page 322.)

Probe for Flow-Field Surveys

Significant reduction of response time in flow-field surveys during wind-tunnel tests is possible with a new hot film static-pressure probe. In these tests, surveying a static-pressure distribution in a flow field requires an extremely large number of runs unless the probe response time is reduced

considerably. The new probe incorporates two hot film sensors, an unheated film for temperature compensation and a heated film for pressure measurement, and a sonic orifice for flow control
(See page 303.)

High-Speed Wafer Slicer

Silicon ingots are sliced quickly into wafers for solar cells by the reciprocating blades of a new wafer slicer. The light, sturdy blade heads

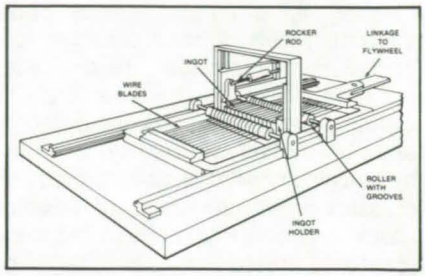

operate at high speed with little vibration. As a result, production rates are high, cuts are accurate, and little material is wasted. The machine slices two ingots simultaneously; the two bladeheads are synchronized so that both accelerate in opposite directions at the same rate. This balanced arrangement reduces power requirements, vibration, and sideways motion that would otherwise widen the kerf.
(See page 324.)

Explosively Actuated Opening for Rapid Egress

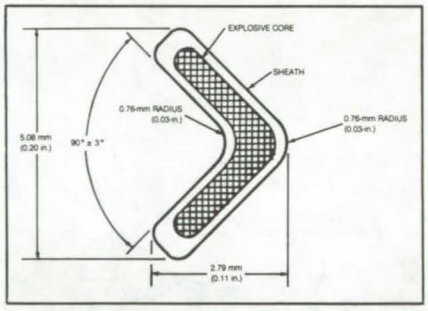

An emergency pyrotechnic-actuated egress system for use in light general-aviation airplanes allows the pilot to bail out from the left side of the airplane by creating an opening where no door exists. The pyrotechnic approach is an add-on system based on previous experience gained in escape modules. It is simple and highly responsive, requiring minimal modifications to the airplane. The system is initiated mechanically when the pilot pulls a pivoting handle. From that point, the system functions automatically. Safety features are incorporated to prevent inadvertent actuation on the ground and in flight.
(See page 312.)

Electronic Components and Circuits

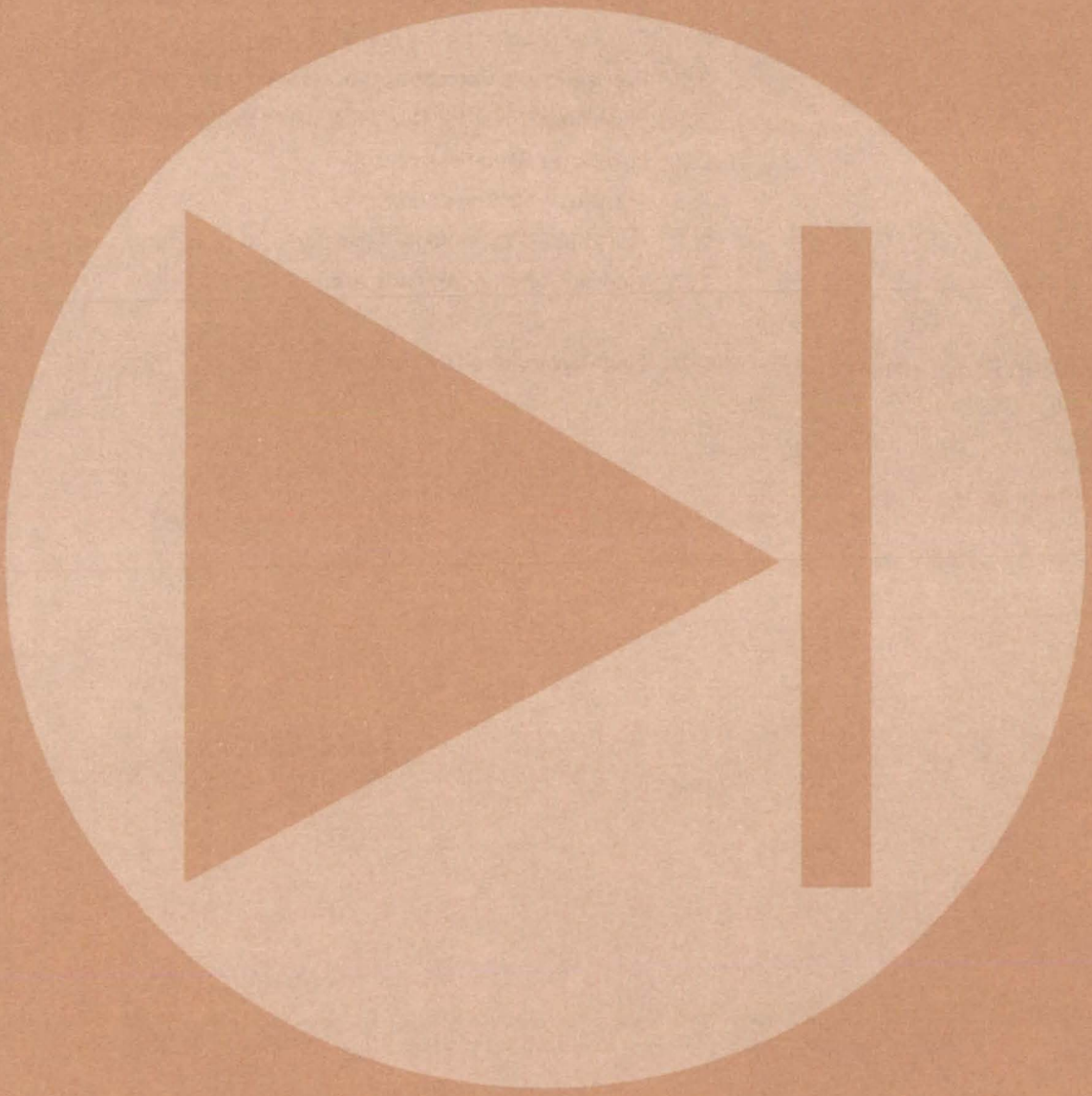

Hardware, Techniques, and Processes

247 Wideband Amplifier With Subpicosecond Stability
248 Boltless Seal for Electronic Housings
249 Unequal-Split Strip-Line Power Divider
250 High-Density Terminal Box for Testing Wire Harness
251 Failure Detector for Power-Factor Controller
252 Precise Phase Comparator for Nearly Equal Frequencies
253 Flashlamp Driver for Quasi-CW Laser Pumping
254 Low-Noise Band-Pass Amplifier
255 Arc-Free High-Power dc Switch
256 Power-MOSFET Voltage Regulator
257 Modular Amplifier/Antenna Arrays

Computer Programs

257 Line-Replaceable-Unit Analysis

Wideband Amplifier With Subpicosecond Stability

RF circuit offers high isolation as well as phase stability.

Goddard Space Flight Center, Greenbelt, Maryland

A wideband amplifier, usable from 30 kHz to 45 MHz is stable enough to distribute the signal from an atomic-frequency standard, such as a hydrogen maser, with negligible degradation of phase stability. For a 5-MHz signal, the amplifier adds a tune jitter of less than 5×10^{-14} s and has a phase delay that changes by less than 1×10^{-12} s for a 1° C change in ambient temperature or a 1-V change in the power supply voltage. When used in a distribution amplifier with a power splitter the circuit provides 90 to 110 dB port-to-port isolation between users.

For temperature stability, all circuit components are contained in a closed metal housing, and the packages of the active circuit elements are embedded in a common heat sink. These provisions not only slow down the effect of ambient temperature changes on individual devices but also reduce temperature differences across devices so that differential temperature effects vanish.

The amplifier package consists of a voltage regulator powering a driver transistor and an integrated-circuit unity-gain buffer amplifier, coupled in a feedback circuit (Figure 1). The transistor provides the requisite gain for the input signal, while the unity-gain buffer ensures signal isolation and provides high signal drive capability. The voltage regulator, besides furnishing a steady voltage to the transistor and unity-gain buffer, reduces crosstalk from similar devices connected to a common power supply.

In a typical application, nine wideband amplifiers and an eight-way power splitter are used to make an eight-output distribution amplifier (Figure 2). As mentioned previously, this provides 90 to 110 dB of isolation between user ports

(continued on next page)

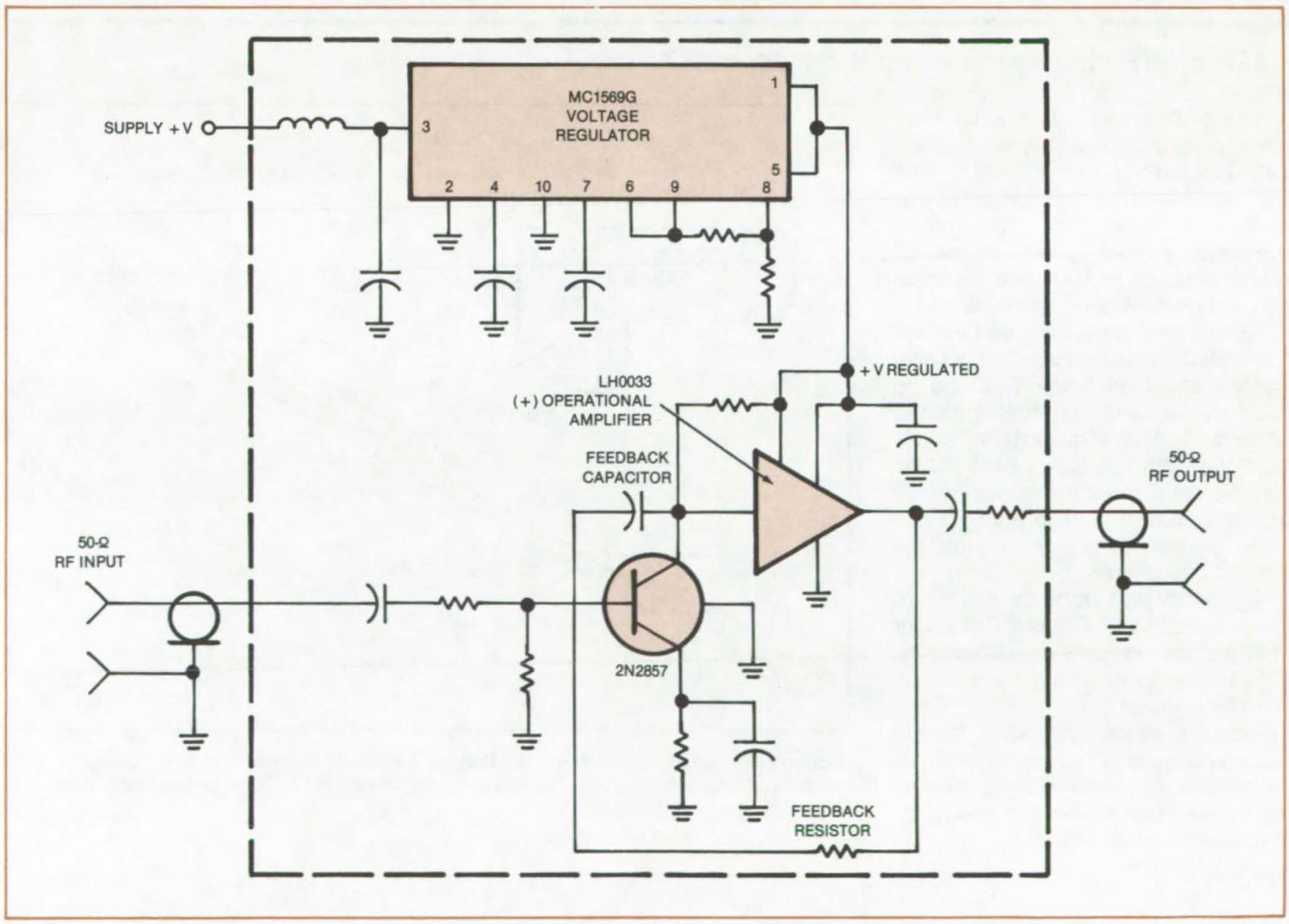

Figure 1. A **Wideband RF Amplifier** provides gain through its transistor, isolation through its operational amplifier and voltage regulator, and thermal stability through its heat sinking and mechanical design. The signal gain into a characteristic impedance of 50 Ω is determined by the values of the feedback resistor and capacitor. The gain ranges from 1 to 10.

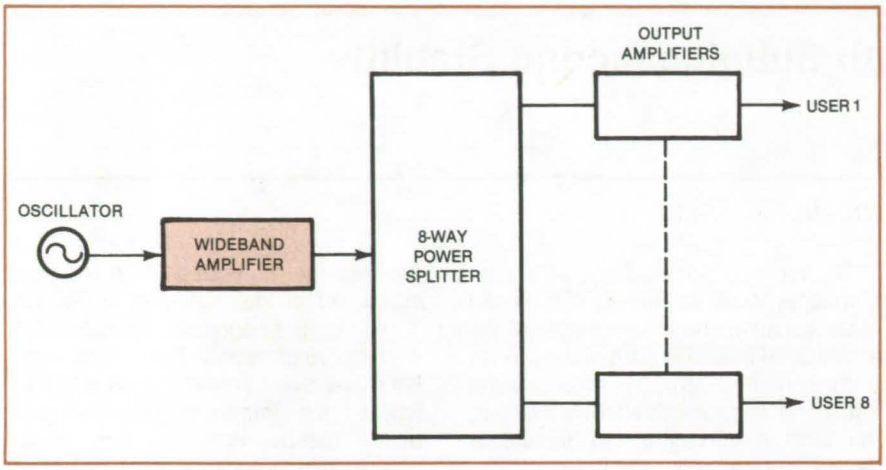

Figure 2. An **Eight Output Distribution Amplifier** is assembled using the wideband amplifiers.

and also provides greater than 120 dB back-to-front isolation at 5 MHz. In this application, amplifier gains are usually adjusted to provide 1-V RMS output on all output ports.

This work was done by Victor S. Reinhardt and William A. Adams of **Goddard Space Flight Center.** *For further information, Circle 1 on the TSP Request Card.*

This invention is owned by NASA, and a patent application has been filed. Inquiries concerning nonexclusive or exclusive license for its commercial development should be addressed to the Patent Counsel, Goddard Space Flight Center [see page A5]. Refer to GSC-12646.

Boltless Seal for Electronic Housings

Slip-on clip protects against interference and contamination.

NASA's Jet Propulsion Laboratory, Pasadena, California

Spring clips seal housings for electronic circuitry, preventing electromagnetic interference from entering or leaving the housings. The clips also keep dust out of the housing. Since no bolts are used, a housing can be opened quickly; and unlike bolts, the clips can be used on thin-walled housings.

A clip is installed by being slipped over the mated flanged edges of a housing box and cover (see figure). Because the clip is made of a spring material such as phosphor bronze, it clamps the flanges together tightly but nevertheless can be removed if it is pulled away from the box. The two ends of the clip are bent outward so that they can engage the flanged edges easily.

This work was done by Russell H. Dawe and James T. Evans of Caltech for **NASA's Jet Propulsion Laboratory.** *For further information, Circle 2 on the TSP Request Card.*

Inquiries concerning rights for the commercial use of this invention should be addressed to the Patent Counsel, NASA Resident Office-JPL [see page A5]. Refer to NPO-14818.

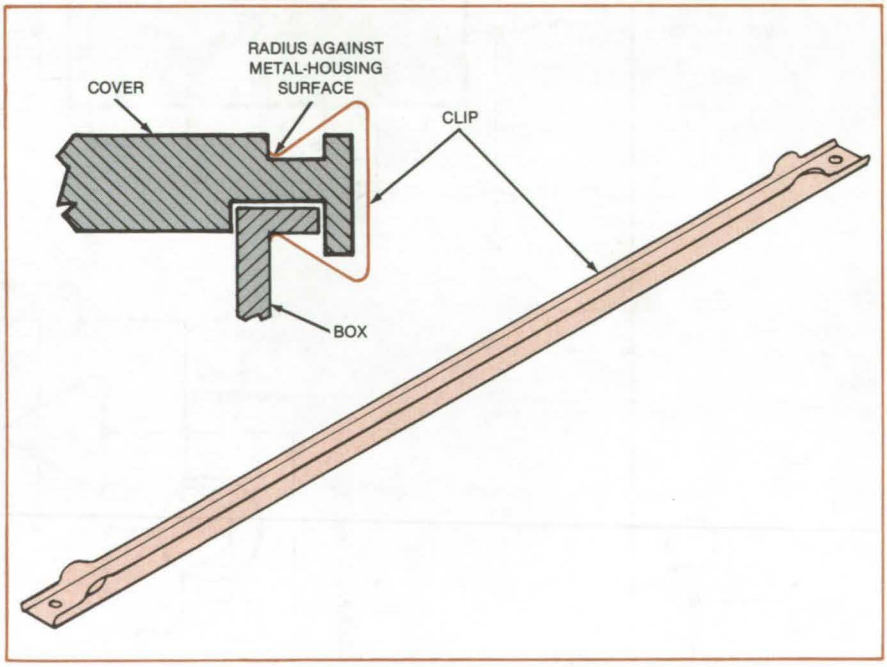

Spring Clip (right) is slipped over the flanged edges of the cover and box of an electronic housing (cross section, left). The seal was developed for an X-band array amplifier.

Unequal-Split Strip-Line Power Divider

Output power ratio is determined by the location of the input tap.

Langley Research Center, Hampton, Virginia

Corporate feed networks for antenna arrays often require unequal power dividers to excite the array with a nonuniform amplitude distribution. Depending on amplitude taper, the number of elements, and design of the network, the required power-split ratio may not be the same for all power dividers and may vary over a wide range of values.

A simple technique for designing such strip-line or microstrip power dividers can be used for unequal, but inphase, power split. The technique allows power splits ranging from equal to as large as required, with the advantage of using the same line impedances and line spacings for all splits. The output power ratio is determined by selecting the location of the input port in a manner analogous to the tap point for an electric-power transformer.

Although various couplers and dividers have been designed and implemented in strip line or microstrip for unequal power split, if the ratio of power split exceeds about 8 decibels, the narrow line widths due to the required high line impedances are impractical to construct. For power splits exceeding 10 decibels, side-coupled quarter-wave lines can be used, although they require multilayered construction. In a power distribution network that includes a wide range of power divisions, a variety of unequal power dividers, line widths, and line spacings may be required.

In the new technique, the unequal power split is obtained by exciting both input ports of a quadrature hybrid with equal amplitudes but different phases. The signals at the two output ports are then the superposition of the response of the hybrid to two input signals. By properly selecting the phase difference between the input signals, the signals combine at the output ports so that the output amplitude ratio can be any value desired, while an inphase relationship is maintained at the output.

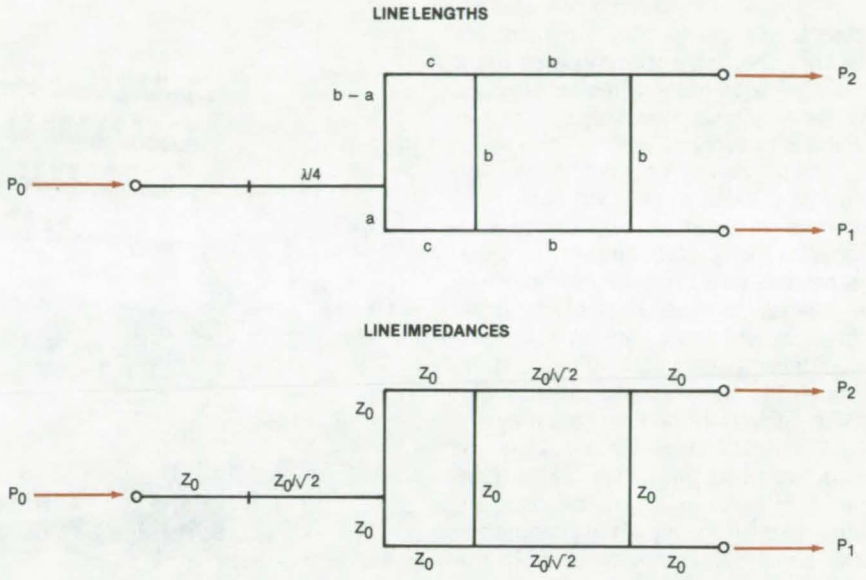

A **Simple-Tee Equal Power Divider** is connected to the inputs of the hybrid by unequal line lengths to produce the phase difference at the inputs to the hybrid.

For the configuration shown in the figure, the ratio of the output power split is determined by the position of the input port. Since the power split depends only on the ratio, a/b, once the physical parameters (dielectric constant, dielectric thickness, line widths, and line lengths) have been established for an equal power divider and a quadrature hybrid at the design frequency, all unequal power dividers for a distribution network can be designed by simply selecting the proper location of the input tap point.

Three experimental unequal power splitters were fabricated in strip line output power ratios at 1,413 MHz of 0.5, 0.25, and 0.1 (-3, -6, and -10 dB). A quarter-wave transformer was included in the input line for impedance matching. At the design frequency, the measured power split agrees with the design values within the accuracy of the network analyzer system used to make the measurements. Although the power split and phase vary with frequency, the usable bandwidth is adequate for certain applications. For example, the frequency band 1,363 to 1,463 MHz has been allocated for an L-band radiometer phased array with a cosine distribution, which is currently being built. The simplicity of the design of the unequal power splitter makes it attractive for such narrow-band phased-array applications where a tapered-amplitude distribution is required for side-lobe reduction.

This work was done by Marion C. Bailey of **Langley Research Center.** *Further information may be found in NASA TM-81870 [N80-31684/NSP], "A Simple Stripline Design for Uneven Power Split" [$5]. A copy may be purchased [prepayment required] from the National Technical Information Service, Springfield, Virginia 22161.*

LAR-12797

High-Density Terminal Box for Testing Wire Harness

Miniature sockets double circuit capacity.

NASA's Jet Propulsion Laboratory, Pasadena, California

A compact terminal box provides access to complex wiring harnesses for testing. The box accommodates more than twice as many wires as previous boxes — 256 single contacts vs. 122 — in the same volume.

Like previous "breakout" boxes, the new box takes in wires via cable connectors and distributes them to contacts on the box face. Instead of separate insulated jacks in a metal face panel, the new box uses pairs of small military-standard metal sockets in a precision-drilled plastic panel (Figure 1). Although the contacts are packed much more densely in the new box, they are clearly identified by number. They are also identified with their cable connector by color — red stripes associate the sockets from one of the connectors, and black associates those from the other.

Before a socket is assembled on the panel, a wire is crimped on its pin. The wire and its socket are inserted in a hole in the faceplate, and the socket is pressed into place. The unattached end of each wire is then crimped on the proper pin of one of the two 128-pin connectors mounted on the end of the box.

A shorting plug (Figure 2) provides continuity for wires when they are not being tested. The shorting plug connects the two members of a socket contact pair. It also includes a socket for a test probe. Thus, the complete wiring joined by a socket pair can be tested without removal of the shorting plug.

This work was done by Wallace B. Pierce and Walter G. Collins of Caltech for **NASA's Jet Propulsion Laboratory.** *For further information, Circle 3 on the TSP Request Card.*
NPO-15147

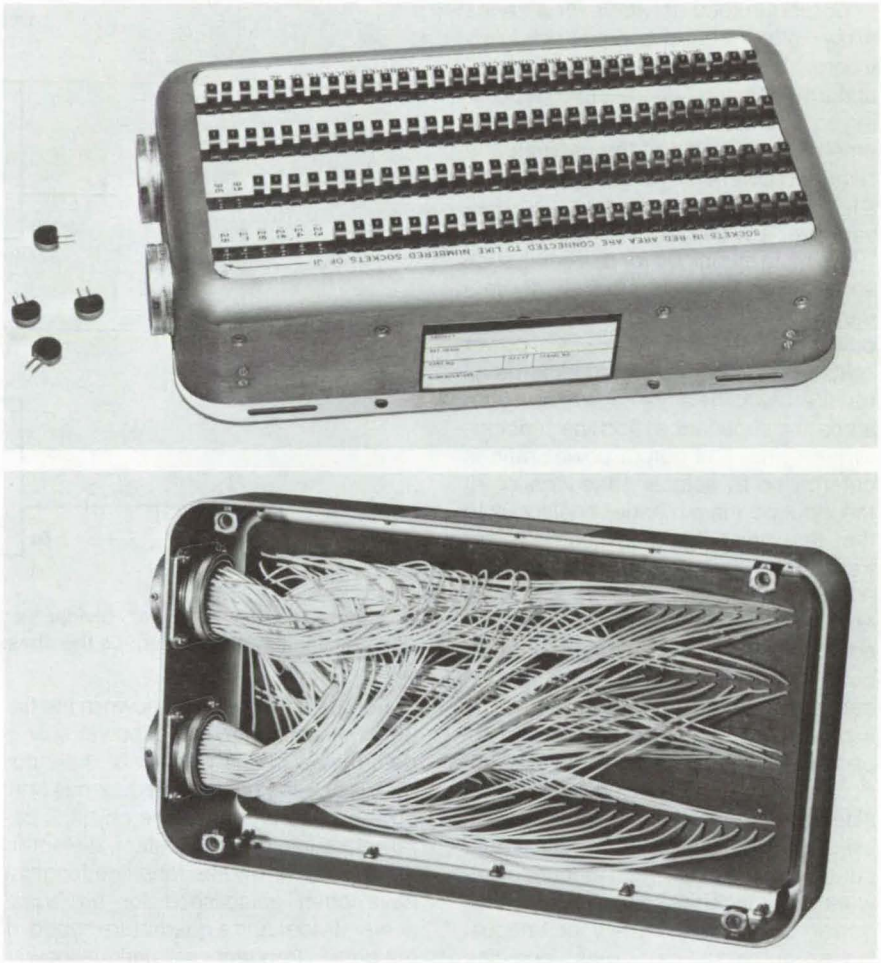

Figure 1. A **Terminal Box Provides Access** to 128 circuits via 256 terminals. Shorting plugs are removed at the lower left corner of the box (top view) so that segments of circuits can be probed. Complete circuits can be probed through central sockets in the shorting plugs. Inside the box, wires lead from the miniature socket pins to external connectors (bottom view).

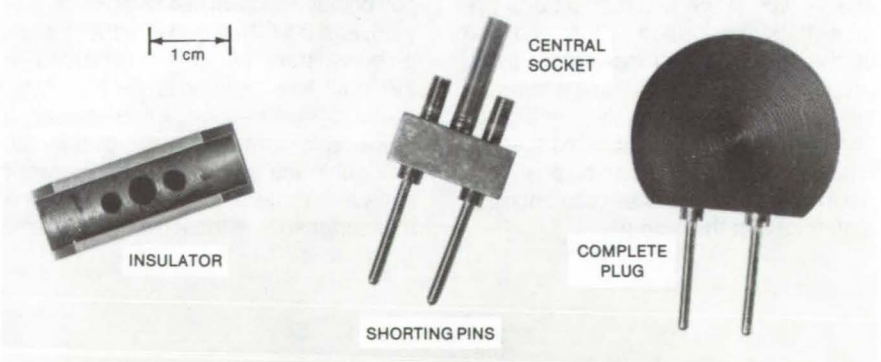

Figure 2. A **Shorting Plug** (right) contains a pair of pins (center) that are held by an insulator (left). A central socket in the shorting pin accepts a test probe.

Failure Detector for Power-Factor Controller

Circuit prevents motor overheating due to switch failure.

Marshall Space Flight Center, Alabama

New protective circuits have been developed for power-factor ac motor controllers. These circuits prevent the direct current and consequent motor heating that would normally result from the failure of a solid-state switch in the controller.

Switch failure modes include a short circuit or an open circuit in one direction only. In either case, the resulting unbalanced waveform includes a steady-state component that may cause the motor to overheat. One of the new circuits turns the switch (a Triac, or equivalent, switch) fully on in both directions if it detects a short in either direction. Another circuit turns the switch off if it detects an open in either direction. In either case, balance is restored.

The single-phase power-factor controller of Figure 1 is equipped with a short detector, shown within the dashed line. The combination of R_1 and C_1 acts as a low-pass filter. Amplifier A_1 has a gain of unity. In normal operation, the switch voltage is symmetrical, and the output voltage V_1 of R_1C_1 is near zero.

If the switch shorts in either the positive or negative direction, V_1 departs from zero, resulting in $V_3 = +|V_1| \approx 10$ volts at the input of comparator A_2. A_2 then switches to its full negative output (-15 V), causing gate current for the switch to flow through resistor R_8, thus holding the switch fully on in both directions. The values of R_4, R_5, and R_6 are so chosen that A_2 remains latched in the negative-output condition until the power is turned off. (Therefore full power is applied to the motor until then.) The positive charging current through C_2 assures that A_2 goes into the positive-output state when power is restored to the repaired circuit.

Unbalance due to an open circuit also trips comparator A_2. However, an additional circuit is needed to apply the corrective measure. Because the switch will not respond to the turn-on current in the direction of open-circuit failure, V_3 remains at about $+10$ V.

As shown in Figure 2, V_3 is fed to low-pass filter $R_{20}C_{20}$, the time constant of which is 1 to 2 seconds, about 20 times that of R_1C_1. If V_3 remains at $+10$ V, indicating an open-circuit failure, then it will survive the delay of $R_{20}C_{20}$ and trip comparator A_{10}. The output of A_{10} then swings fully positive ($+15$ V). This positive voltage is fed through resistor R_{24}, which equals the gate-current-limiting resistor R_{26}. Thus, the negative voltage from comparator A_2 is balanced, the net voltage at the switch gate is essentially zero, and the switch turns off. The combination of D_{21} and R_{24} latches A_{10} in the positive-output state until the power is removed. When power is applied to the repaired circuit, charging current through C_{21} insures that A_{10}

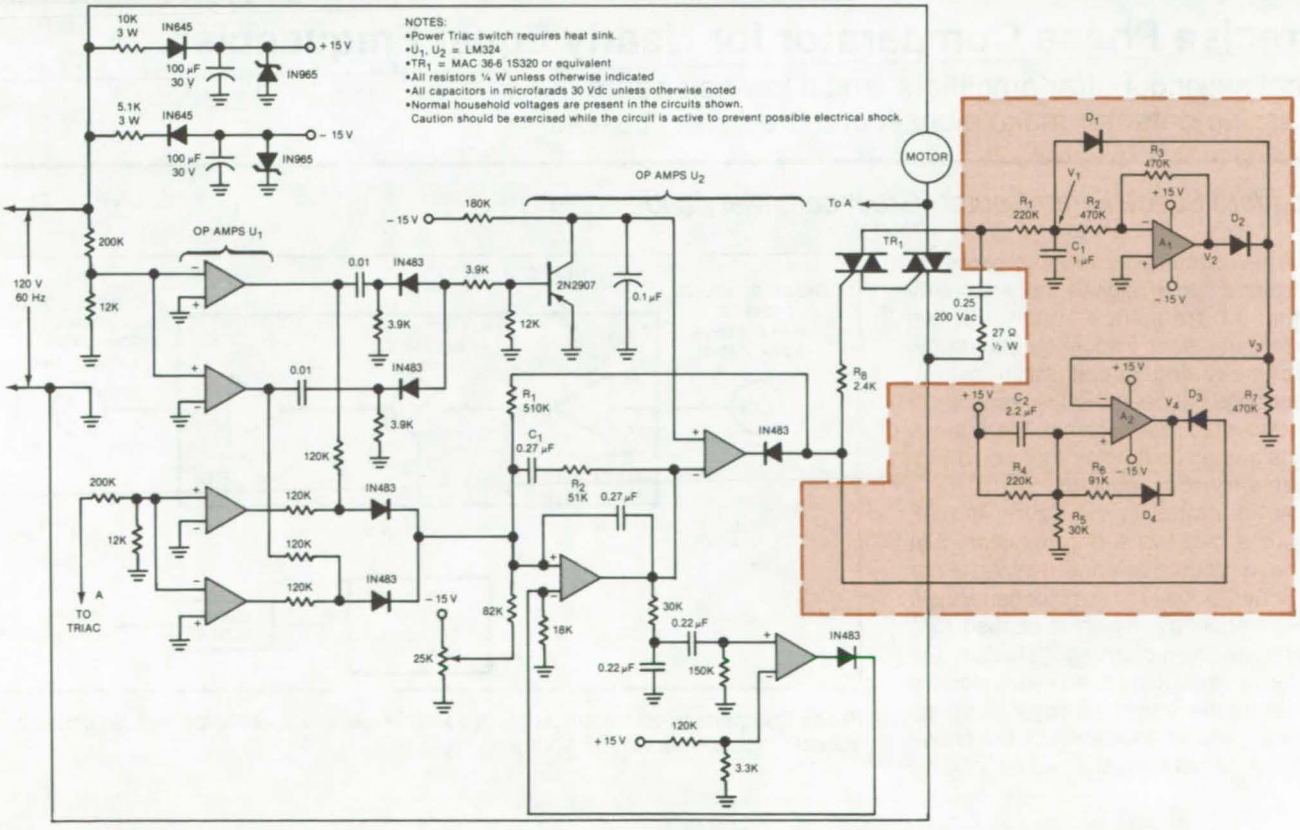

Figure 1. A **Single-Phase Power-Factor Controller With Short Detector** compensates for a short-circuit failure in either direction by applying full power to the motor. The short-detector circuit is shown within the dashed line.

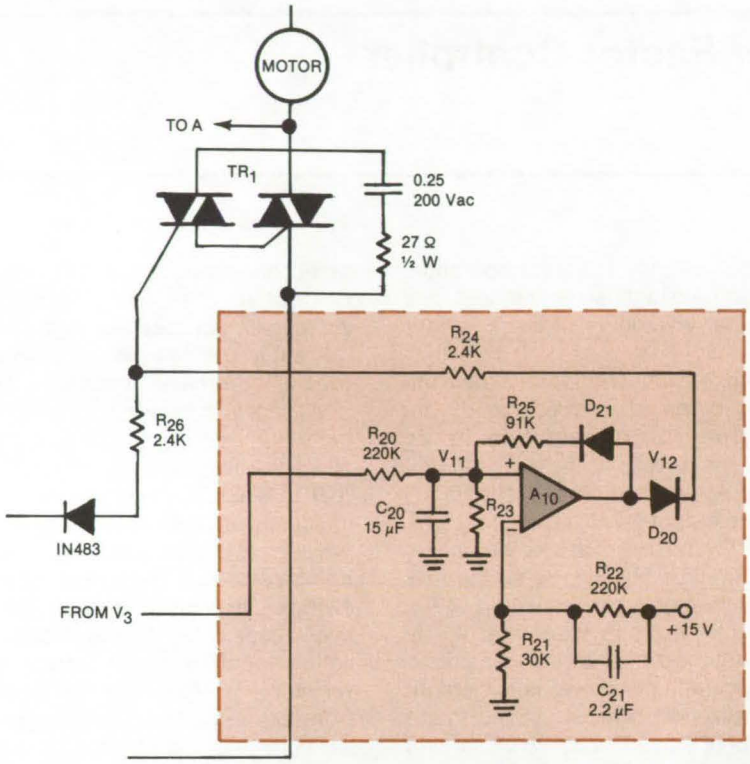

Figure 2. A **Single-Phase Power-Factor Controller With Open Detector** compensates for an open-circuit failure in either direction by turning off power to the motor. The open-detector circuit is shown within the dashed line. The remainder of the circuit to the left (not shown here) is the same as in Figure 1.

goes into the normal negative-output condition.

This work was done by Frank J. Nola of ***Marshall Space Flight Center.*** *For further information, Circle 4 on the TSP Request Card.*

This invention is owned by NASA, and a patent application has been filed. Inquiries concerning nonexclusive or exclusive license for its commercial development should be addressed to the Patent Counsel, Marshall Space Flight Center (see page A5). Refer to MFS-25607.

Precise Phase Comparator for Nearly Equal Frequencies

Heat sinking, buffer amplifiers, and a low-noise zero-crossing detector make picosecond precision possible.

Goddard Space Flight Center, Greenbelt, Maryland

A new circuit precisely compares the phases of two RF signals that are nearly equal in frequency, such as two hydrogen-maser frequency standards. The measuring circuit minimizes interactions between the two sources. It is also stabilized against thermal effects and against noise that could produce erroneous readings.

As illustrated in the figure, the RF sources feed two buffer amplifiers that drive a double-balanced mixer. Four matched diodes in the mixer generate a beat frequency, which is applied to a low-noise zero-crossing detector; the detector is coupled to an event clock to measure the time of the edge crossings and to yield an indication of the phase difference between the two RF inputs.

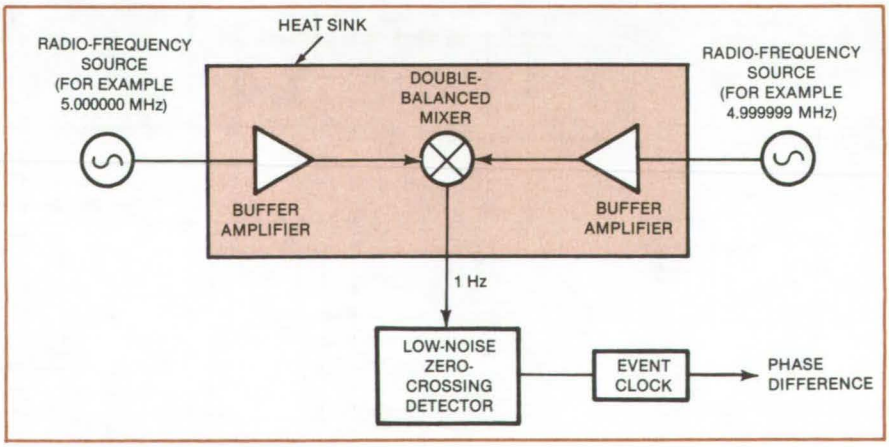

Phase Comparison with a precision of 1×10^{-12} second is achieved in this circuit that accepts inputs from two RF sources.

Temperature stability is achieved by mounting the amplifiers and mixer on a common circuit board with the active elements embedded in a common heat sink (a thick metal plate). The two amplifiers are powered through individual voltage regulators, which are also embedded in the heat sink and which increase RF isolation by reducing crosstalk through the power supply.

This circuit can resolve phase differences corresponding to a time difference of 5×10^{-14} s between the two compared frequency standards for periods of several hundred seconds. For periods of up to several days, the circuit can resolve phase differences corresponding to 1×10^{-12} s.

This work was done by Victor S. Reinhardt and William A. Adams of **Goddard Space Flight Center.** *For further information, Circle 5 on the TSP Request Card.*

This invention is owned by NASA, and a patent application has been filed. Inquiries concerning nonexclusive or exclusive license for its commercial development should be addressed to the Patent Counsel, Goddard Space Flight Center [see page A5]. Refer to GSC-12645.

Flashlamp Driver for Quasi-CW Laser Pumping

Active lamp-driver circuit maintains constant current during the pumping pulse and simmer current between pulses.

Goddard Space Flight Center, Greenbelt, Maryland

If an optically pumped laser is illuminated with stable pulses of light, the laser emission achieves the quasi-continuous characteristics (fixed pulse width and pulse profile) that are essential for ultraprecise ranging applications. A circuit has been developed for generating the required current pulses in a flashlamp for laser pumping. The circuit maintains a constant high-current level through the lamp while it is lighted and a low simmer current through the lamp while it is not lighted. The lamp current is switched between these two modes by a transistor; the transistor is therefore called a current-mode switch.

The active lamp-pulse driver circuit is shown in the figure. The small dc power supply keeps capacitor C_1 charged and maintains a partially-ionizing simmer current flowing in the lamp, once the lamp has been ignited. When the transistor is turned on, it allows a high current to flow during an incomplete discharge of C_1. The monostable multivibrator sets the pulse interval by applying voltage to the noninverting terminal of the base-drive amplifier. A tap on emitter resistor R_2 delivers a feedback signal to the inverting terminal of the amplifier, thereby controlling the amplitude of the current during the pulse.

A flash-time interval greater than 100 microseconds is usually necessary to give adequate damping time to relaxation oscillations in the laser being pumped. The typical drive-current pulse is approximately 350 microseconds long and transfers an instantaneous power of about 120 kilowatts to the flashlamp. The duty cycle is 0.1 percent.

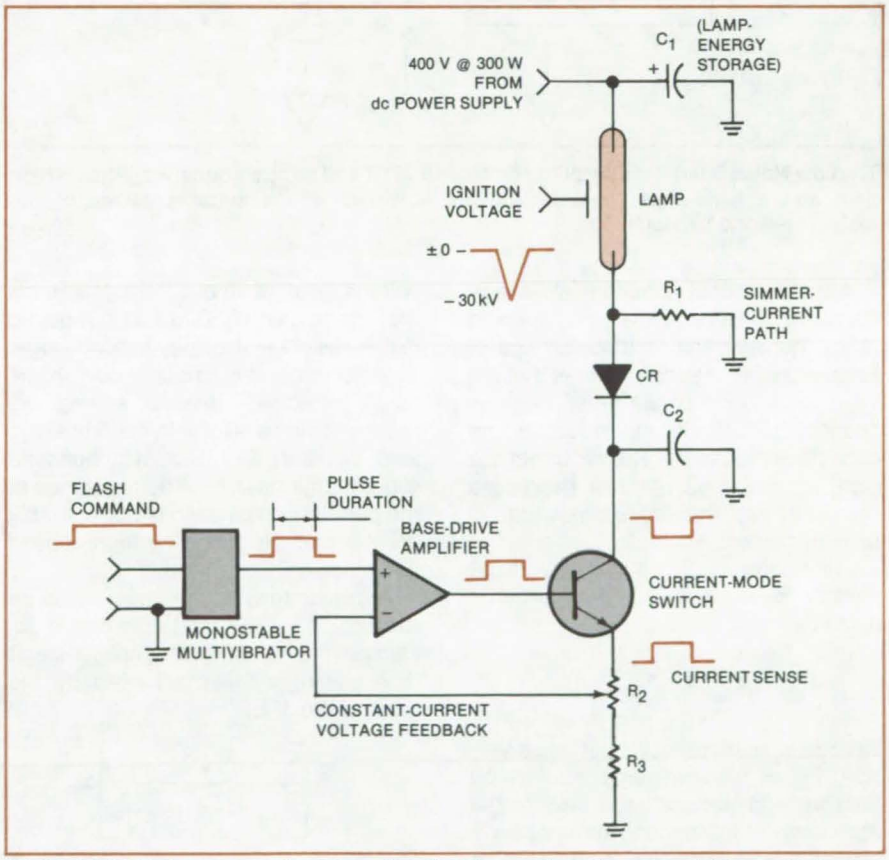

Stable Light Pulses are emitted from the flashlamp when the monostable multivibrator goes high, in part because the unsaturated transistor switch has a negative feedback control that keeps the lamp current constant.

This work was done by K. Edward Logan of International Laser Systems, Inc., for **Goddard Space Flight Center.** *For further information, including details of circuit operation and waveforms of current, lamp output, and laser output, Circle 6 on the TSP Request Card.*

This invention is owned by NASA, and a patent application has been filed. Inquiries concerning nonexclusive or exclusive license for its commercial development should be addressed to the Patent Counsel, Goddard Space Flight Center (see page A5). Refer to GSC-12566.

Low-Noise Band-Pass Amplifier

Circuit uses standard components to overcome a common limitation of JFET amplifiers.

Goddard Space Flight Center, Greenbelt, Maryland

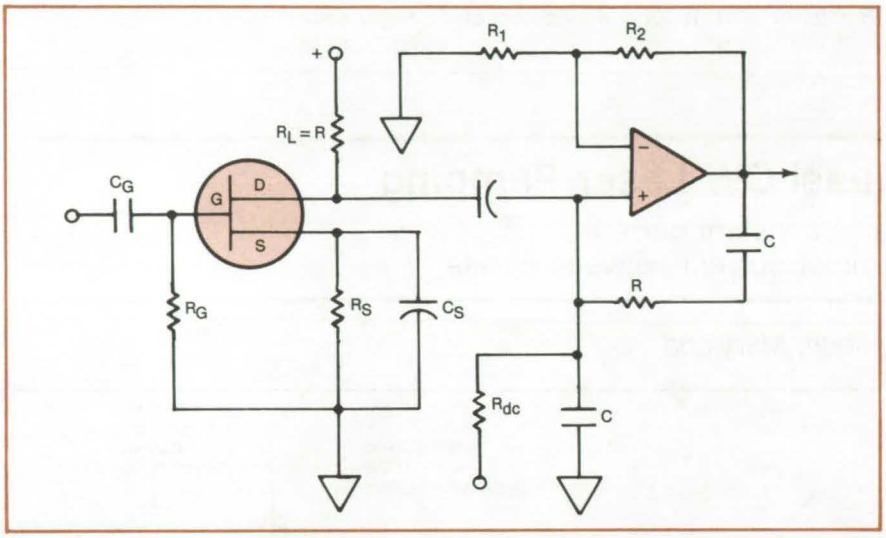

The **Low-Noise Band-Pass Amplifier** employs a JFET and an operational amplifier. A high gain and a band-pass characteristic are achieved with a suitable choice of the resistances and capacitances.

A conventional junction-field-effect-transistor (JFET) amplifier is ac-coupled to the noninverting input of an operational amplifier in such a manner that the input impedance of the latter includes negative resistance and inductive and capacitive reactance. The net effect is a high first-stage gain with a band-pass characteristic; that is, a simulated LC resonance condition.

The equivalent first-stage input noise voltage, E_{in}, of a two-stage amplifier is given by

$$E_{in}^2 = E_1^2 + E_2^2/k^2$$

where E_1 = first-stage input noise voltage, E_2 = second-stage input noise voltage, and k = voltage gain of the first stage. If the second-stage noise is large, then a high first-stage gain is necessary to minimize its effect.

The low-noise condition in a JFET usually requires a large quiescent current. In turn, this requires a small load resistor, resulting, in practice, in a voltage gain of about 7 to 10. But a first- stage gain of 50 to 100 is required in the presence of a noisy second stage. At resonance, the circuit shown in the figure effectively places a negative resistance in parallel with the first-stage load resistor, R_L, with a magnitude slightly larger than R_L. The resistance of the parallel combination is considerably greater than R_L, resulting in increased first-stage gain.

A straightforward analysis yields an expression for the total admittance (including the operational-amplifier-stage driving-point admittance) seen by the drain of the JFET:

$$Y = \left[\frac{1}{R} - \frac{\varrho R}{R^2 + \frac{1}{\omega^2 C^2}}\right] + j\left[\omega C - \frac{\varrho/\omega C}{R^2 + \frac{1}{\omega^2 C^2}}\right]$$

where $\varrho = R_2/R_1$.

The susceptance vanishes at a resonant frequency

$$\omega_{res} = \frac{(\varrho - 1)^{1/2}}{RC}$$

At resonance, the expression for the admittance simplifies to $Y_{res} = (2 - \varrho)/R$. The ac first-stage load resistance has effectively been multiplied by $1/(2-\varrho)$, while the dc value still allows the required large quiescent current. If for example, $\varrho = 1.9$, then the effective load resistance is increased to 10R, which multiplies the first-stage gain to 10 times its unloaded value.

Since the operational-amplifier-stage gain equals $1 + \varrho$, the overall gain at resonance is given by

$$K_V \approx \frac{g_m R}{2 - \varrho}(1 + \varrho)$$

where g_m = the JFET transconductance, and its drain resistance is considered to be very large. This expression may also be written as

$$k_V \approx [\text{unloaded gain}] \times \frac{1 + \varrho}{2 - \varrho}$$

Thus, the circuit provides a band-pass characteristic and the required high first-stage gain, as well as high overall gain. The circuit should find use as a low-noise amplifier, for example as the first stage in an instrumentation system.

This work was done by Leonard Kleinberg of **Goddard Space Flight Center.** *No further documentation is available.*

This invention is owned by NASA, and a patent application has been filed. Inquiries concerning nonexclusive or exclusive license for its commercial development should be addressed to the Patent Counsel, Goddard Space Flight Center (see page A5). Refer to GSC-12567.

Arc-Free High-Power dc Switch

Power contacts carry no current while they open or close.

Lyndon B. Johnson Space Center, Houston, Texas

A hybrid switch allows high-power direct current to be turned on and off without arcing or erosion. The switch consists of a bank of transistors in parallel with mechanical contacts. The transistor bank makes and breaks the switched circuit; the contacts carry current only during the steady-state "on" condition.

Originally designed for the Space Shuttle orbiter, the hybrid switch can be used also in high-power control circuits in aircraft, electric autos, industrial furnaces, and solar-cell arrays. With its arc-free closure, the device could also be operated in potentially explosive atmospheres. The switch operates at a maximum of 330 Vdc, in versions with current ratings of 100, 300, 500, 600, 1,000, and 1,500 Adc.

To close the hybrid switch, an operator sets a switch on a control panel to the "close" position (see figure). This actuates a motor, which moves a set of contacts, S_1, together. S_1, designed for low current and voltage, energizes a dc/dc converter, which biases the transistor bank into saturation. The transistors then apply 270 Vdc power to the load. About 10 milliseconds later, the motor closes a second set of contacts, S_2, designed for high current and voltage. S_2 short-circuits the transistors and carries the full current load. When the motor has closed S_2, it is turned off automatically. The dc/dc converter remains energized because S_1 stays closed. The power drawn by the converter is less than 2 watts.

To open the hybrid switch, the operator sets the control panel switch to "open." The motor opens S_2, and the transistors again furnish power to the load since the transistor bank has been kept fully saturated by the converter. About 10 milliseconds after S_2 opens, the motor opens S_1. The transistor bank is then deenergized, and no further power is delivered to the load.

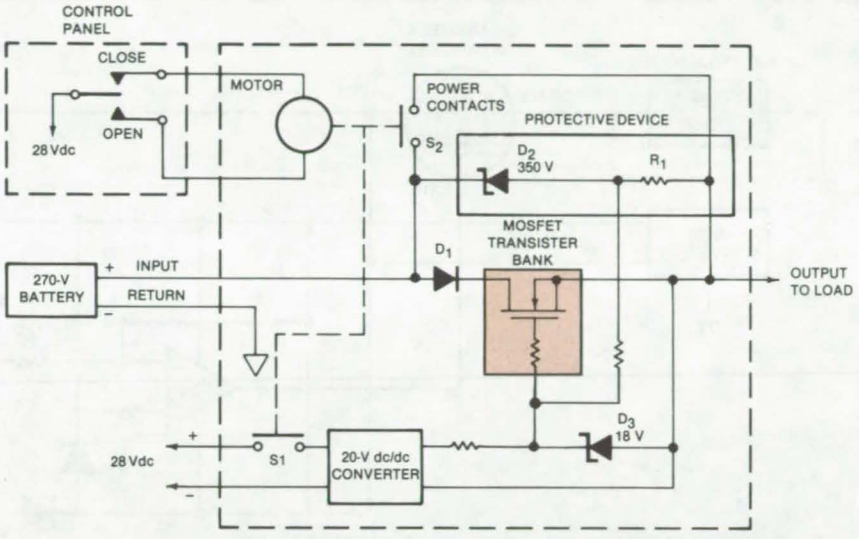

A Bank of MOSFET's delivers current to the load when power contacts S_2 are in the process of opening or closing. Contacts S_1 energize the MOSFET bank for a brief period before S_2 closes and after S_2 opens. The power contacts are therefore never subjected to arcs when they are joined or separated. The 1,500-A version of the switch measures 7-½ by 15 by 10 inches (19 by 38.1 by 25.4 cm).

The transistor bank is composed of parallel groups of metal-oxide-semiconductor field-effect transistors (MOSFET's). With these devices, the auxiliary circuitry is simpler than if bipolar transistors were used. The MOSFET's for this application must have a drain-to-source voltage rating of 400 V and a drain-current rating of 11 A. "On" resistance must be low — less than about 0.3 Ω. Each parallel group of MOSFET's contains up to six transistors (adding more than six devices to the group makes it difficult to balance the drain-current distribution among the members). A 100-A switch contains 12 MOSFET's divided into two groups. A 1,500-A switch contains 150 MOSFET's divided among 25 groups.

A series diode, D_1, protects the transistor bank from negative transient voltages and positive reverse currents from the bus while the bank is deenergized. D_1 is reverse-biased by output transient voltages greater than the battery voltage. Zener diode D_3 protects the transistor gates from overvoltage.

A protective device composed of diode D_2 and a resistor protect the deenergized transistor bank from positive transient voltages greater than 350 Vdc. When such a transient occurs, D_2 conducts and creates a voltage drop across R_1 that turns on the transistor bank. The voltage drop from drain to source of the parallel transistors is thereby reduced, and damage to them is prevented. Although the transient is passed on to the load, it is ordinarily so short — 100 μs long at most — that only minimal voltage is developed across the load.

This work was done by Wilson N. Miller and Ormal E. Gray of Rockwell International Corp. for **Johnson Space Center.** *No further documentation is available.*

MSC-20091

Power-MOSFET Voltage Regulator

Parallel MOSFET's act as a high-current dc regulator and switch.

Lyndon B. Johnson Space Center, Houston, Texas

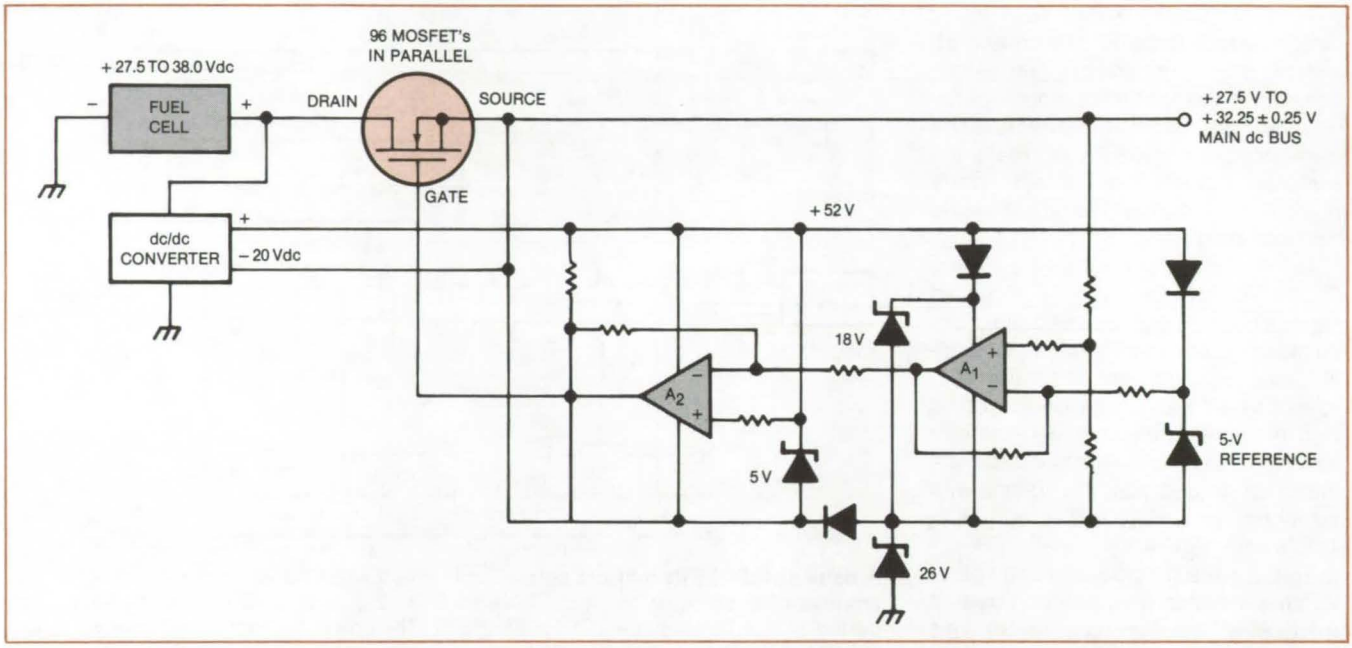

Ninety-six Parallel MOSFET Devices with a two-stage feedback circuit form a high-current dc voltage regulator that also acts as a fully-on solid-state switch when fuel-cell output falls below the regulated voltage. Ripple voltage is less than 20 mV, and transient recovery time is less than 50 ms.

A high-current voltage regulator based on metal-oxide-semiconductor field-effect transistors (MOSFET's) is highly efficient, dissipating only 115 watts of power at a current output of 450 amperes. The control element is a parallel combination of 96 MOSFET devices, which thus act as though they have a single source, gate, and drain. Developed to regulate the output of fuel cells on board the Space Shuttle, the MOSFET regulator can be used wherever large direct currents must be controlled. It can be applied, for example, to inverters, industrial furnances, photovoltaic solar generators, dc motors, and electric autos.

MOSFET's have a positive temperature coefficient of resistance; thus as the internal temperature of a single device rises because of increased current, internal resistance also rises, tending to limit the current and to divert it to other MOSFET's in the parallel combination. A bipolar transistor with its negative coefficient behaves in just the opposite way, tending to draw more current as its temperature rises. The MOSFET regulator is therefore not subject to the current runaway that can lead to catastrophic failure in overloaded bipolar regulators.

The MOSFET's are the series element in a series static regulator (see figure), which maintains the main dc bus at 32.25 ± 0.25 volts when the fuel-cell output exceeds 32 volts. When the regulator is in the active range (fuel-cell voltage in excess of 32 volts), the MOSFET output (source) voltage is compared with a reference voltage. The difference is amplified by A_1 and A_2 and presented as an error signal at the gate of the MOSFET's. A 20-V dc-to-dc converter, powered by the fuel cell, provides the necessary turn-on bias for the MOSFET's and the operating voltage for A_2. An 18-V Zener diode provides the operating voltage for A_1; the 26-V Zener offsets the return voltage of A_2 so that that amplifier operates at a reasonable level. Protection against lightning-induced voltage transients as high as 96 V is furnished by the 18-V Zener across A_1.

The fuel-cell output can range from 27.5 to 38 Vdc. When the fuel-cell voltage drops below 32 V, the MOSFET's act as a fully-saturated, turned-on solid-state switch.

The normal operating-current range is 50 to 450 A. The regulator can carry abnormally high currents for short periods (until fault-isolating fuses blow) without being damaged. For example, it can carry 1,000 A for 60 s (570 W dissipation) and 4,000 A for 400 ms (9,120 W dissipation). The final temperature of each MOSFET does not exceed 104.3° C for the 4,000-A fault.

This work was done by Wilson N. Miller and Ormal E. Gray of Rockwell International Corp. for **Johnson Space Center.** *For further information, Circle 7 on the TSP Request Card.*
MSC-20059

Modular Amplifier/Antenna Arrays

Solar cells would feed energy directly to amplifier/antenna modules.

Lyndon B. Johnson Space Center, Houston, Texas

Two proposed solar-powered microwave transmitter modules would include amplifiers in direct contact with the antenna dipoles (see figure) so that the metalization of the dipoles serves as heat-dissipation areas for the amplifiers. Each module utilizes 3-watt amplifiers with dipoles spaced on a grid that has 1.3-wavelength spacing. Clusters of 16 modules delivering about 50 watts of transmitter power would be arranged in a phased array controlled from a single source.

Of the two designs, one is a high-Q circuit that is efficient but mechanically complex, while the other is simpler but less efficient. In either case, the anticipated mass is less than 1 gram per watt.

In the high-Q design, the antenna elements are printed on a 3-mil (0.08-mm) sheet (Kapton® , or equivalent) spaced one-quarter wavelength away from the metalized back surface of the solar-cell blanket. Each amplifier uses lumped-element circuits and "bump"-mounted GaAs FET's, all on a 0.5- by 1-cm sapphire substrate. The modules are fed by balanced lines from the receiver and are supplied with dc power by feedlines extending across the space from the solar blanket to the antenna sheet.

The alternative concept calls for a plastic grid, 20 mils (0.5 mm) thick, between the solar blanket and the antenna elements. This arrangement yields lower circuit efficiency, so two-stage, 3-watt chips are employed.

[Kapton® is a trademark of E. I. du Pont de Nemours & Co.]

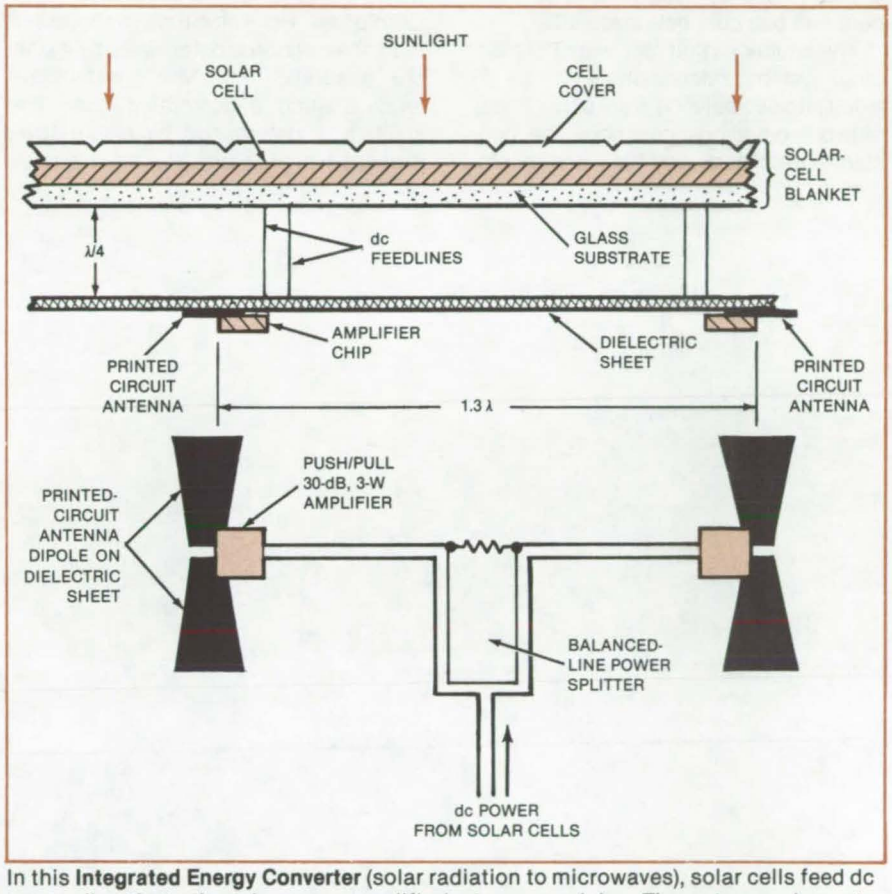

In this **Integrated Energy Converter** (solar radiation to microwaves), solar cells feed dc power directly to the microwave amplifier/antenna modules. The antenna elements also serve as heat sinks for the amplifiers.

This work was done by Erwin F. Belohoubek of RCA Corp. for **Johnson Space Center.** *No further documentation is available.*

MSC-18981

Computer Programs

These programs may be obtained at very reasonable cost from COSMIC, a facility sponsored by NASA to make new programs available to the public. For information on program price, size, and availability, circle the reference letter on the COSMIC Request Card in this issue.

Line-Replaceable-Unit Analysis

Interface voltages are determined for LRU's in various configurations.

The shuttle LRU (Line Replaceable Unit) Analysis Program (SLAP) aids in the evaluation of LRU interface voltages in the Shuttle orbiter electrical system. Slap includes a reduced model of the Shuttle LRU circuit. Although primarily intended for analysis of the Shuttle LRU's, SLAP could be adapted for voltage analysis in other situations. A library of subroutines simulates the different types of circuit components. The user may readily add new, or modify existing, component subroutines so that any

(continued on next page)

unusual or nonstandard circuit models may be handed.

The electrical system is modeled by input data describing its power switching devices, circuit breakers, fuses, and diodes. In addition, data concerning load types and bus voltages are included. The arrangement of the circuit elements is determined by user input code numbers and bus connection identifiers.

The equations that represent the electrical system under analysis can be divided into two sets: (1) A set of nonlinear network equations describes the constant-power loads and their controllers. (2) A set of linear-algebraic network equations describes the resistive load.

The equations of each LRU are coupled through the network equations, which determine how the LRU interface voltages and their currents vary as functions of the bus voltages of the distribution panel. In solving the network equations, resistive loads are handled using Ohm's Law. For a single constant-power load, the solution is determined by a simple quadratic. For two constant-low loads sharing a common feeder, the solution is determined by an iterative process which retains the originality of the network equations.

SLAP is written in PL/I for batch execution and has been implemented on an IBM 370 series computer with a central-memory requirement of approximately 635K of 8-bit bytes. SLAP was developed in 1980.

This problem was written by Tedja Oepomo and Timothy V. Prouty of Rockwell International Corp. for **Johnson Space Center.** *For further information, Circle A on the COSMIC Request Card.*
MSC-20183

Electronic Systems

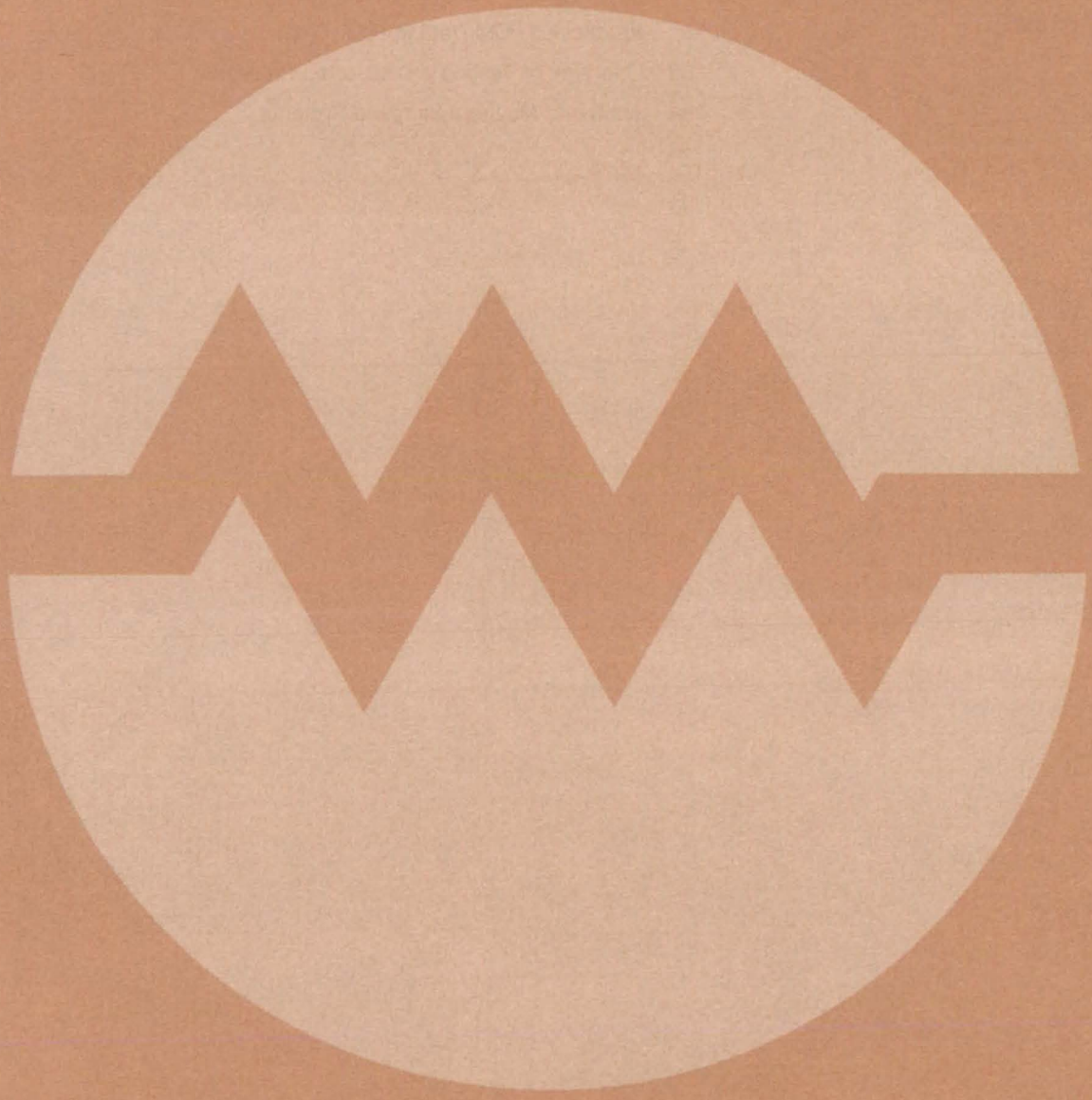

Hardware, Techniques, and Processes

261 Method for Canceling Ionospheric Doppler Effect

262 Programable Interface Handles Many Peripherals

263 Processing PCM Data in Real Time

263 One Way of Testing a Distributed Processor

264 Analyzing Multirate-Sampled Systems

Method for Canceling Ionospheric Doppler Effect

Transponder system achieves zero output-signal shift with suitable choice of frequency-synthesis ratios.

Marshall Space Flight Center, Alabama

Both the dispersive (ionospheric) and nondispersive (motional) components of the Doppler effect are canceled in a novel transmitting and receiving system.

At the S-band frequencies of interest, the index of refraction depends upon frequency and upon the ionospheric electron density along the signal path. To a close approximation, the ionospheric component of the Doppler shift (with an undisturbed ionosphere) is given by

$$\Delta f = -\frac{k}{f}\frac{d}{dt}\int_P \varrho(S,t)dS$$

where k = a constant, f = the signal frequency, $\varrho(t)$ = the electron density, and P denotes that the integral is taken along the signal path from the transmitter to the receiver.

The system shown in the figure exploits the proportionality between the dispersive component of the frequency shift and the reciprocal of frequency to achieve cancellation of the dispersive component at the output. It employs two hydrogen-maser oscillators of output frequency f_h = 1,420.405 MHz — one at the ground station and one on the spacecraft. The one-way downlink frequency, f_0, is generated by processing the maser signal through a frequency synthesizer that multiplies the frequency by P and divides it by Q. Therefore, this signal undergoes an ionospheric Doppler shift of

$$\Delta f_1 = -\frac{kQ}{f_h P}\frac{d}{dt}\int_P \varrho dS$$

This signal is fed to one of the inputs of mixer M_1.

To obtain the uplink frequency, the ground-station maser output frequency is multiplied by R/S. Aboard the spacecraft, a phase-coherent transponder transmits a downlink signal at M/N times the frequency of the received uplink signal. Following the signals up and back down, performing the frequency-shift calculations, and neglecting second-order terms, the shift difference frequency at the output of mixer M_2 is given by

$$\Delta f_2 = -\frac{kS}{f_h R}\left(\frac{N}{M}+\frac{M}{N}\right)\frac{d}{dt}\int_P \varrho dS$$

As shown in the figure, this signal is then multiplied in frequency by SNP/2RMQ and fed to mixer M_3. The M_3 output frequency shift is given by

$$\Delta f_{total} = -\frac{k}{f_h}\left[\frac{Q}{P}-\frac{S^2}{2R^2}\left(1+\frac{N^2}{M^2}\right)\frac{P}{Q}\right] \times \frac{d}{dt}\int_P \varrho dS$$

The ionospheric component of frequency shift can be made to vanish if the frequency multiplication and division ratios are chosen to make the term in brackets equal to zero. The ionospheric Doppler effect is thus canceled when

$$\frac{S^2}{2R^2}\left(1+\frac{N^2}{M^2}\right)\frac{P^2}{Q^2} = 1$$

The motional component of the Doppler effect is canceled for all frequency-synthesis ratios.

In the unified S-band system, the ratios employed were M/N = 240/221, P/Q = 76/49, and R/S = 82/55, leaving a maximum anticipated ionospheric error of 3×10^{-15} in $\Delta f/f$. The system was tested by comparing two adjacent Earth-station hydrogen-maser clocks and simultaneously comparing the spacecraft clock with one of the Earth-station

(continued on next page)

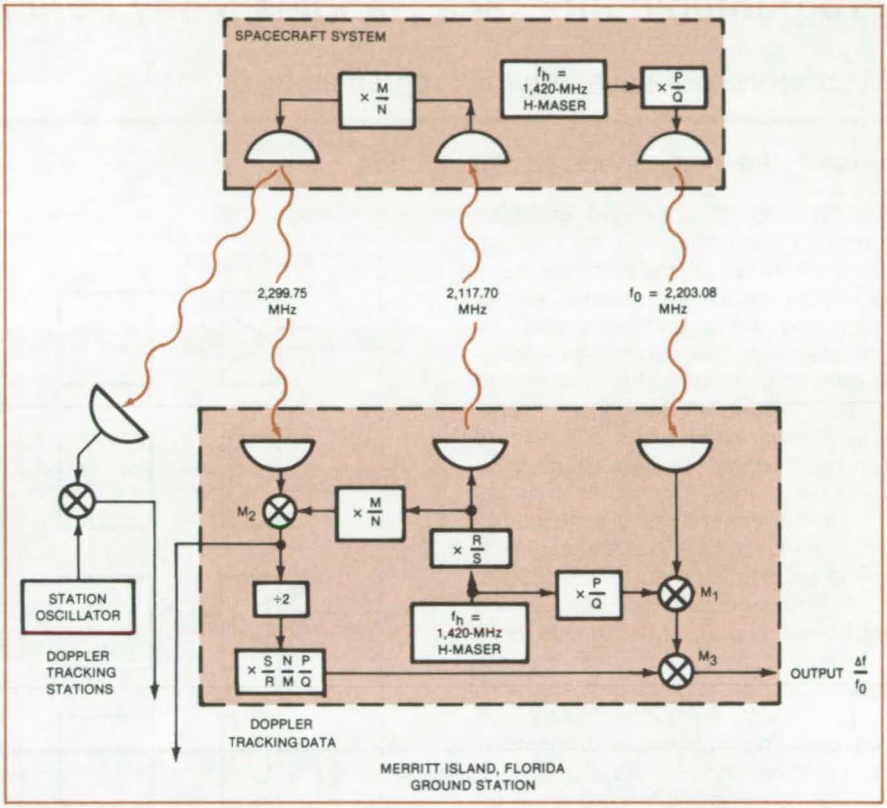

A **Unified Transponder System** with hydrogen-maser oscillators at both stations can compensate for both motional and ionospheric components of the Doppler shift. Appropriate choices of frequency multiplication and division ratios result in a small or zero ionospheric component of frequency shift in the output of mixer M_3.

clocks. The Doppler effects were effectively reduced to a level well below the random frequency variations of the clocks. For averaging intervals from 100 to 1,000 seconds, this was well below a $\Delta f/f$ of 10^{-14}. This type of system can be used for extremely-high-precision time and frequency transfer over long distances where ionization is present.

This work was done by Robert F. C. Vessot of the Smithsonian Institution for **Marshall Space Flight Center.** *For further information, Circle 8 on the TSP Request Card.*
MFS-25599

Programable Interface Handles Many Peripherals

Microprocessor-based unit is programed by the user.

John F. Kennedy Space Center, Florida

A microprocessor-based interface simplifies the interconnection of a peripheral device with the common memory of a network of minicomputers. In the Space Shuttle launch complex, the peripheral is the countdown timing-distribution system; the network of mini's monitors all launch operations. The firmware-controlled interface is reprogramed by the user to interface other peripherals.

The interface consists of a microprocessor, a bidirectional port that connects to the common memory, a bidirectional port that connects to the user-selected peripheral, and an asynchronous serial communications port. Data are accepted and processed from any port, and the results are transmitted through any port. The architecture of the interface is shown in the figure.

Once it has been initialized, the interface continually samples the countdown time in the minicomputer common memory (called a "common data buffer"). Once each second, the time is read, reformatted, and transmitted to the timing-distribution system peripheral. From there, the countdown time is distributed to the many wall displays in the launch complex. On request, the interface can issue discrete output commands or digital data patterns. It can also check for errors in the data it reads.

This work was done by M. Jasinski of IBM Corp. for **Kennedy Space Center.** *For further information, Circle 9 on the TSP Request Card.*
KSC-11132

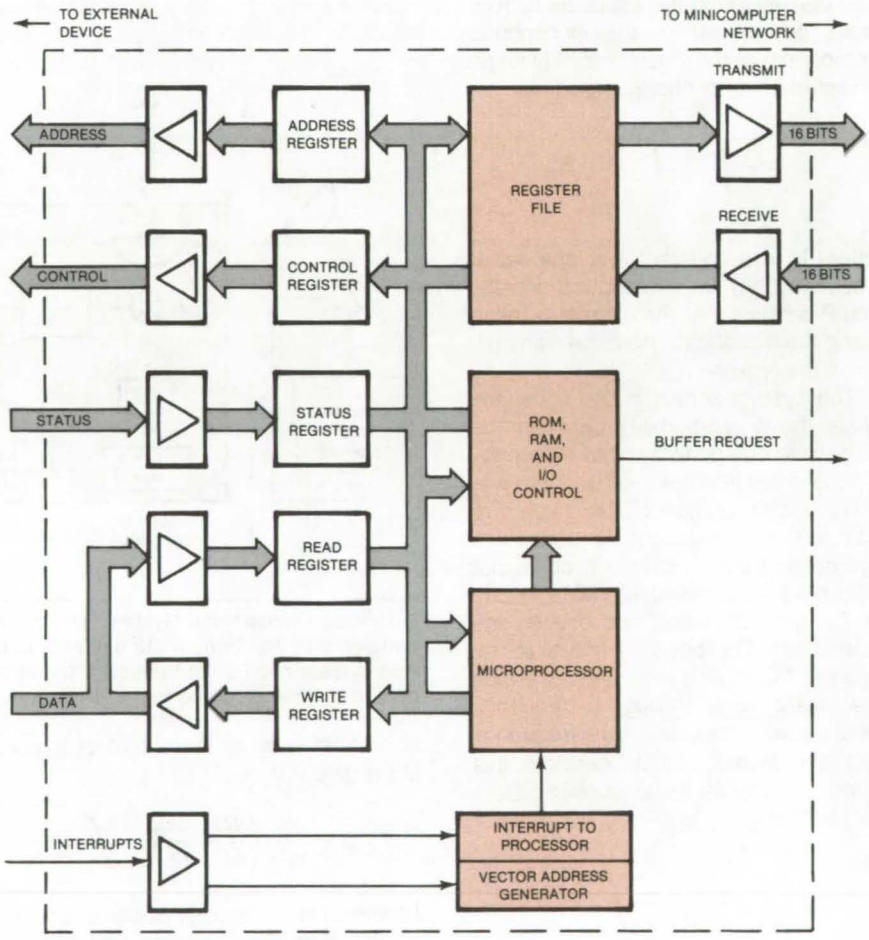

The **Programable Interface** is based around a 6800 microprocessor. It is assembled from 90 integrated circuits.

Processing PCM Data in Real Time

Three CPU's work together to monitor pulse-code-modulated data for errors and changes.

John F. Kennedy Space Center, Florida

A novel hardware configuration makes it possible for the Space Shuttle launch processing system to monitor pulse-code-modulated data in real time. Using two microprogramable "option planes," incoming PCM data are monitored for changes at the rate of one frame of data (80 16-bit words) every 10 milliseconds.

The Shuttle launch processing system includes up to 64 minicomputers. A memory device called a Common Data Buffer (CDBFR) links the computers, allowing them to communicate with each other by using computer-to-computer commands. Each minicomputer has conventional I/O capabilities and up to 64K of memory.

The two option planes associated with one of the minicomputers are seen in the figure. Each has its own CPU, storage registers, and I/O bus. The PCM option plane does most of the processing of the PCM data. Reports to the rest of the network on the results of the processing are made through the CDBFR option plane.

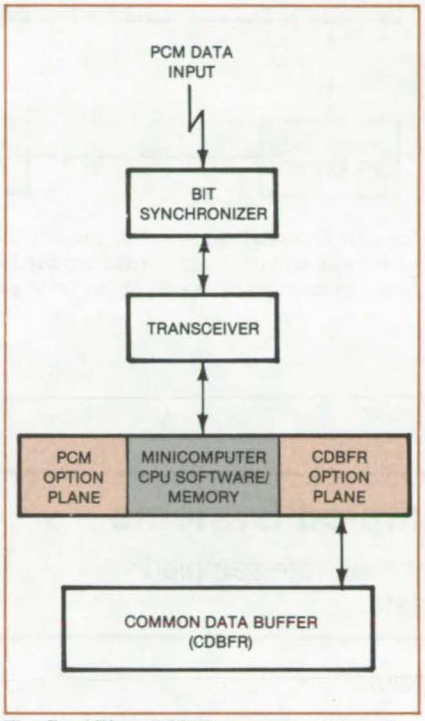

The **Real-Time PCM Processor** utilizes the CPU in the minicomputer and CPU's in two option planes.

Many of the operations required to process the incoming data are done by the PCM option plane. Certain complex operations are done by the minicomputer CPU under control of the PCM option plane. The option plane can also release control of the CPU and do its own processing in parallel. In this parallel mode, the option plane functions as any other peripheral and can communicate with devices connected to its own I/O bus.

The PCM measurement system monitors the incoming data to check magnitudes and to look for changes that fall outside of predetermined limits. When an error or out-of-limits condition develops, the information is reported to the rest of the launch processing system by the CDBFR option plane.

This work was done by T. L. Wissink of IBM Corp. for **Kennedy Space Center.** *For further information, Circle 10 on the TSP Request Card.*

Inquiries concerning rights for the commercial use of this invention should be addressed to the Patent Counsel, Kennedy Space Center (see page A5). Refer to KSC-11131.

One Way of Testing a Distributed Processor

The parallel-processing capabilities of a system of minicomputers are exercised with two programs.

John F. Kennedy Space Center, Florida

The launch-processing system for the Space Shuttle uses a master console and operations consoles at many different locations. All of the consoles interface with front-end data processors and a processed-data recorder through a common data buffer (see figure). This entire system for the checkout, control, and monitoring of a launch is tested with just two computer programs.

The first program, which is executed in the master console, synchronizes test initiation in the operations consoles and also controls test duration. In addition, it monitors the "up" or "down" status of each operations console.

The second program controls the execution in an operations console. An important feature of this program is a scheduler with directory of five subprograms that communicate with or process data from a particular front-end processor (FEP). The scheduler initiates three of these subprograms; and when one terminates, another is called. Thus three of the five subprograms are active at all times. Using this technique, each operations console communicates with a different set of FEP's at any given time.

Software interrupts facilitate the communications between the scheduler and active tasks. Each task is assigned a unique interrupt; and when the task terminates, the interrupt is sent to the scheduler. The scheduler then initiates another task.

The second program monitors the countdown clock and begins initiating tasks when the status changes from Hold to Count. A countdown time of zero terminates the test.

(continued on next page)

The operations consoles all have copies of the second program. These copies are identical except for the program directory and the discretes used for communicating with the master console.

To execute a test, the control program is called in each operations console. The operator then calls the monitor program from the master console. Keyboard commands set the countdown time to a value that represents test duration and start the countdown clock. The control program in each operations console detects the change in status and begins task initiation. All of the front-end processors are exercised from the consoles through the common data buffer, and all data are logged to the processed-data recorder for posttest analysis.

This work was done by R. Edstrom and D. Kleckner of IBM Corp. for **Kennedy Space Center.** *No further documentation is available.*
KSC-11123

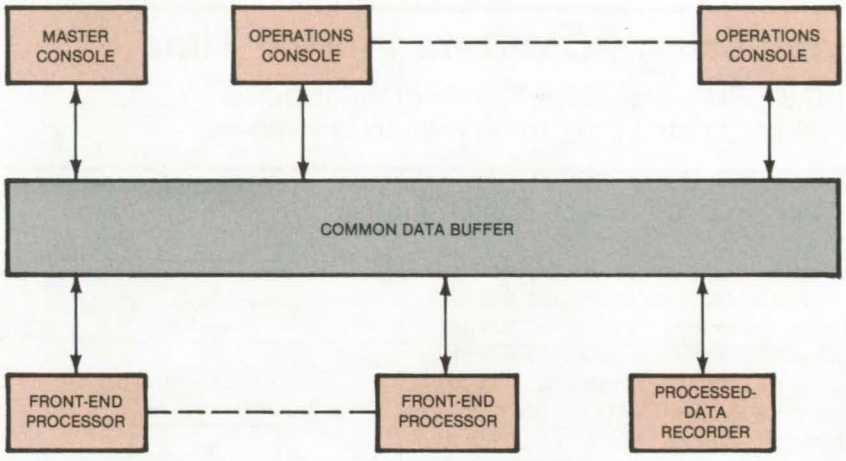

Launch Processing for the Space Shuttle is checked out, controlled, and monitored with this system. The entire system can be exercised by two computer programs — one in the master console and the other in each of the operations consoles.

Analyzing Multirate-Sampled Systems

Method allows stability analysis of multirate-sampled, multiple-variable control-system data.

Marshall Space Flight Center, Alabama

A new method is available for monitoring the stability of a system on the basis of data sampled at multiple rates — in particular, at two rates, one of which is twice the frequency of the other. The method is called Multirate Matrix Frequency Response (MMFR) analysis.

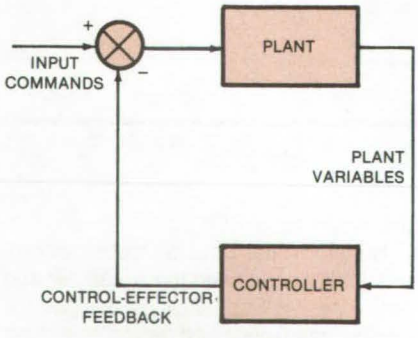

A **Control Loop** is analyzed for stability by means of matrices representing the equations relating plant variables, control-effector feedback signals, and input commands. Since input commands do not affect closed-loop stability, the input commands are nulled for the purpose of stability analysis.

MMFR was used in the Space Shuttle to evaluate the effect of decreasing the sample rate of the an error loop in the ascent-phase digital autopilot. It should also be useful to designers of other control systems and to structural, civil, and mechanical engineers for structure and vibration analysis.

One of the forerunners of MMFR was a method of open-loop frequency-response analysis known as the Generalized Determinant Expansion Routine (GDER). The latter can expand a large determinant with elements composed of polynomials in Laplace transform operator form and can correctly determine the coefficient of the highest order term. Dynamic equations of the plant and the control equations necessary to close the control loops (see figure) are placed in the GDER determinant. The eigenvalues resulting from the expansion determine the total system stability.

A refinement of GDER resulted in the immediate predecessor of MMFR, a program known as Matrix Frequency Response (MFR). A somewhat more direct approach than GDER, MFR made substitution of a complex variable the first step in the frequency-response calculation process. Improved computer speeds and the development of an innovative determinant expansion routine made this approach possible.

In MMFR, a Z-transform frequency decomposition technique is used to reduce a multirate system to an equivalent single-rate system that operates at the faster (or fastest) sample rate. The resulting model is then analyzed by GDER and MFR techniques. Sample-rate ratios other than 2:1 can be accommodated by MMFR, though additional complexity is thereby introduced.

This work was done by Neal Hendrix of **Marshall Space Flight Center.** *For further information, Circle 11 on the TSP Request Card.*
MFS-25541

Physical Sciences

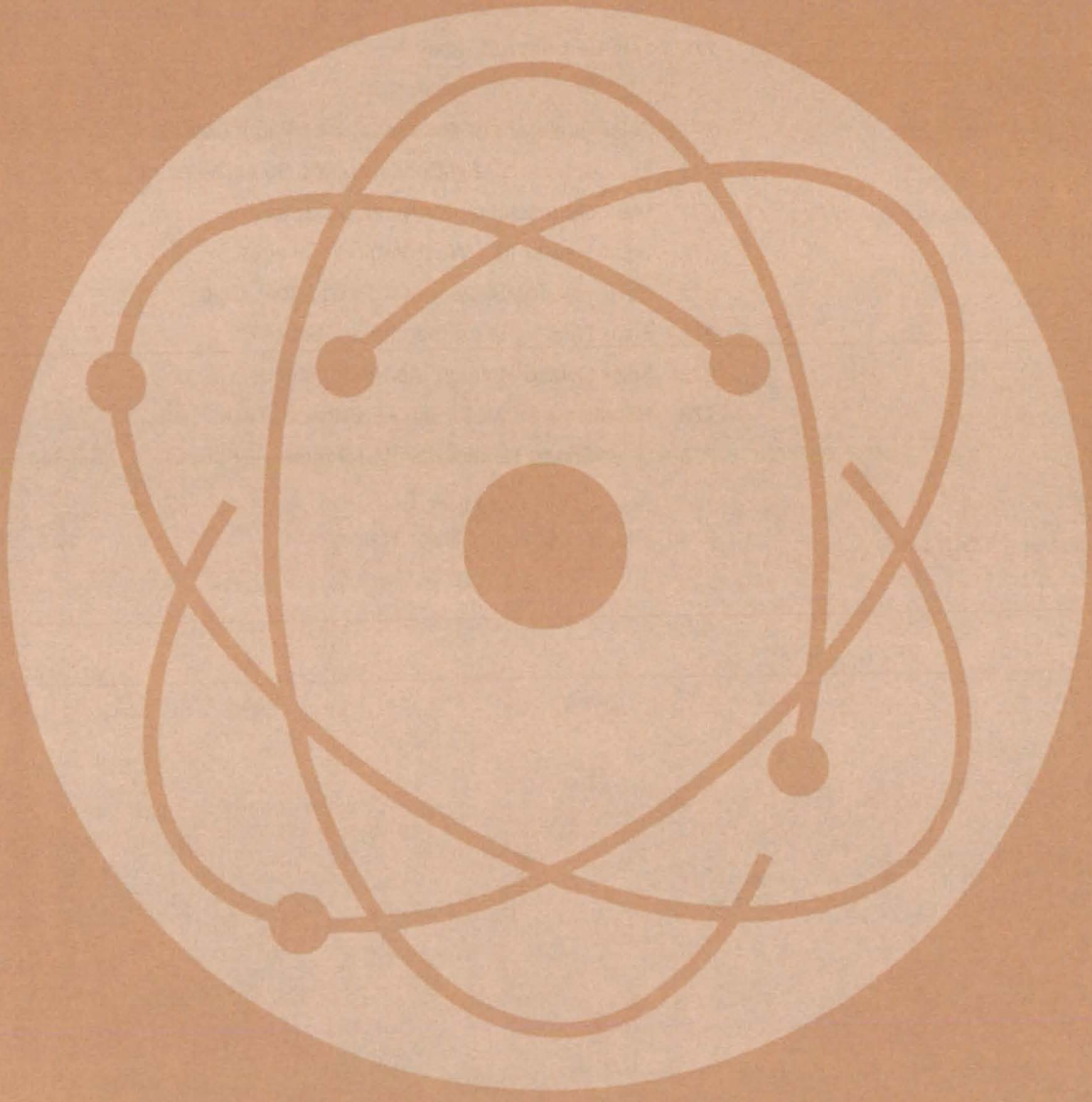

Hardware, Techniques, and Processes

267 Rotating the Plane of Parallel Light Beams
268 Solar-Driven Liquid-Metal MHD Generator
269 Improved Lixiscope
270 Test-Bed Aircraft Scanner

Books and Reports

271 Solar Simulator at Marshall Space Flight Center
271 Evaluation of a Line-Concentrating Solar Collector
271 Manifold Insulation for Solar Collectors
272 Solar Heater in a West Virginia College
272 Solar Heating System at a Racquetball Club
272 Solar Heating in an Elementary School
273 Solar-Cooled Hotel in the Virgin Islands
273 Hot Water for Motor Inn — Garland, Texas
273 Solar Space Heating for Warehouse — Kansas City, Kansas

Computer Programs

274 The Economics of Solar Heating

Rotating the Plane of Parallel Light Beams

A pair of rhomboid prisms displaces and rotates the beam plane.

Ames Research Center, Moffett Field, California

Pairs of rhomboid prisms rotate the plane of parallel light beams and change the beam spacing in new optical systems developed at Ames Research Center. Among other uses, the prism configurations can rotate the plane of parallel laser beams used in a laser velocimeter.

A rhomboid prism laterally displaces a light beam as shown in the figure. By using pairs of rhomboids, the plane of two light beams is rotated. The spacing between the beams is maintained or changed, depending on the length of the prisms used.

The figure also shows an arrangement of two pairs of rhomboid prisms that provides either of two rotation angles, depending on which pair of prisms is rotated into the beams. The prisms are mounted on a disk that is rotated by a motor.

A pair of rhomboid prisms can also be mounted so that each prism is rotated independently about the beam entry point. In that case, the plane of the beams rotates through any angle in a wide range; however, the spacing of the beams changes with the angular setting.

Other prisms, such as the Pechan (a two-prism system) and the Dove, can rotate the plane of two closely spaced beams through any desired angle. However, they are quite bulky for large beam spacings.

In the suggested configurations, the cross section or aperture of the rhomboid prism needs only to be large enough to accommodate one of the beams. With the Pechan and Dove, both beams enter one prism, so the aperture must be large enough to include both beams. Furthermore, the length of the prisms increases in proportion to the aperture.

Both the rhomboid and Pechan prisms are achromatic. Since the beams enter and leave these prisms perpendicularly to the glass surface, no refraction occurs, and beams of all wavelengths follow the same path. The Dove prism is not achromatic because the beam enters and leaves at an oblique angle.

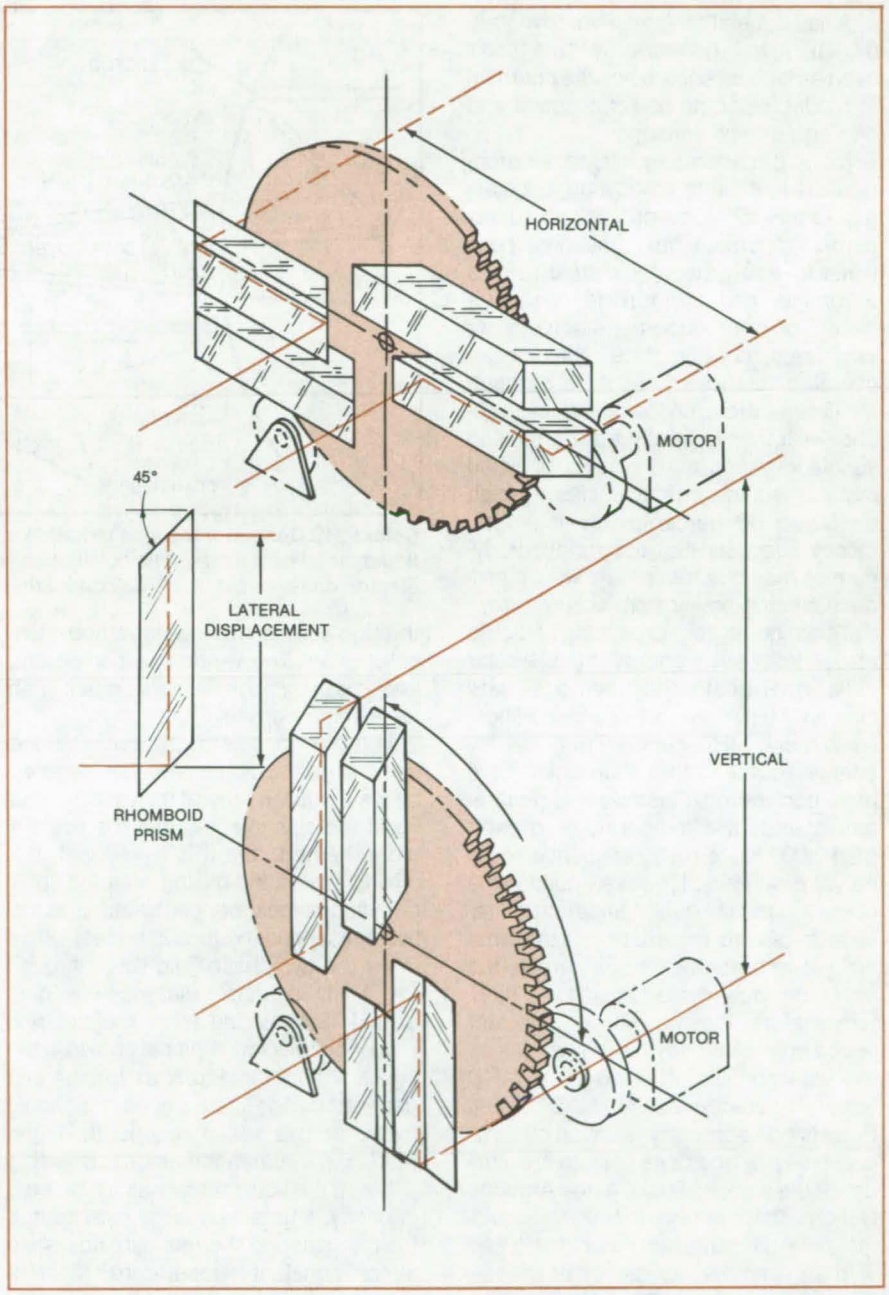

A **Rhomboid Prism** laterally displaces a beam of light. Pairs of rhomboid prisms can rotate the plane of two parallel beams of light and change the spacing of the beams. If each element of a pair is mounted on an independent motor-driven disk, the angle of rotation of the plane of the beams can be varied over a wide range.

This work was done by Kenneth L. Orloff and Haruo Yanagita of **Ames Research Center.** *For further information, Circle 12 on the TSP Request Card.*

Inquiries concerning rights for the commercial use of this invention should be addressed to the Patent Counsel, Ames Research Center (see page 5). Refer to ARC-11311.

Solar-Driven Liquid-Metal MHD Generator

Magnetohydrodynamics appears to be an efficient way to convert solar radiation to electric power.

Langley Research Center, Hampton, Virginia

A liquid-metal magnetohydrodynamic (MHD) power generator with a solar oven as its heat source has the potential to produce electric power in space and on Earth at high efficiency.

Modern generating plants incorporate irreversible thermodynamic losses due to their complex processes: Fuel is burned to create heat, the heat boils water to create steam, the steam drives a turbine, and the turbine powers a generator to produce the electricity. At each step, energy is lost, yielding an overall efficiency of about 35 percent. MHD generators, on the other hand, produce electricity directly from a moving substance such as a plasma or liquid metal, resulting in efficiencies as high as 50 to 60 percent. This high efficiency suggests that magnetohydrodynamics may be an excellent way to produce electric power from solar energy.

Techniques for producing electric power from solar energy include solar cells, thermoelectric methods, and plasma MHD generators. In addition, liquid-metal MHD generators driven by energy sources other than solar have been considered. Plasma MHD generators operated at temperatures greater than 2,000 K are highly-efficient electric power producers. However, continuous operation at such high temperatures results in severe material problems that are yet to be solved. For example, the maximum duty cycle tested for a high-temperature plasma MHD generator lasted only a few days with coal gas as the working fluid. A liquid-metal MHD generator proposed at NASA's Jet Propulsion Laboratory is driven by a nuclear reactor and uses cesium and lithium as the working fluids. At the Argonne National Laboratory, a NaK-N_2 liquid-metal MHD generator was developed with an estimated efficiency of greater than 50 percent at 1,500 K. Various heat sources were considered, but solar energy was not included.

A solar-powered liquid-metal MHD generator proposed at Langley Research Center focuses solar radiation through a transparent window and into a solar oven. The window is cooled and kept clean by an inert working gas such as helium or argon.

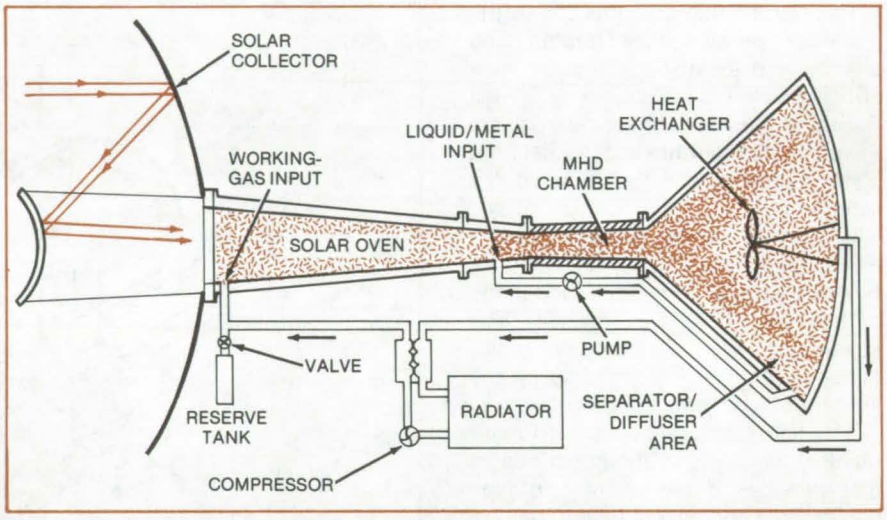

Solar MHD Generator focuses radiation from the Sun to heat a driving gas that pushes a liquid metal past a magnetic coil (not shown above). Power is extracted directly from the electric currents set up in the conducting liquid.

In the oven, solar radiation heats the working gas, which is also compressed by the conical shape of the oven. As the liquid metal is injected into the oven, it too is heated, and it is mixed with the driving gas. In the mixing area the solar radiation is most concentrated, and the two-phase working fluid is hottest.

As the two-phase fluid flows through the MHD channel, electricity is generated. Surrounded by a magnet and power-conditioning unit not shown in the figure, the channel acts as turbine and generator: The gas drives the liquid metal across the magnetic field and thereby generates the electric power.

Since the liquid metal has a high heat capacity, it acts as a large heat source for the gas, and the gas expands at an almost-constant temperature. Most of the enthalpy change in the generator depends on the liquid.

The gas is separated from the mixture in the separator/diffuser and is recouped in the regenerative heat exchanger. The gas is then returned to the solar oven by way of the radiator and compressor. The liquid metal is pumped back into the mixer.

An alternative to the directly-heated solar oven is a heat exchanger similar to that used for a coal-fired liquid-metal MHD generator. In this case the solar radiation is directed to an absorbing material such as graphite in which a heat exchanger is enclosed or to an ensemble of heat-exhanging pipes with multiple fins made of absorbing material.

This system was first conceived for use in space. Using solar energy as a fuel can save considerable costs and payload weight, compared to previous systems. The system could, of course, be adapted for use on Earth. Its principal advantages are that the basic technology exists, that near-term application can be expected, and that it could achieve an efficiency of up to 55 percent. Other methods including plasma MHD generators still require breakthroughs in materials and component development.

This work was done by Frank Hohl of **Langley Research Center** *and Ja H. Lee of Vanderbuilt University. Further in-*

formation may be found in NASA TM-81965 [N81-27926/NSP], "Solar Driven Liquid Metal Magnetohydrodynamic Generator" [$5]. A copy may be purchased [prepayment required] from the National Technical Information Service, Springfield, Virginia 22161.

This invention is owned by NASA, and a patent application has been filed. Inquiries concerning nonexclusive or exclusive license for its commercial development should be addressed to the Patent Counsel, Langley Research Center [see page A5]. Refer to LAR-12495.

Improved Lixiscope

Portable X-ray and gamma-ray imager counts single photons with excellent spatial and energy resolution.

Goddard Space Flight Center, Greenbelt, Maryland

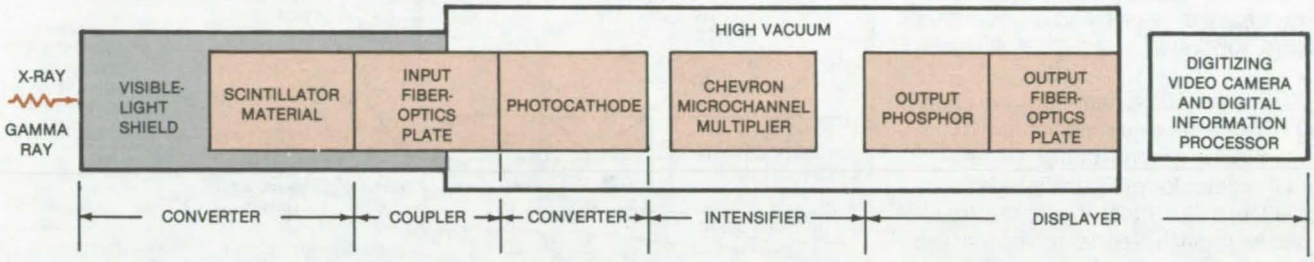

The **Improved Lixiscope** utilizes fast-decay scintillators and multiple or curved microchannel-plate amplifiers to achieve high energy and spatial resolution as well as single-photon counting.

An improved portable X-ray and gamma-ray imaging device — known as a "Lixiscope" — counts single photons and gives excellent energy resolution over its operating range from 20 to 200 keV. The new unit has the same high spatial resolution as the original version.

The previous Lixiscope is described in "Low-Intensity X-Ray and Gamma-Ray Imaging Device," on page 67 of *NASA Tech Briefs,* Vol. 3, No. 1. It is used with or without an attached radiation source in several radiographic applications, including medical diagnostics. The new unit, with its higher energy resolution, is intended for X-ray astronomy, although it could be applied terrestrially wherever a sensitive portable radiation spectrometer is required for the 20-to-200-keV range.

As shown in the illustration of the Lixiscope, the incident photons pass through a shield opaque to visible light but transparent to X-rays and gamma rays. They strike a scintillator that converts them into visible-light photons. The visible-light image is then coupled by optical fibers to an image intensifier, which produces an electron image. Finally, the electron image is impressed on an aluminized phosphor at the output faceplate, which displays the much-intensified visible image.

Significant improvements have been made in the image-intensifier section. Previously, a conventional single-channel microchannel-plate (MCP) amplifier with a peak gain of about 10^4 was used. Ion feedback prevented the realization of the higher gain (about 10^7) needed for single-photon counting.

The new unit uses a dual, triple, or curved microchannel-plate amplifier. The dual, triple, or curved MCP's eliminate the ion-feedback problem. The microchannels are 12 microns in diameter with a total length-to-diameter ratio of approximately 100:1. Since electron multiplications are confined to these narrow channels, image information is preserved during the intensification process. For single-photon counting, NaI, CsI, or other fast-decay phosphors can be used as input scintillators.

When the multiple or curved MCP amplifier is operated at saturation, the gain for a single-electron input is about 10^7. However, since tens to thousands of simultaneous photocathode electrons are produced by each gamma ray, it is necessary to operate below saturation to stay below the charge limitation of the amplifier.

Nonetheless, the multiple or curved MCP amplifier operated below saturation has essentially the same gain characteristic for multiple-electron inputs that it does in the saturated mode for a single-electron input. This is a result of the statistics associated with large numbers of photoelectrons. Thus even when operated below saturation to prevent charge overload, the dual MCP amplifier has sufficiently high gain to allow single-photon counting and to give energy resolution.

This work was done by Lo I Yin of **Goddard Space Flight Center.** *For further information, Circle 13 on the TSP Request Card.*

This invention is owned by NASA, and a patent application has been filed. Inquiries concerning nonexclusive or exclusive license for its commercial development should be addressed to the Patent Counsel, Goddard Space Flight Center [see page A5]. Refer to GSC-12587.

Test-Bed Aircraft Scanner

Versatile line-scanning spectral imaging system has improved optics and electronics.

Langley Research Center, Hampton, Virginia

The test-bed aircraft multispectral scanner (TBAMS) is a line-scanning multispectral imaging system with eight visible/near-infrared channels and one thermal-infrared channel. Key design features of TBAMS are its large size and its modular subsystems mounted on a horizontal baseplate. This unique layout allows easy access to and replacement of the subsystems and their subcomponents.

Sensitive visible/near-infrared imaging is achieved by a modification of the transmission-grating optics (Figure 1) and the detector/preamplifier electronics (Figure 2). In the optics, the transmission grating is reoriented so that the grooved surface faces toward the collimating lens rather than toward the focusing lens. The electronics are modified to optimize the match between the optics and the detector geometry and to optimize the detector/preamplifier for the highest signal-to-noise ratio in the electronic bandwidth required for imaging. Selectable spectral channels are achieved by mounting detectors and signal-processing electronics on interchangeable printed-circuit boards.

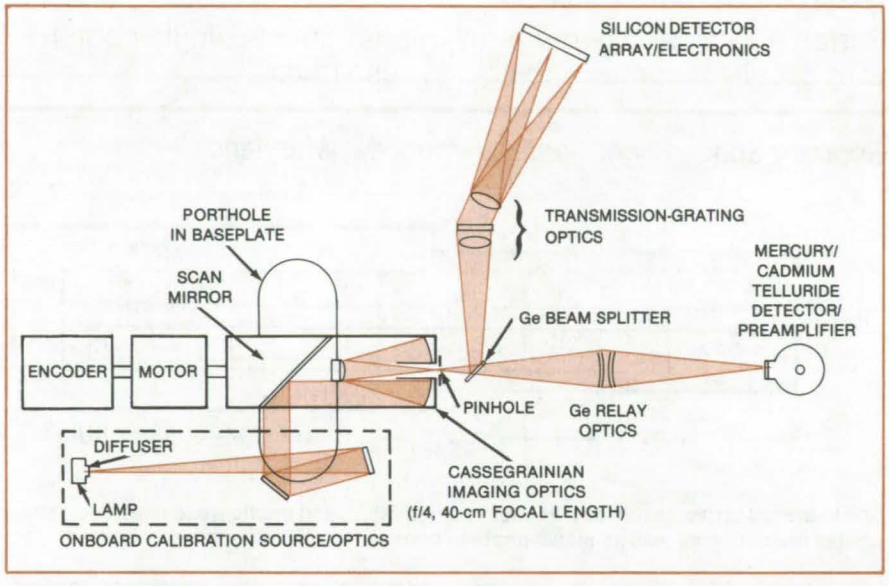

Figure 1. The **TBAMS Optical System,** designed around existing inexpensive parts, sacrifices compactness for the ease of modification.

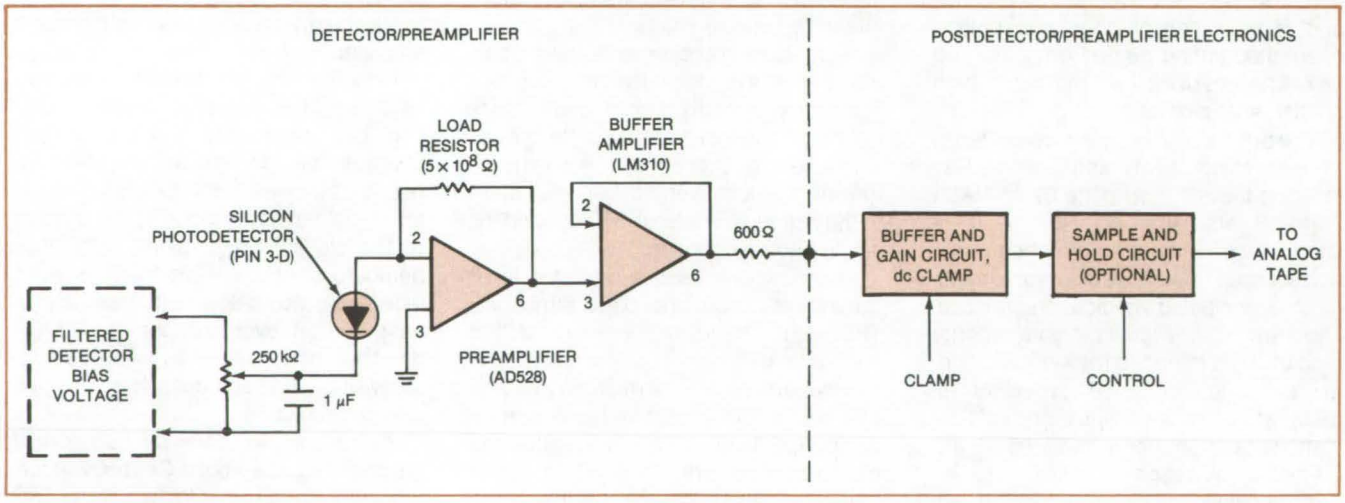

Figure 2. The **TBAMS Electronics** shown here were modified to optimize the signal-to-noise ratio.

The reorientation of the transmission diffraction grating, which improves efficiency in this system, could also improve efficiency in other electro-optical or optical systems that use this component. The data derived from this system will be used in a review of other existing systems for possible improvements in their performance.

This work was done by Daniel J. Jobson, Stephen J. Katzberg, Robert B. Spiers, Charles A. Hardesty, Ernest E. Burcher, and Stewart H. Irwin of **Langley Research Center.** *For further information, Circle 14 on the TSP Request Card.*
LAR-12796

Books and Reports

These reports, studies, and handbooks are available from NASA as Technical Support Packages (TSP's) when a Request Card number is cited; otherwise they are available from the National Technical Information Service.

Solar Simulator at Marshall Space Flight Center

Solar collectors can be evaluated under a variety of conditions.

A solar simulator at Marshall Space Flight Center allows solar collectors to be evaluated indoors, where testing is not subject to the vagaries of the weather and where repeatability of conditions can be ensured from test to test. The subject of a 73-page report, the simulator can establish a variety of conditions that can be set at constant levels over a broad range. The conditions include solar-radiation intensity, spectrum and collimation; solar attitude; and wind speed and direction.

The simulator can be used on collectors employing either an air or a liquid collection medium. It can reproduce such system conditions as collector-fluid flow rate, inlet temperature, and collector tilt and azimuth angles. It provides data on collector efficiency, collector time constant, incident-angle modifier, and stagnation temperature. Simulator measurements compare with outdoor measurements within a few percent.

Solar radiation is simulated by 405 tungsten-halogen lamps, the spectrum of which closely resembles that of the Sun near the surface of Earth. Each lamp is paired with a Fresnel lens, which collimates the radiation. The lamp array illuminates a 4 by 8 ft (1.2 by 2.4 m) surface. The collector under test is placed on a table that tilts and orients it. A load simulator supplies it with air or liquid collection fluid. Two portable floor fans provide wind.

A data-acquisition system accommodates 256 channels of analog or digital data. It measures and records absolute and differential temperatures, flow rate, absolute and differential pressure, wind velocity, and total solar radiation. Measurements of diffuse and direct solar radiation can be made if they are needed.

The report describes the Sun simulator, the solar-collector system simulator, the overall simulation setup, and instrumentation. It provides detailed operating procedures, including instructions for solar field mapping, system startup and shutdown, and adjustment of air and liquid supplies.

This work was done by Wyle Laboratories for **Marshall Space Flight Center.** *Further information may be found in DOE/NASA CR-161825 [N81-30523/NSP], "Design Data Package and Operating Procedures for MSFC Solar Simulator Test Facility" [$14]. A paper copy may be purchased [prepayment required] from the National Technical Information Service, Springfield, Virginia 22161. The report is also available on microfiche at no charge. To obtain a microfiche copy, Circle 15 on the TSP Request Card.*
MFS-25742

Evaluation of a Line-Concentrating Solar Collector

Sun-tracking accuracy is found to affect efficiency critically.

Results of a performance evaluation of a line-concentrating solar collector are contained in a 45-page report. The collector employs a parabolic trough to direct Sunlight to a line along its focal axis, along which lies a black-chrome-plated receiver tube covered by a glass tube containing still air. The reflective trough has an aluminum-mirror surface covered with a metallized acrylic film. It is 7 ft 2½ in. wide and 20 ft ½ in. long (2.1 by 6.1 m). The maximum operation temperature and pressure of the receiver are 650° F and 250 lb/in.^{2} (343° C and 1.7 MPa), respectively. The trough can rotate through an angle of 270°.

The performance evaluation included measurements of the collector time constant (the time for the temperature difference between inlet and outlet to drop to 0.368 of its value for full illumination), Sun-tracking accuracy, thermal efficiency, all-day performance (efficiency vs. time for various inlet temperatures), and collector heat loss. An array of four collectors, positioned end to end, was used for the evaluation. The array was driven by a single drive mechanism which was controlled by an electronic tracking device.

Tracking accuracy was found to be critical. Efficiency drops as much as 10 percent when the reflector leads or lags the sun by only 1°.

The evaluation report tabulates test conditions, tracking angles and speed for the twenty-first day of each month, and performance data as a function of time for a few test days. The report presents graphs of solar radiation, heat loss, efficiency, and tracking accuracy vs. sky conditions (clear, intermittent clouds, and cloudy).

This work was done by Wyle Laboratories for **Marshall Space Flight Center.** *Further information may be found in NASA CR-161856 [N82-10502/NSP], "Performance Evaluation of the Solar Kinetics T-700 Line Concentrating Solar Collector" [$7.50]. A paper copy may be purchased [prepayment required] from the National Technical Information Service, Springfield, Virginia 22161. The report is also available on microfiche at no charge. To obtain a microfiche copy, Circle 16 on the TSP Request Card.*
MFS-25778

Manifold Insulation for Solar Collectors

Thermal resistance must be high or else solar-collector efficiency will be low.

If fluid is distributed to and gathered from an array of solar collectors by an external manifold rather than an internal one, the effectiveness of the manifold insulation has a major influence on efficiency. The results of a computer analysis of the effects of various manifold insulations are detailed in a 23-page report.

The results show that efficiency falls off sharply for manifold insulations having values of thermal resistance, R, of 2.0 h-ft^2-°F/Btu (0.35 m^2-°C/W) or less. Values of R of 7.0 or more denote little

(continued on next page)

heat loss and performance degradation.

The analysis used a simple FORTRAN program. The program can be modified easily to provide additional information or to accommodate alternative input data. The program is based on the following assumptions:

- The collectors in an array are identical and use a liquid as the collection medium.
- The liquid flow rate through each collector is identical.
- External manifolds, when used, are made of constant-diameter tubing and are uniformly insulated.
- Manifold heat loss can be determined from the tube area, the insulation resistance, and the temperature difference between the mean fluid temperature and the ambient temperature.
- The external manifolds receive no heat from the Sun.

The report describes the required input data and presents the equations that govern the computer model. It provides graphs comparing collector efficiencies for representative manifold sizes and insulations. An important conclusion is a realistic determination of effective collector area must include an allowance for external manifolds and spacing between adjacent collectors.

This work was done by Wyle Laboratories for **Marshall Space Flight Center.** *Further information may be found in NASA CR-161852 [N82-10501/NSP], "An Analytical Comparison of the Efficiency of Solar Thermal Collector Arrays With and Without External Manifold" [$7.50]. A paper copy may be purchased [prepayment required] from the National Technical Information Service, Springfield, Virginia 22161. The report is also available on microfiche at no charge. To obtain a microfiche copy, Circle 17 on the TSP Request Card.*
MFS-25779

Solar Heater in a West Virginia College

Report covers a flat-plate collector and associated equipment.

The solar space-heating and hot-water system installed at Alderson-Broaddus College, Philippi, West Virginia, is described in an 87-page document. The system, which is designed to supply 35 percent of the 51,000-ft^2 (4,700-m^2) building, uses an antifreeze solution as the heat-exchange medium. It employs 3,150 ft^2 (295 m^2) of single-glazed flat-plate solar collectors with coated copper absorbers. Water warmed by the solar-heated antifreeze solution is stored in two 3,000-gallon (11,000-liter) steel tanks. The system operates in conjunction with a heat pump and electric water heaters.

The document contains a description of the building and its solar-energy system; specifications for the solar-energy system, including collectors, coolant, storage tanks, circulation equipment, piping, controls, and insulation; acceptance test data; and a discussion of problems with the installation, their solution, and recommendations for dealing with excess solar energy during summer months. The problems were largely of an administrative rather than a technical nature. Also included in the document is an as-built drawing of the system.

This work was done by J. E. Sturm, Inc., for **Marshall Space Flight Center.** *Further information may be found in DOE/NASA CR-161756 [N81-25491/NSP], 'Solar Heating and Hot Water System Installed at Alderson Broaddus College, Philippi, West Virginia' [$9.50]. A paper copy may be purchased [prepayment required] from the National Technical Information Service, Springfield, Virginia 22161. The report is also available on microfiche at no charge. To obtain a microfiche copy, Circle 18 on the TSP Request Card.*
MFS-25706

Solar Heating System at a Racquetball Club

Space heat and hot water are provided.

An Arlington, Virginia, racquetball club obtains heat and hot water for its support areas (reception room, lounge, and lockers) from solar collectors. As detailed in a 93-page report, the system contains 2,520 ft^2 (234 m^2) of flat-plate solar collectors and a 4,000-gal (15,000-l) storage tank. The heat-transfer fluid is a nontoxic antifreeze solution composed of equal parts of water and propylene glycol.

The hot-water portion of the system consists of a copper preheat coil, 60 ft (18 m) long and 1¼ in. (3.2 cm) in diameter in the storage tank, and a recirculation loop between the preheat coil and the existing electric water heaters. The space-heating portion consists of two water-to-air heat exchangers in the ducts of the existing space-heating and cooling system, supplied with water from the storage tank.

The report explains the modes of operation of the system and details an acceptance-test plan. It presents a maintenance procedure and a maintenance checklist. It describes the operation of controls, and provides project drawings and a list and description of parts. The manufacturers' specifications for the internal manifold selector, temperature controllers, valves, switches, motors, and pumps are detailed.

This work was done by ARC Associates for **Marshall Space Flight Center.** *Further information may be found in NASA CR-16179 [N81-28518/NSP] "Solar Heating and Hot Water System Installed at Arlington Racquetball Club, Arlington, Virginia — Final Report" [$9.50]. A paper copy may be purchased [prepayment required] from the National Technical Information Service, Springfield, Virginia 22161. The report is also available on microfiche at no charge. To obtain a microfiche copy, Circle 19 on the TSP Request Card.*
MFS-25720

Solar Heating in an Elementary School

A Virginia school was designed for solar heating.

A solar-heating and hot-water system installed in an elementary school in Virginia is described in a 154-page report. The 63,525-ft^2 (5,902-m^2) James Hurst School in Portsmouth, which houses 842 kindergarten through fourth-grade students, was designed for solar heating. Solar energy furnishes more than half the 636 million-Btu (6.71×10^{11}-J) annual heat requirement.

Flat-plate liquid-medium collectors are mounted on a south-facing portion of the roof sloped at 53°. The gross area of the 192 collectors is 3,630 ft^2 (337 m^2). Hot water from the collectors is stored in

an insulated steel tank in a storage shed attached to the school. For space heating, the solar-heated water is pumped from the storage tank to heating coils in air-handling units. For domestic hot-water preheating, the water is pumped to a shell-and-tube-type heat exchanger.

The building is zoned into four heating/cooling areas. Each area has an air-handling unit that is controlled by a central monitoring unit. The ground floor contains a perimeter zone, an internal zone, and a cafeteria/multipurpose-area zone. The second floor is a single zone. Back-up heat is provided by an oil-fired boiler.

The report contains a discussion of the design philosophy and an acceptance-test report. It provides instructions for installation, maintenance, and operation. It also furnishes mechanical drawings and manufacturers' data on pumps, valves, controllers, and other components.

This work was done by Portsmouth Public Schools for **Marshall Space Flight Center.** *Further information may be found in DOE/NASA CR-161830 [N81-31625/NSP], "Solar Heating and Hot Water System Installed at James Hurst Elementary School, Portsmouth, Virginia" [$14]. A paper copy may be purchased [prepayment required] from the National Technical Information Service, Springfield, Virginia 22161. The report is also available on microfiche at no charge. To obtain a microfiche copy, Circle 20 on the TSP Request Card.*
MFS-25747

Solar-Cooled Hotel in the Virgin Islands

Sun energy supplies about one-third of the cooling requirements for public areas.

A solar cooling system at Frenchman's Reef Hotel in Saint Thomas, U.S. Virgin Islands, provides cooling for public areas including ballrooms, restaurant, lounge, lobby, and shops. Chilled water from the solar-cooling system is also used to cool hot water from the hotel's desalinization plant.

The performance of the cooling system is described in a 21-page report. The system consists of 956 solar-collector modules, two 2,500-gal (9.5-m^3) storage tanks, two absorption chillers, a combined controller and data logger, and associated pumps, piping, and valves. Each of the collector modules (which are mounted on the hotel roof) contains eight evacuated glass-tube solar collectors within a compound parabolic-cusp reflector. The effective collection area of a module is about 14 ft^2 (1.3 m^2). Water heated in the collectors is stored in the connected tanks and is drawn from one of them as needed. The hot water is used by itself to operate one of the chillers or in combination with steam generated by exhaust heat from the diesel electric generators of the hotel. A second chiller operates on the steam alone to provide cooling at night and during cloudy periods.

In tests in March 1980 and August 1981, 31.4 and 34.5 percent, respectively, of the energy to the chiller was contributed by the solar-energy system. With a hot-water pump the capacity of which matches the system design-flow specifications of 450 gal/min (28 l/s), it is expected that the solar-energy system will deliver more of the available energy to the chiller.

The report briefly describes the system and its operation. Performance constraints are discussed and the results of the performance tests are summarized.

This work was done by Harry Harber (innovator) of **Marshall Space Flight Center.** *Further information may be found in DOE/NASA TM-82442 [N81-33611/NSP], "Solar Cooling System Performance, Frenchman's Reef Hotel, St. Thomas, U.S. Virgin Islands — Final Report" [$6]. A paper copy may be purchased [prepayment required] from the National Technical Information Service, Springfield, Virginia 22161. The report is also available on microfiche at no charge. To obtain a microfiche copy, Circle 21 on the TSP Request Card.*
MFS-25776

Hot Water for Motor Inn — Garland, Texas

Solar collectors supply rooms and laundry.

A solar-collector array provides 39.9 percent (in December) to 84.7 percent (in August) of the domestic hot-water needs of the Day's Inn in Garland, Texas. The system provides hot water for showers and sinks in the inn rooms and for the laundry.

A 35-page report describes the system and its operation and presents the projected system performance. It details calibration and maintenance procedures and lists and describes the equipment that makes up the system.

Forty-four Daystar flat-plate collectors with a gross area of 998 ft^2 (92.7 m^2) are located on the roof of the inn. Pipes to and from the collector array penetrate the roof above the laundry room, where the 1,000-gal (3,800-l) storage tank and control unit are located. The control unit houses all pumps, differential thermostats, relays, meters, gages, and all valves except for a check valve in the collector-return line and four gate valves on the roof. Water from the storage tank flows through a tube-in-shell heat exchanger in the control unit, thereby heating the domestic water.

This work was done by Day's Inn of America, Inc., for **Marshall Space Flight Center.** *Further information may be found in DOE/NASA CR-161802 [N81-28515/NSP] "Solar Domestic Hot Water System Manual for Day's Inn, Garland, Texas" [$6.50]. A paper copy may be purchased [prepayment required] from the National Technical Information Service, Springfield, Virginia 22161. The report is also available on microfiche at no charge. To obtain a microfiche copy, Circle 22 on the TSP Request Card.*
MFS-25726

Solar Space Heating for Warehouse — Kansas City, Kansas

Simple modular design adapts to a variety of occupancy patterns.

A 48,800-ft^2 (4,500-m^2) warehouse/office building in Kansas City, Kansas, uses solar heating for the 39,000-ft^2 (3,600-m^2) warehouse portion and conventional heating and cooling for the 9,800-ft^2 (900-m^2) office portion. The building is divided into 20 equal units, each with its own solar-heating system. The modular design enables multiple units to be combined to form offices or warehouses of various sizes as required by tenants.

As described in a new report, each unit has 20 double-glazed flat-plate solar collectors of 400 ft^2 (37 m^2) total area,

(continued on next page)

tilted at 53° from the horizontal and facing 3° east of south. Air serves as the heat-transfer medium, so that no freeze protection is required. When the collector temperature is insufficient to heat the air being circulated through the system, the air is heated by electric-resistance duct coils. Return air is drawn through the collectors and circulated back into the warehouse space.

There is no mass heat storage other than that due to the mass of the building and of the materials stored in the warehouse area. This eliminates the need for more extensive ductwork and controls and prevents valuable storage space from being taken up by the heat-storage medium.

It is estimated that the solar-heating system will supply 56.2 percent of the heating requirements of the warehouse area. An additional energy saving is expected: The building envelope is well insulated, and the energy required to heat the building without solar assistance will be 30 to 35 percent less than in comparable buildings.

This work was done by Ducat Investments Inc. for **Marshall Space Flight Center.** *To obtain a copy of the report, "Solar Space Heating Installed at Kansas City, Kansas — Final Report," Circle 23 on the TSP Request Card.*
MFS-25712

Computer Programs

These programs may be obtained at very reasonable cost from COSMIC, a facility sponsored by NASA to make new programs available to the public. For information on program price, size, and availability, circle the reference letter on the COSMIC Request Card in this issue.

The Economics of Solar Heating

Program assesses the economic feasibility of solar energy for single-family residences and light commercial applications.

A solar heating system typically supplies from 50 to 70 percent of the average home heating and hot water load. This savings in conventional-fuel cost over many years is the incentive for spending the extra money to install the solar heating system. Because of the possibility of extended periods of bad weather, a full-sized conventional heating system is required as a backup to the solar heating system.

The question of whether to spend the extra money depends on how much the system will save and how long it will take to obtain those savings. The SHCOST computer program helps to answer these questions by assessing the economic feasibility of solar energy for single-family residences and light commercial applications.

There are several important economic considerations in "sizing" a solar heating system. "Sizing" means selecting a collector area and a collector performance and then determining the percentage of the annual energy load that can be provided by solar energy. As the collector area increases, the solar-energy system carries a greater percentage of the annual load. For low collector areas, not much Sunlight is captured and, hence, little heat is supplied. A relatively large amount of money is invested to displace a small amount of conventional heating. At high collector areas a similar cost phenomena occurs. Adding collector area when it is already high provides only a very small increase in the percentage of the total load carried by the solar-energy system.

Using classic life-cycle costing techniques, the collector area that minimizes the life-cycle cost of the system can be computed. From an economic standpoint, however, this may not be the most attractively-sized solar-energy system to the homeowner or for a light commercial application. Homeowners are usually more interested in a lower initial cost, fewer years to positive cash flow, fewer years to recover downpayment, and a shorter payback period than are determined in a classic minimum-life-cycle cost analysis.

SHCOST analyzes life-cycle costs as well as sensitivity studies to aid the designer in selecting the most economically attractive solar system for a single-family residence or a light commercial application. SHCOST includes a fairly comprehensive list of cost elements from which the user may select. It is assumed that the total heating load has been determined. Starting with an initial collector area and performance characteristics, the GFL method is used to determine the percentage of the heating load carried by the solar system.

SHCOST studies a range of values of certain parameters. The parameters that may be varied are collector area, discount rate, inflation rate, downpayment factor, property-tax rate, and income-tax rate. The output consists of tabular data on the sizing parameters and the sensitivity studies. Plotter output may be generated for the annual cash flow results and for the life-cycle cost as a function of any of the sensitivity analysis parameters.

SHCOST is written in ASCII FORTRAN for batch execution and has been implemented on a UNIVAC 1100 series computer with a central memory requirement of approximately 25K of 36-bit words. For plotter output, a Cal-Comp plotting system or equivalent is required. SHCOST was developed in 1979.

This program was written by J. Alan Forney of **Marshall Space Flight Center.** *For further information, Circle B on the COSMIC Request Card.*
MFS-25391

Materials

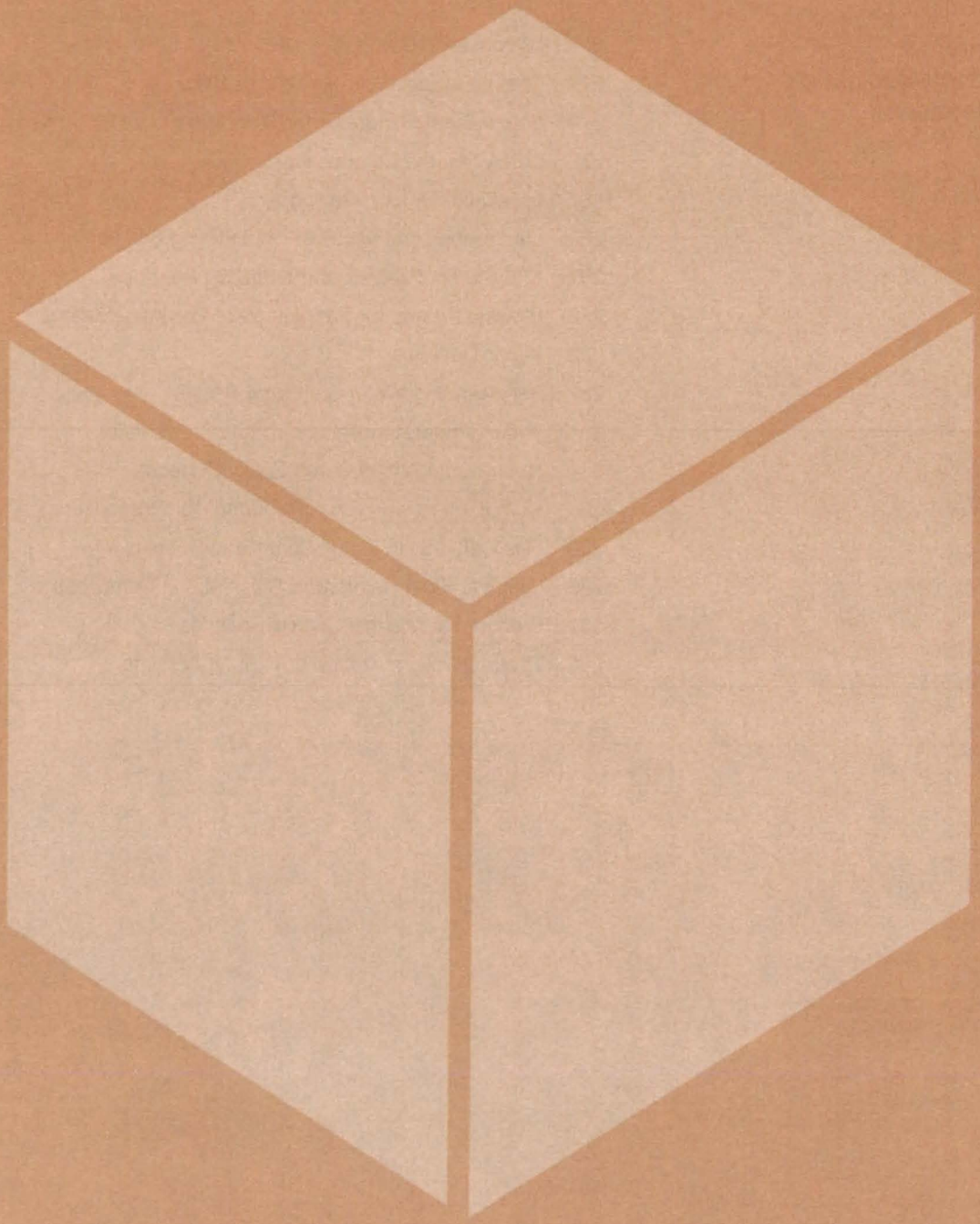

Hardware, Techniques, and Processes

277 Silicone/Acrylate Copolymers

277 Coal as a Substitute for Carbon Black

278 Sound-Burst Generator for Measuring Coal Properties

279 Catalyzing the Combustion of Coal

280 Low-Gold-Content Brazing Alloys

280 Electrochemical Assay of Gold-Plating Solutions

281 XPS Study of SiO_2 and the Si/SiO_2 Interface

282 Blowing Agents for Fabrication of Polyimide Foams

282 Vapor Detector

283 Regenerating Water-Sterilizing Resins

284 Wide-Temperature-Range Torque-Stripe Paint

284 Neutralizing Amine-Cured Epoxy Surfaces

285 Heat-Exchange Fluids for Sulfuric Acid Vaporizers

286 Gas Diffusion in Fluids Containing Bubbles

286 Graphite-Fiber-Reinforced Glass-Matrix Composite

287 Binders for Thermal-Control Coatings

288 Thermal Polymerization of N-Butyl Acrylate

Silicone/Acrylate Copolymers

Durable, clear polymer films protect photovoltaic cells.

NASA's Jet Propulsion Laboratory, Pasadena, California

The search for a protective coating for the ethylene vinyl acetate encapsulant of photovoltaic cells has led to polymers that combine the hardness of acrylates with the elongation of silicones. Combining the monomers in various ratios produces copolymers with a wide range of physical and mechanical properties. Blends eventually selected for application would have to exhibit dirt and scratch resistance, weatherability, durability, cost-effectiveness, ultraviolet absorbance, and transparency to longer wavelengths.

Silicones and acrylates were chosen for investigation, in part because of their demonstrated weatherability. In the two-step synthesis, an acrylate functional fluid is prepared by reacting an acrylate functional silane with a polydimethylsiloxane fluid. The acrylate functional fluid is then reacted with butyl acrylate, methyl methacrylate, and ultraviolet-absorbing monomers in the presence of a catalyst.

Experiments in the two-step process were carried out, beginning with the reaction between methacryloxypropyltrimethoxysilane and a silanol functional polydimethylsiloxane (see figure). Potassium acetate was used to accelerate the reaction. An excess of the first ingredient was used to promote end capping of the polydimethylsiloxane chains rather than coupling. Methanol and the excess ingredient were removed by heating in a vacuum. The potassium acetate was removed by filtration.

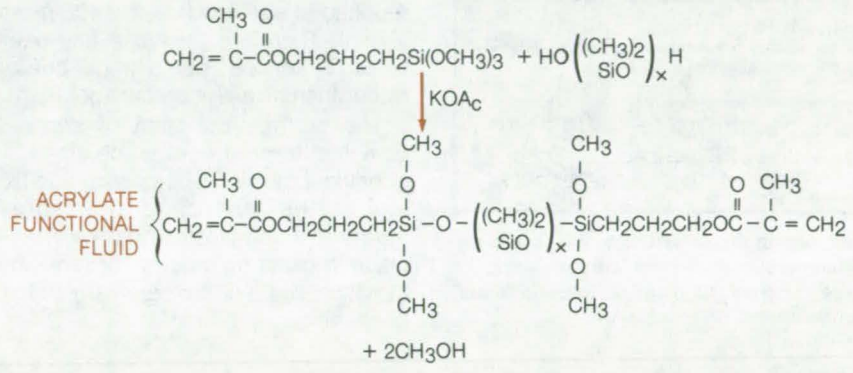

	PARTS BY WEIGHT
ACRYLATE FUNCTIONAL FLUID	20
BUTYL ACRYLATE	40
METHYL METHACRYLATE	40
ACRYLATE FUNCTIONAL ORTHOHYDROXYBENZOPHENONE (ULTRAVIOLET ABSORBER)	1.0
CHAIN REGULATOR	0.35
AZOBISISOBUTYRONITRILE (CATALYST)	0.5
TOLUENE (SOLVENT)	200

A **Two-Step Process** forms silicone/acrylate copolymers. An acrylate functional fluid is prepared in the reaction shown in the upper part of the figure. The resulting fluid is reacted with other ingredients in the proportions shown in the table to produce the copolymer.

The acrylate functional fluid was reacted in toluene at 100° C with the other ingredients in the ratios shown in the figure. Films of the resulting polymer were formed by simply pouring or spraying the mixture and allowing the solvent to evaporate. The films showed good weatherability.

Questions remain concerning the degree of copolymerization versus oligomerization of the ultraviolet absorber. Further work is also needed to optimize the formulation and the process conditions.

This work was done by William E. Dennis of Dow Corning Corp. for **NASA's Jet Propulsion Laboratory.** *For further information, Circle 24 on the TSP Request Card.*
NPO-15523

Coal as a Substitute for Carbon Black

Finely divided coal produced by spraying may be an inexpensive reinforcing agent for rubber products.

NASA's Jet Propulsion Laboratory, Pasadena, California

According to a new proposal, sprayed coal powder formed by the extrusion of coal heated to a plastic state may be an inexpensive substitute for carbon black. Tests have been suggested for evaluating the proposal.

Carbon black is used extensively in the rubber industry as a reinforcing agent in such articles as tires and hoses. It is made from natural gas and petroleum, both of which are in short supply.

The useful properties of carbon black as a reinforcing agent depend on fine particle size (average diameters less than 0.5 μm) and active chemical groups on the particle surface. The

(continued on next page)

CARBON BLACK REPLACEMENT TO BE EVALUATED
Premium-grade carbon black
Commercial pulverized coal
Sprayed coal
Raw coal, pulverized in a ball mill
Extruded coal, pulverized in a ball mill

ELASTOMERS TO BE USED IN THE EVALUATION
Natural rubber (an unsaturated elastomer used in heavy-duty truck and airplane tires)
Styrene-butadiene rubber (SBR) (an unsaturated rubber used in automobile tires)
Ethylene-propylene rubber (EPR) (a saturated rubber used for general-purpose applications)

Reinforcing-Agent Studies will compare different substitutes for carbon black, in three different rubbers, at three different temperatures.

surface chemistry may be the dominant factor: When carbon black is heated to a sufficiently high temperature, it loses its reinforcement property because of removal of the active chemical groups from the particle surface.

Ground coal and coke have been considered as substitutes for carbon black in the past, but cannot economically be reduced in size much below 400 mesh (37μm). Therefore their use has been limited to service as an extruder or filler rather than as a reinforcing agent.

The surface condition of sprayed coal is different from that obtained by grinding, however. The cooling and fixing of the surface during spray atomization of plastic coal can take place in oxidizing, neutral, or reducing atmospheres, with either fast or slow quenching.

Because carbon blacks behave differently in different elastomers, it is suggested that three typical rubbers be used in evaluating the coal substitutes (see table). Five carbon blacks and coals would be used. The compounded elastomers would be molded into a sheet during vulcanization. Mechanical testing would be carried out at 80°, 20°, and -40° C (176°, 68°, and -40° F) to determine and compare elastic modulus and tensile strength, mechanical hysteresis, and failure behavior for the three elastomers. Approximately 300 to 400 grams of carbon black of each type would be required.

This work was done by Raymond O. Kushida of Caltech for **NASA's Jet Propulsion Laboratory.** *For further information, Circle 25 on the TSP Request Card.*
NPO-15461

Sound-Burst Generator for Measuring Coal Properties

Digital instrument transmits two sine-wave outputs.

Marshall Space Flight Center, Alabama

The acoustical properties of coal can be measured accurately and with relative ease with the aid of a digital two-channel sine-wave sound generator. The generator is expected to provide information for the development of acoustic devices for measuring the thickness of coal in longwall mining.

In particular, the generator is expected to provide data for a computer model of sound-wave propagation in coal. Such a model will help in determining the preferred frequency range and sensing techniques. The generator can be used in the measurement of such properties as sound speed, attenuation rate, characteristic impedance, and the relationship of these properties to the structure and composition of coal.

The sound generator produces two bursts of identical sinusoidal waveform with an adjustable separation between the starting times of the bursts. Unlike conventional pulse generators, the sine-wave generator produces bursts with well-defined frequency spectrum, precisely-controllable relative phases, readily determined beginning and end, and adjustable duration. These attributes contribute to the accuracy of measurements.

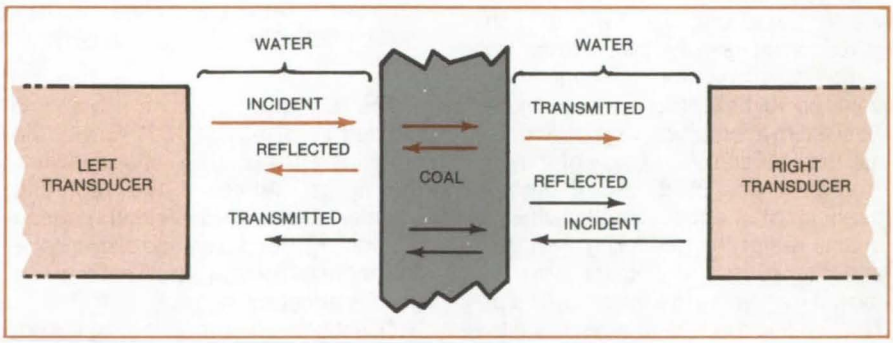

In **Echo-Cancellation Measurements,** sound bursts are sent to a coal sample from opposite directions. The transmitted and reflected amplitudes and phases are measured by the transducers to determine coal properties.

The generator produces its outputs with digital logic circuitry based on complementary metal-oxide-semiconductor (CMOS) technology. The frequency of the sine waves is adjustable up to 500 kHz. The delay between bursts in the two channels can be varied from one-tenth to 100 periods of a sinusoid. The main components are:

- A clock, which produces the master frequency;
- Two basic sine-wave generators (one for each channel) — each generator contains a five-flip-flop walking-ring counter and an amplifier; and the phase-shifted flip-flop outputs are summed to build up a rising and falling step-function wave, which after being filtered becomes a sine wave;
- Burst counters, which allow an adjustable number of trigger pulses to pass to the sine-wave generators so that each generator produces the desired number of sinusoids for each burst; and

- A delay counter, which starts the second burst counter and its sine-wave generator after an adjustable number of master clock pulses.

The sound transducers for the coal measurements operate at 100 to 200 volts peak-to-peak and present a largely capacitive load. On the other hand, the sine-wave outputs come from CMOS operational amplifiers, which are low-output-impedance devices with 10-volt peak-to-peak output voltage. A buffer circuit with a step-up transformer matches the source to the load.

Because the generator produces two sound bursts with a controllable delay between them, it can be used for echo-cancellation measurements. The coal specimen is placed in a water medium between two transducers (see figure). One sine-wave channel is applied to the left transducer, and the other channel is applied to the right transducer. From measurements of amplitude and phase shift of the received bursts, sound speed and attenuation factor are computed.

This work was done by W. J. Hadden, Jr., J. M. Mills, and A. D. Pierce of the Georgia Institute of Technology for **Marshall Space Flight Center.** *For further information, Circle 26 on the TSP Request Card.*
MFS-25438

Catalyzing the Combustion of Coal

Coating coal with calcium potassium acetate increases its heat-power output by 2 percent.

NASA's Jet Propulsion Laboratory, Pasadena, California

The reaction rate of coal in air can be increased by contacting or coating the coal with a compound such as calcium acetate. The enhanced reaction rate generates more heat, reducing the furnace size. The increase in combustion rate is about 26 percent, and internal pollutants in the powerplant are reduced.

Twenty experiments were conducted to assess the catalytic action of additives to coal. Mixtures of calcium and potassium acetates were found to have a stronger synergistic effect than either one alone. The coal sample used was Illinois No. 6 bituminous, ground to 200 mesh (<74 mircons). The coal was soaked in catalyst concentrations of 2 percent, 1 percent, and 0.6 percent by weight of coal sample and then was dried to remove the water.

The catalyst-treated coal is consumed at lower temperature than the raw coal; and its initial sharp reduction in weight is frequently accompanied by flame, unlike the raw coal (see figure). Also, when samples are suddenly heated by insertion into a furnace at 1,000° C and then removed after devolatilization, the treated samples keep glowing red, while the untreated samples turn unreactive.

The combustion reaction of coal follows the Arrhenius equation

$$dW/dt = -WB \exp(-E/RT)$$

where W is the weight of the sample at time t, E is the activation energy for the reaction, B is a proportionality factor, R is the universal gas constant, and T is the temperature of the sample at time t. A small reduction in activation energy due to the catalyst might greatly increase the combustion rate.

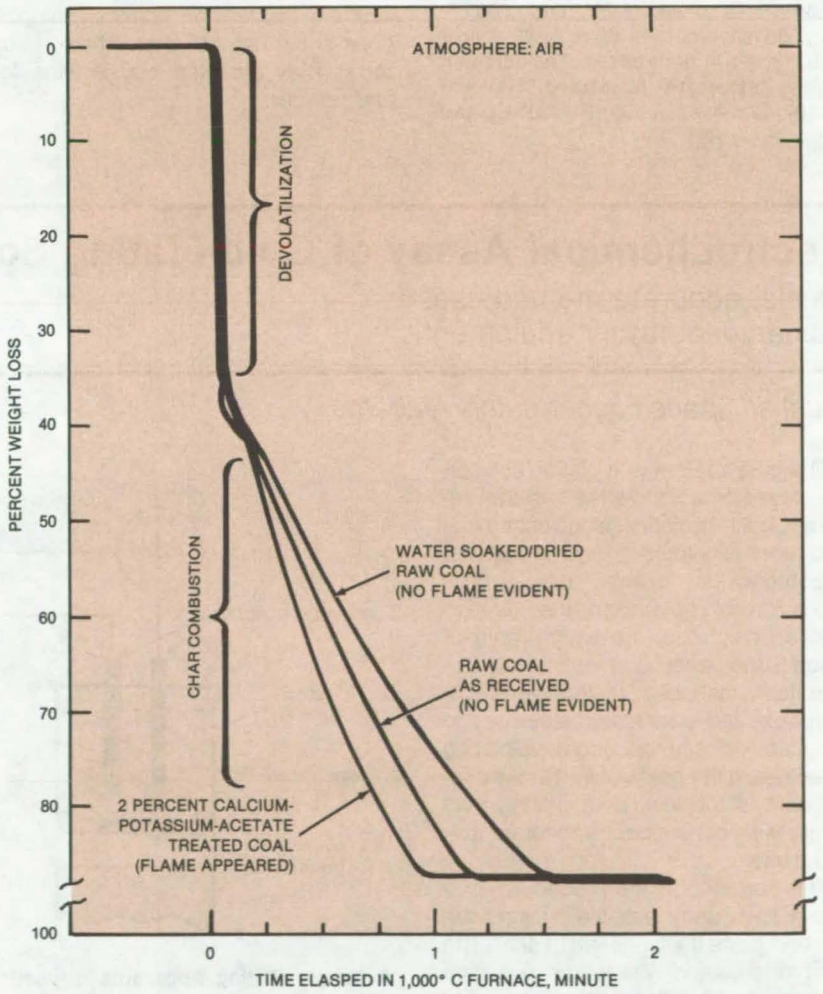

Weight Loss of Coal was measured by thermogravimetric analysis for samples suddenly introduced into a preheated furnace at 1,000° C. The treated samples reach minimum weight before the untreated samples, thus indicating a greater combustion rate.

This work was done by Marshall F. Humphrey and Won Dokko of Caltech for **NASA's Jet Propulsion Laboratory.** *For further information, Circle 27 on the TSP Request Card.*
NPO-15456

Low-Gold-Content Brazing Alloys

Two new alloys for brazing at 1,760° to 1,850° F are stronger and have better gap-filling capability.

Marshall Space Flight Center, Alabama

Element \ Alloy	R.I. 48	R.I. 49
Au	19	30
Ni	7	10
Pd	6	10
Mn	25	16
Cu	43	34

Nominal Percentage Compositions of low-gold brazing alloys for high-temperature applications are shown here. Alloy R.I. 48 is used between 1,760° and 1,850° F. R.I. 49 is used between 1,790° and 1,850° F. Alloy density is less than 0.380 lb/in.^{3} (0.10 N/cm^3) in both cases. The ultimate tensile strength is above 100 ksi (7×10^5 N/m^2) at +800° F (430° C) and −300° F (−185° C).

Two new brazing alloys are used for brazing in the temperature range between 1,760° and 1,850° F (954° and 1,010° C). They are much stronger than previous high-temperature alloys of their type and have better gap-filling capability and excellent wetting. They are also nonagressive and have good oxidation and salt-spray resistance. Neither is brittled by a hydrogen environment.

The new alloys have lower gold content than other gold brazes for their temperature range and therefore are far less expensive. The nominal compositions of the two alloys are shown in the table. They are produced in wire, foil, and powder.

These alloys were developed for vertical tube/tube brazing in the Space Shuttle main-engine flight nozzle, but they can be used for many nonspace applications. They are excellent for brazing at temperatures where no suitable alloys existed — especially for step brazing copper.

This work was done by Alexander Brennan and R. D. McKown of Rockwell International Corp. for **Marshall Space Flight Center.** *No further documentation is available.*

Inquiries concerning rights for the commercial use of this invention should be addressed to the Patent Counsel, Marshall Space Flight Center [see page A5]. *Refer to MFS-19629.*

Electrochemical Assay of Gold-Plating Solutions

Simple, accurate method uses ordinary laboratory equipment.

Marshall Space Flight Center, Alabama

The gold content of a plating solution is assayed by a simple method that requires only ordinary electrochemical laboratory equipment and materials. The technique involves the electrodeposition of gold from the solution onto an electrode, the weight gain of which is measured.

Suitable fast assay methods are economically and practically necessary in the electronics and decorative-plating industries. If the gold content in the plating bath is too low, poor plating may result, with consequent economic loss to the user.

The first step in the procedure is to take a 10-ml sample of the plating solution and place it in a 250-ml beaker. The sample is diluted with water to a total volume of 100 ml. An alkaline-cyanide complex bath is prepared from the dilute solution by the addition of 10 pellets of potassium hydroxide and 3 to 4 grams of potassium cyanide.

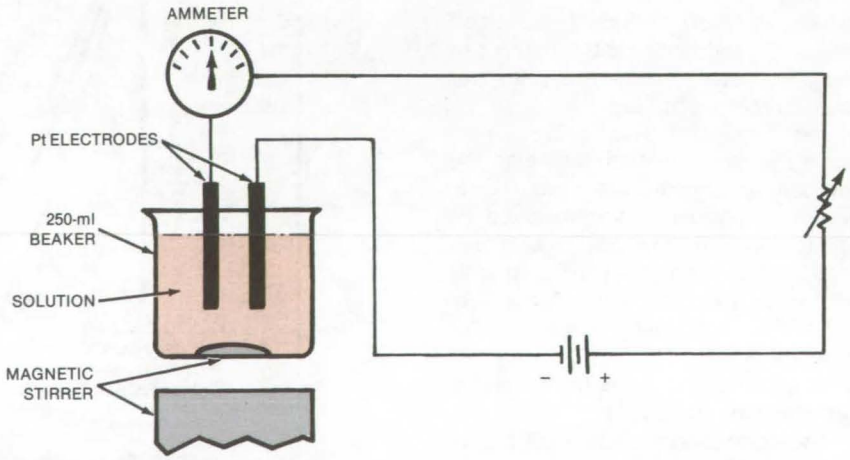

A Simple Plating Apparatus is used for electrochemical assay of the gold-plating solution. The gold is plated out of the solution onto one of the platinum electrodes, and the electrode weight gain is noted.

Before insertion of the platinum electrodes (see figure), the cathode weight is measured and recorded. After insertion, the current density is adjusted to 75 to 100 amperes per square foot (800 to 1,100 amperes per square meter). Plating is continued for sufficient time to remove all gold from the solution. Typical plating time may be as long as 24 hours, though this may be reduced to as little as one-half hour through the use of larger electrodes. After plating, the cyanide solution must not be allowed to become acidic and must be properly disposed of for safety.

The electrode is removed from the beaker, washed in distilled water, then rinsed with isopropyl alcohol, and dried in air for 1 hour. The electrode weight is again measured and recorded. Correlation of the electrode weight gain with the volume of the sample gives a measure of the concentration of gold in the solution.

This work was done by R. Chiodo of Rockwell International Corp. for **Marshall Space Flight Center.** *No further documentation is available.*
MFS-19639

XPS Study of SiO_2 and the Si/SiO_2 Interface

X-ray photoelectron spectroscopy shows structure-induced redistribution of valence charge in a 30-Å region.

NASA's Jet Propulsion Laboratory, Pasadena, California

The crystal structure of the thin SiO_2 film on silicon and of the Si/SiO_2 interface has been studied by X-ray photoelectron spectroscopy (XPS), in conjunction with chemical profiling, and resolution enhancement. XPS is an analytical technique for understanding the electronic structure of atoms close to the surface in solids, in preference to the bulk structure of the material. The study found evidence for core-level chemical shifts arising from changes in the local structural environment in amorphous SiO_2 (a-SiO_2, and at the Si/SiO_2 interface.

The experimental studies were conducted employing a modified commercial spectrometer. A series of 3- to 6-Ω-cm <100> n-type silicon wafers was prepared, following a standardized cleaning procedure, and then oxidized in HCl-cleaned quartz tubes with dry oxygen at 1,000° C with no anneal. A wet chemical etching procedure was used to depth-profile these samples. This method used nonaqueous solvents, millisecond exposure times, and a high-purity dry N_2 ambient to minimize perturbations of the sample chemistry. All spectra were taken at 300 K with control of the secondary electron background to minimize charging effects and establish near-flat-band conditions.

The observed spectra in the Si2p region are displayed in the figure as a function of oxide thickness. The peak at 98.9 eV corresponds to the silicon substrate and that at 103.2 eV to silicon in SiO_2. The substrate Si2p peak first acquires obvious intensity on this scale for oxide thickness less than 50 Å, consistent with the electron escape depth of ~36 Å for the spectrometer geometry and the photon energy employed ($AlK\alpha_{1,2}$, 1,486 eV). The actual position of the substrate Si2p line follows the substrate surface potential and thus depends upon the charge-induced interface field and the level and type of doping.

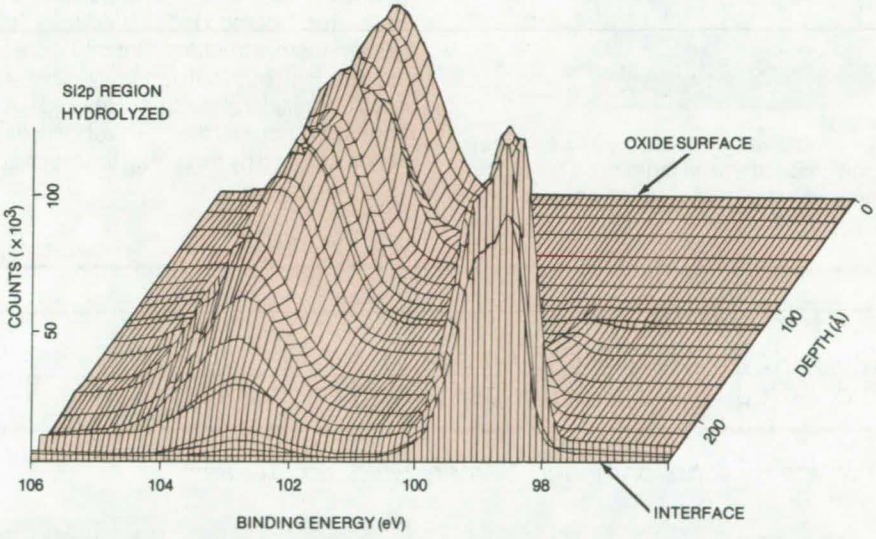

The Si2p Spectra in the silicon dioxide and silicon substrate binding-energy region are plotted here versus oxide thickness, measured from the outer (vacuum) surface. Equipotential lines are drawn at 0.1 eV spacing.

The high-resolution spectra in the figure contain chemical and structural information that can be examined using advanced deconvolution methods. The observed XPS spectra may be understood as a sequential convolution of several functions, each with a well-defined physical interpretation. Because the natural line shape, the characteristics of the spin orbit doublet (2:1 intensity ratio, 0.602 eV splitting), the instrument-broadening function, and some aspects of the noise process can all be determined with reasonable (though varying) precision, it is possible to reconstruct some of the features of the noninstrumentally broadened spectrum.

This work was done by Frank J. Grunthaner, Paula J. Grunthaner, Richard P. Vasquez, Blair F. Lewis, Joseph Maserjian, and Anupam Madhukar of Caltech for **NASA's Jet Propulsion Laboratory.** *For further information, Circle 28 on the TSP Request Card.*
NPO-14968

Blowing Agents for Fabrication of Polyimide Foams

Foaming caused by internal chemicals allows control over density and cellular structure.

Lyndon B. Johnson Space Center, Houston, Texas

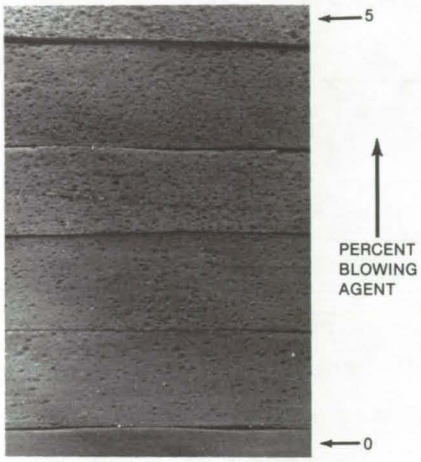

The **Cellular Structure** of these polyimide foams is more open for higher concentrations of blowing agent.

Polyimide foams have applications as fillers for seat cushions, wall panels, floor sheets, and thermal and acoustical insulation [see *NASA Tech Briefs*, Vol. 5, No. 3, pp. 384 – 387 (MSC-16921, MSC-18704, MSC-18707, and MSC-18708)]. Polyimide resin can be foamed by an agent that is generated within the matrix of the powder precursor. This blowing agent is a mixture of the water and methanol that are byproducts of the condensation/polymerization reaction in the resin. The expansion of these two compounds produces a cellular foam structure that is flexible and resilient but that tends to have a very-fine cellular structure. However, a more open structure with lower density can be attained by modifying the mechanism of foam formation. The more-open cell structure contributes to improved recovery of the foams.

Sodium bicarbonate, Celogen HT 550, and Expandex 5 PT (or equivalent materials) all produce a flexible structure with more open cells. The standard concentration of any of these blowing agents is 2.5 percent, but various concentrations can be used to achieve different density values. The figure shows, as an example, the effect of concentrations of Celogen HT 500 agent on the cell structure of polyimide resins.

This work was done by John Gagliani, Usman A. K. Sorathia, and Raymond Lee of International Harvester Co. for **Johnson Space Center.** *No further documentation is available.*
MSC-18993

Vapor Detector

Monoethylhydrazine and nitrogen tetroxide vapors are visually monitored with a canister containing color-changing gels.

Lyndon B. Johnson Space Center, Houston, Texas

Continuous visual monitoring of leaks of nitrogen tetroxide (N_2O_4), monoethylhydrazine, and other hydrazine fuels is possible with a new vapor detector. Like litmus paper, which changes color to indicate pH, vapor-indicating gels change color to indicate the presence of vapors. The detector, which was developed for monitoring vapors in the Space Shuttle thrustor bell, eliminates the need for removing covers to take samples.

The detector is a canister (see figure) consisting of a screw-in base and a clear plastic tube that contains two colors of silica gel. A yellowish silica gel containing p-dimethylaminobenzaldehyde indicates monoethylhydrazine vapor by turning orange and then red. The silica gel indicating N_2O_4 is blue in color but becomes bronze upon exposure to the vapor; it contains $CoCl_2$ and will turn pink if exposed to moisture.

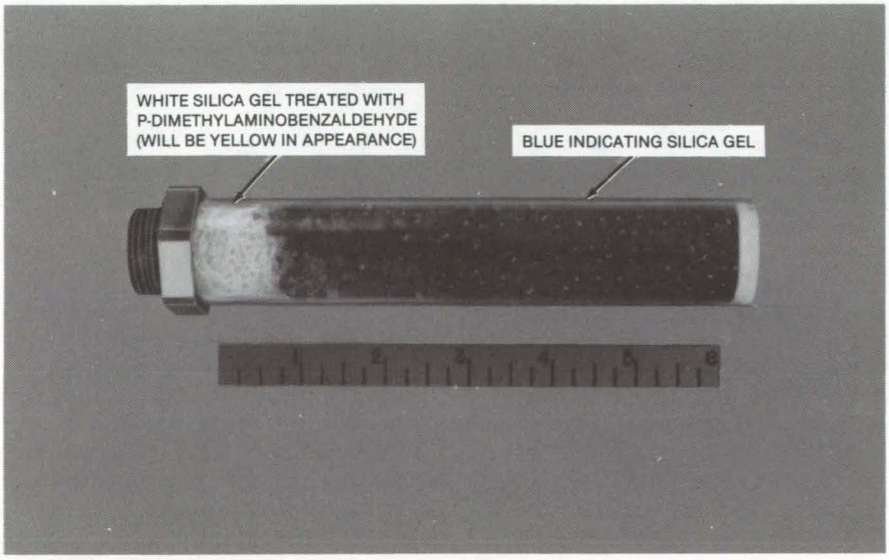

Silica Gels within a canister change color to indicate the presence of vapors.

Screw-top canisters containing gel for indicating N_2O_4 are commercially available. These canisters can be modified by replacing some of the blue gel with a preparation of the yellowish monoethylhydrazine-indicating gel.

To prepare 450 grams of the hydrazine-fuel indicator, 500 ml of a 5-percent solution are made by dissolving 25 grams of p-dimethylaminobenzaldehyde in methyl alcohol in a 2,000-ml steel beaker. After most of the material is dissolved, 10 drops of concentrated hydrochloric acid are added, turning the solution a clear yellow. With the solution still in the beaker, 450 grams of 6-to-16 mesh silica gel are added.

Due to solvent absorption, the silica cracks and would be ejected from the beaker unless the beaker were covered until cracking subsided to the point where the gel could be removed. The gel is removed with a scoop and placed on filter paper in a large Buchner funnel. After most of the liquid drains off, the solid is transferred to a flat pan and dried at approximately 60° C to remove the alcohol. The yellowish silica can then be packaged for storage or added to a canister that contains the blue silica gel.

This work was done by Henry M. Waddell, George C. Garrard, and Donald W. Houston of Rockwell International Corp. for **Johnson Space Center.** *No further documentation is available.*
MSC-18989

Regenerating Water-Sterilizing Resins

Iodine crystals restore anion-exchange resins.

Lyndon B. Johnson Space Center, Houston, Texas

An iodine-dispensing resin can be regenerated after its iodine content has been depleted, without being removed from the water system. The resin is used to make water potable by killing bacteria, fungi, and viruses. [See also the related article "Improved Microbial-Check-Valve Resins" (MSC-18377) in Vol. 4, No. 3 of *NASA Tech Briefs*, page 392.]

The regeneration technique may become the basis of a water purifier for very long space missions. Enough crystalline iodine for multiple regenerations during a mission can be stored in one small cartridge. The cartridge could be inserted in a waterline as necessary on signal from an iodine monitor or a timer. The convenience of regenerating the resin without removing it from the water system will be attractive in terrestrial applications as well.

Water flowing through the iodine crystals in the cartridge carries iodine to the resin, where iodine accumulates. When the depleted iodine in the resin has been replaced, the cartridge is removed.

Experiments have demonstrated the effectiveness of the regeneration method. For example, an iodine bed that had been washed until it produced only 40 parts per million of I_2 in effluent water was installed in a waterline containing a resin bed. The iodine bed remained in the line until the effluent water from the resin bed had built up to 1.8 ppm I_2 (see figure), at which point it was removed. The effluent from the resin bed immediately dropped below 1 ppm and gradually declined to 0.2 ppm.

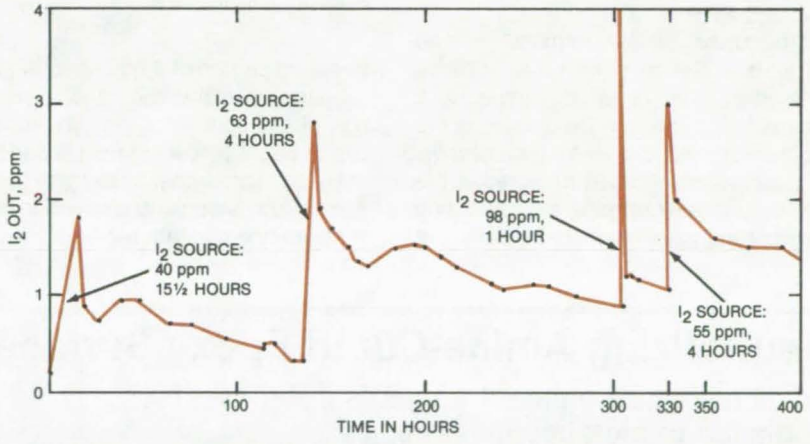

The **Temporary Insertion of an Iodine Bed** in a waterflow line (indicated by spikes) quickly regenerates a resin bed. The resin is a commercially-available quaternary ammonium ion-exchange resin.

Next, a somewhat more-potent iodine bed was installed — one that produced an effluent containing 63 ppm I_2. The new iodine bed was removed when the resin bed effluent had risen to a concentration of 3 ppm I_2. The resin effluent immediately dropped to 2 ppm and gradually declined to 1 ppm. (An I_2 concentration of about 2 ppm is considered both microbicidal and taste-free.)

At that point, a fresh bed of iodine crystals, producing 98 ppm I_2 in its effluent, was installed. The resin effluent climbed to 4 ppm in only an hour, when the iodine bed was removed. The resin effluent immediately dropped to 1.2 ppm, then gradually dropped to 1 ppm.

Finally, a 55-ppm-effluent iodine bed was installed. The resin effluent rose immediately to 3 ppm but quickly returned to 2 ppm, where it remained for 4 hours. The iodine bed was removed, and water was circulated through the resin bed overnight. In the morning, the resin effluent concentration was 1.6 ppm.

The sharp rise in resin effluent concentration that occurs when the iodine bed is first connected is not expected to be a problem. Most purifiers feed a storage tank with a volume that will dilute the iodine content to acceptably low levels.

This work was done by Gerald V. Colombo and David F. Putnam of Umpqua Research Co. for **Johnson Space Center.** *No further documentation is available.*
MSC-20001

Wide-Temperature-Range Torque-Stripe Paint

Urethane-based material retains its useful properties in extreme heat and cold.

Marshall Space Flight Center, Alabama

A "torque-stripe" paint withstands a wide range of temperatures, from −320° to +180° F (−196° to +82° C). The paint, brushed on an electrical connector, serves as both a locking agent and an indicator of a loosened connection: A crack in the paint stripe is readily visible and shows that a torqued connector has loosened.

The new paint can be used on electrical connectors or machine bolts that are exposed to extremes of heat and cold. Conventional torque-stripe paints, in contrast, become brittle, shatter, and fall off at liquid-nitrogen temperature (−320° F).

The basis of the formulation (see table) is a urethane resin that adheres well over the required temperature range, helps to retain the torque on the connector, and shows a crack clearly. Silica powder is added to increase the viscosity of the urethane base and thus prevent the paint from seeping into the threaded portion of the connector (such seepage would make intentional separation of the connector virtually impossible). A bright yellow pigment is added to make the light-amber base more visible. Ammonium phosphate is added to make the urethane nonflammable.

Component	Units by Weight
Urethane (Uralite 3124, Part A)*	100
Urethane (Uralite 3124, Part B)*	32
Ammonium Phosphate	30
Silica Powder (Cabosil)*	10
Yellow Pigment	1

*Equivalent materials could be substituted.

The Formulation of Torque-Stripe Paint ensures adhesion, nonflammability, viscosity, and visibility.

A connector is first cleaned with a lint-free cloth dampened with Freon (or equivalent) solvent. A urethane primer is applied to the surfaces to be painted. A band of catalyzed urethane is brushed onto the connector joint and allowed to cure for 24 hours at room temperature. The cure can be hastened by the application of heat. The paint is typically applied 0.050 to 0.080 inch (1.3 to 2 mm) thick.

Connectors subjected to 10 thermal-shock cycles over the required temperature range showed no signs of deterioration. The paint doubled the torque needed to loosen the connectors, whether at room temperature or liquid-nitrogen temperature, and gave an obvious indication of loosening.

This work was done by E. R. Mills of Rockwell International Corp. for **Marshall Space Flight Center.** *No further documentation is available.*
MFS-19644

Neutralizing Amine-Cured Epoxy Surfaces

An isocyanate treatment prevents corrosion to metal conductors.

Goddard Space Flight Center, Greenbelt, Maryland

Surfaces of amine-cured epoxies can be made noncorrosive by a simple treatment. Amines are a preferred curing agent because they react with epoxies in a predictable way, but they form a corrosive alkaline layer on the cured resin. Such a surface attacks aluminum and copper. Amine-cured epoxies are therefore corrosive to conductors in contact with the epoxy surface.

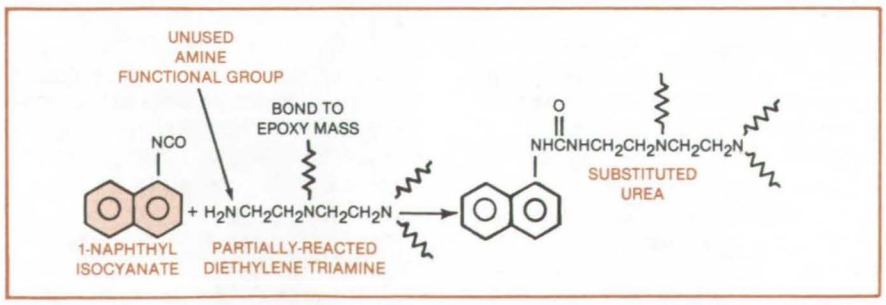

The Isocyanate Reagent Reacts with the unused amine functional group on the amine curing agent (diethylene triamine). The end result is neutral substituted urea.

Unreacted amine curing agents and amine functional groups remain on the resin surface after curing. Aliphatic amines are particular offenders. Moisture and carbon dioxide in the air hinder the cure at the surface, allowing unreacted groups to form. Nevertheless, aliphatic amines are favored because they react at room temperature and cure fast. Aromatic amines, in contrast, do not form a corrosive layer; they do not react significantly with carbon dioxide or water. However, they need high temperature to cure epoxies.

The new surface treatment is a rapid, convenient, and effective method for converting unused amines and amine functional groups into neutral, noncorrosive substituted urea. The reaction pro-

ceeds at room temperature, takes only a few minutes, and leaves no corrosive residue.

For best results, the surface should first be washed with alcohol to remove as much as possible of the unreacted amine. Then it should be dried, since residual moisture or alcohol may consume some of the treatment reagent, and neutralization may then be incomplete.

The reagent, a mono-isocyanate or a mono-isothiocyanate, is brushed on the cured epoxy surface. The preferred reagent is 1-naphthyl isocyanate because it has a low vapor pressure, and its vapor is less irritating than that of other reagents. The isocyanate group on the 1-naphthyl isocyanate molecule reacts with the unused amines and amine groups on the surface, rendering them neutral (see figure).

An excess of reagent should be used. It should be brush-mixed once or twice while it is reacting. Finally, the surface should be rinsed with acetone followed by alcohol. Rinse waste should be collected in one receptacle so that the alcohol can destroy the cyanate.

The isocyanate treatment is more effective than previous methods of reducing surface corrosiveness. For example, rinsing with a solvent cannot completely remove unreacted amine groups because they may be bonded at one end of the molecule to the base material. Reducing the amine content helps little because there will still be unreacted groups on the surface. Sanding or abrading removes the surface layer, but often is not practical. Curing in dry air or an inert atmosphere reduces surface alkalinity but usually not enough.

This work was done by Sheng Y. Lee of **Goddard Space Flight Center.** *For further information, Circle 29 on the TSP Request Card.*

This invention is owned by NASA, and a patent application has been filed. Inquiries concerning nonexclusive or exclusive license for its commercial development should be addressed to the Patent Counsel, Goddard Space Flight Center [see page A5]. *Refer to GSC-12686.*

Heat-Exchange Fluids for Sulfuric Acid Vaporizers

Some polymers seem promising as heat-exchange fluids for use in thermochemical cycles in hydrogen production.

NASA's Jet Propulsion Laboratory, Pasadena, California

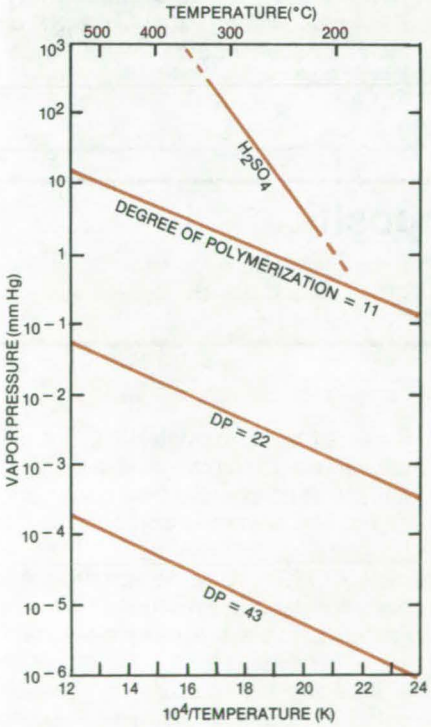

Vapor-Pressure Data are shown for sulfuric acid and perfluoropolypropylene oxide materials of various degrees of polymerization.

Some fluorine-substituted organic materials meet the criteria for heat-exchange fluids in contact with sulfuric acid. The most promising candidates are perfluoropropylene oxide polymers with a degree of polymerization (DP) between 10 and 50. It is desirable to have the DP in the high range because the vapor pressure of the material decreases as the DP increases, and hence the high-DP liquids have lower loss due to vaporization (see figure).

In some thermochemical cycles for hydrogen production, the oxygen release step is the thermal decomposition of sulfuric acid. To vaporize the H_2SO_4 at 330° C, it can be mixed with an immiscible nonreactive hot liquid. The liquid used for this purpose must:

a. Be chemically stable to concentrated sulfuric acid at temperatures of 300° to 400° C,
b. Have low miscibility with sulfuric acid at those temperatures,
c. Have low vapor pressure at those temperatures to prevent loss by vaporization,
d. Be liquid at room temperature, and
e. Be relatively inexpensive.

While the fluorocarbon fluids meet these criteria, possible problems include:

a. The commercial polymer liquids are impure and tend to evolve hydrogen fluoride during the first hour or so of contact with sulfuric acid at the operating temperatures. However, boiling the polymer for several hours at 350° C removes the impurities.
b. The highly fluorinated fluids may react violently with such metals as aluminum and magnesium and their alloys. Thus the pumps, valves, and holding tanks of a system must be chosen with care.

The perfluoroethers, although stable to oxygen and ozone, are decomposed by halogenated Lewis acids, such as $AlCl_3$, SbF_5, and CoF_5. Therefore any use in cycles other than service with sulfuric acid should be evaluated with this behavior in mind.

This work was done by Daniel D. Lawson and Gene R. Petersen of Caltech for **NASA's Jet Propulsion Laboratory.** *For further information, Circle 30 on the TSP Request Card.*
NPO-15015

Gas Diffusion in Fluids Containing Bubbles

Mathematical model represents behavior of bubbles in such liquids as molten glass.

NASA's Jet Propulsion Laboratory, Pasadena, California

A mathematical model describes the movement of gases in a fluid containing many bubbles. The model makes it possible to predict the growth and shrinkage of the bubbles as a function of time.

The model will aid in designing experiments on low-gravity processing of materials. In particular, it is expected to help in developing processes for the production of high-quality optical glasses in space. Glass containing bubbles would be unacceptable. Since bubbles arise from gases dissolved in molten glass, the ability to predict gas transport under varying conditions will be useful.

Previously, most such analyses of gas transport have focused on single-bubble systems. Those that have been directed toward multiple-bubble systems have been limited to steady-state rather than varying conditions.

The new model overcomes the complexities involved in the analysis of varying conditions by making two simplifying assumptions. It treats the bubbles as point sources, and it employs an approximate expression for the gas concentration gradient at the liquid/bubble interface. Among other things, the model shows that, for a given ratio of gas concentration at the interface to that in the bubble, bubbles shrink more rapidly when they are initially small and are widely spaced (see figure).

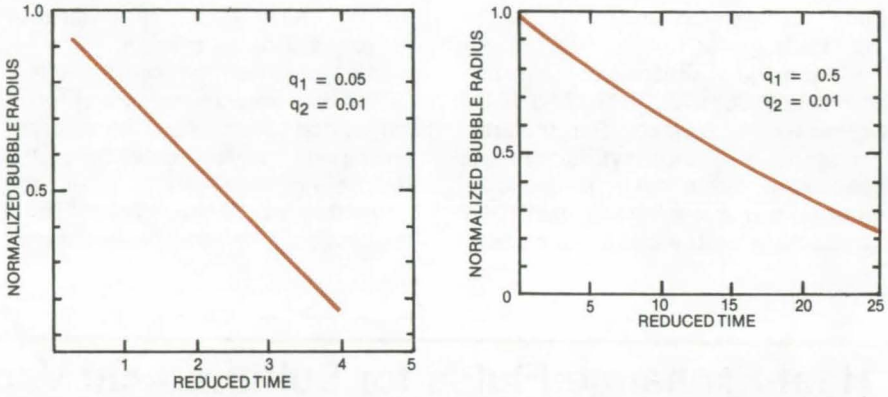

Bubbles Shrink More Rapidly when q_1 is small than when it is large. The quantity q_1 represents the ratio of bubble diameter to the distance between bubbles; q_2 represents the ratio of gas concentration at the interface to gas concentration in the bubble.

This work was done by Michail Zak and Michael C. Weinberg of Caltech for **NASA's Jet Propulsion Laboratory.** *For further information, Circle 31 on the TSP Request Card.*
NPO-15060

Graphite-Fiber-Reinforced Glass-Matrix Composite

G/Gl composites exhibit excellent strength, fracture toughness, and dimensional stability at elevated temperatures.

Langley Research Center, Hampton, Virginia

New applications for composites are creating new demands for high-performance matrix systems. Requirements for higher operating temperatures and greater environmental and dimensional stability exceed the capabilities of most resin-matrix systems. Metal-matrix composities, one approach to the solution of these problems, suffer from fiber/matrix incompatibility and have significantly greater densities than resin-matrix systems. Another approach is the use of graphite-fiber-reinforced glass-matrix composites (G/Gl).

G/Gl is a structural composite material made of graphite fibers embedded in a borosilicate glass. It is made by passing graphite-fiber yarn through a slurry containing a suspension of fine glass particles in a carrier liquid and winding on a drum to produce a prepregged uniaxial tape. After drying, the tapes are cut into appropriate lengths and laid up in a graphite die in the desired stacking scheme (e.g., uniaxial or cross-plied).

The stack is consolidated by hot pressing in a furnace. First, the furnace is heated to approximately 1,273 K under vacuum to remove all volatiles. The furnace atmosphere is then changed to argon, and heating is continued to the hot-pressing temperature of approximately 1,723 K. While the temperature is held constant, a pressure of approximately 6.9 MPa is applied to the stack for a minimum of 15 minutes. While maintaining full pressure, the consolidated composite is allowed to cool to about 873 K, where the pressure is removed; and then cooling is continued to ambient temperature. This consolidation

process can be used to fabricate either flat plates or structural shapes such as hat sections directly from prepregged tapes. Alternatively, structural shapes can be made from previously-consolidated flat plates by a secondary hot-forming operation.

G/GI is relatively lightweight (for a 60-percent-fiber volume fraction, specific gravity of about 2.0) with little or no porosity. It has a low coefficient of thermal expansion and a fracture toughness similar to that of graphite-reinforced plastics. High strength-to-density and stiffness-to-density ratios make it more structurally efficient than any other known material over the temperature range 600 to 800 K. It is thermally stable: Strength and fracture toughness are maintained at temperatures up to 800 K. G/GI is resistant to thermal and mechanical fatigue and should have a chemical inertness similar to that of monolithic borosilicate glass. It is wear-resistant with a low coefficient of friction and is machinable by carbide and diamond tools and electric-discharge method.

G/GI is expected to find applications in structures that require dimensional and environmental stability and resistance to thermal cycling and oxidation at temperatures up to at least 700 K. It is suitable for strong lightweight structures at use temperatures above those of graphite/epoxy and graphite/polyimide composites. G/GI is also expected to find application where chemical inertness must be be combined with mechanical reliability, such as in chemical ware, piping, process equipment, and cookware.

This work was done by Karl M. Prewo of United Technologies Corp. and Dennis L. Dicus of **Langley Research Center.**

Further information may be found in:

NASA CR-165711 [N81-24181/NSP], "Research on Graphite Reinforced Glass Matrix Composites" [$12.50], and

NASA CR-159312 [N80-32440/NSP], "Research on Graphite Reinforced Glass Matrix Composites" [$9.50].

Copies of these reports may be purchased [prepayment required] from the National Technical Information Service, Springfield, Virginia 22161.

LAR-12764

Binders for Thermal-Control Coatings

Improved coatings are tough and resistant to abrasion.

Marshall Space Flight Center, Alabama

Methyl trialkoxysilane hydrolysates have been found to be superior binders for radiative thermal-control coatings. Using sprayed test panels, candidate coating formulations were optimized with respect to binder/pigment ratio, ethanol content, pigment particle size, coating thickness, and curing conditions.

Prior silicone-bound thermal-control coatings are susceptible to handling damage. They are subject to damage by the absorption of high-energy ultraviolet radiation. They also outgas at low-pressures, contaminating adjacent surfaces — a particular disadvantage when used near contamination-sensitive optics in a vacuum.

The new coatings are based on trialkoxysilane monomers of the general type $R\text{-}Si(OR')_3$, where R represents a methyl (CH_3) group and R′ represents an ethyl (CH_2CH_3) group. Alternatively, a monomer could consist of a chain-extended alkoxysilane of the general structure shown in the upper half of the figure. The latter monomer would be used as a comonomer with methyl triethoxysilane to produce cured coatings with improved toughness and resistance to cracking.

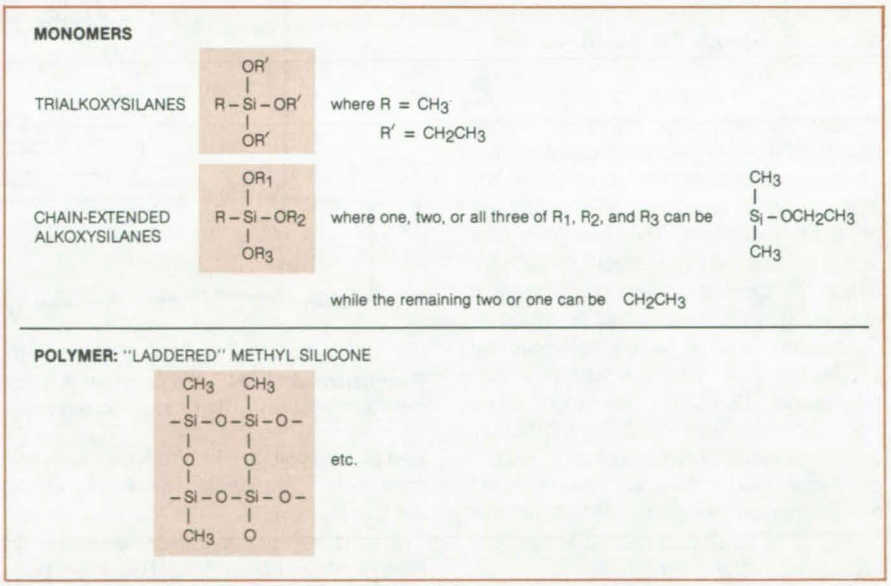

Trialkoxysilane Hydrolysate Binders are made from monomers of trialkoxysilanes or chain-extended alkoxysilanes of the types shown above. The monomers are believed to polymerize to ladder-type structures like the methyl silicone shown below.

A test preparation of a typical optimized coating began with the acetic acid-catalyzed hydrolysis of methyl triethoxysilane with 2.5 mole-equivalents of water over a 24-hour period at room temperature. The hydrolysate was directly mixed with premilled TiO_2 (12 grams pigment/26 grams binder) to yield a sprayable consistency. Panels were sprayed to give a nominal cured-coating thickness of 2 mils (0.05 mm). Cure was effected by drying in air for

(continued on next page)

24 hours at room temperature, followed by 24 hours at 160° F (71° C).

The resulting coating was extremely tough and abrasion-resistant, with an absorptance of 0.02 and an emittance of 0.89. The coating survived a mandrel bend test and thermal cycling from −160° F (−107° C) to +160° F (71° C) with no significant damage. Vacuum ultraviolet exposure for 500 hours at 1 equivalent Sun resulted in no visible degradation. An extremely low outgassing rate was observed at 100° C and 10^{-6} torr.

The new binders are believed to have a laddered structure like that shown in the lower part of the figure. This structure reduces the number of $Si\text{-}CH_3$ groups available for damage via ultraviolet radiation.

This work was done by William J. Patterson and James E. Curry of **Marshall Space Flight Center.** *For further information, Circle 32 on the TSP Request Card.*

This invention is owned by NASA, and a patent application has been filed. Inquiries concerning nonexclusive or exclusive license for its commercial development should be addressed to the Patent Counsel, Marshall Space Flight Center [see page A5]. *Refer to MFS-25620.*

Thermal Polymerization of N-Butyl Acrylate

A novel combination of methods results in a polymer with desirable properties.

NASA's Jet Propulsion Laboratory, Pasadena, California

A simple new polymerization method enables the production of n-butyl acrylate polymer of the desired high molecular weight, without the disadvantages that usually attend the more conventional methods. The new process, which is a hybrid of thermal, solution, and emulsion polymerization methods, involves the controlled thermal polymerization of the monomer at moderate temperatures without the use of catalysts or additives.

Poly-(n-butyl acrylate) is of interest as a possible solar-cell encapsulant because of its ultraviolet stability and a glass-transition temperature sufficiently low to give it good resistance to temperature extremes. The catalysts and additives used in conventional polymerization processes can limit long-term ultraviolet and environmental stability. Furthermore, each of the conventional processes suffers from a particular disadvantage: Bulk polymerization gives poor control over product molecular weight; solution polymerization gives undesirably low molecular weight; and emulsion polymerization results in the retention of soap and catalyst-fragment impurities in the polymer.

To prepare the polymer by the new method (see figure), one begins by mixing n-butyl acrylate monomer, methanol, and water in a stirred reaction vessel under an inert atmosphere. The mixture is then heated to a temperature and for an amount of time that depend upon the desired degree of conversion. The polymer clings to the walls of the reaction vessel, and the solvents are decanted at the end of the reaction period. The resulting polymer is subsequently purified by dissolving it in a solvent such as methylene chloride and then evaporating the solvent.

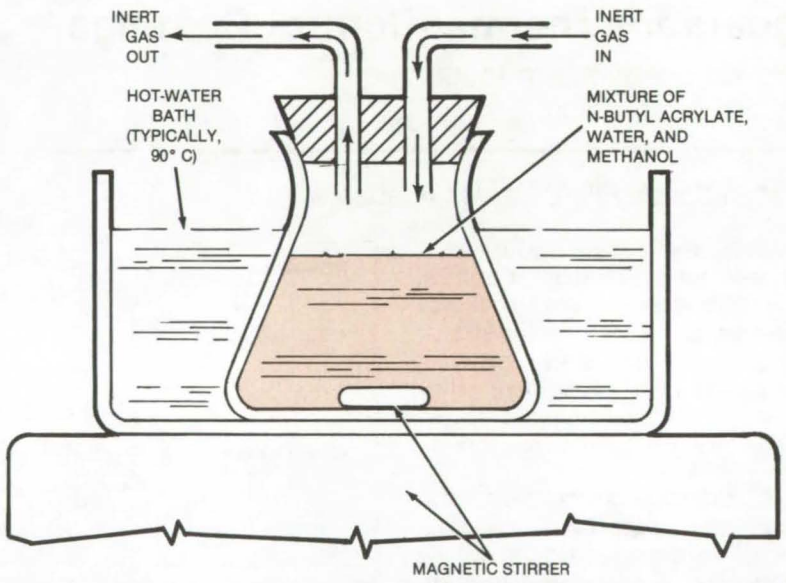

Polymerization of N-Butyl Acrylate is accomplished by heating the ingredients under an inert atmosphere. The process is simple and easy to control.

The ratios of monomer to water to methanol are not critical. The water dissipates the heat of polymerization, thus preventing thermal runaway that promotes undesired cross-linking and degradation and thereby allowing the reaction to proceed to the desired high-molecular-weight conclusion. In pure methanol, a lower-molecular-weight polymer is produced. Thus, the monomer/water/methanol ratios can be adjusted to control the degree of cross-linking and the molecular weight of the product.

In a typical experiment, 10 ml of monomer, 40 ml of methanol, and 40 ml of water were stirred into a 250-ml flask. The flask was heated by immersion in a 90° C bath for 24 to 96 hours, maintaining the flask at about 85° C internally. After 90 hours, 90 percent conversion was achieved. Other experiments were run at different temperatures and for different durations. In all cases, a superior high-quality polymer was obtained.

This work was done by John D. Ingham of Caltech for **NASA's Jet Propulsion Laboratory.** *For further information, Circle 33 on the TSP Request Card.*

NPO-15010

Life Sciences

Hardware, Techniques, and Processes

291 Cuff for Blood-Vessel Pressure Measurements

Computer Programs

292 Environmental-Analysis Routine Library

Cuff for Blood-Vessel Pressure Measurements

A noninvasive sensor can be used for long-term monitoring.

Ames Research Center, Moffett Field, California

The pressure within a blood vessel is measured by a new cufflike device without penetration of the vessel. The device continuously monitors blood pressure for up to 6 months or longer without harming the vessel. It is especially useful for vessels smaller than 4 or 5 millimeters in diameter.

Up to now, measurement of pressure in small blood vessels has required the insertion of a hypodermic needle. Such invasive methods, however, damage the vessel wall, disturb blood flow, and cause clotting. Thus they do not always give reliable pressure measurements over prolonged periods.

The new device is used on an exposed vessel. It is therefore invasive to the body, although not to the arterial system. The vessel is clamped between a solid half cylinder and a hollow half cylinder (see figure) held together by retaining rings. A pressure transducer in the solid semicylinder presses against the vessel and detects internal pressure through the pliable vessel wall. An electrical lead connects to the pressure transducer, which has a flexible pressure-sensing area 3.5 millimeters in diameter.

The flat surface of the transducer compresses the vessel over about 20 percent of its normal circumference. Tests show that this compression ensures enough contact for a linear relationship between transducer output and pressure. The constriction does not affect blood flow significantly. In fact, the blood-pressure waveform and level are unaffected by reductions in vessel cross section up to about 30 percent.

The cuff measures pressure in vessels ranging from 1 to 30 millimeters in diameter. It is equally suitable for the small pressures in veins and the large pressures in arteries. It furnished accurate data for studies of the carotid, coronary, and renal arteries.

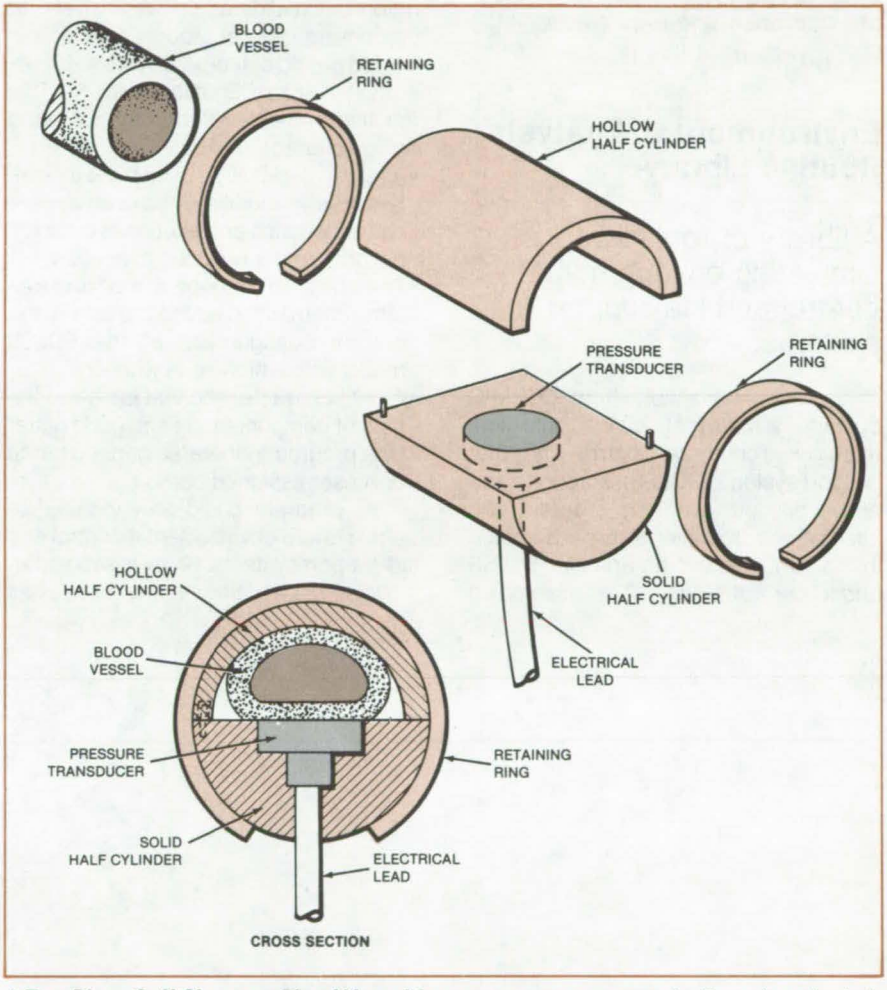

A **Two-Piece Cuff Clamps a Blood Vessel** for pressure measurements. It can be adapted for pressure measurements in flexible hoses and other fluid lines.

The cuff can be constructed in configurations other than that of a two-piece clamp. For example, it can be made as a single-piece hollow cylinder with a longitudinal slot to admit the blood vessel, or an elastic strap can be used to hold the blood vessel against the pressure transducer.

This work was done by Masashi Shimizu of the National Research Council for **Ames Research Center.** *For further information, Circle 34 on the TSP Request Card.*

Inquiries concerning rights for the commercial use of this invention should be addressed to the Patent Counsel, Ames Research Center (see page A5). Refer to ARC-11264.

Computer Programs

These programs may be obtained at very reasonable cost from COSMIC, a facility sponsored by NASA to make new programs available to the public. For information on program price, size, and availability, circle the reference letter on the COSMIC Request Card in this issue.

Environmental-Analysis Routine Library

A library of routines for simulating environmental-control and life-support systems.

A program available from COSMIC contains a library of routines that simulate environmental-control and life-support systems (ECLSS). Through interactive dialogue with the program, the user selects routines to be assembled into a simulation of a particular ECLSS under consideration. The assembled routines are then loaded and executed to calculate the transient performance parameters of the ECLSS under prescribed boundary conditions.

The environmental-analysis library program models various ECLSS configurations. Consideration was given to processing several models over an extended period of time such as one for operational Space Shuttle payloads. This resulted in the resulted in the following design characteristics:

- A restart capability in which the user interactively modifies the component characteristics and exercises different options from a previous execution;
- The ability to produce a modeled-system schematic to advise the user of the current configuration of the ECLSS model with which he is working;
- A print characteristic that identifies the type of component at each node either by a program-generated generic name or a user-assigned name.

The program could be expanded to handle future environmental-control and life-support systems. Since it is modular, it allows the addition of new routines as they are required. In addition, the consumables bookkeeping system is compatible with advanced closed-system (regenerative) ECLSS components.

The execution procedure includes various input and output options that are entered interactively through user-prompted displays. Output generally includes fluid-property data, atmospheric-property data, consumables data, stores data, and a modeled-system schematic.

The system is written in FORTRAN IV for interactive execution and has been implemented on a UNIVAC 1100 series computer with a central memory requirement of approximately 46K of 36-bit words. The system requires a Hazeltine 4000 graphics terminal, a UNIVAC 494 controller, and the DISSPLA software system. It was developed in 1980.

This program was written by Karen Parker and John Torian of TRW Co. for **Johnson Space Center.** *For further information, Circle C on the COSMIC Request Card.*
MSC-18925

Mechanics

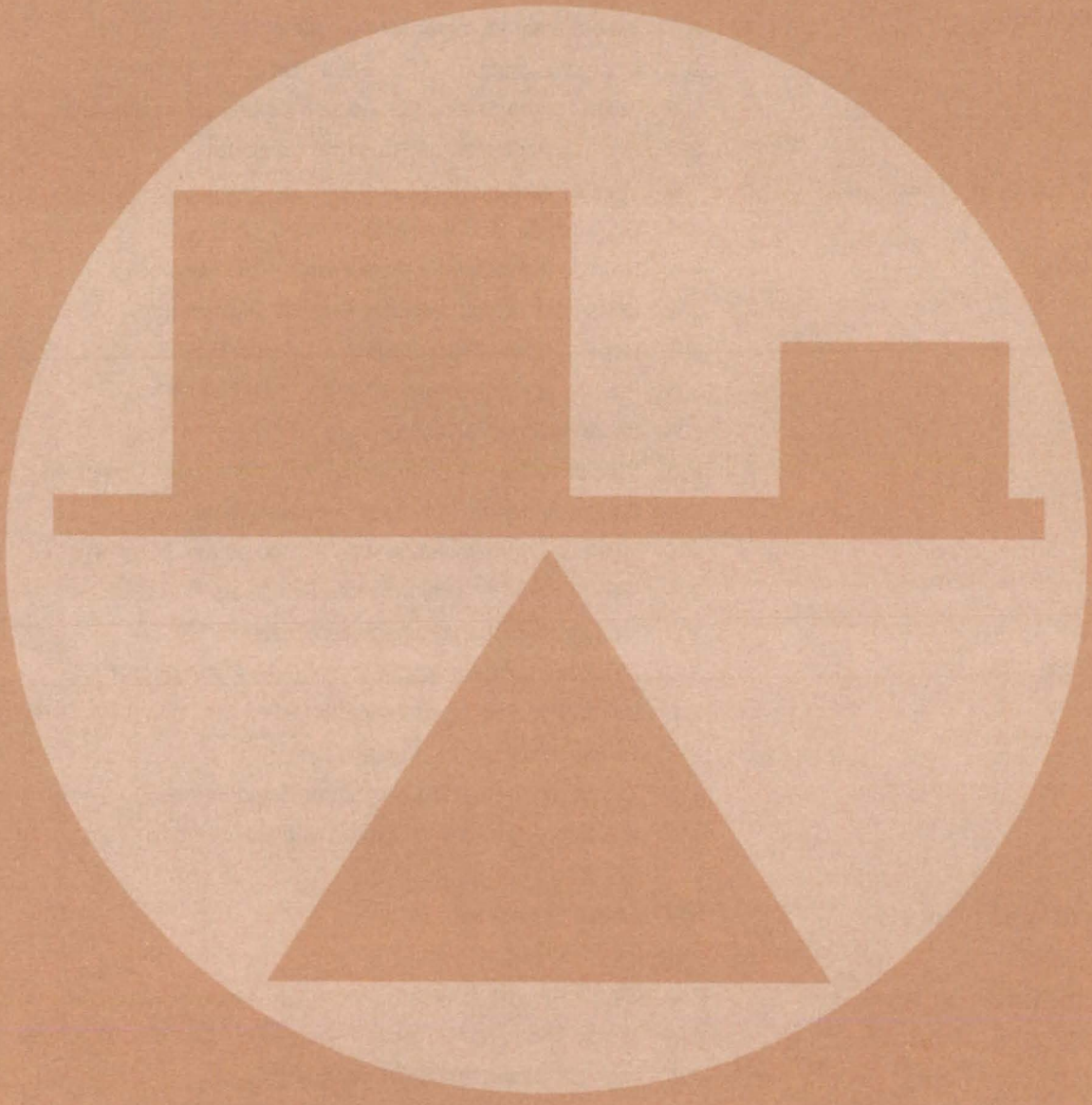

Hardware, Techniques, and Processes

295 Fast-Acting Electrohydraulic Servo
296 Improved Magntic-Field-Component Resolvers
297 Simple Magnetometer for Autopilots
298 Ultrasonic Instrument for Evaluation of Composites
298 Small Fixture Strains Composites for Environmental Tests
299 Solution Accounts for Structural Damping
300 Tile-Gap Measurement Tool
301 Gage for Surface Waviness
301 New Configuration for Compression-Test Fixture
302 Mass-Loss Buttons Monitor Material Degradation
303 Hot Film Static-Pressure Probe for Flow-Field Surveys
304 Predicting the Strengths of Angle-Plied Laminates
304 Improved Tensile Test for Ceramics
305 Predicting Tensile Strengths of Boron/Aluminum Composites
306 Double-Adhesive Tape Test Reduces Waste
307 Detecting Contamination With Photoelectron Emission
308 New Apparatus Tests Pressure-Suit Joints
309 Modular Engine Instrumentation System
310 Algorithm for Unsteady Potential Flow About Airfoils
310 Using Nomarski Interference to Detect Microcracks in Glass
311 Torque Simulator for Rotating Systems
312 Explosively Actuated Opening for Rapid Egress
313 Vibration Analysis With Finite Dynamic Elements

Books and Reports

313 Elastic Surface Wrinkling

Computer Programs

314 Structural Design With Stress and Buckling Constraints
314 Plastic and Large-Deflection Analysis of Nonlinear Structures
315 High-Lift Separated Flow About Airfoils

Fast-Acting Electrohydraulic Servo

Servosystem drives an airflow valve to 500 hertz.

Lewis Research Center, Cleveland, Ohio

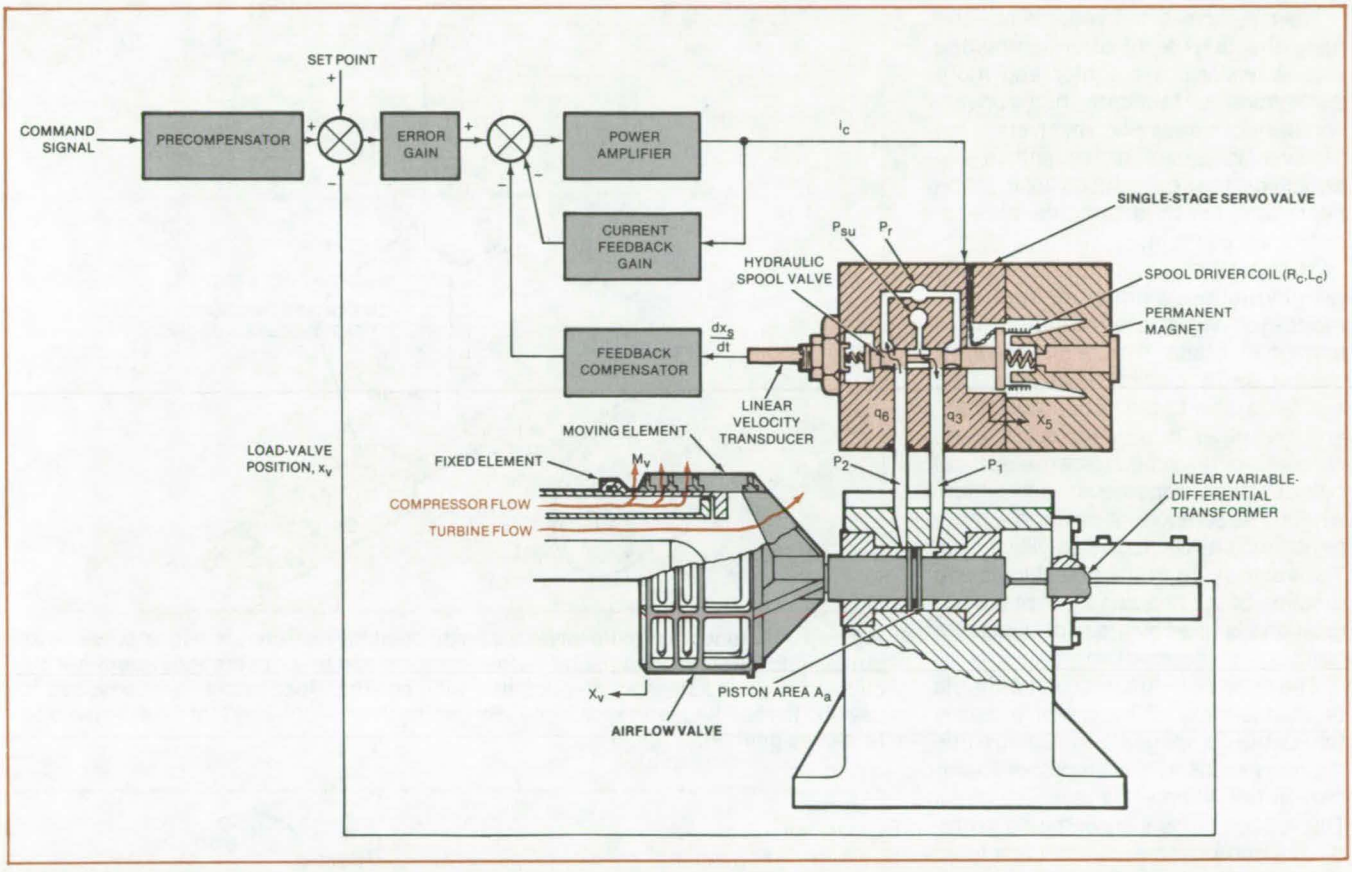

The Electrohydraulic Servo controls the moving elements of the airflow valve. The position of the moving element and attached piston is monitored by a linear variable-differential transformer. A single-stage servo valve lets fluid into and out of the piston volume in response to feedback signals from the LVDT.

A fast-acting electrodydraulic-actuation servosystem has been developed for application to the control of an airflow valve. The servosystem employs a high-power single-stage servo valve to obtain dynamic response beyond that of systems designed with conventional two-stage servo valves.

The schematic diagram of the airflow valve shows its actuator and the servosystem for positioning the valve. The airflow valve was designed to provide a contolled compressor exit area for a small axial-flow compressor that was driven by an air turbine. The flow paths for the compressor and turbine are shown in the cross-sectional view of the airflow valve.

The piston position signal from the linear variable-differential transformer (LVDT) is fed into an electronic controller where it is differenced with a precompensated command signal and a manual set-point signal. The precompensator is a second-order lead-lag circuit designed to extend the linear response of the servosystem. The error signal is amplified and applied to a power amplifier that is used to drive the coil on the electrohydraulic servo valve.

The electrohydraulic servo valve is a single-stage four-way spool valve positioned mechanically by the sum of the forces exerted by the springs at either end of the spool and the current-driven coil. The spool valve controls the hydraulic fluid supply into the actuator piston chambers to position the piston. Velocity feedback provides damping sufficient to insure stable operation. The fixed element in the airflow valve was coated with a solid lubricant to prevent excessive wear and galling.

This servosystem exhibited a dynamic response of −3 decibels at 490 hertz for excitation amplitudes of 20 percent of full stroke with a 1.1-kilogram (2½-pound) inertia load. Full stroke corresponds to 0.635 cm, or an airflow valve area of 40 cm^2.

This work was done by John A. Webb, Jr., Oral Mehmed, and Carl F. Lorenzo of **Lewis Research Center.** *Further information may be found in NASA TP-1678 [N80-29369/NSP], "Single-Stage Electrohydraulic Servosystem for Actuating an Airflow Valve with Frequencies to 5000 Hertz" [$6.50]. A copy may be purchased [prepayment required] from the National Technical Information Service, Springfield, Virginia 22161.*

LEW-13730

Improved Magnetic-Field-Component Resolvers

New optical, capacitive, and potentiometric devices have applications in aircraft navigation systems.

Langley Research Center, Hampton, Virginia

New resolvers for vectorially summing the outputs of aircraft-mounted magnetometers are lighter and more economical to fabricate than conventional electromagnetic resolvers. One resolver is based on potentiometric principles, the second uses polarization filters, and the third has a variable-capacitance element.

In aircraft navigation systems using two induction magnetometers, the magnetometers are mounted in a horizontal plane with their sensitive axes at right angles to one another: One axis is parallel to the direction of flight, and the other is perpendicular. Each magnetometer produces an electrical output signal proportional to the intensity of the component of Earth's magnetic field parallel to the sensitive axis. The vector sum of the two signals is a function of the heading error of the aircraft and is used by the pilot to make a heading-error correction.

The potentiometric resolver consists of an assembly of inexpensive, easily fabricated components, including a mechanical crank to drive a pair of linear-motion potentiometers (see Figure 1). The voltage outputs are summed to produce a composite signal that is a function of the heading error.

Figure 2 shows the polarized-light resolver. It generates the sine/cosine functions by photoresistive elements illuminated by light, the intensity of which is modified by linearly polarized filters.

The printed-circuit capacitive resolver is shown in Figure 3. It consists of two capacitor plates separated by sheets of dielectric material and a rotatable metallic shield. Both plates consist of active cruciform electrodes surrounded by grounded shields. The input electrode is electrically separated into four separate arms. The ac output of each magnetometer drives diametrically opposite pairs of these arms, and inverting amplifiers are used to reverse the phase of one arm of each pair so that opposite arms are driven at a 180° phase difference. The output electrode is capacitively coupled to each of the input electrodes and modulated in such a

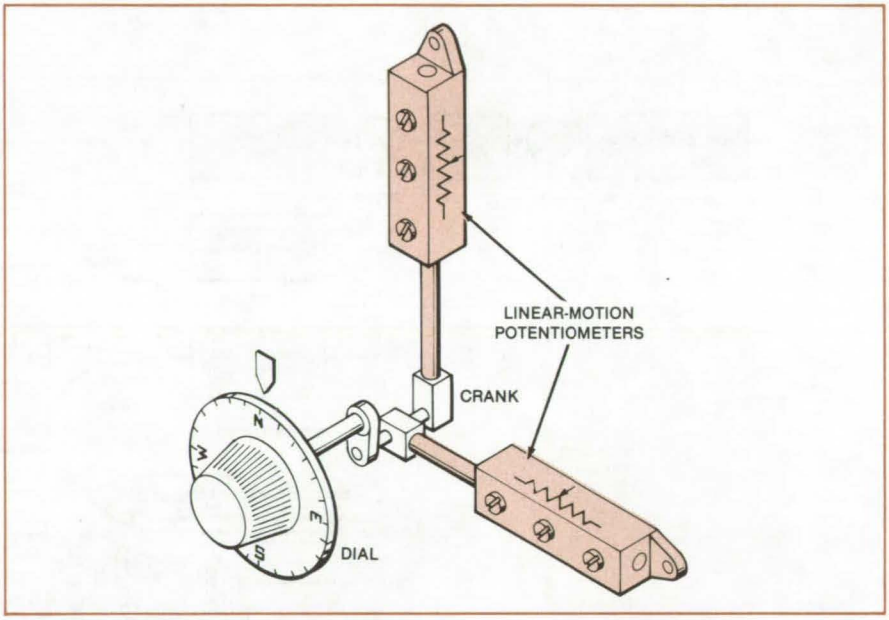

Figure 1. A **Potentiometric Resolver** is used to combine two aircraft magnetometer-output signals. Each magnetometer output is processed by an operational-amplifier circuit and applied across a potentiometer winding. The wiper outputs are combined to develop the heading-reference signal. By turning the dial, the operator sets the heading reference direction.

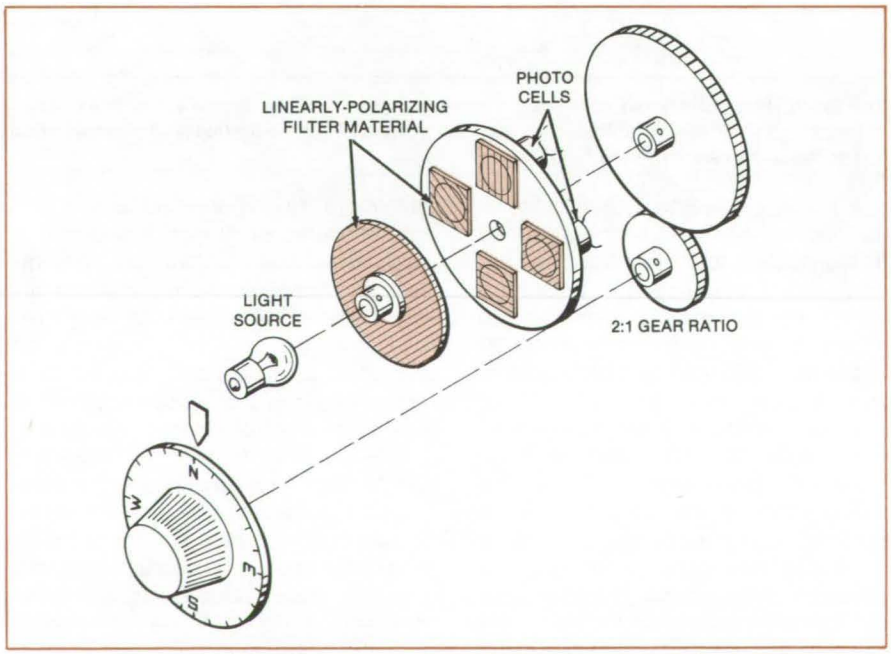

Figure 2. In the **Optical Resolver,** the heading reference is set when the operator turns the dial to the desired compass reading. This adjusts the relative polarization orientation of the filter elements. The magnetometer signals are applied to the photocells.

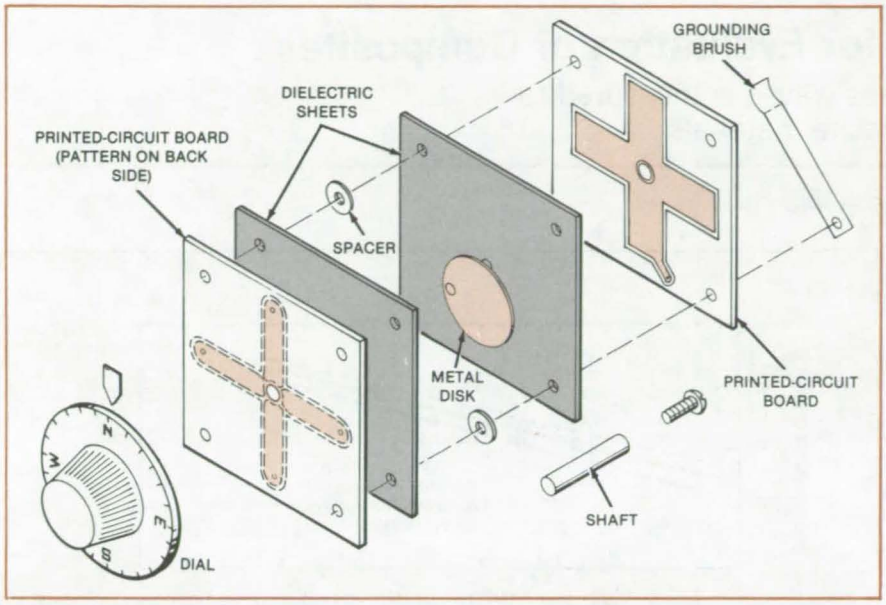

Figure 3. The **Capacitive Resolver** has a metal disk that rotates between cross-shaped electrodes. The position of the disk determines the heading reference. The magnetometer signals are applied to the plates in the foreground, and the heading error is extracted from the plate in the background.

way that the final amplified and demodulated signal voltage yields the desired heading-error signal.

This work was done by H. Douglas Garner of **Langley Research Center.** *For further information, Circle 35 on the TSP Request Card.*

Inquiries concerning rights for the commercial use of this invention should be addressed to the Patent Counsel, Langley Research Center [see page A5]. Refer to LAR-12638.

Simple Magnetometer for Autopilots

An inexpensive, heading-reference system uses readily available components.

Langley Research Center, Hampton, Virginia

A simple, low-cost magnetometer is suitable for heading-reference applications in autopilots and other directional-control systems. The sensing element utilizes a commercially-available transformer core; and the supporting electronics consist of one transistor, two readily-available integrated-circuit chips, and associated resistors and capacitors.

The figure illustrates the magnetometer sensor and electronics. The output is a dc signal between ±3.5 volts, proportional to the component of Earth's magnetic field that is parallel to the sensitive axis of the instrument. When used with recently-developed northerly-turning-error-compensation techniques, which compensate for errors caused by the vertical component of the magnetic vector, the new magnetometer would be a low-cost, zero-drift, ultra-reliable heading reference for aircraft autopilots.

This work was done by H. Douglas Garner of **Langley Research Center.** *For further information, Circle 36 on the TSP Request Card.*
LAR-12832

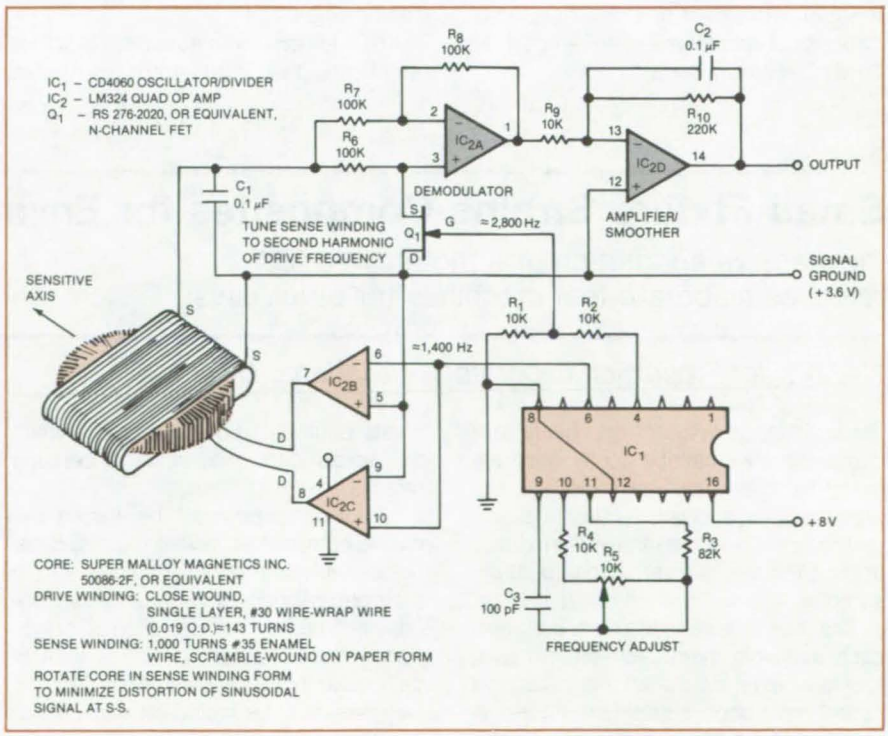

The **Reliable Magnetometer** features simple circuitry using low-cost, commercially available components.

Ultrasonic Instrument for Evaluation of Composites

The attenuation of acoustic stress waves is measured to determine the strength of composite materials.

Lewis Research Center, Cleveland, Ohio

Fiber-reinforced polymer composites are replacing metals in a variety of structures where high strength-to-weight ratios and other unique properties are important. The significant advantages of these materials are somewhat offset beause of inherent variations in mehanical strength and integrity of component parts. The fabrication process used in forming composite materials allows the chance for microvoid formation and similar hard-to-detect imperfections to be present in the final product.

For these materials to reach their full potential, it is necessary for an advanced nondestructive-testing technique to characterize quantitatively the defects and physical properties of the composite-material components. This test technique must assure that defective materials are not put into service and that serviceable materials are not discarded.

A new portable ultrasonic inspection instrument measures the strength of composite materials. This new commercial instrument has similar specifications to prototypes developed at Lewis Research Center.

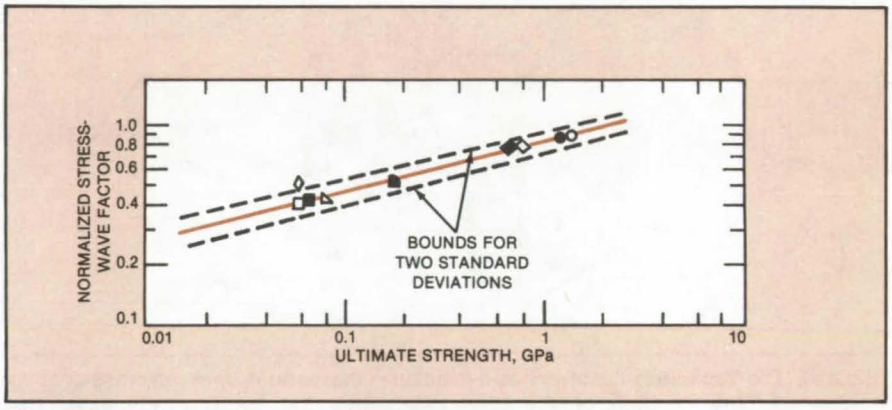

The **Ultimate Strength of a Composite Material** is related to the normalized stress-wave factor, a measure of the attenuation of the stress wave.

Ultrasonic pulses are injected by the instrument into the material being tested. The pulses excite stress waves that are detected by the instrument, allowing it to calculate a "stress-wave factor," which is a measure of the attenuation of the waves as they pass through the material. As shown in the figure, the normalized stress-wave factor is related to the ultimate strength of the composite.

In addition to measuring ultimate strength, the instrument can also assess the integrated effect of all flaws in a localized region of the composite. This device may ultimately help to reduce energy consumption and improve efficiencies of vehicles by allowing the use of composite materials to their full potential in critical application areas.

This work was done by Alex Vary of **Lewis Research Center** *and Allen Green of Acoustic Emission Technology Corp. For further information, Circle 37 on the TSP Request Card.*
LEW-13716

Small Fixture Strains Composites for Environmental Tests

Inexpensive adaptation of a motorcycle tool releases elaborate test machines for other uses.

NASA's Jet Propulsion Laboratory, Pasadena, California

Qualification tests for graphite/epoxy composites — usually costly because many samples must be tested — are made less expensive by a simple strain-test fixture. Used in quantity, the fixtures apply precisely similar loads to many samples.

The inexpensive fixture is a commercially-available motorcycle-chain repair tool to which a steel shim and calibrated screw have been added (see figure). A small rectangular sample of a composite panel is held in the fixture while the screw and shim apply a bending stress.

Many samples must be tested because composites, unlike metals, deteriorate with time under a load or strain; their behavior under various loads, periods of time, and environmental conditions must be determined. For statistically meaningful data, a large number of samples must be tested for each set of conditions.

In the past, 24 to 100 test samples were tested in commercial strain devices for fixed periods, after which the sample strength was measured. Separate duplicate samples were tested after 1, 2, 4, 8, and 16 weeks. Such tests were conducted for various combinations of temperature and humidity under load. With the new fixture, a strain machine is used only briefly, to establish the amount of displacement needed to produce 50 percent or other desired strain

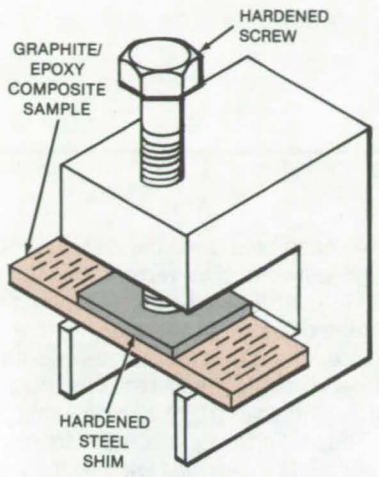

A **Fixture for Long-Term Strain Tests of Composites** is based on a tool for repairing motorcycle chains. (In normal use the tool forces a rivet out of a chain element.) As modified for composite testing, the tool has a precision screw and a shim.

on only one sample.

Samples are cut from large sheets of graphite/epoxy composite by precision diamond saws. Sample dimensions are typically ¼ by 1 by 0.070 inch (0.635 by 2.54 by 0.178 cm). Each sample is inserted in a fixture. With a torque wrench, the screw is turned until the shim just touches the sample. A calibration mark is made on a 360°-angle calibration sheet atop the fixture. Next, the screw is turned through a fixed arc known to advance it against the sample by the required deflection. (Alternatively, a dial indicator can be used to measure the travel of the screw.)

Conventional environmental testing then proceeds. The fixtures and their samples are placed in humidity ovens. They are removed after the requisite number of weeks and subjected to the short-beam shear test in a testing machine.

This work was done by Fred W. Tervet of Caltech for **NASA's Jet Propulsion Laboratory.** *For further information, Circle 38 on the TSP Request Card.*
NPO-15062

Solution Accounts for Structural Damping

A finite-element model includes nonlinear, nonviscous internal damping.

Langley Research Center, Hampton, Virginia

A new analytical technique determines the dynamic response of damped structures dominated by internal structural damping mechanisms. Though structural damping is often negligible compared with damping due to air friction and friction in joints, structural damping can be of major importance in structures having heavy damping treatments or in outer-space structures.

When structural damping is the dominant damping mechanism, its nonlinearity must be considered since there is experimental evidence showing that structural damping is basically a nonlinear nonviscous phenomenon. Although linear viscous or hysteretic damping models give adequate results in many engineering applications, nonlinear nonviscous models are needed to represent realistic structural damping in free-vibration or nonperiodic-vibration situations.

One objective of the method is to incorporate many different structural damping functions, viscous or nonviscous, in a structure through finite-element damping matrices. A second objective is to develop and evaluate an efficient solution technique for problems with nonviscous damping.

The technique first considers incorporating nonviscous damping in a structure through the use of the finite-element method. Damping is included through the stress/strain constitutive law by the addition of strain-rate-dependent terms. Then, the general equations for representing damping matrices are derived through the principle of virtual work.

To solve the set of nonlinear equations resulting when nonviscous damping is present, a solution technique is developed by modifying the Newmark method to accommodate an iterative solution and to treat the nonviscous damping as a pseudoforce. The solution technique was checked for accuracy and convergence in single- and multiple-degree-of-freedom problems and was found to be accurate and efficient for initial-condition problems with small nonviscous damping. Finally, the approach is demonstrated by determining the effects of a specific nonviscous damping model on the transient motion of a free-free Timoshenko beam.

Thus, the modeling of structural damping through strain and strain-rate terms in the constitutive law of a material is shown to be an effective analytical tool because it readily leads to the calculation of damping matrices in the finite-element method, which yields equations of motion that can be solved to investigate the effect of damping. The practicality of this method is yet to be verified experimentally.

This work was done by Louis A. Roussos of **Langley Research Center,** *M. W. Hyer of Virginia Polytechnic Institute and State University, and E. A. Thornton of Old Dominion University. For further information, Circle 39 on the TSP Request Card.*
LAR-12863

Tile-Gap Measurement Tool

Hand-held tool accurately measures gap width.

Lyndon B. Johnson Space Center, Houston, Texas

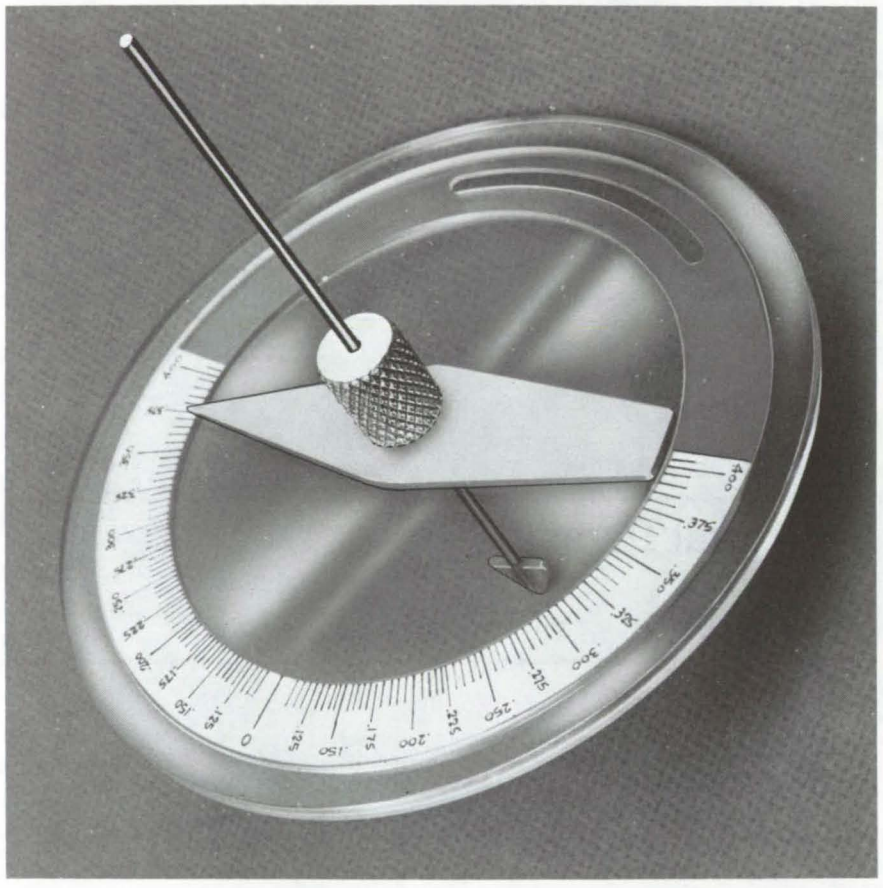

Figure 1. The **Pointer on Gap-Measurement Tool** indicates the width of a gap, in inches, on a calibrated scale.

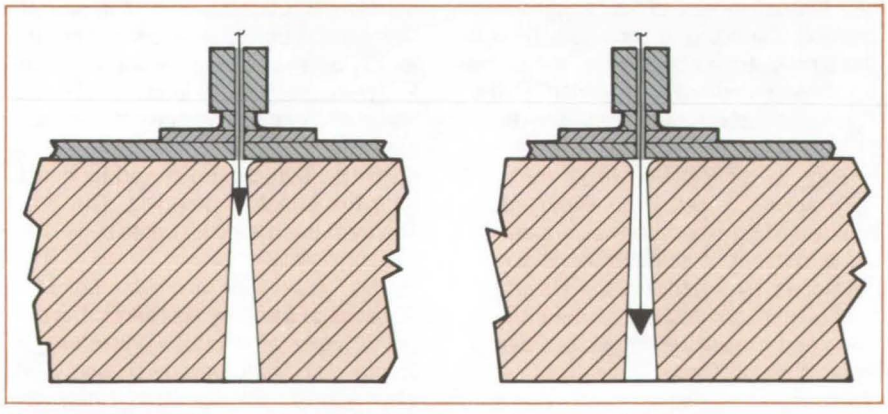

Figure 2. The **Depth of Blade Can Be Adjusted** so that tapered or irregular gaps can be measured. When the knob is loosened, the blade can be moved from the shallow position at left to the deep one at right. The blade appears broader at right because it is turned more fully toward the viewer, since the gap is wider.

A hand-held tool measures small gaps between tiles rapidly and accurately, even when the gap is tapered or indented below the surface. The tool indicates the gap dimensions on a calibrated disk. Its measurements are accurate within ±0.003 inch (76 μm).

The tool consists of a flat blade on a shaft held by a knurled knob on the calibrated disk (Figure 1). To measure the width of a gap, the user inserts the blade into the gap and turns the blade into contact with the walls. With the blade firmly in contact with the wails, the user turns the pointer on the disk scale to zero. Next, the user rotates the knob in the opposite direction until the blade again contacts the walls. The pointer then indicates the width of the gap.

To change the depth at which the gap width is measured, the user loosens the knurled knob so that the blade shaft can be moved up or down, then tightens the knob. The user can thus make measurements at progressively smaller or larger depths in the gap (Figure 2).

The tool was developed for determining the gap between tiles on the Space Shuttle. It may be of use in other applications requiring the precise setting of gaps between tiles or other structures.

This work was done by Donald H. Helman and Andrew R. Keir of Rockwell International Corp. for **Johnson Space Center.** *No further documentation is available.*

MSC-20057

Gage for Surface Waviness

Three dial indicators with adjustable spacing give a quick check of surface figure.

Lyndon B. Johnson Space Center, Houston, Texas

A new device gives qualitative readings of the flatness, curvature, or waviness of a surface. It was designed to check for waviness in the surface of the Space Shuttle prior to the installation of heat-resistant tiles, but it could be used to measure the regularity or irregularity of other surfaces.

As the figure shows, the waviness indicator consists of a frame that is supported by two fixed feet and one movable foot plus three dial indicators that can be located with various spacings in the frame. The dial gages are preset to read zero on a controlled flat surface. Then when the measurement device is applied to a surface under test, the dial readings reveal any irregularities. As the device is moved about on the surface, the dials indicate any departure from true planar contour.

The sliding foot is positioned so that its distance from the fixed feet is equal to the width of the area to be measured — e.g., the distance between stringers or rivet lines. Then the dial indicators are spaced equidistantly on the frame. In the unit already in use, the indicators can be as close as 4 inches (10.16 cm). They read positive or negative displacements to within 0.001 inch (0.025 mm).

This work was done by George W. Williams of Rockwell International Corp. for **Johnson Space Center.** *No further documentation is available.*
MSC-20055

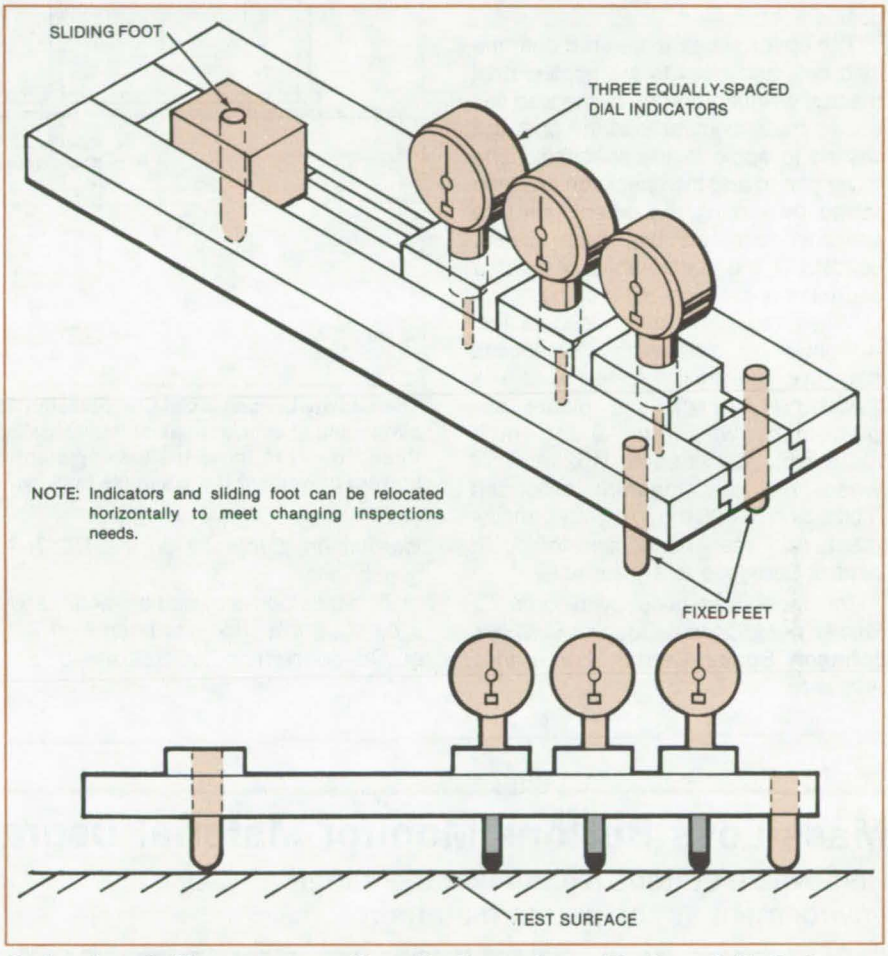

Surface Irregularities are measured by noting the readings of the three dial indicators on this simple, inexpensive instrument. The original device was built to check the contours of the Space Shuttle prior to tile installation.

New Configuration for Compression-Test Fixture

Gravity-loading fixture is accurate and controllable.

Lyndon B. Johnson Space Center, Houston, Texas

In a variation of the usual axial-compression test fixture, the specimen raises a platen until the specified load is applied. Previous fixtures compress the specimen between platens that are moved toward each other. The new configuration gives better control over the load and allows it to be measured more accurately. Testing can be stopped abruptly if necessary to prevent buckling or other damage to the specimen.

As shown in the figure, the specimen is placed between upper and lower platens. The platens are supported by a base and a threaded steel post. The

(continued on next page)

lower platen rests on a nut and is constrained laterally by a lubricated ridge. Tie rods attached to an adjacent post prevent the lower platen from rotating. A large wheel extending beyond the lower platen is used to turn the nut, producing upward or downward motion of the lower platen. A load cell is located in a pivot hole at the top of the threaded steel post.

The upper platen is lowered onto the load cell, and weights are applied until the true weight recorded by the load cell equals the maximum load the operator wishes to apply to the specimen. The lower platen and the specimen are then raised by turning the wheel until the specimen contacts the upper platen. Loading of the specimen is seen as a decrease of the load-cell reading.

When the fixture was used to test a lightweight fiber/epoxy composite structure, the maximum test load was 2,800 lb (1,270 kg), and platen displacement was only 0.010 inch (0.25 mm). Six inches (152 mm) of wheel rim displacement produced 0.001 inch (0.025 mm) of platen movement. An experienced operator could control loading to ±2 lb (±9 N).

This work was done by George C. Shanks of McDonnell Douglas Corp. for **Johnson Space Center.** *For further information, Circle 40 on the TSP Request Card.*

This invention is owned by NASA, and a patent application has been filed. Inquiries concerning nonexclusive or exclusive license for its commercial development should be addressed to the Patent Counsel, Johnson Space Center [see page A5]. Refer to MSC-18723.

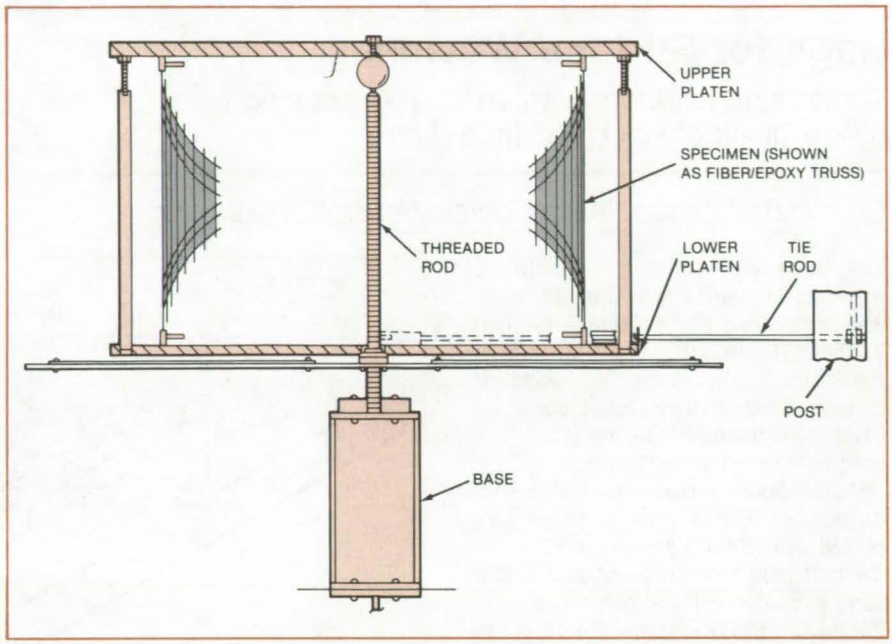

The **Gravity-Loaded Axial-Compression Test Fixture** is operated by raising the lower platen and specimen against the weighted upper platen. The wheel turns the nut on the threaded rod to move the lower platen up or down. The limiting rods prevent further upward movement if the sample buckles.

Mass-Loss Buttons Monitor Material Degradation

Removable buttons experience the same environment as the parent material.

Lyndon B. Johnson Space Center, Houston, Texas

Small button-sized samples attached to a parent material are a simple way of monitoring the degradation of the parent in harsh environments. The samples determine the effects of multiple exposures to environmental extremes without disturbing the fit or function of the parent. They are less costly and more convenient than the complex instrumentation normally required to measure the complete temperature/pressure time history of the parent component.

For the reinforced carbon-carbon (RCC) panels of the Space Shuttle, such samples are in the form of RCC buttons three-fourths of an inch (1.9 cm) in diameter. The buttons are clipped to the Shuttle leading-edge panels.

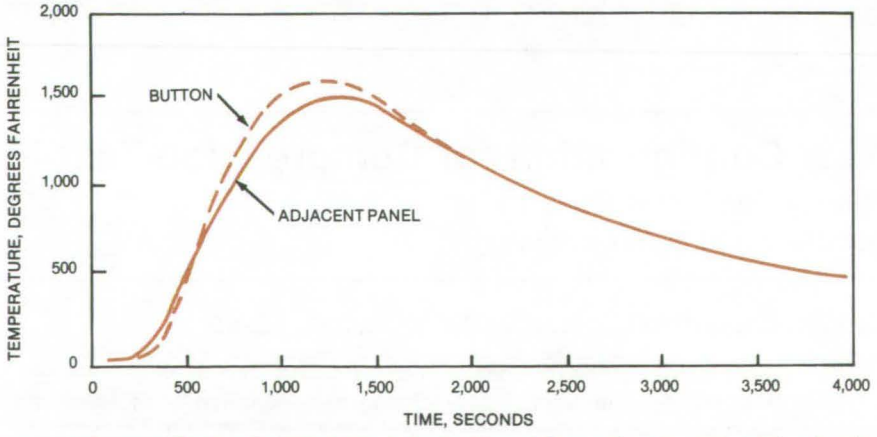

Temperatures of Button Samples and Adjacent Panel Areas closely track each other in reentry simulation. The greatest mass loss is expected to occur after the first 1,800 seconds of reentry, while temperatures and pressures are high.

The strength of the panels is reduced by subsurface oxidation, which is manifested as mass loss, during reentry. When the strength drops to the point where the panel can no longer support loads with an adequate margin of safety, the panel must be replaced. By sharing the same history as the panels, the buttons make it possible to monitor degradation. The buttons are removed and weighed after a mission to determine the amount of mass loss.

In simulated Space Shuttle reentries with thermocouples attached to buttons and to adjacent panel areas, the temperatures of the buttons closely matched those of the panels (see figure). To complete the characterization of the buttons, their cumulative mass loss is correlated with the panel mission life.

This work was done by Charles N. Webster of Vought Corp. for **Johnson Space Center.** *No further documentation is available.*
MSC-18903

Hot Film Static-Pressure Probe for Flow-Field Surveys

The use of two hot film sensors and a sonic orifice reduces response time to milliseconds.

Langley Research Center, Hampton, Virginia

A new hot film static-pressure probe (see figure), designed at Langley Research Center, significantly reduces response time in flow-field surveys during wind-tunnel tests. The probe incorporates two hot film sensors, an unheated film for temperature compensation and a heated film for pressure measurement, and a sonic orifice for flow control.

A conventional static-pressure probe has four equally spaced orifices from 10 to 20 tube diameters downstream of its conical tip. In a uniform stream the probe senses the static pressure of the stream at the orifices within 1 or 2 percent, but for low static pressures the response time through the length of tubing required to link it to a transducer could be on the order of 35 to 40 seconds. Therefore, surveying the static-pressure distribution in a flow field requires an extremely large number of runs unless the probe response time is reduced considerably.

To reduce response time, a pressure-measuring setup is used that consists of a pair of hot film sensors inside the probe tubing just downstream of the exterior orifices. A low mach number is maintained nearly constant over the sensors by placing a small flow-controlling orifice just downstream of them and connecting the probe to a vacuum pump. The front sensor is operated without overheat; its resistance change is proportional to the change in the temperature of the gas. The rear sensor is operated in an overheat ratio (operating temperature to environmental temperature) of 1.5 to 1.8, and its output is directly proportional to the static pressure. The front sensor reading is used to compensate for the effect of temperature on the rear sensor.

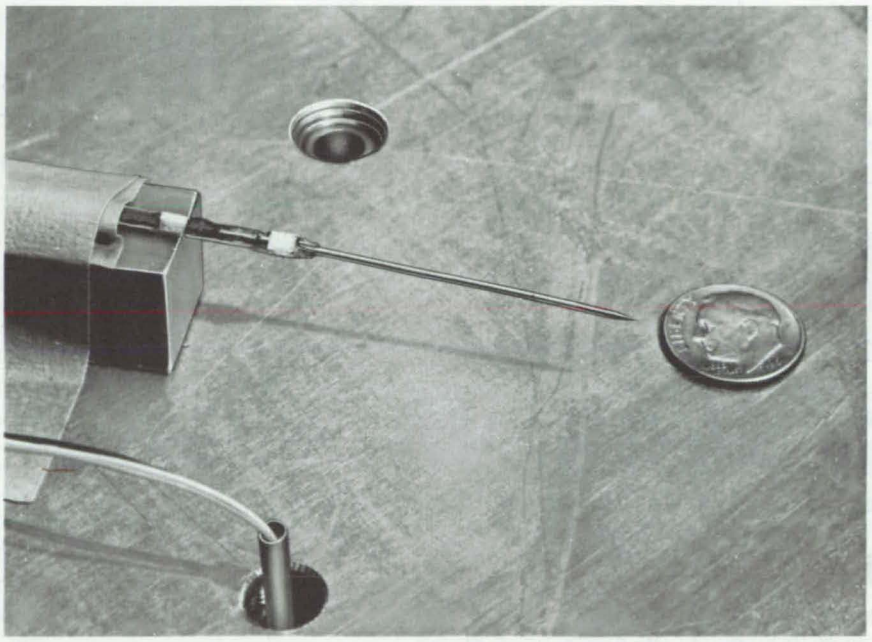

Hot Film Probe measures static pressure while compensating for gas temperature.

For operation, the probe is calibrated for the test gas of interest over the range of environmental temperatures and static pressures that are anticipated during the wind-tunnel tests. The calibration is then used to determine the pressure from the probe sensor readings recorded during the wind-tunnel test. The hot-film-probe settling time for the two-film design is just a few milliseconds, allowing complete flow-field surveys to be made in one or two runs (with only a slight loss in measurement accuracy) rather than with the large number of runs previously required.

This work was done by Leonard M. Weinstein and George C. Ashby, Jr., of **Langley Research Center.** *For further information, Circle 41 on the TSP Request Card.*

Inquiries concerning rights for the commercial use of this invention should be addressed to the Patent Counsel, Langley Research Center [see page A5]. Refer to LAR-12799.

Predicting the Strengths of Angle-Plied Laminates

Method suitable for use with a pocket calculator determines physical properties of composite laminates.

Lewis Research Center, Cleveland, Ohio

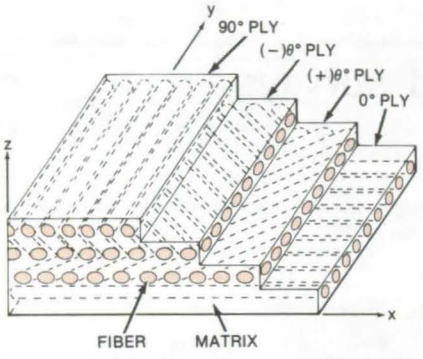

Figure 1. **Layers of Composite Material** are each angled so that the fibers within each layer are alined in a different direction from the fibers in the other layers.

The unique properties associated with composite materials have resulted in increased usage in a wide variety of applications. Composite materials can significantly reduce the weight and increase the strength of load-bearing structures. Laminated fiber composites are increasingly being used in high-performance aircraft and land vehicles.

The determination of mechanical properties of angle-plied laminates (see Figure 1) is required for the initial design of structural components from fiber composites. The material properties of these components are determined using composite mechanics and laminate theory as calculated through the use of computer programs. This analysis by computer programing is expedient and quite general. It does not, however, provide the researcher/user with insight and instant feedback of the laminate behavior and capability as he or she proceeds with the design and analysis of the component.

A simplified, convenient procedure has been developed that can be used to determine the elastic and strength properties of angle-plied laminates. This method is suitable for use with a pocket calculator. It consists of simple equations and graphs of ($\pm\theta$) ply combinations (Figure 2) from the most frequently used composites. This procedure makes use of the well-known transformation equations, the ply stress influence coefficients, and the ply uniaxial strengths. It can handle all types of composites including interply and intraply hybrids.

This work was done by C. C. Chamis of **Lewis Research Center.** *Further information may be found in NASA TM-81404 [N80-16107/NSP], "Prediction of Fiber Composite Mechanical Behavior Made Simple" [$6.50]. A copy may be purchased [prepayment required] from the National Technical Information Service, Springfield, Virginia 22161.*

LEW-13733

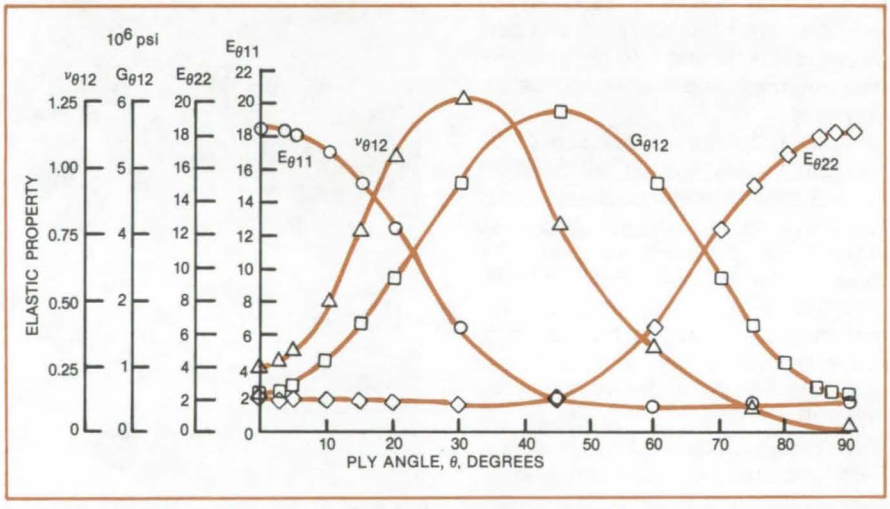

Figure 2. The **Elastic Properties** of graphite-fiber/epoxy (AS/E) $\pm\theta$ laminates are an example of the simple graphs of ply combinations from the most frequently used composites. These graphs can be utilized to determine the elastic and strength properties of angle-plied laminates.

Improved Tensile Test for Ceramics

Test destroys only a shallow surface layer.

Lyndon B. Johnson Space Center, Houston, Texas

The tensile strength of such low-strength brittle materials as ceramics can be measured by a new method without destroying the entire test sample. The samples are inexpensive to prepare and can be used for the fabrication of parts after testing.

The method consists of bonding a pull rod to a specimen and pulling the rod and specimen apart in a conventional tensile-test machine. The measured stress at the breaking point is an indication of the tensile strength of the specimen and can be correlated with conventional destructive tensile tests.

The pull rod, 0.5 in.^{2} (3.2 cm^2) in cross section, is bonded to the specimen with a thermoplastic adhesive (see figure).

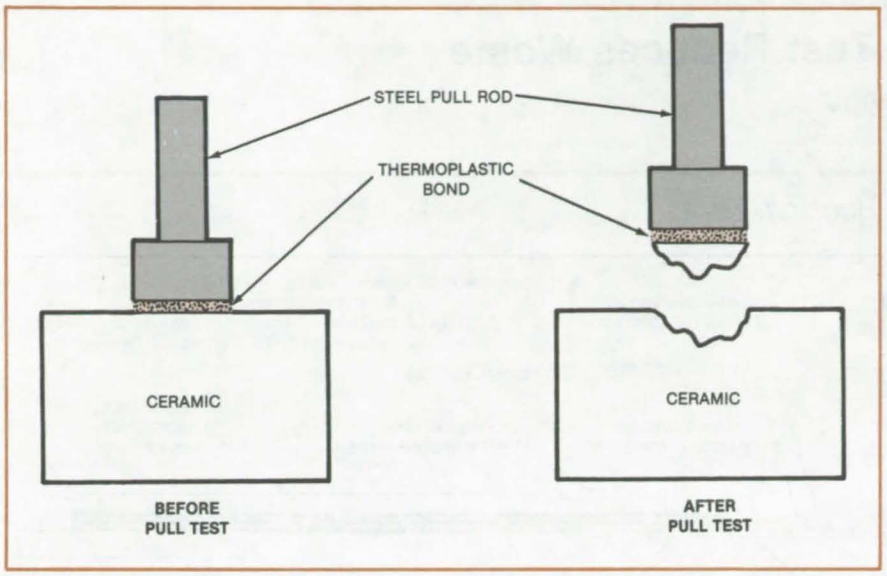

For **Almost-Nondestructive Tensile Testing** of ceramics, a steel pull rod is bonded to a sample of the ceramic. The assembly is then pulled apart in a conventional tensile-test machine.

The stress required to pull the rod vertically from the material is then measured. When the pull rod is torn from the surface of the specimen, a downward-pointing conelike volume of material pulls away with it. The cone base has the same shape and area as the bonded pull-rod cross section and is usually less than 0.1 inch (2.5 mm) in height. Machining away the material surrounding the cone-shaped hole left in the specimen makes it ready for other uses.

The method was developed for measuring the tensile strength of the Space Shuttle thermal-protection tiles. It should be useful as a manufacturing inspection procedure for low-strength brittle materials.

This work was done by Richard A. Osiecki of Lockheed Missiles & Space Co., Inc., for **Johnson Space Center.** *No further documention is available.*
MSC-20105

Predicting Tensile Strengths of Boron/Aluminum Composites

Using derived formulas, calculated and experimental results agree to within 3 percent.

Lewis Research Center, Cleveland, Ohio

The development of strong, high-modulus ceramic fibers has given impetus to the use of composite materials as structural replacements for high-strength metal alloys. One of the most successful of these materials is the boron/aluminum (B/Al) composite in which standard aluminum alloys are reinforced with continuous high-strength boron fibers. The improved structural properties of the B/Al composite stem primarily from the fiber. The resultant product is not only much stronger and stiffer than the best high-strength aluminum alloys but it also can be used effectively at significantly higher temperatures.

In designing for the mechanical behavior of B/Al composites containing high volume-fractions of fiber, the simplifying assumption is generally made that the fibers and thus the composite behave as brittle elastic materials. Although this assumption is approximately valid at low temperatures (near room temperature and below), it can produce serious design errors for elevated-temperature applications. This is due to the fact that boron fibers are not truly elastic materials but deform and fracture in a manner that is both time and temperature dependent. Thus for tensile stresses applied along the fiber direction and at elevated temperatures, there exists a need to design for the fiber-controlled creep and stress-rupture behavior of B/Al composites.

To develop a predictive theory to account for these time/temperature effects, a series of deformation and fracture studies was performed on commercial boron fibers over wide ranges of stress, stress application time, and temperature. Within these ranges, it was determined that the deformation strain, fracture strain, and fracture stress of the boron fiber could be described by very simple time/temperature-dependent equations. By combining these single-fiber results with fracture theory for metal matrix composites, design formulas were also derived that describe B/Al composite tensile and stress rupture strengths as a function of time and temperature. Calculated short-time tensile strengths for B/Al composites were found to agree to within 3 percent with experimental strength data between 70° and 750° F (20° and 400° C). Because the design equations are based on boron fiber deformation, they can also be used for understanding and predicting the time/temperature-dependent mechanical behavior of other composite systems reinforced by boron fibers.

This work was done by James A. DiCarlo of **Lewis Research Center.** *Further information may be found in NASA TM-81474 [N80-21452/NSP], "Predicting the Time-Temperature Dependent Axial Failure of B/Al Composites" [$6.50]. A copy may be purchased [prepayment required] from the National Technical Information Service, Springfield, Virginia 22161.*
LEW-13745

Double-Adhesive Tape Test Reduces Waste

New way of measuring peel strength uses half as much material.

Lyndon B. Johnson Space Center, Houston, Texas

A new method for testing the peel strength of a particular thermal-control tape used on the Space Shuttle orbiter radiators requires only half the amount of tape of the method previously employed. Since each of the 60 rolls of tape applied to the Space Shuttle radiators must be peel-tested, the cost saving with the new method is substantial.

The new method consumes only 4 feet (1.2 m) of each 100-ft (30.5-m) roll, whereas the old method consumed 8 feet (2.4 m). The method also avoids the cost of labor and materials to prepare a second test coupon and can be adapted for testing other types of double-faced-adhesive tapes in military, industrial, and consumer applications.

The thermal-control tape consists of layers of FEP, silver, Inconel metal, adhesive, Kapton film, and a second adhesive layer (see Figure 1). Because two adhesive bonds are involved — one against the aluminum sheet and one against the Inconel metal layer, both bonds must be tested. Previously, each peel test was conducted on a separate 4-ft cutting of tape. Now, however, a single 4-ft cutting is used.

The tape cutting is applied to a 12- by 12-inch (30.5- by 30.5-cm) aluminum coupon in three strips, each extending 4 inches (10.2 cm) beyond the edge of the coupon (Figure 2). Each strip is slit longitudinally into 1-inch (2.54-cm) ribbons. A ribbon is peeled back away from the aluminum, while the peeling force is measured, to about half the specimen length, as directed in ASTM standard D-903. At that point, the Kapton film separating the two adhesive layers is carefully cut through. Peeling is resumed; then the peel force represents the strength of the bond to the Inconel.

This work was done by Larry C. Lee and Madison W. Reed of Vought Corp. for **Johnson Space Center.** *No further documentation is available.*
MSC-20047

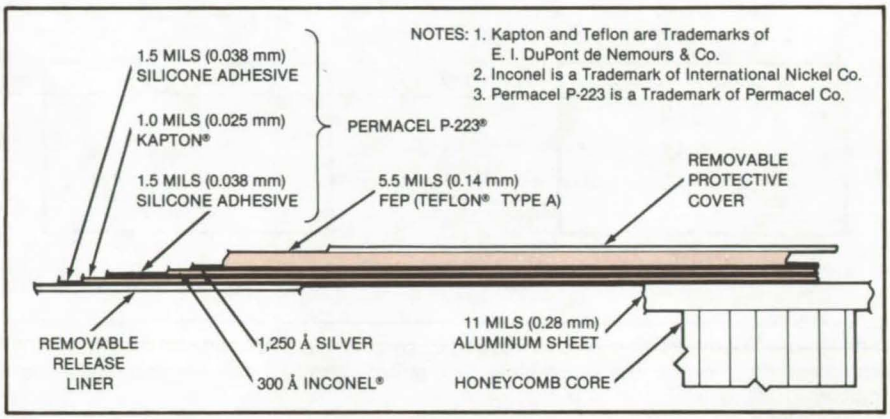

Figure 1. **Double-Adhesive Tape** sticks to an aluminum sheet on one side of its Kapton film carrier and to an Inconel/silver/FEP structure on the other side. A liner on the aluminum side is removed just before the tape is applied, and a protective overlay on the topmost FEP layer is removed after installation.

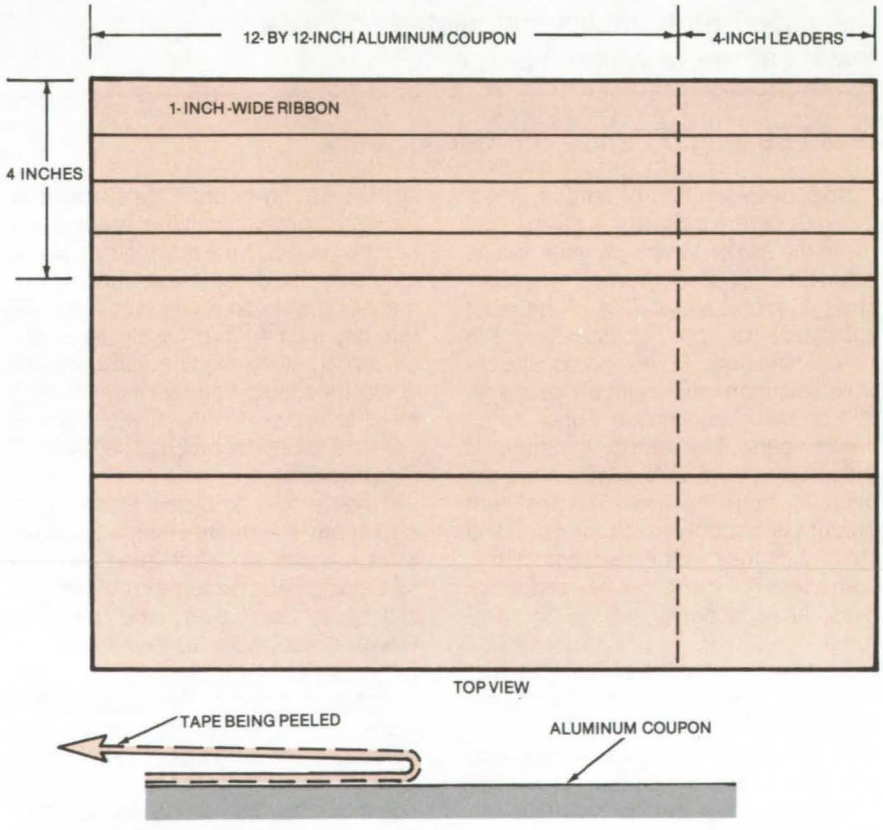

Figure 2. **Aluminum Test Coupon** (top), representing a radiator panel, is covered with three strips of double-adhesive tape, each 4 inches (10.2 cm) wide. The strips are then slit into 1-inch (2.54-cm) ribbons. Each ribbon is peeled back to about half the width of the coupon to measure the peel strength of the adhesive/aluminum bond (bottom). After the Kapton film interadhesive layer is cut, the ribbon is peeled back farther to measure the strength of the bond to the Inconel metal layer.

Detecting Contamination With Photoelectron Emission

Instrument finds areas of unacceptably high contamination so they can be cleaned selectively.

Marshall Space Flight Center, Alabama

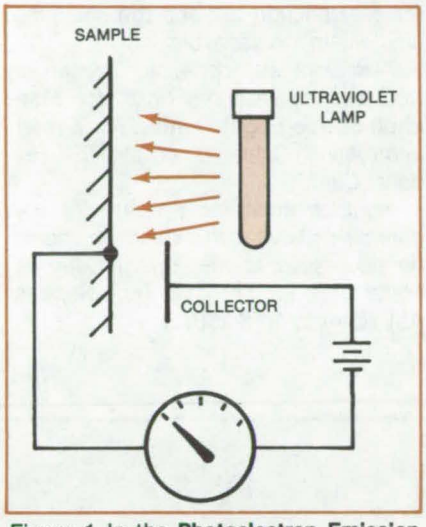

Figure 1. In the **Photoelectron Emission Detector** an ultraviolet lamp producing light at 2,500 Å is moved over a surface while a collector on the lamp gathers electrons emitted by the surface.

Photoelectron emission from aluminum or epoxy-painted aluminum can be used to reveal the presence and the concentration of surface contaminants. [See the article in *NASA Tech Briefs*, Vol. 6, No. 2, page 190, "Surface-Contamination Inspection Tool for Field Use" (MFS-25581).] The emission can be used to locate those parts of a surface that are excessively contaminated and to which coatings cannot be reliably bonded. Cleaning can then be done on the areas that most need it.

The photoelectron emission technique is based on the fact that aluminum and epoxy surfaces emit electrons when they are exposed to ultraviolet light, while such emissions are attenuated by contaminating films. Thus, the photoelectron current from a contaminated surface will be less than that from an uncontaminated one.

A contamination-measurement probe based on the photoelectron principle consists of an ultraviolet lamp to which a current-collector electrode is attached (Figure 1). As the lamp scans the surface, the collected photoelectron current is measured and recorded. Cur-

(continued on next page)

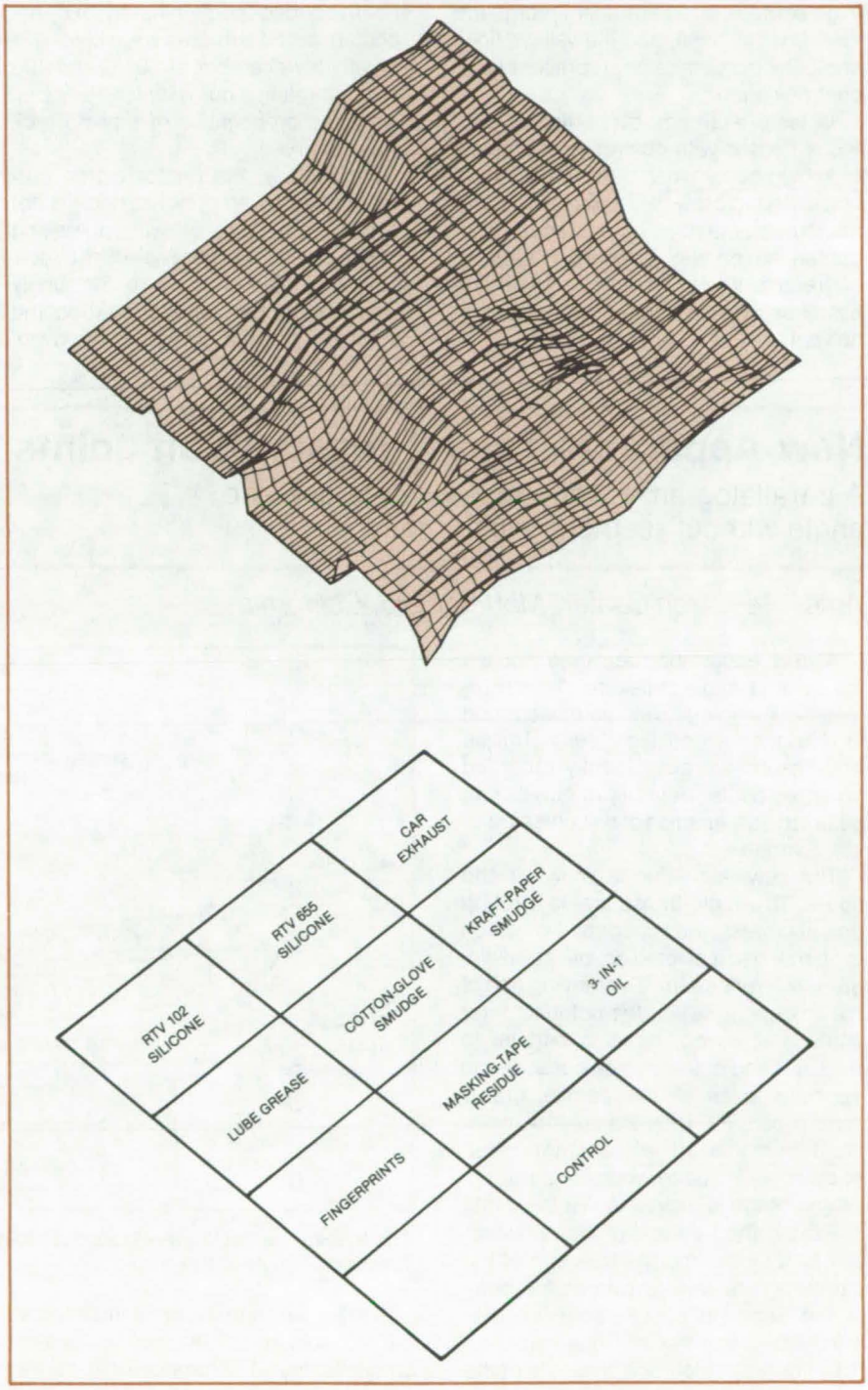

Figure 2. **Photoelectron Emission Map** (top) for an epoxy-painted panel shows contaminated areas as depressions and clean areas as peaks. This map is for a demonstration panel measuring 1 ft (30.5 cm) square divided by pencil lines into 12 equal areas. Nine of the areas were coated with selected contaminants, as indicated by the diagram at the bottom.

rents below a certain value indicate that contamination is excessive and will result in poor bonding.

The emission data can be plotted by a computer as a contamination map — a diagram showing the peaks and valleys of photoelectron current sensed by a probe as it moves over the aluminum or epoxy surface (Figure 2, left). The peaks (high photoelectron emission) represent low contamination, and the valleys (low photoelectron emission) represent high contamination.

In tests, adhesion properties of surfaces treated with controlled quantities of known contaminants (Figure 2, right) correlated closely with photoemission measurements for the surfaces. The contamination was removed to various degrees by wiping the surfaces with dry tissue or tissue saturated with cleaning solvent.

The following adhesion tests were then performed:

- Pressure-sensitive tapes were applied to the surfaces, and the forces required to peel back the tapes were measured.
- Contaminated surfaces were bonded to uncontaminated ones with foam and were measured for lap-shear strength.
- Foam-bonded contaminated and uncontaminated surfaces were placed in a humidity chamber at 60° C and 100 percent relative humidity for 16 hours, while the propagation of a pilot crack was observed.

Interestingly, the photoelectron current emitted by an epoxy surface is not constant, but drops off with increasing time of exposure to ultraviolet light. After about 2 minutes of exposure, the supply of electrons apparently starts to become depleted. After the UV light is removed, the photoelectron emission does not recover.

Fortunately, the photoelectron depletion effect does not hamper the new probe since it moves continuously over the surface, scanning a swath 9 inches (23 cm) wide. The probe moves at a rate of typically 1 ft/s (30 cm/s), a speed slow enough to ensure sensitivity but fast enough to keep the scanning time within a reasonable limit.

This work was done by T. Smith of Rockwell International Corp. for **Marshall Space Flight Center.** *For further information, Circle 42 on the TSP Request Card.*

Inquiries concerning rights for the commercial use of this invention should be addressed to the Patent Counsel, Marshall Space Flight Center [see page A5]. *Refer to MFS-25619.*

New Apparatus Tests Pressure-Suit Joints

A parallelogram linkage measures torque and angle without restricting joint motion.

Ames Research Center, Moffett Field, California

A new apparatus measures applied torque and angle-of-flexure in pressurized flexible joints, such as those found in diving suits and flight suits. Torque and flexure are permanently recorded on an x-y plotter. A family of curves can be taken as a function of suit pressure or other variables.

The new test setup is shown in the figure. The angle transducer is a rotary potentiometer, the wiper shaft of which is clamped to a pivoted double-parallelogram reference arm. The moving end of the linkage, to which the potentiometer shaft is attached, remains parallel to the fixed end of the linkage because the opposite sides of the parallelograms remain parallel. Thus the potentiometer shaft remains at a constant reference angle in space when the parallelogram linkage is moved to flex the joint.

Flexing the free end of the pressure-suit joint by moving the free end of the parallelogram linkage rotates the body of the angle-transducer potentiometer with respect to the shaft. Thus the potentiometer resistance is a measure of the flexure angle of the joint.

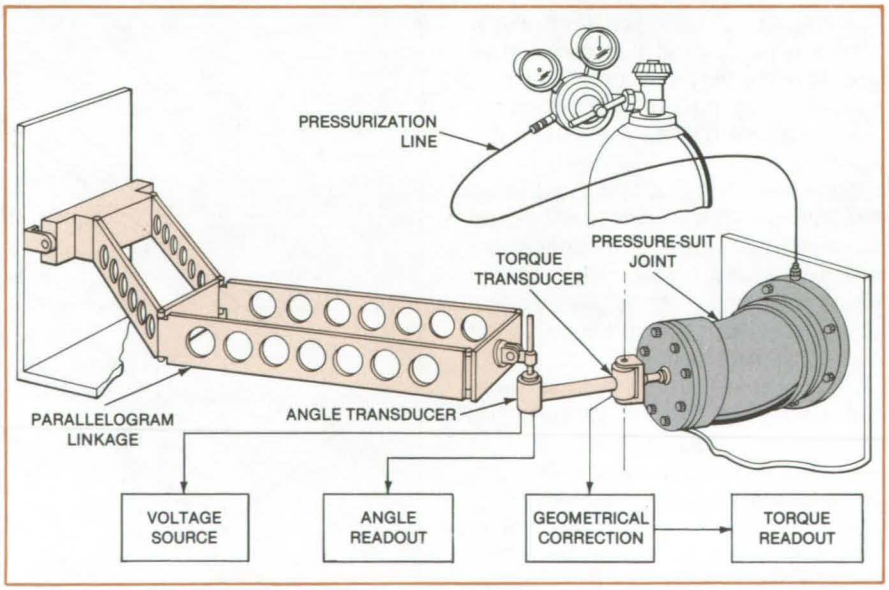

The **System for Testing Pressure-Suit Joints** measures torque applied to the joint as a function of angle-of-flexure.

The torque transducer is mounted at the movable end of the joint under test. Since its signal is proportional to the torque at the location of the transducer, the signal is multiplied by a geometrical correction factor to convert it to the torque acting at the point of flexure of the joint under test.

In some tests, measurements of additional variables may be required. Some

types of pressure joints, such as the rolling convolute design, must be measured during flexure because the torque drops to zero as soon as the joint becomes static. In this case the rate-of-change of the angle is an important variable; the angle signal could be differentiated to produce a rate signal. The apparatus could also measure torque-versus-angle in mechanical linkages.

This work was done by Hubert C. Vykukal and Bruce Webbon of **Ames Research Center.** *For further information, Circle 43 on the TSP Request Card.*

Inquiries concerning rights for the commercial use of this invention should be addressed to the Patent Counsel, Ames Research Center [see page A5]. Refer to ARC-11314.

Modular Engine Instrumentation System

Modules measure key combustion parameters of reciprocating engines.

Lewis Research Center, Cleveland, Ohio

Research intended to improve the performance of internal-combustion engines has always been hindered by a lack of understanding of the combustion process. Data from these processes have been tedious to obtain and analyze.

A system (see figure) that provides information and measurements never obtained before in real time has been developed. This system shows not only the real-time measurements but also the results of computations of key combustion parameters in a meaningful and easily understood display.

A number of important parameters, such as indicated mean effective pressure and mass fraction burn rate, are displayed, each by its own module. All parameters are shown versus crank angle positions so that the jitter often seen in time-domain displays as a result of engine speed variation is virtually eliminated. The modules themselves fit into standard racks, and thus new parameters can easily be introduced and displayed by simply adding the required modules.

A standard commercially-available shaft encoder plus data from the pressure transducer act as the principal drivers to the device. Otherwise, this is a stand-alone system because no external computer is required.

In addition to the utility of the system in visualizing and understanding the combustion process, it is anticipated that if further developments in the miniaturization of instruments and suitable algorithms were to occur, this system could eventually be adapted to onboard control of automotive engines.

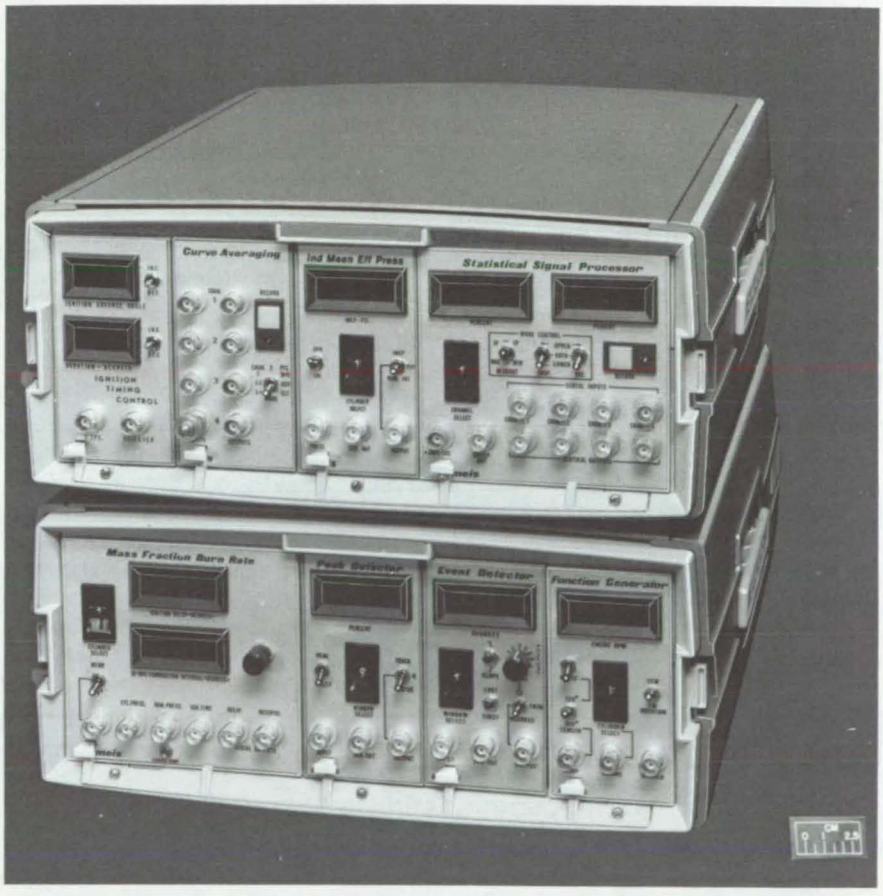

The **Engine Instrumentation System** is assembled from commercially available modules such as these. Eventually, the modular system could be developed into an onboard controller for automobile engines.

This work was done by W. J. Rice and A. G. Birchenough of **Lewis Research Center.** *Further information may be found in NASA TP-1757 [N81-11315/NSP], "Modular Instrumentation System for Real-Time Measurements and Control on Reciprocating Engines" [$5]. A copy may be purchased [prepayment required] from the National Technical Information Service, Springfield, Virginia 22161.*

Inquiries concerning rights for the commercial use of this invention should be addressed to the Patent Counsel, Lewis Research Center [see page A5]. Refer to LEW-13729.

Algorithm for Unsteady Potential Flow About Airfoils

Algorithm efficiently solves the unsteady-potential-flow equations in conservation form.

Ames Research Center, Moffett Field, California

An implicit finite-difference scheme efficiently computes the unsteady potential flow about airfoils. The formulation uses density and velocity potential as dependent variables. Conservation form is retained to assure that shock-wave location and speed are computed correctly.

The unsteady-potential-flow mass- and momentum-conservation equations are written and transformed to a time-varying, sheared-rectilinear, body-conforming coordinate system (see figure). This allows the boundary conditions to be directly imposed on the instantaneous airfoil surface. An implicit scheme time-integrates the equations. Then, a finite-difference equivalent of the differential equations is constructed, introducing artificial viscosity to capture shocks. The result is a linear system of equations in the dependent variables. A numerically-stable approximate factorization of these equations is constructed to enable an efficient alternating-direction algorithm to solve the equations.

The use of artificial viscosity results in improved shock resolution compared to the results obtained when artificial compressibility is used. The retention of density as a second dependent variable eliminates the separate calculation of density that is required in other formulations.

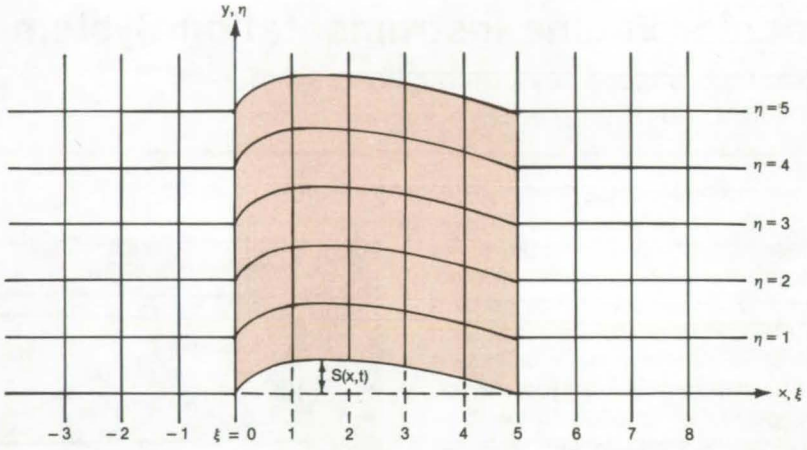

A Time-Varying, Sheared-Rectilinear Coordinate System [$\xi = x, \eta = y - S(x, t)$] is used to impose the airfoil boundary conditions. $y = S(x, t)$ represents the instantaneous coordinates of a point on a fluttering airfoil surface.

The scheme fills a need for a method to calculate efficiently the unsteady potential flow about airfoils and to predict flutter and other unsteady aeroelastic phenomena in transonic flow regimes. Wind-tunnel testing is less desirable than computation because of the extensive facilities required, and linearized solutions about steady flows are valid only in limited applications. Previous finite-difference methods were more complex and less efficient.

This work was done by Richard Chipman of Grumman Aerospace Corp. for **Ames Research Center.** *For further information, Circle 44 on the TSP Request Card.*
ARC-11378

Using Nomarski Interference to Detect Microcracks in Glass

Technique can find applications in the inspection of glass and glasslike materials.

Goddard Space Flight Center, Greenbelt, Maryland

Nomarski interference-contrast microscopy has been proposed as a technique for detecting, measuring, and observing Griffith microcracks in glass and glasslike substances (for example, quartz and glasslike ceramics). It would facilitate research into the cause and elimination of these flaws, along with the short-and long-term effects of temperature, humidity, and other conditions.

Griffith microcracks cause a weakening of finished or unfinished components. These cracks appear to worsen with age, further weakening the structure and causing the degradation of critical optical-surface contours. Conventional methods for observing these cracks include ion exchange and variations thereof and various chemical and electrochemical processes. These are time consuming and damaging to the test piece. The Nomarski interference-contrast technique is nondestructive.

With the application of the technique to an optical problem at Goddard Space Flight Center, a controlled grinding/lapping process was found to eliminate the flaws. It is expected that the Nomarski interference-contrast technique will find wide use in the inspection of glass and other materials.

This work was done by Charles M. Fleetwood, Jr., of **Goddard Space Flight Center.** *No further documentation is available.*
GSC-12649

Torque Simulator for Rotating Systems

Torque is generated by magnetism, and rotation is sensed optically.

Langley Research Center, Hampton, Virginia

A new torque brake simulates varying levels of friction in the bearings of a rotating body. Originally developed to simulate friction in the free-rolling tail of a rocket, the new torque brake could help in the design of windmills and other rotating systems.

The simulator produces a constant torque, selectable between 0 and 6 inch-pounds (0 and 0.7 m-N), for various flow fields and for rotation speeds from 20 to 1,000 rpm. Output signals give a measure of torque and rotation speed.

Previous tests to determine rocket aerodynamic-control characteristics could only be made with fixed-tail or free-tail configurations. The new system allows for the first time an in-depth study of the effects of tail-fin spin rates on pitch-, yaw-, and roll-control characteristics.

As illustrated in Figure 1, the tail rotates on bearings and is coupled to an electromagnet by a sliding ring, which makes up part of the magnetic path. The magnet is mounted on a strain-gage torque balance, which measures the torque between the tail and the model.

The ring coupling is attracted to the electromagnet with a force proportional to the current in the coil. The magnetic force between the two parts produces the torque. A nonmagnetic hard surface coating is flame-sprayed onto the sliding surfaces to reduce wear and to create a magnetic gap to eliminate residual magnetism, which would otherwise produce a large torque after the applied current is removed.

The speed transducer is an infrared emitter and phototransistor mounted in the coil slot. A reflecting ring with alternate black and white segments is mounted in the torque-brake ring to cause a pulsed output from the photospeed transducer.

The rotating wheel shown in Figure 2 contains 60 segments, allowing a direct reading in rpm on the counter front-panel display. A calibrated torque-command voltage fed into the servoamplifier circuits drives the torque brake. The torque is sensed by the strain-gage balance, which produces a feedback signal for servocontrol. This signal is fed to the notch filter, which dampens vibrations in the balance.

The tail may rotate in either direction, producing a feedback signal of either polarity. The full-wave rectifier circuit insures that the signal at the summing amplifier is of the correct polarity. The torque limit circuit limits the torque to any preset value and prevents damage to the balance should the torque command be set too high. The system holds the preset value constant to 0.01 inch-pound (0.001 m-N) throughout its speed range of 20 to 1,000 rpm.

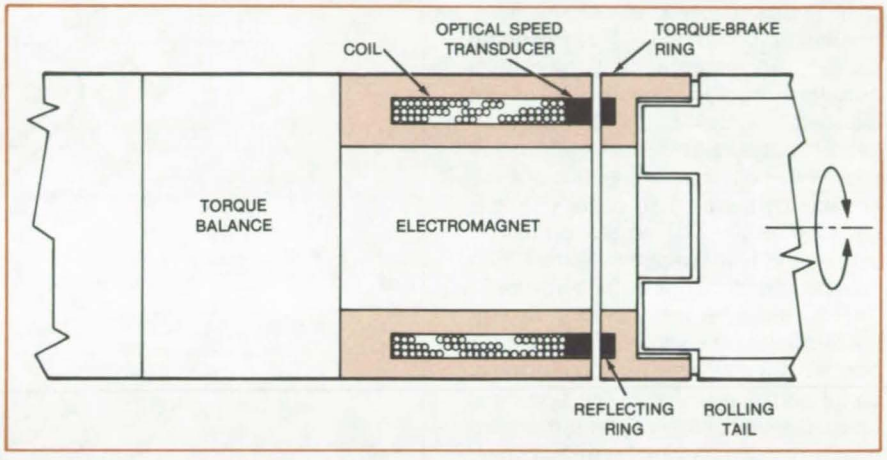

Figure 1. The **Rolling-Tail Torque Brake** uses magnetic force to produce friction between a rotating part and a stationary part.

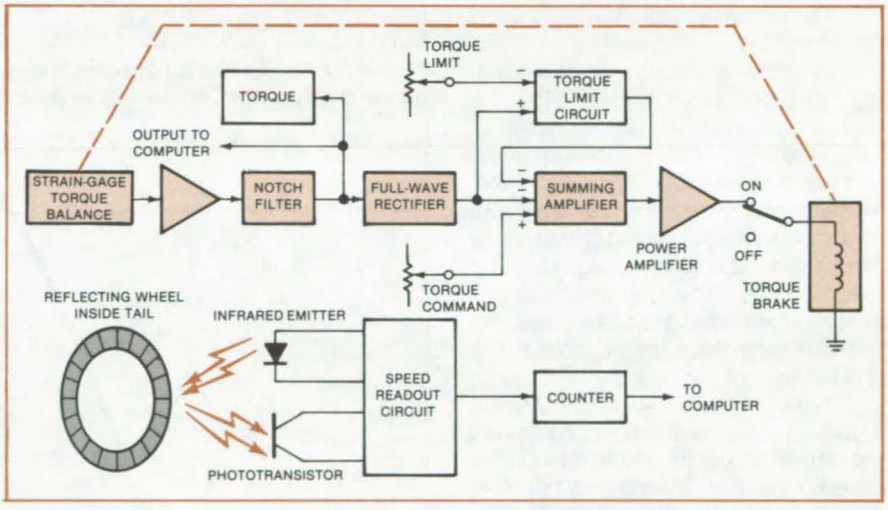

Figure 2. The **Simulator Electronics** produce a positive or negative feedback signal, depending on the direction of rotation.

This work was done by William T. Davis of **Langley Research Center.** *No further documentation is available.*

Inquiries concerning rights for the commercial use of this invention should be addressed to the Patent Counsel, Langley Research Center [see page A5]. *Refer to LAR-12751.*

Explosively Actuated Opening for Rapid Egress

Add-on, minimal-modification system uses a flexible linear-shaped charge.

Langley Research Center, Hampton, Virginia

In support of a stall/spin flight-research program at Langley Research Center, an emergency pyrotechnic-actuated egress system has been qualified for use in a light general-aviation airplane. This system allows the pilot to bail out from the left side of the airplane by creating an opening where no door exists. The egress system is simple and highly responsive, requiring minimal modifications to the airplane.

The new emergency system uses a small quantity of explosive [less than 0.4 ounce (11.3 gm)] to sever and jettison a panel from the airplane. The system is initiated mechanically when the pilot pulls a pivoting handle. From that point, the system functions automatically. Safety features are incorporated to prevent inadvertent actuation on the ground and in flight.

A pyrotechnic-actuated egress opening is more advantageous than a mechanical system on the basis of structural modification, performance, and potential for success. A mechanical system would require considerable structural modification and reanalysis to incorporate a door and release mechanisms. The pyrotechnic approach is an add-on system based on previous experience gained in the F-111 and B-1 escape modules.

A flexible linear-shaped charge (see Figure 1) provides the energy to sever the aircraft structure and to jettison the severed material. The inboard explosive fragments and sound/pressure wave are contained by a closed volume around the explosive (see Figure 2.). Constructed of aluminum angle and channel, the lightweight containment structure flexes to dissipate the explosive energy in metal deformation and heat. Closed-cell foam, installed in the closed volume, prevents the entry of such contaminants as water and dust and also further seals the closed volume by filling vent paths.

The severed structure is jettisoned by the explosive pressure wave driving against an externally-mounted cold-rolled steel strip. This exterior strip is mounted on the material to be jettisoned, directly opposite the flexible

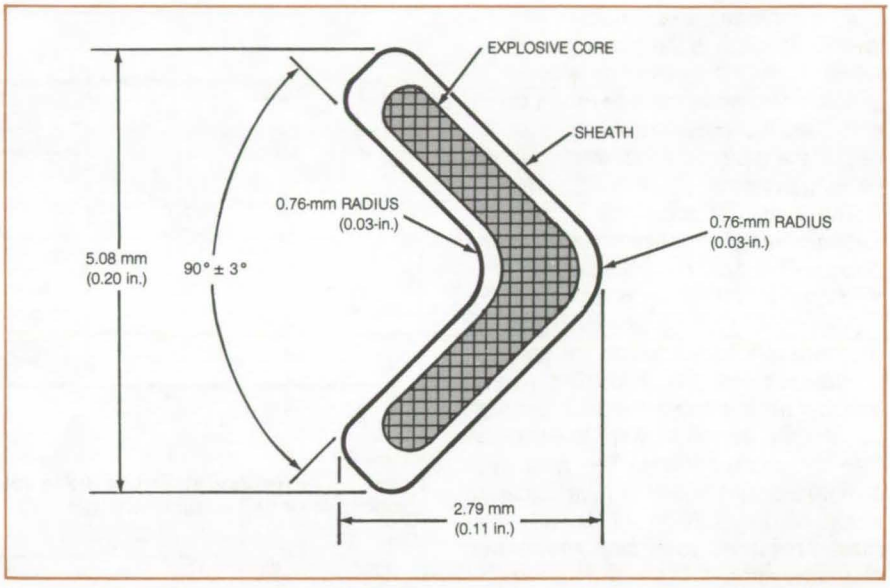

Figure 1. A **Flexible Linear-Shaped Charge** (0.3-gram/meter, 15-grains/foot, less than 0.4 ounce total) provides explosive energy to create an opening and to jettison a panel.

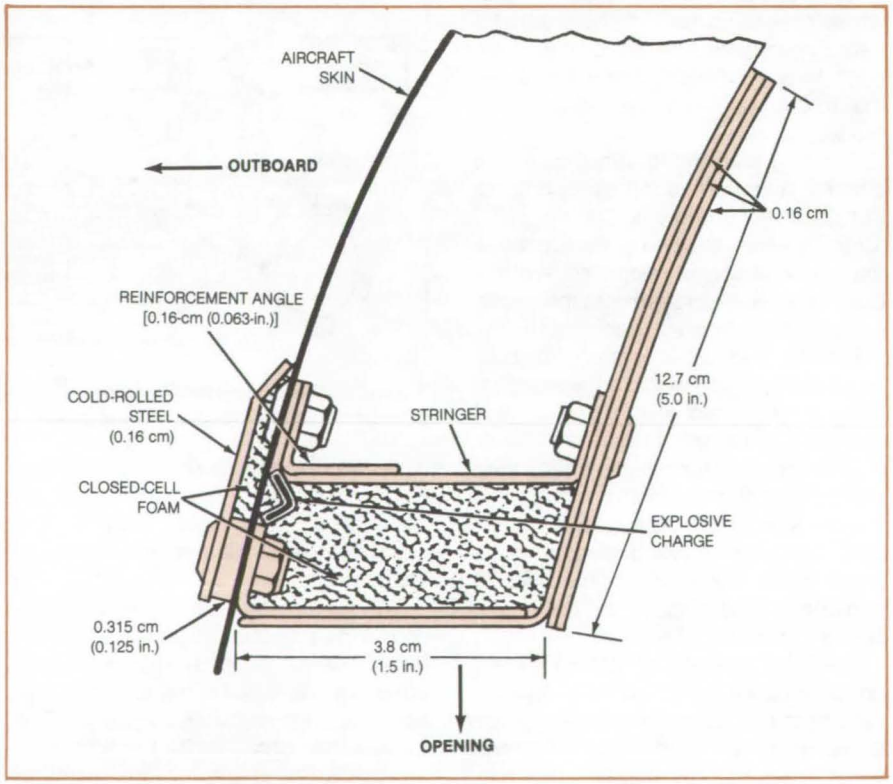

Figure 2. A **Container Around the Explosive Charge** protects the pilot from the effects of the explosion. The exterior steel strip receives most of the force of the explosion to jettison the severed panel.

linear-shaped charge. The resulting severed edges of the opening are neat and smooth, presenting minimal interference to the pilot on egress.

System reliability has been demonstrated by previous aerospace applications and by functional tests. The pyrotechnic components and performance principles have been qualified on such aircraft systems as the F-111 and B-1 escape modules. All functional parameters have been tested, and they demonstrate substantial performance margins. The system requires no maintenance except for a 5-year replacement cycle on the detonator. This technology is suitable for creating egress openings or for other requirements in any vehicle or structure of similar construction.

This work was done by Laurence J. Bement of **Langley Research Center** *and James W. Bailey and Ronnie Perry of LTV Corp. Further information may be found in NASA TM-80235 [N80-21293/NSP] "Emergency In-Flight Egress Opening for General Aviation Aircraft" [$4]. A copy may be purchased [prepayment required] from the National Technical Information Service, Springfield, Virginia 22161.*

Inquiries concerning rights for the commercial use of this invention should be addressed to the Patent Counsel, Langley Research Center [see page A5]. Refer to LAR-12624.

Vibration Analysis With Finite Dynamic Elements

Structural discretization by finite dynamic elements yields equations for fast solution by computer.

NASA's Jet Propulsion Laboratory, Pasadena, California

To enhance the usefulness of computers in solving engineering problems, new techniques are being developed for numerical analysis of structural dynamics. Two aspects of this analysis — structural discretization with finite dynamic elements and the solution of the resulting equations — have been applied in detail to membrane and plane stress/strain continua.

In essence, a finite dynamic element is a mathematical representation of a structural element with higher-order dynamic correction terms. The adoption of finite dynamic elements (FDE's) in place of finite elements permits the use of a coarser mesh and significantly reduces the solution time for problems in the free vibrations of structures. The FDE's achieve essentially the same level of solution accuracy as higher-order finite elements, without the increased solution cost that is inherent with the FE's. A new, triangular, plane stress/strain element is shown in the figure.

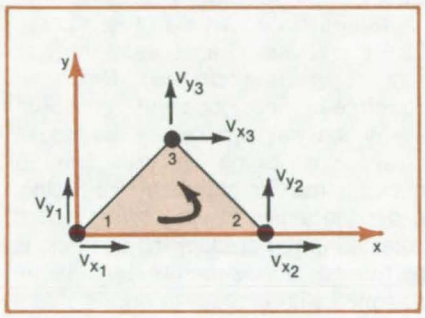

A **Triangular Plane Stress/Strain Element** used in the dynamic element method of numerical analysis is shown with the in-plane displacement velocities V_x and V_y at each corner.

This work was done by Kajal K. Gupta of Caltech for **NASA's Jet Propulsion Laboratory.** *For further information, Circle 45 on the TSP Request Card. NPO-15087*

Books and Reports

These reports, studies, and handbooks are available from NASA as Technical Support Packages (TSP's) when a Request Card number is cited; otherwise they are available from the National Technical Information Service.

Elastic Surface Wrinkling

Instability phenomena in elastic surfaces subject to compressive stresses are examined theoretically.

A new report describes a theoretical study of waves on the surfaces of elastic mediums. The theory is potentially applicable to such practical problems as aircraft panel flutter, nondestructive testing, piezoelectric transducer design, the distortion of optical surfaces, and tolerance studies of very precise machine parts.

The physical model for the study is the free surface of an elastic body streamlined by the flow of an inviscid fluid. The equations of motion are formulated from the principle of virtual work, for small surface displacements and corresponding fluid velocities. Motion of the whole body is not considered: Rather, the potential-energy term in the equation of motion includes only elastic strain energy due to displacements at and near the surface, and the kinetic-energy term likewise includes only velocities in the surface region.

An equation is obtained for the motion of the surface in a direction perpendicular to itself. The equation is further specialized by setting the potential energy for shearing deformations in the fluid equal to zero for the inviscid case and by incorporating the stress/strain relations for an isotropic elastic body.

The resulting wave equation serves as a boundary condition relating the three-dimensional equations of fluid and elasticity for the two mediums. The equation is also of interest in itself since

(continued on next page)

it can be used to derive qualitatively some basic dynamic properties of the free surfaces of elastic bodies. Consideration of the propagation of high-frequency oscillations with small displacements transverse to the surface leads quite naturally to results that depict instabilities — that is, waves that grow from infinitesimal to finite amplitudes. Microroughness or wrinkling is an instance of this.

The onset of wrinkling can be described by a quantitative criterion, which shows that the stability of the smooth surface shape decreases with an increase in tangential compressive stress and/or in fluid velocity. Surface contraction appears to have a low-compression regime in which smoothness is not affected and a high-compression regime in which free-surface filaments can be considered to buckle when the longitudinal stress exceeds a limiting value.

The theory has been applied to a cylindrical linear elastic shaft rotating in an inviscid fluid. Even when the shaft transmits no torque to a load, the equations show that wrinkles will be induced by the mere rotation of the shaft when the angular velocity exceeds the critical value.

This work was done by Michail Zak of Caltech for **NASA's Jet Propulsion Laboratory.** *To obtain a copy of the report, Circle 46 on the TSP Request Card.*
NPO-15091

Computer Programs

These programs may be obtained at very reasonable cost from COSMIC, a facility sponsored by NASA to make new programs available to the public. For information on program price, size, and availability, circle the reference letter on the COSMIC Request Card in this issue.

Structural Design With Stress and Buckling Constraints

Weight is minimized for a given layout subject to prescribed constraints.

The structural designer is seldom required to create a structure that will only serve its primary function. Usually the designer is expected to meet such additional objectives as minimum weight and cost.

DESAP 2 synthesizes linear-elastic structures under static loads. Its objective is to find the element sizes (cross-sectional areas, plate thicknesses, and the like) that minimize the total structural weight without changing the layout of the structure.

The primary constraints used in the DESAP 2 synthesis algorithm are upper limits on stresses and lower bounds on buckling loads. The stress limits may be prescribed in the form of yield criteria, local instability criteria, or both. Any number of load conditions may be imposed on the structure for the stress-constrained design. However, for considerations of economy, only one load condition may be imposed for the buckling-constrained design. Secondary constraints consisting of minimum allowable element sizes and size proportion constraints may also be imposed.

The design procedure employed in DESAP 2 is an iterative process with each iteration consisting of four parts. First a prebuckling analysis of the current design is performed. Next, the structure is redesigned with respect to stress constraints based on the results of the prebuckling analysis. Then a buckling analysis of the current design, under the action of the internal forces obtained in the prebuckling analysis, is performed. The structure then is redesigned with respect to buckling with the element sizes determined in step two being used as minimum size constraints. The classical stress-ratio method is employed with respect to stress constraints. This procedure will drive the final design to the fully stressed design, which does not necessarily coincide with the minimum weight distribution of the material. For the constraints on the general buckling loads, the redesign procedure is derived directly from an optimality criterion. Consequently, the element sizes converge toward the minimum weight design.

Inputs to DESAP 2 consist of an initial finite-element model of the structure and a set of constraint conditions. Basic structural elements available in DESAP 2 include three-dimensional bars, three-dimensional beams, quadrilateral and triangular-plane stress elements, quadrilateral shear panels, quadrilateral and triangular plate elements, and a special boundary element. The boundary elements can be used to model elastic supports, to enforce displacements or rotations, and to allow the computation of support reactions. Allowances have been made for such element-size-dependent loads as thermal stresses and gravity loading. Outputs from DESAP 2 consist of a redesign history, the final structural weight, and the redesigned element sizes.

DESAP 2 is written in FORTRAN IV for batch execution and has been implemented on an IBM 370-series computer with a central memory requirement of approximately 330K of 8-bit bytes. DESAP 2 was developed in 1977.

This program was written by J. Kiusalaas and G. B. Reddy of The Pennsylvania State University for **Marshall Space Flight Center.** *For further information, Circle D on the COSMIC Request Card.*
MFS-25234

Plastic and Large-Deflection Analysis of Nonlinear Structures

System considers bending and membrane stresses, general three-dimensional bodies, and laminated composites.

The Plastic and Large Deflection Analysis of Nonlinear Structures (PLANS) system is a collection of five computer programs for the finite-element static-plastic and large-deflection analysis of a variety of nonlinear structures. Four of the programs, BEND, HEX, REVBY, and OUT-OF-PLANE MG, employ finite-element techniques to calculate static structural responses. The four analysis programs are capable

of treating problems that contain bending and membrane stresses, thick and thin axisymmetric bodies, general three-dimensional bodies, and laminated composites. Each program is associated with a distinct physical problem class and has its own finite-element library. The fifth program, SATELLITE, is a math-model preprocessor for data debugging, plotting of input geometries, and node resequencing.

BEND computes the static-elastic, elastic-plastic, and elastic-cyclic-plastic response of arbitrary built-up thin-walled structures where bending and membrane effects are equally important. The BEND element library includes a three-node uniform strain triangle, a six-node linearly-varying strain triangle, both a four- and a five-node hybrid triangle for use as a transition element, a two-node uniform strain stringer, a three-node linearly-varying strain stringer, a variety of cross sections for beams that may be subjected to bending about two planes as well as torsion, and a higher-order triangular plate element with bending and membrane capabilities.

HEX performs the static-elastic, elastic-plastic, and elastic-cyclic-plastic response of arbitrary three-dimensional solid structures. For modeling, HEX offers a family of isoparametric hexahedron elements consisting of a basic 8-node hexahedron and higher order hexahedrons with up to 12 additional midside nodes.

REVBY was developed for the static-elastic, elastic-plastic, and elastic-cyclic-plastic analysis of orthotropic axisymmetric solids of revolution subjected to axisymmetric loadings. Three different elements are available in REVBY for the analysis of both thick and thin bodies of revolution. These consist of a revolved triangular element, a thin shell element, and a thin-ring stiffener element.

OUT-OF-PLANE MG is used for the static nonlinear analysis of built-up thin-walled structures, including the effects of combined material and geometric nonlinearities; however, bending and membrane effects are not considered significant. The OUT-OF-PLANE MG element library includes a three-node uniform stress triangle, a six-node linearly-varying stress triangle, both a four- and a five-node hybrid triangle for use as a transition element, a two-node uniform stress stringer, a three-node linearly-varying stress stringer, and a variety of cross sections for beams that may be subjected to bending about two planes as well as torsion.

SATELLITE is a data preprocessor for the BEND, REVBY, and OUT-OF-PLANE MG programs. The SATELLITE program checks and plots the undeformed math model to aid the user in detecting modeling errors. An option is also included for reordering the node numbers such that the minimum semibandwidth is achieved, thus improving the efficiency of the analysis programs.

All four of the analysis programs employ the "initial strain" concept within an incremental procedure to account for the effect of plasticity and to include the capability for cyclic-plastic analysis. The solution procedure for treating material nonlinearities alone reduces to the incremental analysis of an elastic body of identical shape and boundary conditions but with an additional set of applied "pseudoloads." This solution technique does not require modification of the element stiffness matrix at each incremental load step. Combined material and geometric nonlinearities are treated in the OUT-OF-PLANE MG program by using the "updated" or convected coordinate approach.

The PLANS programs are written in FORTRAN IV for batch execution and have been implemented on both a CDC CYBER 175 computer and an IBM 370-series computer. Most of the PLANS programs for the CDC are segmented with the largest having a central memory requirement of approximately 256K (octal) of 60-bit words. Most of the PLANS programs for the IBM are overlaid with the largest having a central memory requirement of approximately 730K of 8-bit bytes. PLANS was developed in 1975 and updated in 1977.

This program was written by R. G. Thomson, R. J. Hayduk, M. P. Robinson, and B. J. Durling of **Langley Research Center** *and A. Pifko, H. S. Levine, H. Armen, Jr., A. Levy, and P. Ogilvie of Grumman Aerospace Corp. For further information, Circle E on the COSMIC Request Card.*
LAR-12816

High-Lift Separated Flow About Airfoils

The effect of massive boundary-layer separation is included.

In the design and analysis of high-performance airfoils, aerodynamicists would like not only to be able to compute cruise behavior but also to predict airfoil pressure distributions at high-lift, high-angle-of-attack conditions. Since such conditions are characterized by large regions of separated flow and are dominated by strong viscous interaction effects, inviscid methods are not applicable.

TRANSEP calculates the flow field about a low-speed single-element airfoil at high-angle-of-attack and high-lift conditions with massive boundary-layer separation. Since TRANSEP includes the effects of weak viscous interactions, it can also be used for subsonic/transonic airfoil design and analysis. The approach used in TRANSEP is based on the direct-inverse method and its ability to use either the displacement surface or pressure as the airfoil boundary condition.

In the present TRANSEP code, the turbulent boundary layer is computed using the Nash-Macdonald method. For the laminar portion, the boundary layer is computed using a compressible Thwaites method. These integral methods are efficient and reliable and yield excellent predictions for displacement-thickness values. Internally, the transition point is determined from a Granville-type correlation based upon the difference between the local momentum-thickness Reynolds number and the value at the laminar instability point combined with the pressure gradient history.

The calculation procedure used in TRANSEP is an iterative successive-column-relaxation scheme with the separation point and separated pressure level being permitted to vary. This scheme has been found to generate values that quickly converge.

TRANSEP inputs consist of airfoil geometry, free-stream conditions,

(continued on next page)

angle-of-attack, and solution-control parameters. Outputs for each grid in the massive separation solution include iteration history, laminar boundary-layer values, turbulent boundary-layer values, final boundary-layer results, pressure distribution, and wave drag coefficient.

TRANSEP is written in FORTRAN IV for batch execution and has been implemented on a CDC CYBER 70-series computer with a central memory requirement of approximately 103K (octal) of 60-bit words. TRANSEP was developed in 1980.

This program was written by Leland A. Carlson of Texas A. & M. University for **Langley Research Center.** *For further information, Circle F on the COSMIC Request Card.*
LAR-12853

Machinery

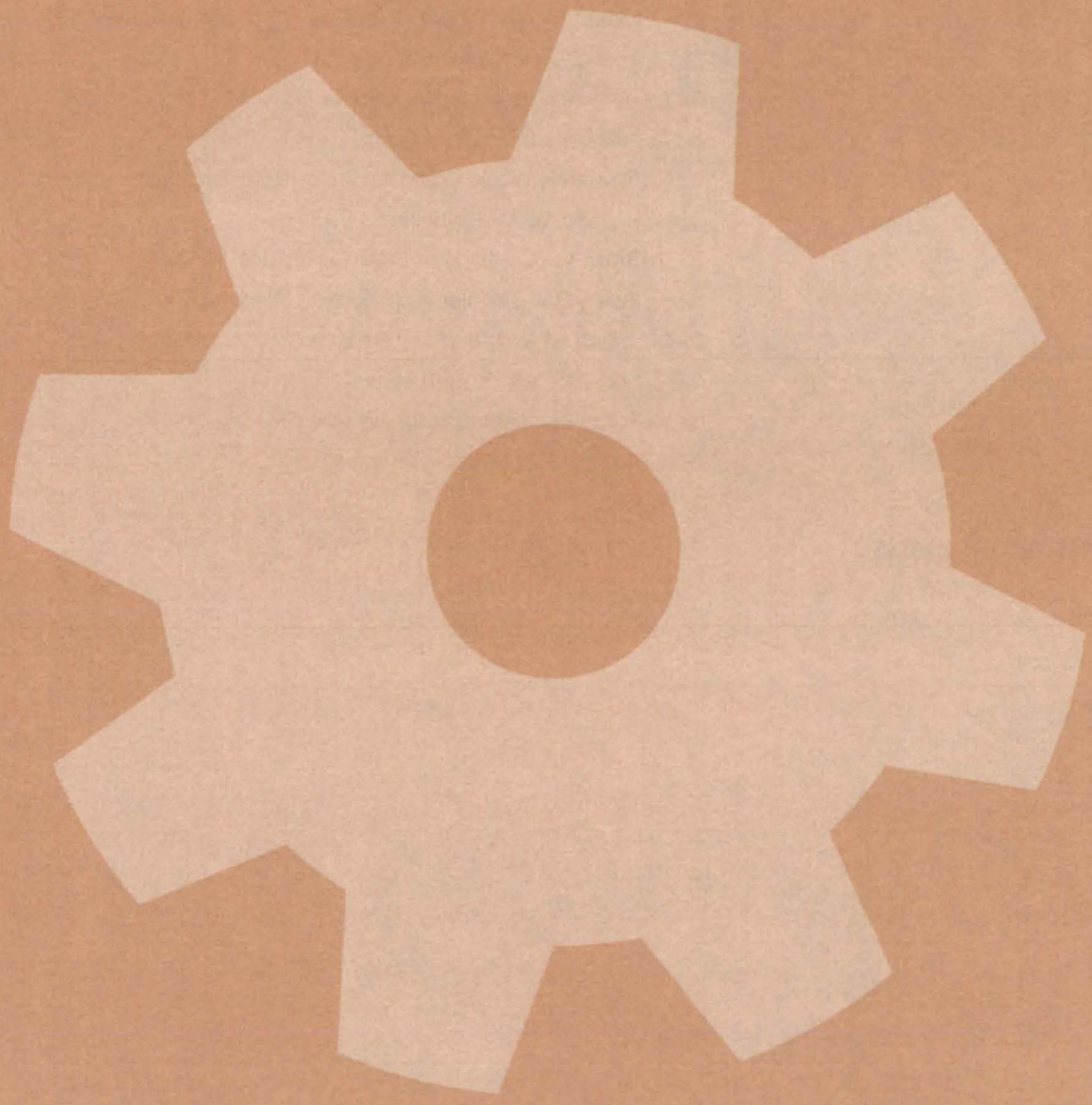

Hardware, Techniques, and Processes

319 A Simple Tiltmeter

320 "Teaching" an Industrial Robot To Spray

320 Hybrid Position/Force Control of Robot Manipulators

321 Precise Restraightening of Bent Studs

322 Universal Assembly for Captive Bolts

323 Articulated Vacuum Chuck

323 Flywheels Would Compensate for Rotor Imbalance

324 High-Speed Wafer Slicer

325 Brushless Cleaning of Solar Panels and Windows

326 Safety Bolt Doubles as a Bushing-Removal Tool

327 Improved Nozzle Would Reduce Cryogenic Boiloff

328 Staking Tool for Hard Metals

329 Force Augmentation for Relief Valve

329 Damping Vibration at an Impeller

Books and Reports

330 Tests of 38 Ball-Bearing Greases

A Simple Tiltmeter

Differential capacitance measurement on a bubble level measures angular orientation.

Ames Research Center, Moffett Field, California

A simple tiltmeter indicates angular orientation to within 0.05 second of arc. Its sensor is a modified spirit level (or bubble level) such as those used on surveyor's transits.

As shown in Figure 1, the vial of the level is covered by aluminum-foil electrodes. One electrode is a reference electrode, covering all of the outside of the vial except the surface over the path of the bubble. The other two electrodes, located symmetrically on either side of the center position for the bubble, are as long and wide as the bubble.

An electrical indication of the bubble position is obtained by a differential meaurement of the capacitances between each sensing electrode and the reference electrode. The liquid in the vial has a dielectric constant of about 80, while the bubble volume has a dielectric constant of 1; the difference in dielectric constant in between the sensing electrodes and the reference produces the changes in differential capacitance.

The measuring circuit for the tiltmeter (see Figure 2) uses a 300-kHz oscillator to excite a diode bridge, which produces a voltage output that depends on the difference in capacitances appearing at either side of the bridge. The circuit has a full-scale output of ±0.7 volt, with stable resolution of 1 millivolt. Measurement resolution is determined by the vial geometry; a level vial with 2 mm deflection for a tilt of 5 arc-seconds easily resolves 0.05 arc-second.

The tiltmeter was developed for an experiment on forecasting seismic events by changes in Earth's magnetic field. A shift in the orientation of the magnetic sensors — caused by settling of the ground, for instance — could produce erroneous signals on the order of those expected from impending seismic activity. In this application a tilt resolution of 0.4 arc-second is adequate, so the higher precision of commercial tiltmeters is not required.

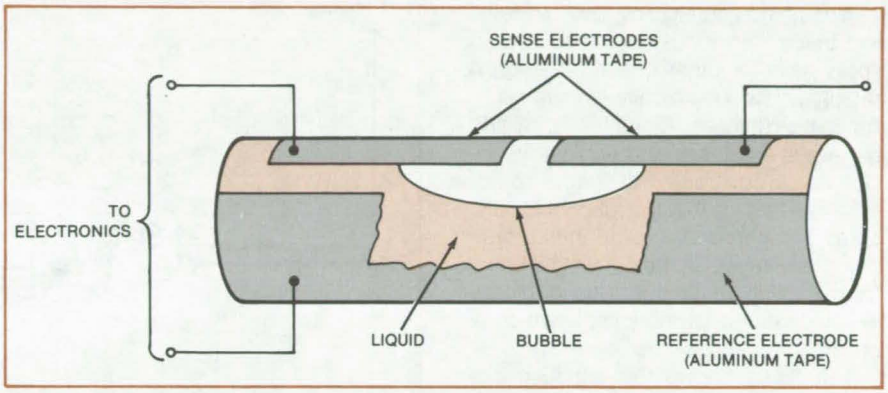

Figure 1. A **Bubble Vial** with external aluminum-foil electrodes is the sensing element for a simple indicating tiltmeter. To measure bubble displacement, a bridge circuit detects the difference in capacitance between the two sensing electrodes and the reference electrode.

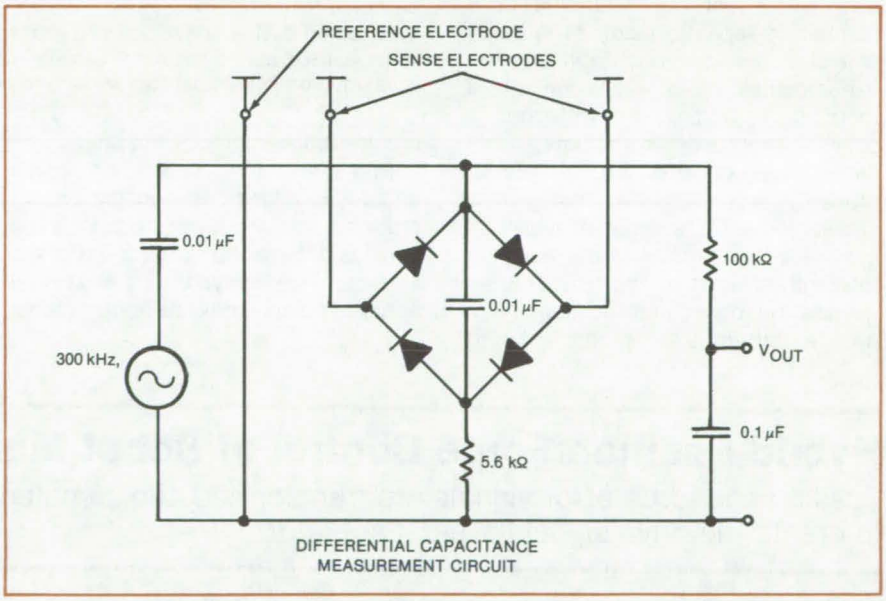

Figure 2. Using this **Differential Capacitance Measurement Circuit,** a tiltmeter level vial with 2 mm deflection for 5 arc-seconds of tilt easily resolves 0.05 arc-second. The four diodes are CA3039, or equivalent.

This work was done by Michael G. Dix, Dean R. Harrison, and Thomas M. Edwards of **Ames Research Center.** *For further information, Circle 47 on the TSP Request Card.*

Inquiries concerning rights for the commercial use of this invention should be addressed to the Patent Counsel, Ames Research Center [see page A5]. *Refer to ARC-11344.*

"Teaching" an Industrial Robot To Spray

A spacing device establishes the spray-head positions for the point-by-point manipulator pattern.

Marshall Space Flight Center, Alabama

A spacing-and-leveling device helps to "teach" an industrial robot how to spray paint (or other coating materials) rapidly and economically over large irregular structures. A point-to-point grid pattern is established to achieve precision spray coverage; the spacer rod or tube makes sure that the robot holds the spray gun perpendicular to the surface being coated and at the correct distance from it. This technique was originally developed for applying an ablative composition to a solid rocket booster.

The figure shows the teaching aid, with its three-point contact and line level, attached to a spray-gun head held by the flexible arm of the manipulator. Point-to-point programing is a system in which the moving pattern of the robot manipulator is "taught" by recording of a number of separate points. The exact time of recording for each point is determined manually — unlike a continuous recording in which a fixed number of points is recorded per unit time. When the recording switch on the handle is depressed, the position of the manipulator at that moment is recorded on a disk for storage. After removal of the teaching tool and initiation of the playback sequence, the robot-controlled sprayer applies a pattern that is constant and precise to the tolerance required.

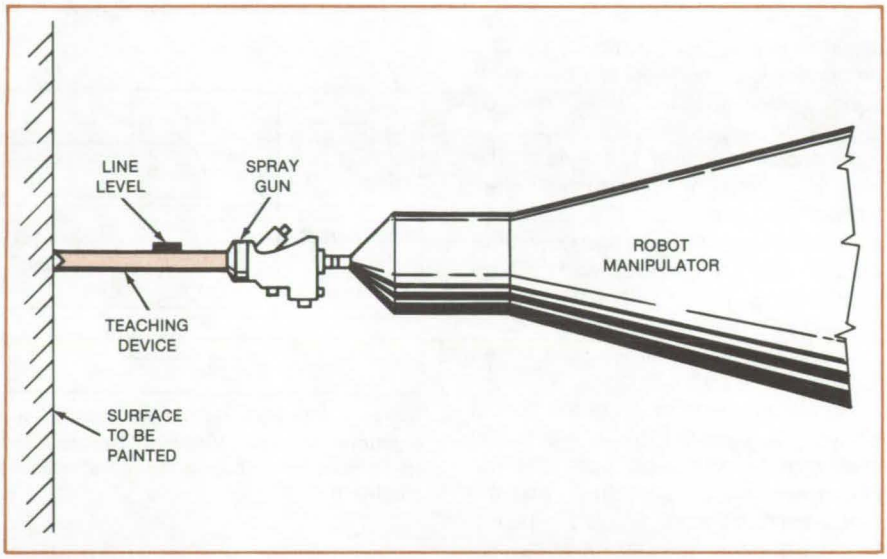

A **Teaching Device,** consisting of a spacer rod or tube with a three-pointed tip and a line level, is used during pattern "teach-in" to make sure that a robot manipulator holds a spray gun perpendicular to a surface to be sprayed and at the right distance from it.

For slanted surfaces, an angle adapter is added between the spacer rod and the line-level indicator. The angle is determined by the slope of the surface to be sprayed, thus allowing a perpendicular spray pattern against even slanted surfaces.

This work was done by A. R. Evans and G. K. Sweet of United Space Boosters Inc. for **Marshall Space Flight Center.** *No further documentation is available.*
MFS-25523

Hybrid Position/Force Control of Robot Manipulators

Position and force error signals are transformed and summed to create the drive signal for each actuator.

NASA's Jet Propulsion Laboratory, Pasadena, California

In a proposed method for the task-oriented control of a robot manipulator, the position and force error signals for each task degree of freedom are used to calculate appropriate control parameters in task coordinates. These are transformed by projection onto the joint space of the manipulator. The final control signal for each axis is a weighted sum of the force and position control parameters provided onto it. Thus there is a continuous control of each actuator responsive to both position and force simultaneously, and there is no need to switch explicitly from one to the other.

As the manipulator operates within a given control regime, there is a gradual changeover shaped by the projection of the changing manipulator geometry. Regimes, which involve the specification of orthogonal position and force control directions in task coordinates, are naturally task dependent and are specified at the time tasks are set up.

In robot manipulators that are used for manufacturing processes, warehouse storage and retrieval, and the like, both the force and the position trajectory (or velocity or acceleration) of each movement must be specified for each task degree of freedom. For example, the simple task of inserting a pin in a socket (see figure) requires position con-

trol along the z-axis and force limiting along the other two axes to prevent scraping against sides of the socket and pin.

The control of these dual modes of operation has involved complex concepts and methods in the past. One approach was to multiplex the sensing and control for each actuator and to choose which mode to employ in each time interval. Thus one actuator might be carrying out a position correction while ignoring the force error caused thereby, while another was responding solely to force error. The result was an output that dithered.

This new hybrid control technique does not require the operator to supply complex transform matrices. The control trajectories are easily visualized in terms of the task to be performed.

This work was done by John J. Craig and Marc H. Raibert of Caltech for **NASA's Jet Propulsion Laboratory.** *For further information, Circle 48 on the TSP Request Card.*
NPO-14997

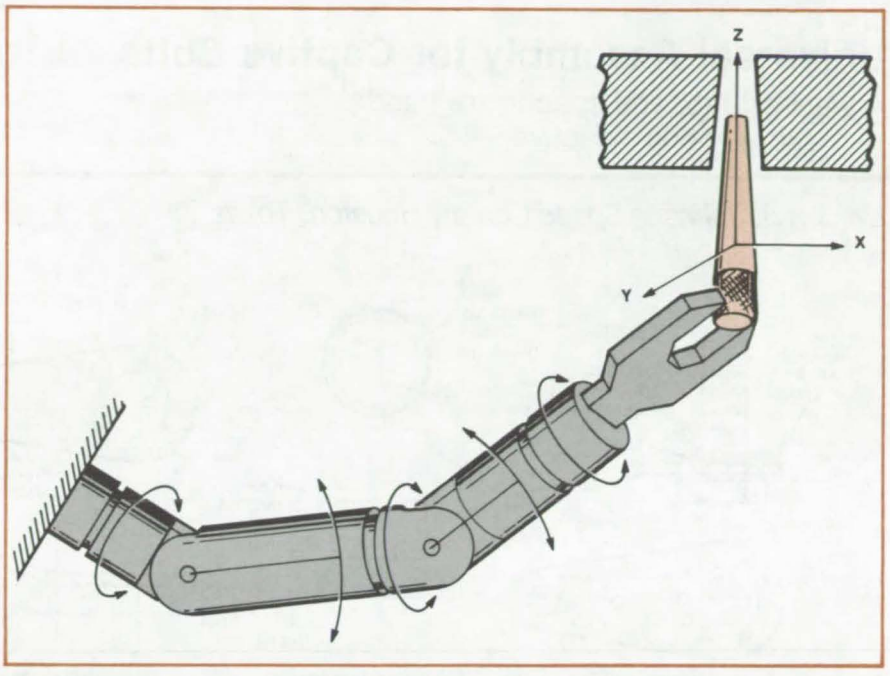

Programed Manipulator control that combines both position trajectories and forces may allow this pin to be inserted in the socket without heavy scraping of the sides.

Precise Restraightening of Bent Studs

A special tool quickly bends studs back into shape.

Marshall Space Flight Center, Alabama

Studs that are used to position and fasten cover plates on hatches, engines, manifolds, or other housings can become bent — sometimes to the extent that the plate cannot fit over them. Replacement of the bent studs is not always desirable because of the time expense, and difficulty involved, as well as the possibility of damage to the housing. Instead, the studs can be bent by a precisely controlled amount to return them to their original locations within the required tolerance.

A special tool, shown in the figure, is used to straighten the discrepant studs. A nut is threaded onto the end of the stud to protect the thread and present a flat surface for thrust and measurement. Then, with a straightening tool in place, pressure is applied to the hydraulic ram until the pressure gage reaches its minimum reading; the dial indicator is set to read zero at that point. Pressure is applied to bend the stud the desired amount, then is released, and then is reapplied just enough to produce the minimum gage reading again. The amount of permanent set is then measured with the dial indicator, and the cycle is repeated until the stud reaches its proper position. Bending direction is reversed by exchanging the positions of the hydraulic ram and the dial indicator.

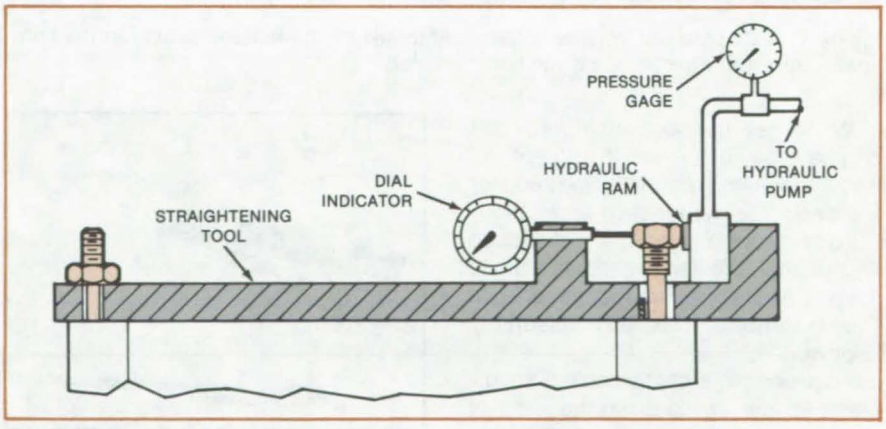

A **Stud Is Straightened** accurately and safely by force applied by a hydraulic ram, with deflection being measured by a dial indicator. The ram and indicator can be interchanged for straightening in the reverse direction.

This work was done by R. E. Boardman of Rockwell International Corp. for **Marshall Space Flight Center.** *No further documentation is available.*
MFS-19632

Universal Assembly for Captive Bolts

A washer, tab, and spacer are used to make any bolt "captive."

Lyndon B. Johnson Space Center, Houston, Texas

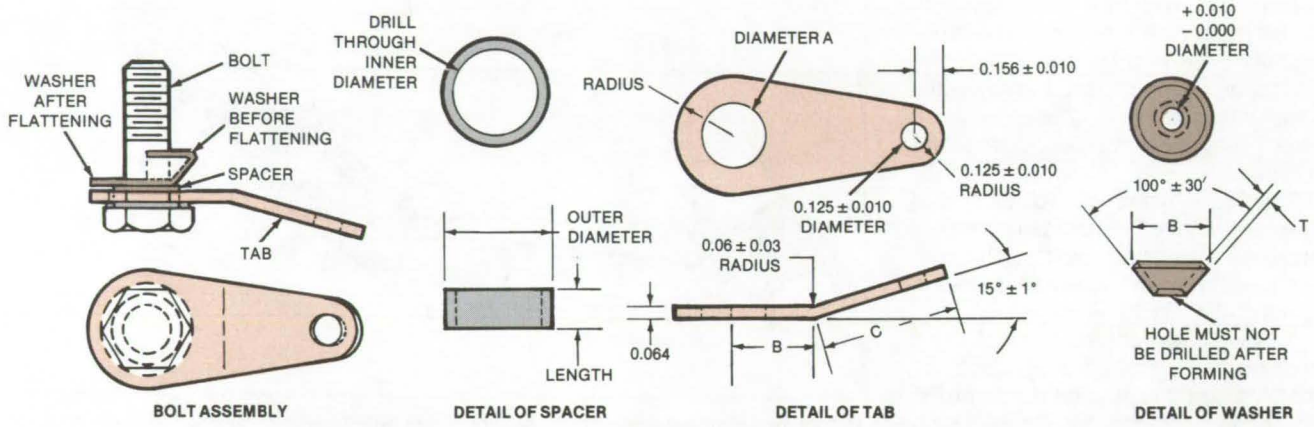

BOLT	SPACER			TAB				WASHER		
NOMINAL DIAMETER	LENGTH ± .010	INNER DIAMETER	OUTER DIAMETER ± .010	A ± .010	B ± .03	C ± .03	R ± .010	DIAMETER A	DIAMETER B ± .010	T
.190	.109	.191	.312	.332	.41	.59	.328	.190	.420	.020
.250	.109	.257	.375	.395	.41	.59	.328	.250	.480	.032
.312	.109	.316	.438	.458	.41	.59	.328	.312	.540	.032
.375	.109	.377	.500	.520	.59	.53	.453	.375	.600	.032
.438	.109	.453	.625	.645	.59	.53	.453	.438	.720	.040
.500	.109	.516	.688	.708	.59	.53	.453	.500	.845	.040
.562	.109	.578	.812	.832	.75	.50	.546	.562	1.030	.040
.625	.109	.641	.875	.895	.75	.50	.546	.625	1.094	.040
.750	.109	.766	1.000	1.032	1.00	.50	.750	.750	1.312	.040

Figure 1. A **Cup-Shaped Washer** is flattened to secure the tab and spacer to the bolt. The table shown gives the dimensions of the spacer, tab, and washer for a given bolt diameter.

With a new method, virtually any bolt can be easily converted to a "captive" bolt. The method eliminates the need for a separate design for each application.

As shown in Figure 1, a cup-shaped washer that is flattened secures a tab to the bolt. A wire (see Figure 2) attached to the tab holds the bolt assembly captive.

To assemble a captive bolt, a snugly fitting spacer is slid down the shaft of the bolt, and a tab with an opening slightly larger than the spacer is slipped over the spacer. After this combination is in place, a cup washer is placed over it. The dimensions of the spacer are such that the tab fits loosely on the finished bolt and can turn freely about it without coming off.

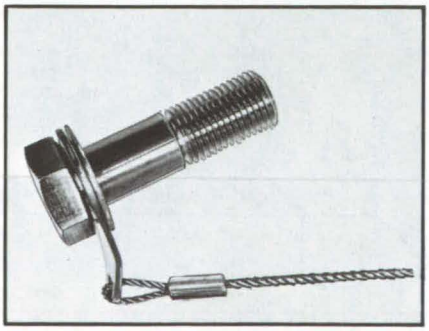

Figure 2. The **Captive Bolt** when it is not in use can hang loosely from the wire attached to its tab.

By threading the bolt into a flat-faced surface, the cup washer is flattened to grip the bolt shaft and secure the spacer and tab. Flattening the washer can also be done during installation of the bolt. The washer, tab, and spacer are all made of corrosion-resistant steel.

This work was done by Michael L. Marke and Berge Hagopian of Rockwell International Corp. for **Johnson Space Center.** *No further documentation is available.*

MSC-18905

Articulated Vacuum Chuck

A pull tool conforms to the work surface.

Lyndon B. Johnson Space Center, Houston, Texas

A vacuum chuck originally developed to pull-test Space Shuttle surface tiles conforms to complex surface contours. Its gripping surface is a polyurethane panel embedded with links of roller chain. The panel flexes under vacuum to adjust to the surface contour, and then bolts are tightened to lock the configuration. Possible applications of the new chuck are in pull-testing contoured surfaces, holding assemblies together for repairs, or for handling unusually-shaped parts.

As shown in the photograph, eight hexagonal-cap bolts can be tightened to lock an array of slotted plates after vacuum is applied. (The vacuum line is not visible in the photo.) In all, there are 112 plates arranged in 8 groups of 14 each. The bottoms of the plates are linked by lengths of roller chain embedded in the polyurethane. A load can be applied to the clevis at the top of the chuck.

This work was done by Scott A. Peterson of Rockwell International Corp. for **Johnson Space Center.** *For further information, Circle 49 on the TSP Request Card.*
MSC-18933

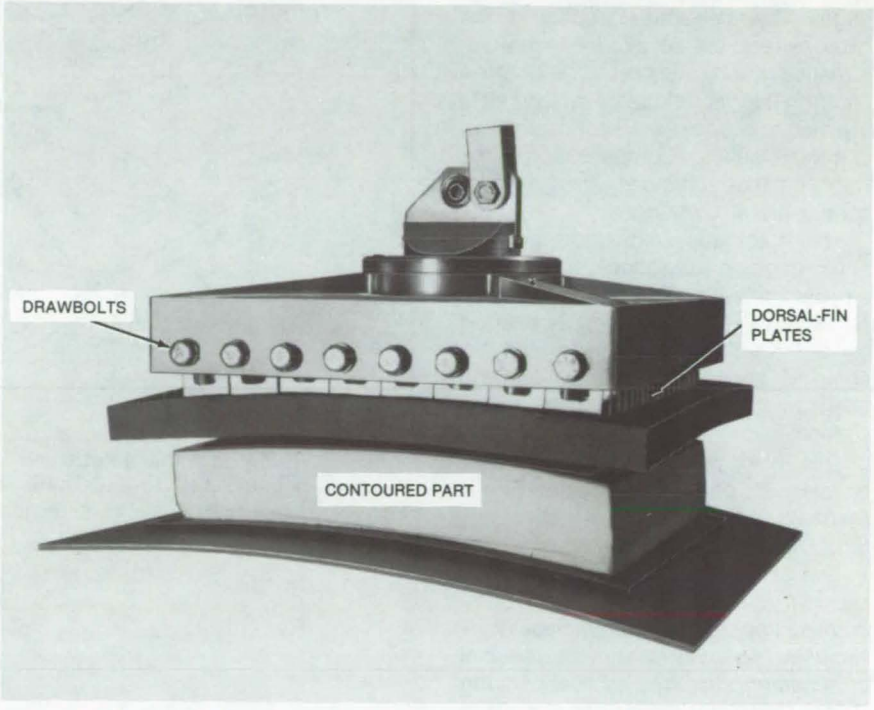

Articulated Vacuum Chuck conforms to the contoured part. The vacuum is applied, and then the drawbolts are tightened, freezing the chuck shape with that of the work.

Flywheels Would Compensate for Rotor Imbalance

Gyroscopic action is proposed to cancel dynamic imbalance in rotating structures.

Goddard Space Flight Center, Greenbelt, Maryland

A concept for correcting imbalance in spinning bodies exploits the gyroscopic action of flywheels attached to the body. The speeds of the flywheels would be automatically regulated to null the dynamic forces transmitted to the bearings.

Although originally developed for space platforms, the concept should also be useful for compensating rotating bodies on Earth. For example, it may be applied to a large industrial centrifuge, particularly if its balance changes during operation.

Imbalance forces arise to some extent in any body rotating about a fixed axis and connected to a fixed platform. This is because manufacturing imperfections make it impossible to produce a truly symmetrical body and to locate the spin axis precisely at an axis of a principal moment of inertia. Moreover, the axis of rotation may be quite different from the axis of symmetry. For example, a parabolic antenna reflector is symmetric about the boresight axis, which is not generally coincident with the spin axis. Although weights can be attached to a body to improve its balance, such compensation is always approximate.

In the new gyroscopic compensation method, the spinning body, or rotor, is supported on a stable platform by a bearing assembly and driven by a motor. Two additional motors are fixed on the rotor so that their axes of symmetry are perpendicular to one another and also perpendicular to the rotor spin axis (see figure). Flywheels are mounted on the shafts of the auxiliary motors.

The objective in the technique is to spin the motor/flywheel combinations so

(continued on next page)

that their gyroscopic torques compensate for the imbalance forces of the spinning rotor. The compensation relieves forces on the bearings and removes the disturbance to the stable platform.

In operation, the rotor is accelerated to its operating speed. The jitter produced in the platform by rotor imbalance is sensed by accelerometers or strain gages. The speed and direction of the two flywheels are adjusted — either automatically or by an operator — until the platform jitter is reduced. The flywheels are then rotated at fixed speeds to maintain the imbalance compensation. If the rotor balance changes, the flywheel speeds are also changed.

For automatic imbalance control, strain gages can produce signals with amplitudes that are instantaneously proportional to force components exerted by the rotor. These signals can be sampled, applied to dc amplifiers, and used to control the flywheel motor speeds.

This work was done by John A. Hrastar, Sr., of **Goddard Space Flight Center.** *For further information, Circle 50 on the TSP Request Card.*

This invention is owned by NASA, and a patent application has been filed. Inquiries concerning nonexclusive or exclusive license for its commercial development should be addressed to the Patent Counsel, Goddard Space Flight Center [see page A5]. Refer to GSC-12550.

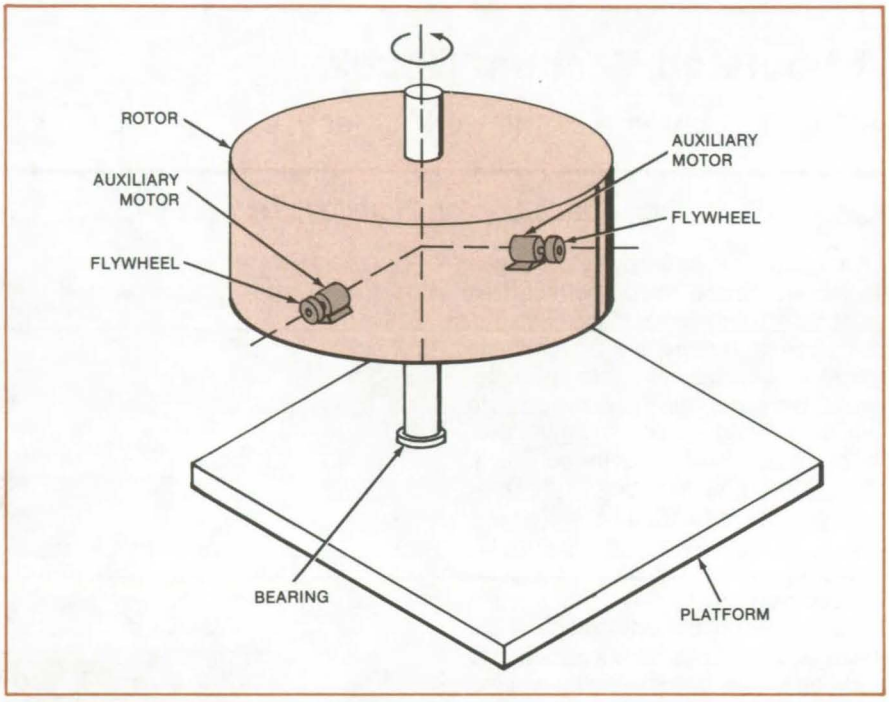

Spinning Flywheels Within a Rotor can null imbalance forces in the rotor. The flywheels axes are perpendicular to each other and to the rotor axis. Feedback signals from accelerometers or strain gages in the platform control the flywheel speeds and rotation directions.

High-Speed Wafer Slicer

Machine conserves silicon while it speeds up solar-cell production.

NASA's Jet Propulsion Laboratory, Pasadena, California

A multiblade cutter slices silicon ingots into solar-cell wafers quickly and with little waste. Its speed and blade pressure ensure a high wafer-production rate. Lightweight, balanced construction minimizes blade vibration and reduces the sideways motion that would otherwise widen the kerf and waste silicon.

A typical commercial reciprocating cutter for silicon ingots 3 in. (7.6 cm) in diameter moves a 220-lb (100-kg) bladehead over an 8-in. (20.3-cm) stroke at a rate of 100 ft/min (30 m/min) or less. In contrast, the new bladehead (see figure) weighs only 37 lb (17 kg), has a stroke of 16 in. (41 cm), and travels at more than 400 ft/min (120 m/min). The higher speed results in longer blade life and better cutting action.

The new machine employs wire blades for lightness, as well as a lightweight structure for supporting and tensioning the blades. As a result, relatively little mass is accelerated with each sawing motion, and the blade comes up to speed faster. Moreover, because the stroke is longer than on a conventional machine, the blades cut through the silicon much faster for a given rate of sawing motion. Two ingots are sliced simultaneously; the two bladeheads (only one is seen in the figure) are synchronized so that both accelerate in opposite directions at the same rate. This balanced arrangement reduces power requirements and vibration.

The ingots are placed in holders on the machine. A flywheel rotating at 150 r/min alternately pulls and pushes

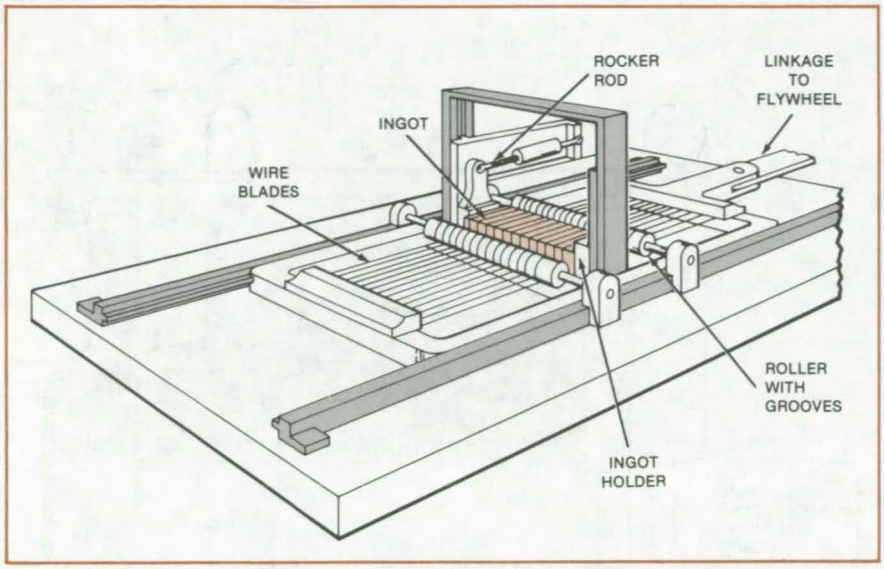

Silicon Ingots Are Sliced into wafers for solar cells by reciprocating wire blades. One-half of the cutter appears in this view; an identical bladehead and ingot holder are located on the opposite side of the flywheel. Bladeheads are light in weight but sturdy so that the machine operates at high speed with little vibration. As a result, production rates are high, cuts are accurate, and little material is wasted. The wires are 30 in. (76.2 cm) long and 5.7 mils (0.14 mm) in diameter. They are impregnated with 30-micron diamond particles on their lower surfaces.

the bladeheads. The ingots are pushed up against the lower surfaces of the reciprocating wire blades. At the same time, a rod pushes and pulls the top of the ingot holder, rocking the ingots through a 30° arc 10 times per minute. This shortens the length of contact between blade and ingot and increases the cutting pressure. The combination of high pressure and speed causes microcracks in the ingot and in the diamond particles in the blade cutting edge, thereby continually renewing the cutting edge and speeding the cutting process.

The wire blades are held in grooves on guide rollers so that their unsupported length is reduced. As a result, their deflection is minimized.

This work was done by Frederick Schmid, Chandra P. Khattak, and Maynard B. Smith of Crystal Systems, Inc., for **NASA's Jet Propulsion Laboratory.** *For further information, Circle 51 on the TSP Request Card.*
NPO-15463

Brushless Cleaning of Solar Panels and Windows

Air jets would scrub panels without damaging them.

NASA's Jet Propulsion Laboratory, Pasadena, California

A machine proposed for cleaning solar panels and reflectors uses multiple vortexes of air, solvent, and water to remove dust and dirt. It uses no brushes that might abrade solar surfaces and thereby reduce their efficiency — a particularly important advantage when reflectors are made of a relatively soft material such as aluminized plastic film. The machine can be readily automated and can be used on curved surfaces such as parabolic reflectors as well as on flat ones. The cleaning fluids are recycled, so that large quantities of water and solvent are not needed.

The concept is not limited to solar panels, but can be applied to other surfaces as well — for example, operating-room walls and the windows of high-rise buildings. It can be adapted to blowing heated air over surfaces for defrosting or drying and to applying coatings. Originally, it was developed

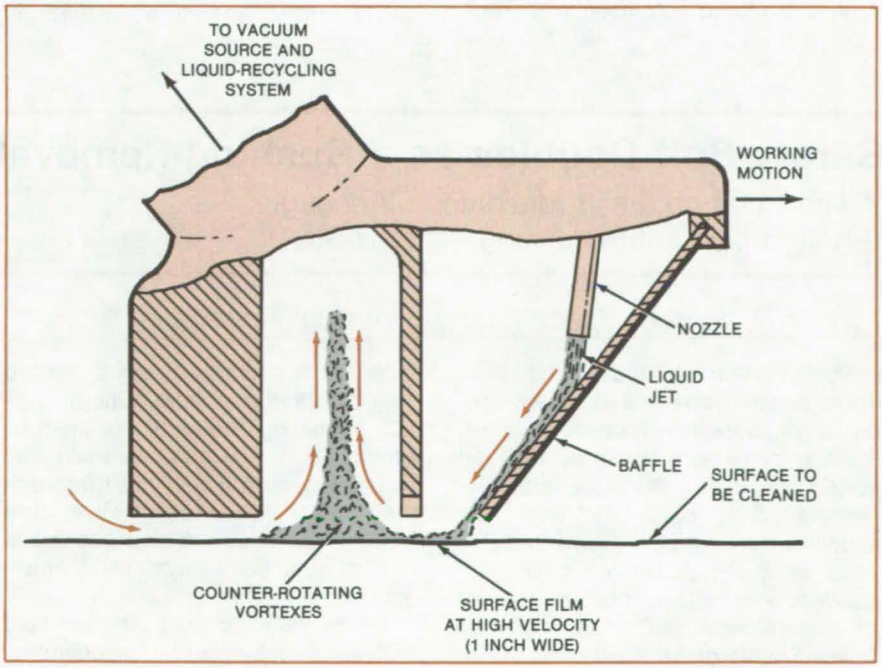

Figure 1. **A Cleaning Head** swirls detergent or other liquid over the surface of a solar panel by the combined action of air jets and vacuum.

for sampling microorganisms on surfaces. Other possible applications are:

- laying solvent film and soaking heavily contaminated surfaces prior to cleaning,
- postcleaning treatment to remove residue,
- electrical neutralization of charged surfaces, and
- tandem arrangement of more than one cleaning head to perform operations requiring different liquids or gases in a single sweep.

The cleaning vortexes are generated in two-chambered cleaning heads (see Figure 1). Several such heads are arranged in a row and scan the solar-panel surface. A cleaning liquid (usually a detergent, water, or a solvent) is applied to the panel surface from the nozzle shown at the right. A small gap between the head and the panel surface allows air to be drawn into the nozzle from outside and to aid in vortex formation. A gap of 0.020 to 0.040 inch (0.5 to 1 mm) is effective.

Inside the left chamber, a jet of air swirls over the film of cleaning liquid while a vacuum tube exhausts air. The vortex thus created agitates the film, dislodging and dissolving dirt particles, and draws off the liquid and the particles. The vortex removes oil and filmlike contaminants as readily as it does dirt particles. A hand-held prototype of the nozzle removes 90 to 98 percent of particles 5 microns or larger in diameter.

In a proposed automatic version of the cleaner, a mobile cleaning apparatus holds the heads, which are fed and drained by flexible hoses. A stationary unit holds liquid and vacuum supplies and a filter for separating the air from the liquid after collection. The heads sweep a panel vertically, then advance sideways for another sweep, performing this sequence until the entire panel has been scanned (Figure 2). If the combination of heads sweeps at a rate of 0.5 ft/s (15.2 cm/s), a row of 12 such units of 1-ft (30.5-cm) width will clean a panel quickly without excessive supply and withdrawal rates for air and liquid.

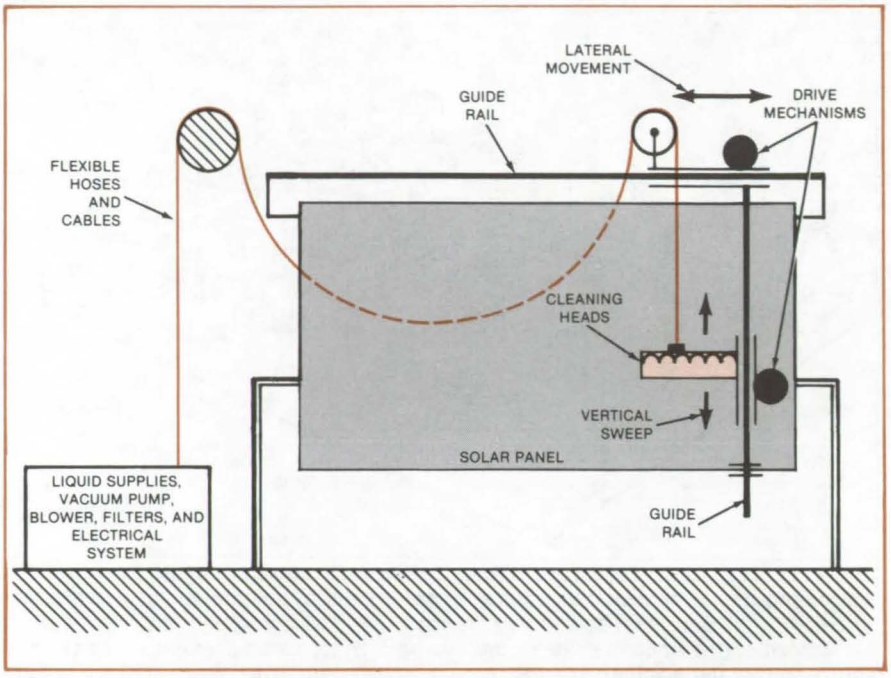

Figure 2. A **Scheme for Automatic Cleaning** has cleaning heads scanning the panel as it sweeps vertically and moves laterally. Heated detergent and water are carried to the head by flexible hoses. Vacuum and air supplies are also connected by hoses. Logic circuitry controls the movement of the head and the opening and closing of valves.

This work was done by Horst W. Schneider of Caltech for **NASA's Jet Propulsion Laboratory.** *For further information, Circle 52 on the TSP Request Card.*
NPO-14922

Safety Bolt Doubles as a Bushing-Removal Tool

A short dog on a self-retaining bolt engages a hole drilled in the bushing.

Lyndon B. Johnson Space Center, Houston, Texas

Bushings that are fitted to close tolerances and that have limited access can be removed without damage to their housing by using a bolt with an integrated locking dog. Such self-retaining positive-locking bolts (HI-SAFE®, or equivalent) are normally used as fasteners in critical joints where an accidentally loosened bolt could cause damage or injuries. However, workers on the Space Shuttle orbiter found that these same bolts could be used to remove bushings on the orbiter structure without damaging the delicate thermal-protection tiles. Such bolts could also be used to remove bushings from such machinery as automotive engine blocks, transmissions, and gearboxes or from water pumps with "blind" rotor-support bushings.

Before installing the bushing, a hole is drilled in one side of it to accommodate the short dog on the bolt. The bolt for removing the bushing (see figure) has a button that releases or retracts the short dog. To remove the bushing, the proper-diameter bolt with the dog retracted is inserted into the bushing, and the dog is released by removing pressure from the button. The bolt is then rotated until the dog engages the hole in the bushing. When the bolt is pulled out, the bushing comes with it.

Depressing the button disengages the locking dog from the bushing.

Other methods for removing limited-access bushings utilize tools that pass through the bushing bore and then extend fingers to engage the far end of the bushing. During extraction, these fingers, which are in tension, are prone to break. However, since the dog on the bolt is in shear, it is less likely to break. [HI-SAFE® is a registered trademark of the Hi-Shear Corp.]

This work was done by Charles E. Haverkamp of McDonnell Douglas Corp. for **Johnson Space Center.** *No further documentation is available.*
MSC-20032

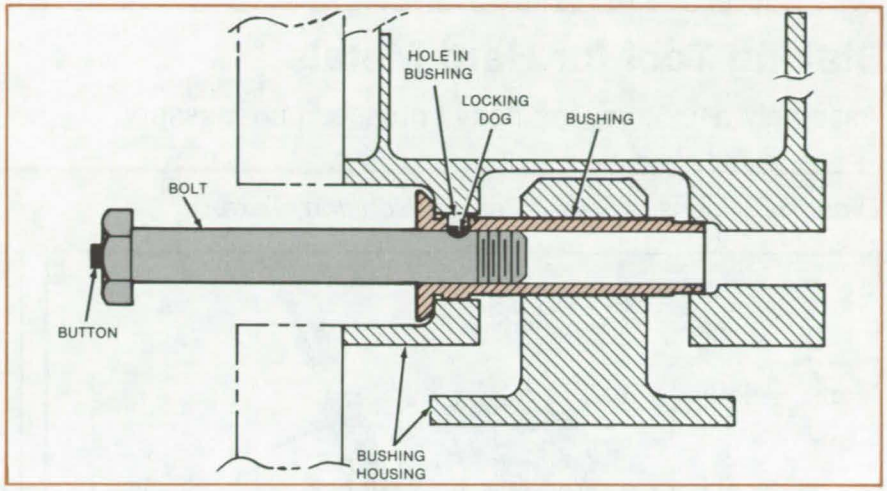

The **Locking Dog on the Bolt** engages the hole in the bushing by releasing the button. Pulling the bolt out brings the bushing out with it.

Improved Nozzle Would Reduce Cryogenic Boiloff

Slots would prevent flow from reaching the fluid surface.

Marshall Space Flight Center, Alabama

A proposed modification to the fluid-inlet nozzle for cryogenic storage tanks promises to reduce the loss of fluid from boiling. The modification consists of substituting a slotted orifice for a bellmouthed one. The orifice is mounted in a perforated cylinder (see figure).

The slots impart a swirling motion to the fluid, creating a circumferential flow along the inner surface of the cylinder. Nonuniform flow is confined to a conical region along the cylinder axis. After the fluid passes through the perforations in the cylinder, it flows radially into the tank. The area of the slots would be chosen to optimize the flow characteristics of the nozzle.

With the bellmouthed orifice used previously, the flow has large axial components along the inner surface of the perforated cylinder. Even after the fluid passes through the perforations, much of it has enough axial velocity to reach the surface of the fluid, where it boils off. The radial spray from the improved nozzle would greatly reduce this effect.

This work was done by Elvis D. Simon and Wayne E. Simon of Martin Marietta Corp. for **Marshall Space Flight Center.** *No further documentation is available.*
MFS-25589

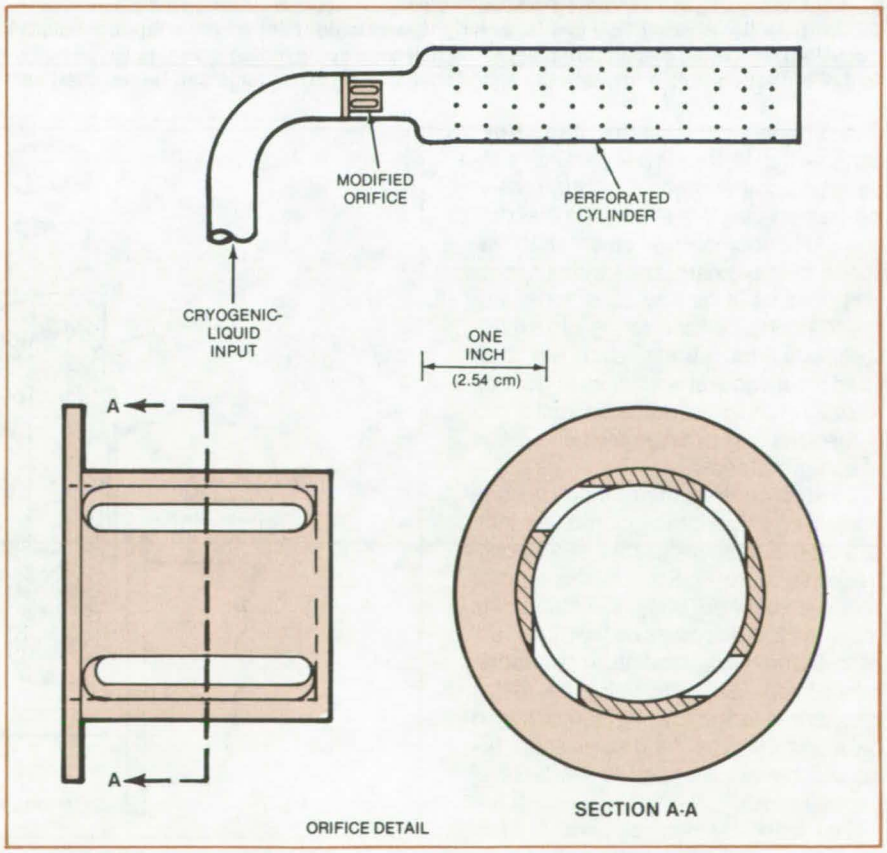

The **Improved Nozzle** has a slotted orifice that would impart a swirling motion to the cryogenic liquid inside the cylinder. The nozzle is installed with its axis vertical. Since most of the flow out of the cylinder would be radial, the fluid spray would not reach the liquid surface.

Staking Tool for Hard Metals

Assembly device makes heavy presses unnecessary.

Lyndon B. Johnson Space Center, Houston, Texas

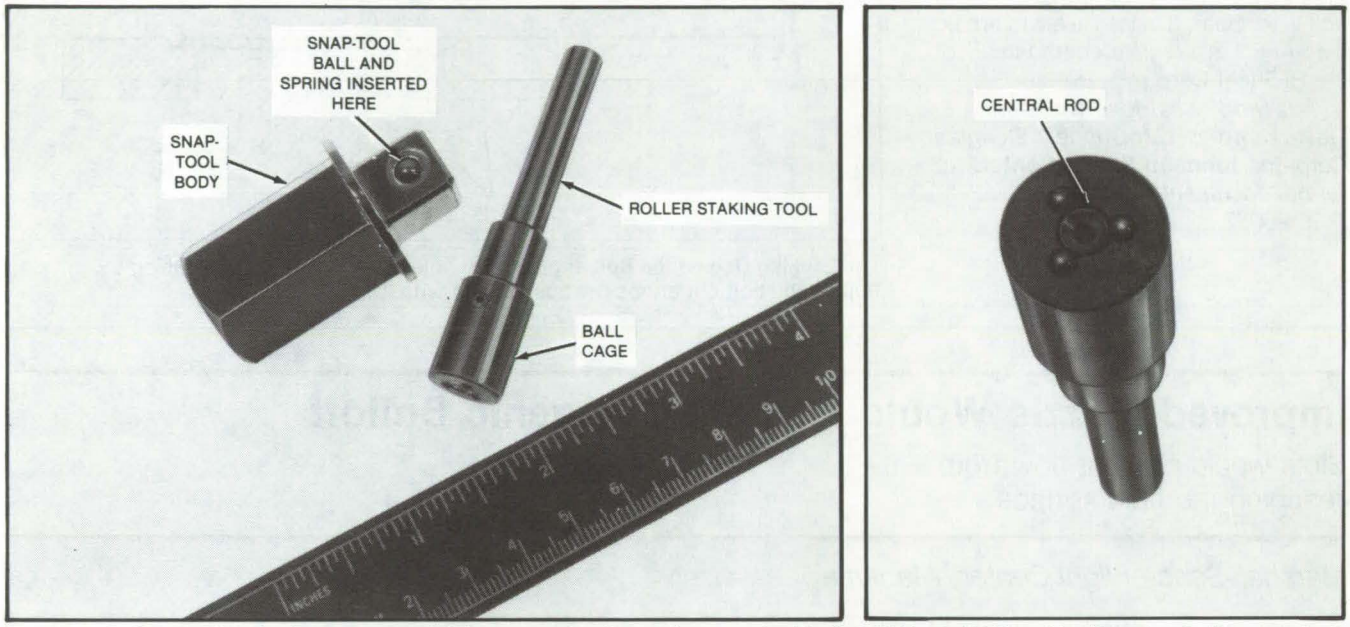

Figure 1. **Roller Staking Tool** (center and right) was used to insert the snap-tool ball, 0.187 inch (4.75 mm) in diameter, in the snap-tool body (left). The three equidistant balls in the ball cage apply rolling pressure to the body. The tip of the central rod contains a recess in a ball pilot that centers and seats the snap-tool ball. The brass cage can be removed easily so that worn cage balls can be replaced.

A simple tool stakes hard-steel parts — that is, forces one part into a recess on another, deforming the receiving part so that it restrains the inserted one. The tool allows small machine shops to stake hard steel without massive presses. It can be used, for example, to insert a ball and spring into a hard-steel snap-tool body such as that used to turn socket wrenches (Figure 1). Its use is not limited to hard steel; it can be used as well to assemble parts made of softer materials.

The tool consists of a mandrel, a cage containing three balls [each 0.094 inch (2.3 mm) in diameter], and a sliding central rod (Figure 2). For the staking of a ball in a snap-tool body, the mandrel is mounted in a drill press so that it can apply pressure while rotating. The mandrel central rod seats the ball. The rolling pressure exerted by the three caged balls swages the hard-steel snap-tool body, which is clamped to the base of the drill press.

This work was done by John A. Stein of Rockwell International Corp. for **Johnson Space Center.** *No further documentation is available.*
MSC-20009

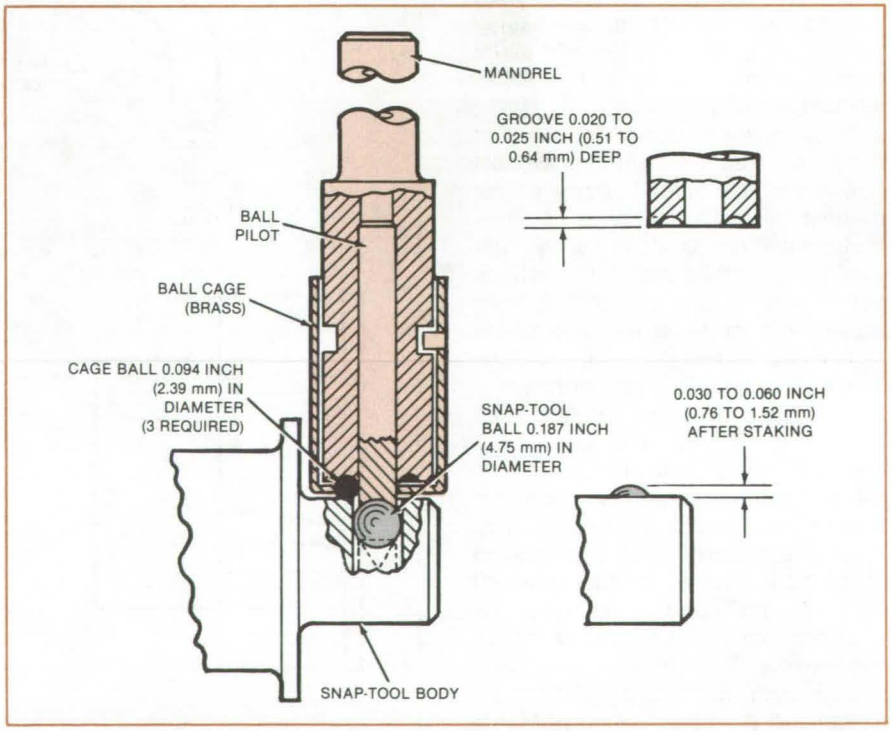

Figure 2. **At the Start of the Staking Operation,** the central rod (or ball pilot) pushes a ball into a hole in a snap-tool body. The three rolling cage balls swage the hard steel at the periphery of the hole so that the body retains the ball. The ball protrudes 0.030 to 0.060 inch (0.76 to 1.52 mm) from the hole after staking.

Force Augmentation for Relief Valve

Flow through a pressure-actuated valve assists in keeping it open.

Lyndon B. Johnson Space Center, Houston, Texas

A simple design change for a poppet relief valve enables the flow through the valve to exert additional force to help keep the valve open. Although originally intended for relief valves for liquid oxygen and liquid nitrogen in the Space Shuttle orbiter, the concept is applicable to pressure- or flow-actuated valves for a wide range of fluids and temperatures.

As shown in the figure, the modification consists in adding a shroud ring around the edge of the poppet. Once the upstream-to-downstream pressure differential suffices to open the poppet against the spring and frictional forces, the flow exerts an additional opening force. The flow must reverse itself somewhat in order to clear the shroud ring, and so the additional force is a function of the rate-of-change of fluid momentum. The maximum flow-pressure differential is reduced, since the additional force causes the valve to open more fully than it otherwise would.

The improved design enabled a relief valve for the Space Shuttle to meet all specified performance requirements in the smallest, lightest configuration. Potential users include processing plants or other fluid-handling facilities.

This work was done by Julian Luger of Parker Hannifin Corp. for **Johnson Space Center.** *No further documentation is available.*
MSC-20065

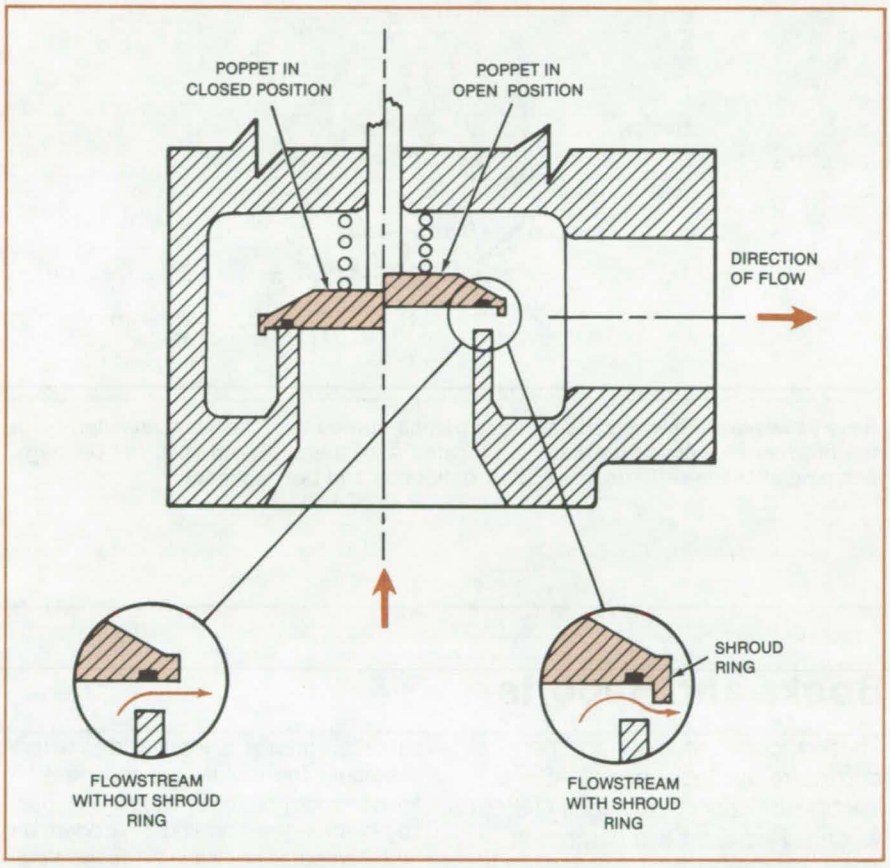

A **Poppet Relief Valve With Force Augmentation** is shown here in cross section with the poppet in closed position (left) and open position (right). The shroud ring increases the opening force exerted by the flow. The static opening pressure is unaffected.

Damping Vibration at an Impeller

Flow through a clearance channel absorbs vibration energy.

Marshall Space Flight Center, Alabama

The vibration of a pump shaft is damped at the impeller — where vibration-induced deflections are greatest — by a shroud and seal. The damping reduces the vibrational motion of the shaft at the bearings and the load the shaft places on them.

The axial-flow inducer in the centrifugal pump is fitted with a cylindrical shroud within a stationary cylindrical seal (see figure). A small amount of the pumped liquid flows in reverse between the shroud and the seal — that is, from the outlet toward the inlet. The reverse flow damps shaft, inducer, and impeller vibrations. The extent of the damping is determined by the pressure differential between inlet and outlet, the clearance between shroud and seal, and the properties of the liquid.

(continued on next page)

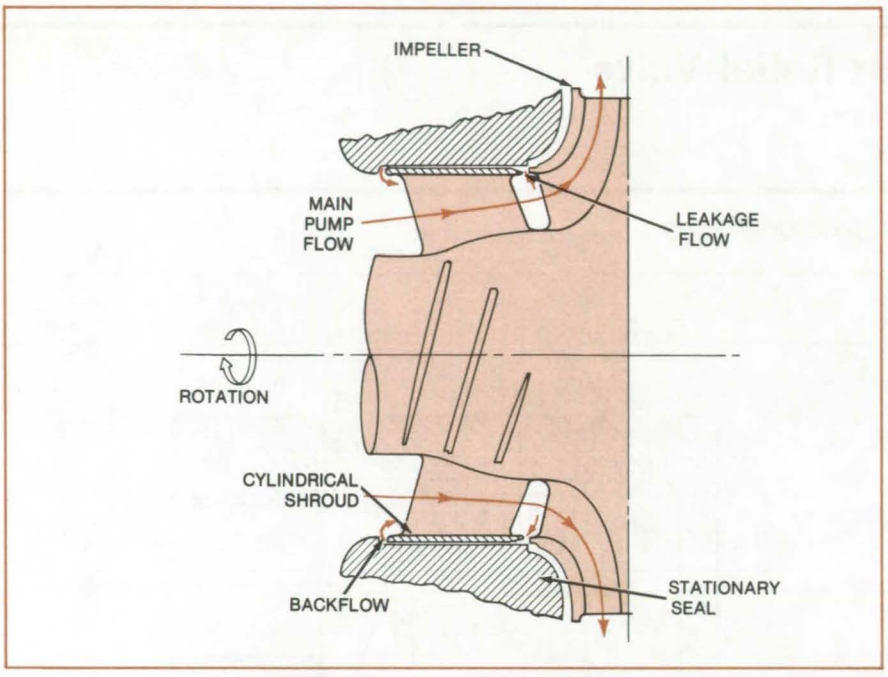

Reverse Leakage Flow of pumped liquid damps vibrations of the pump impeller. Since the impeller is a concentrated mass located a sizable distance from the bearings, damping at the impeller reduces shaft deflection and bearing loads.

This work was done by J. A. Hager and B. F. Rowan of Rockwell International Corp. for **Marshall Space Flight Center.** *No further documentation is available.*
MFS-19645

Books and Reports

These reports, studies, and handbooks are available from NASA as Technical Support Packages (TSP's) when a Request Card number is cited; otherwise they are available from the National Technical Information Service.

Tests of 38 Ball-Bearing Greases

Perfluoroalkylpolyether lubricants have thus far proved best.

A new report presents interim results in a program of long-term tests of ball-bearing greases in vacuum, oxidizing, and otherwise hostile environment. The program is motivated by the need for mechanisms that will operate for long periods in spacecraft or space stations.

Tests reported thus far have included 38 lubricants selected to represent most of the military grease specifications as well as promising nonspecification materials. Twenty motors, each containing two test bearings lubricated with the candidate grease, are set up in each test chamber. The motors are mounted on an aluminum plate furnished with passages for water and liquid nitrogen, so that temperature can be controlled. Since the motors are small ac hysteresis types, there is no problem of overheating or further bearing damage when a motor stalls due to bearing failure, nor is there any brush dust to contaminate the bearings.

To insure a statistical sample, each test set consists of four motors (eight bearings). A set of 20 motors thus allows five different greases to be tested simultaneously. Samples are tested until failure, or else for 1 year. Lubricants that do well in the 1-year tests are selected for further evaluation in 5-year tests.

Test environments include:

- 10 psi (6.9×10^4 N/m^2) oxygen at 90 percent relative humidity;
- Vacuum, ambient temperature (38° C);
- Vacuum, high temperature (93.3° C);
- Vacuum, ambient temperature, with start/stop operation; and
- Low-temperature start (various temperatures).

The evaluations for all tests (except low-temperature start) are based on a go/no-go system: A bearing failure is deemed to occur when the bearing tends to seize, causing the motor to stop. Data recorded in each case include total test time, vacuum or atmosphere conditions, temperature, and total number of on/off cycles where appropriate. Bearings are weighed before and after testing, so that the fractional lubricant weight loss can be calculated. Selected bearings may be disassembled and further examined.

The class of lubricants based on perfluoroalkylpolyether (PFPE) with fluorotelomer thickeners has given the best results in the vacuum tests completed thus far. Other promising materials include some silicone, synthetic-ester, and mineral greases. The test methods and performances of the various lubricants could be of interest in the automotive and industrial communities.

This work was done by E. L. McMurtrey of **Marshall Space Flight Center.** *To obtain a copy of the report, Circle 54 on the TSP Request Card.*
MFS-25624

Fabrication Technology

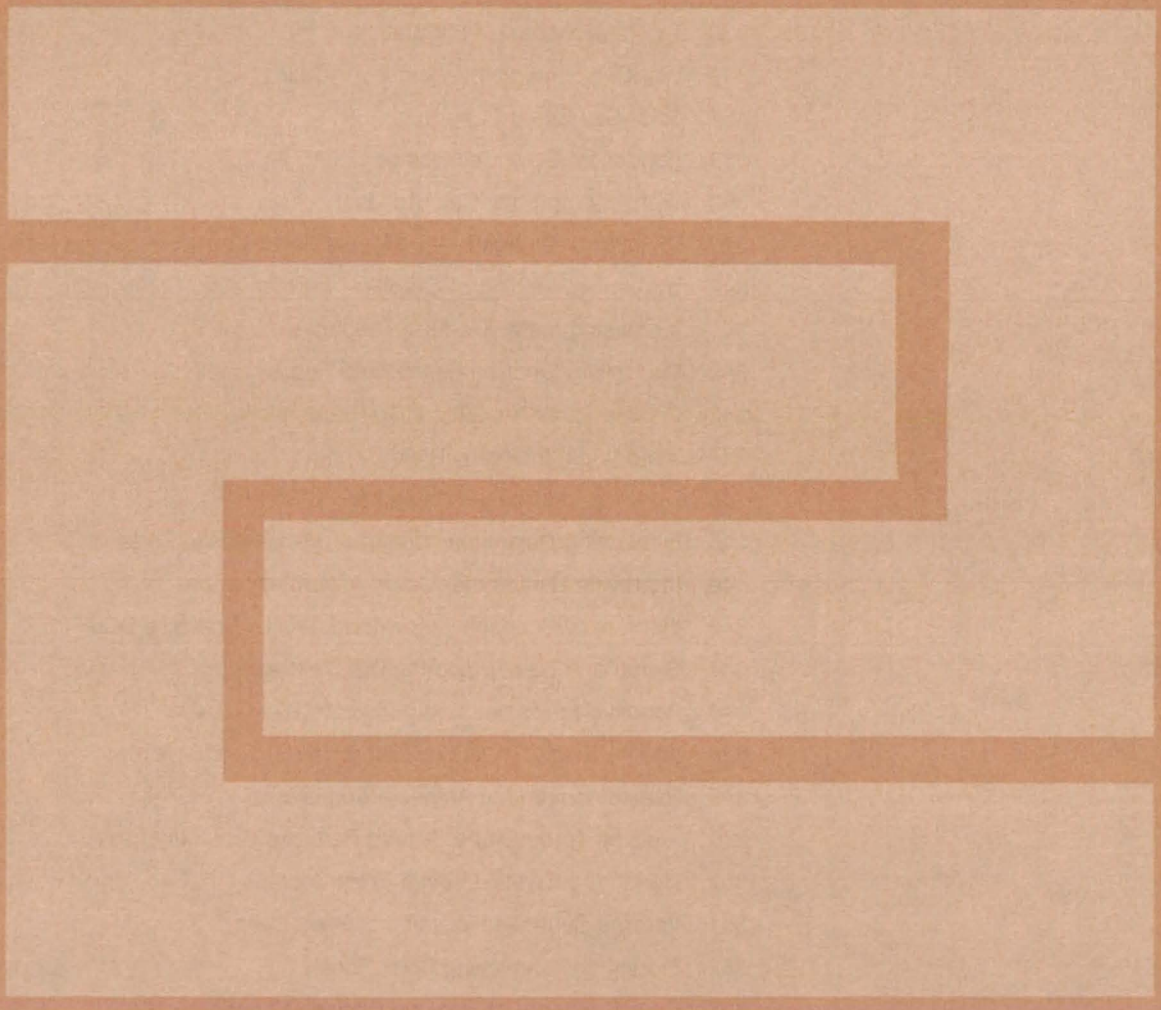

Hardware, Techniques, and Processes

333 Automated Solar-Array Assembly
334 Walking-Beam Solar-Cell Conveyor
334 Vacuum Pickup for Solar Cells
335 Orienting and Applying Flux to Solar Cells
336 Tab Interconnect Work Station
337 Work Station For Inverting Solar Cells
337 Solar-Cell String Conveyor
338 Bonder for Solar-Cell Strings
339 Transporting Solar-Cell Strings
340 Transfer of Strings to the Module Fixture
340 Ultrasonic Welding of Graphite/Thermoplastic Composite
341 Increasing Metal Fracture Toughness
342 Controlling Electron-Beam-Weld Focus
343 Plasma Spray for Difficult-To-Braze Alloys
344 Weld Width Indicates Weld Strength
345 Cleaning Internal-Weld Splatter
345 Eliminating Delamination in Curved Composite Parts
346 Improving Radiometer-Cavity Absorptance
346 Electrically-Conductive Low-Permeability Pressure Seal
347 Clamp and Gas Nozzle for TIG Welding
348 Acoustic Emissions Could Indicate Weld Quality
348 Integral Face Shield Concept for Firefighter's Helmet
349 Radiant Heating of Ampoule Contents
350 Yielding Torque-Tube System Reduces Crash Injuries
351 Monitoring Crystal Growth From Solution
351 Infrared-Controlled Welding of Solar Cells
352 Storing and Deploying Solar Panels
353 Cutting a Tapered Edge on Padding Material
354 Pivot Attachment for Prefabricated Beams

Books and Reports

354 Fabricating Structural Beams

Automated Solar-Array Assembly

An assembly line interconnects cells at the rate of one every 5 seconds.

NASA's Jet Propulsion Laboratory, Pasadena, California

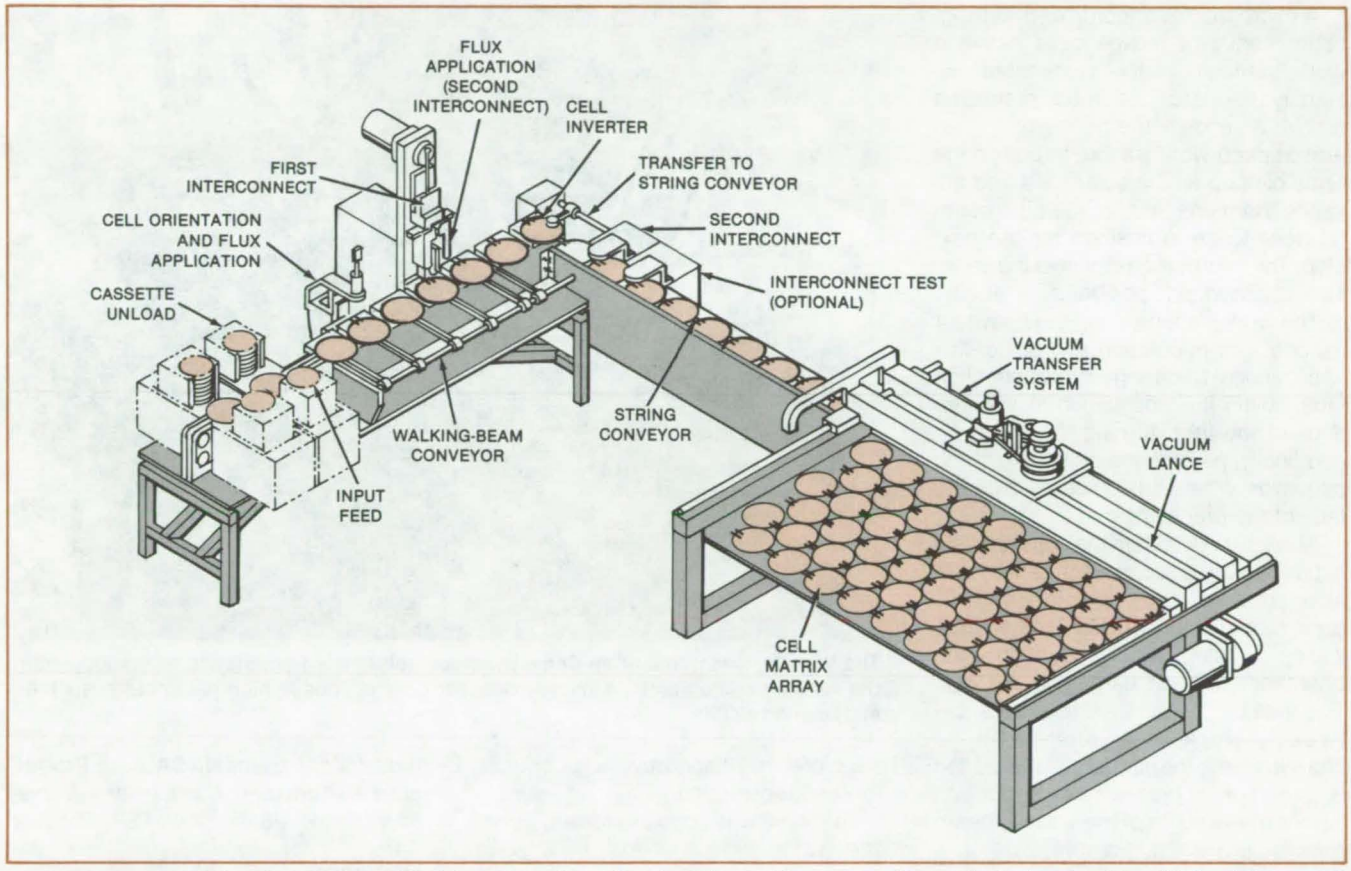

In the **Automated Solar-Module Assembly Line,** the solar cells are unloaded from cassettes, oriented and soldered into strings, and placed into a module up to 2 by 4 ft (61 by 122 cm) in size.

Large arrays are rapidly assembled from individual solar cells by an automated production line developed for NASA's Jet Propulsion Laboratory. The apparatus positions the cells within the array, attaches interconnection tabs, applies solder flux, and solders the interconnections. Cells are placed in either straight or staggered configurations and may be connected either in series or in parallel. They are attached at the rate of one every 5 seconds.

As illustrated in the figure, the solar cells are dispensed from a cassette and transported by belt to a receiving station. A walking-beam conveyor advances the cells through a series of stations. At the first station, the cell orientation is sensed optically, and the cell is rotated into the proper position for tabbing. Solder flux is then applied.

At the second station, tabs are cut from continuous reels of ribbon and are soldered to the fluxed cell by pulsed heating. To improve reliability, each cell is connected to the next by two tabs.

At the third station, solder flux is applied to the free ends of the tabs. The cell is inverted, and further operations are done on the back of the cell to protect the collector side.

The inverted cell is transferred to the string conveyor, where the interconnection to the free ends of the tabs of the preceding cell is made. The attachment is made at the first station and tested at a subsequent station of the string conveyor.

At the end of the string conveyor, a completed cell string is picked up by a vacuum "lance" and placed into a fixture in which the array is assembled. A reject station stores defective strings. Subsequent operations, such as connecting external leads and cleaning, can be performed on the module. (The articles that follow describe the solar-cell assembly line in more detail.)

This work was done by Albert Soffa and Max Bycer of Kulicke & Soffa Industries, Inc., for **NASA's Jet Propulsion Laboratory.** *For further information, Circle 55 on the TSP Request Card.*

NPO-15501

Walking-Beam Solar-Cell Conveyor

Microprocessor control accurately positions cells as they more through the assembly stations.

NASA's Jet Propulsion Laboratory, Pasadena, California

A microprocessor-controlled walking-beam conveyor moves cells between work stations in the automated assembly line described in the preceding article. As shown, the conveyor has an arm at each work station. In unison the arms pick up all the solar cells and advance them one station; then the beam retracks to be in position for the next step. The microprocessor sets the beam stroke, speed, and position.

The work stations along the conveyor include: cell orientation and solder-flux application; soldering interconnection tabs; solder-flux application to the free ends of the tabs; turning the cell over; and finally, passing the cell to the string conveyor, where it is soldered onto the tabs of the preceding cell.

At each work station the cells are held in position by vacuum. Each pickup arm also has a vacuum grip with a soft silicone-rubber vacuum cup (see the following article), which maintains the orientation without damaging the cell. The walking beam transfers cells between work stations with a "handshake"; the vacuum of the station is turned on to hold the cell in position before the vacuum of the walking-beam arm is turned off. Positive control is therefore maintained over cell orientation and registration.

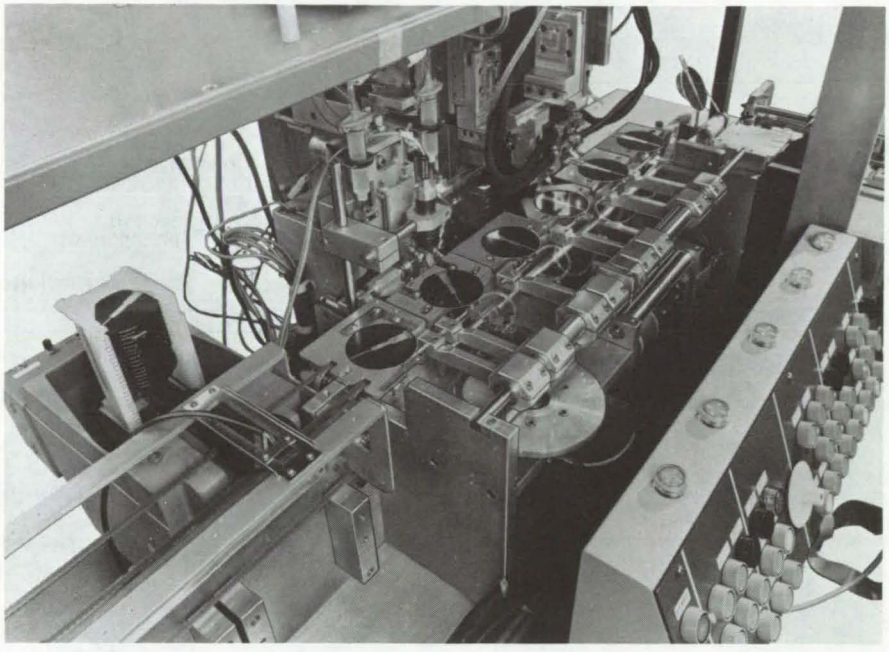

The **Walking-Beam Solar-Cell Conveyor** steps solar cells from station to station, using the vacuum pickup arms. A microprocessor controls positioning parameters, such as stroke and velocity.

This work was done by Howard Feder and Walter Frasch of Kulicke & Soffa Industries, Inc., for **NASA's Jet Propulsion Laboratory.** *For further information, Circle 56 on the TSP Request Card.*
NPO-15503

Vacuum Pickup for Solar Cells

Flexible cup conforms to the shape of the cell back surface.

NASA's Jet Propulsion Laboratory, Pasadena, California

The flexible vacuum cups that handle solar cells along the walking-beam conveyor (see preceding articles) conform to the shape of the cell back surfaces. The cups lift vertically, without tilt that might cause stress on interconnections, inaccurate placement, or damage to the cells.

As the figure shows, the pickup is spring-loaded to allow some overtravel of the cup when it is acquiring a cell or laying it in place. The overtravel assures that the cell is gripped firmly by the cup and placed accurately when it is released.

The vacuum source is a venturi valve mounted on an air manifold. The positive air pressure at the valve orifice generates a vacuum in the line that leads to the vacuum cup.

Each of the pickups along the walking-beam conveyor has its own

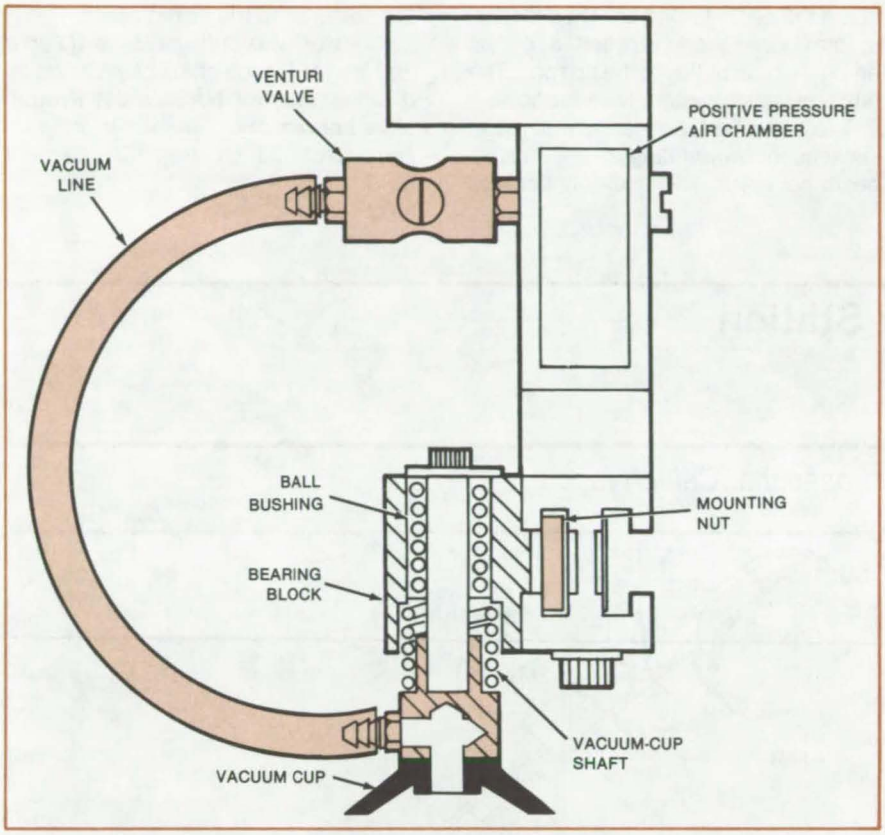

The **Vacuum Cup** in this pickup assembly lifts a silicon solar cell by adhering to the cell back surface. The spring-loaded cup grips firmly without damaging the cell.

vacuum source, so that there is no vacuum cross-coupling that might interfere with the timing of pickups and releases. The pickup housings are individually alined by adjusting a nut accessible at the front.

This work was done by Walter Frasch of Kulicke & Soffa Industries, Inc., for **NASA's Jet Propulsion Laboratory.** *For further information, Circle 57 on the TSP Request Card.*
NPO-15500

Orienting and Applying Flux to Solar Cells

An optical sensor detects the cell orientation for solder-flux application.

NASA's Jet Propulsion Laboratory, Pasadena, California

Solar cells are oriented and fluxed automatically at the first work station along the solar-array assembly line (see preceding articles). In under 2 seconds a rotary drive rotates the cell into the proper position for applying solder flux to the bus pad on the collector side.

A drive wheel in the center of the stage beneath the cell (see figure) urges the cell toward the rear of the station and into contact with two rotating capstans. The capstan wheels contact the edge of the cell without touching the collector surface. The wheels are adjustable to accommodate solar cells either 3 or 3.9 inches (76 or 100 mm) in diameter.

As the cell is rotated by the capstans, it passes beneath an optical sensor. Cell orientation is recognized by the difference in reflectance between the bright,

(continued on next page)

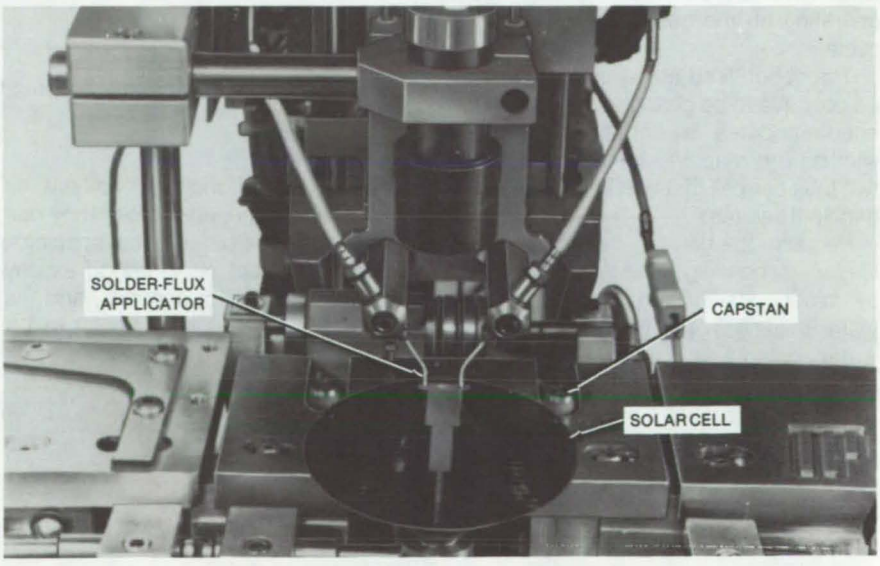

The **Work Station for Orienting and Applying Flux to Solar Cells** is shown with the solar cell in the proper orientation for applying flux.

metalized contact bus pad (where the interconnects will later be soldered) and the dark, active area of the cell, which is antireflection coated.

When the contact bus pad is in the correct position, the capstan drive is disengaged, and a vacuum holddown beneath the cell is turned on. Then the flux system lowers and applies a preset amount of solder flux to the bus pad. The flux application system then retracts.

The cell orientation is maintained at subsequent work stations of the walking-beam conveyor. Two interconnect tabs are soldered to the fluxed areas.

This work was done by Howard Feder and Walter Frasch of Kulicke & Soffa Industries, Inc., for **NASA's Jet Propulsion Laboratory.** *For further information, Circle 58 on the TSP Request Card.*
NPO-15504

Tab Interconnect Work Station

Tabs are cut from metal strip and soldered to solar cells.

NASA's Jet Propulsion Laboratory, Pasadena, California

The second work station along the solar-array assembly line (see preceding articles) automatically attaches two interconnect tabs to each silicon solar cell. The machine feeds, forms, and cuts the tabs from a reel of pretinned metal ribbon, transfers the tabs into position, and solders them to the cell.

A sensor on the workstage detects the presence of a cell at the station. The "pick-and-place" arm brings a pair of tabs and places them in position on the cell. A bonding head then lowers until its tools touch the tabs and heats them for a brief predetermined period. The tools are thermocouple-controlled so that they do not get too hot and damage the cell. Solder on the tabs melts, then resolidifies, forming a bond with the cell (see figure). Finally, the cell is removed, and the pick-and-place arm returns to its original position, where it picks up the next pair of tabs, which were cut to length and formed when the arm was operating on the cell in the preceding cycle.

The ribbon feed uses large reels that do not have to be changed frequently. It accommodates a variety of ribbon widths. The machine feeds and bonds two tabs per cell, but can be modified to handle three tabs.

Because the bonding head is spring-loaded, its bonding force is not affected by minor variations in head travel or wafer thickness. The bonding tools are water-cooled and are controlled individually for such bonding conditions as temperature, time, and force. They can be set for a wide range of tab spacings. The bonding heat pulse period usually lasts from 0.8 to 1.5 seconds, and the postpulse dwell time lasts from 1 to 1.5 seconds.

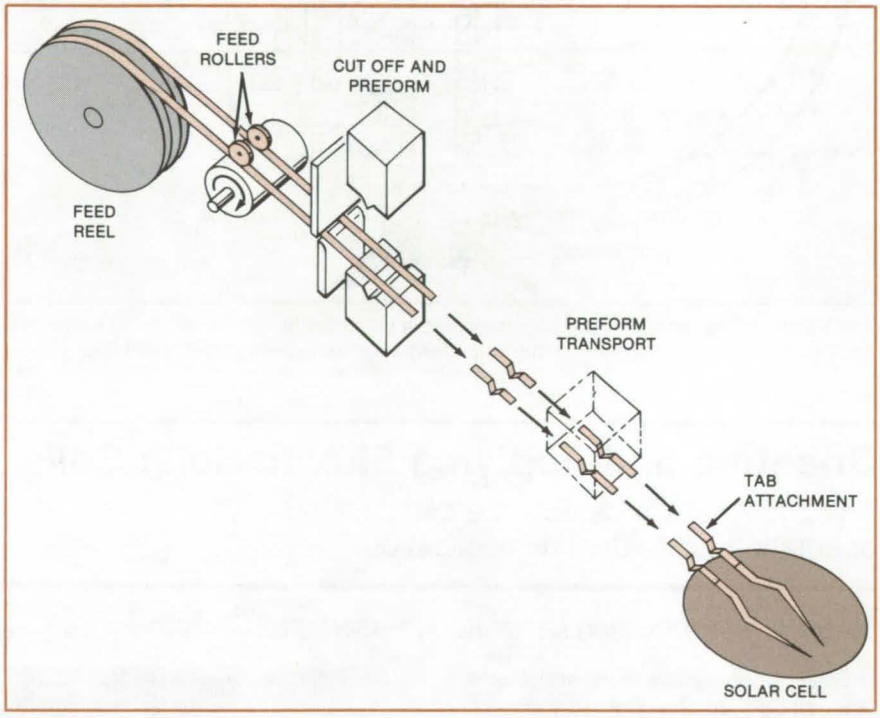

A **Reel Feeds Metal Strips** to a bonding machine that cuts off tabs, forms them, and solders them to a silicon solar cell.

This work was done by George Garwood of Kulicke & Soffa Industries, Inc., for **NASA's Jet Propulsion Laboratory.** *For further information, Circle 59 on the TSP Request Card.*
NPO-15505

Work Station For Inverting Solar Cells

A cell is inverted and centered with only minimal contact with the collector surface.

NASA's Jet Propulsion Laboratory, Pasadena, California

The final work station along the walking-beam conveyor of the solar-array assembly line (see preceding articles) turns each pretabbed solar cell over, depositing it back-side-up onto a landing pad, which centers the cell without engaging the collector surface. The solar cell arrives at the inverting work station collector-side-up with two interconnect tabs attached to the collector side. The tabs are eventually to be soldered to the back of the preceding cell in the next stage of assembly. The cells are inverted so that the second soldering operation takes place in plain view of an operator. Inversion also protects the collector from damage when it is handled at later stages of the assembly. Soldering with the tab ends over the back of the preceding cell eliminates the possibility of solder flowing down during bonding.

The photograph shows the arm that turns the cell over. The walking-beam conveyor places the cell on the arm, collector-side-up. It is held in place by vacuum, which is turned on after the cell is in position but before the vacuum grip of the walking-beam arm is turned off.

The arm then swings over, inverting the cell and depositing it in a landing pad, which has four chamfered pins arranged in a square. The pins are shaped so as to minimize contact with the collector surface. The pins accurately center the cell so that it will be in the correct position for interconnecting to the preceding cell after the walking-beam conveyor moves the cell on to the string conveyor. The interconnects are soldered on the string conveyor.

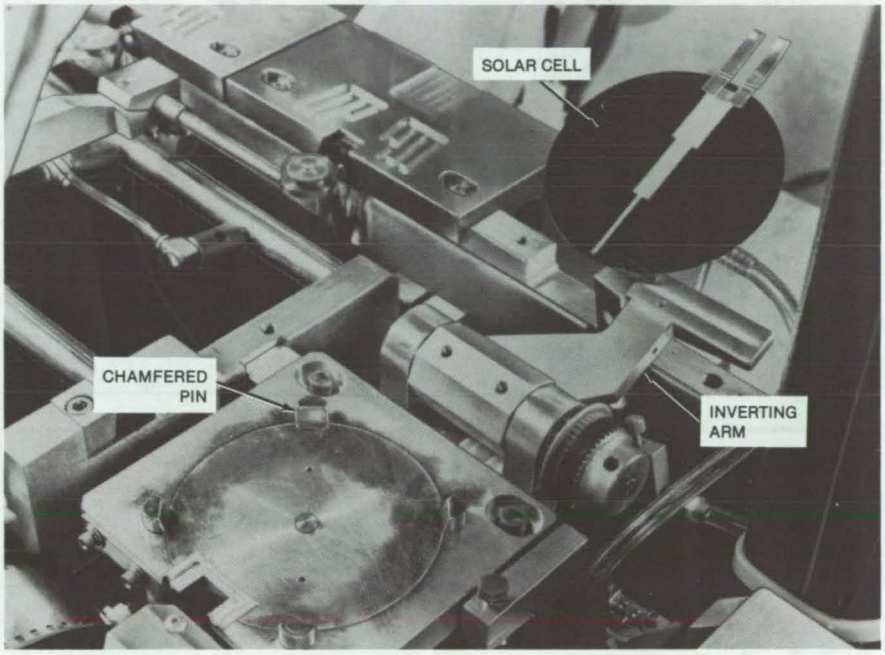

The **Work Station for Inverting Solar Cells** is shown with the solar cell on the inverting arm. The arm is part way through the process of inverting the cell and placing it in the chamfered pins of the landing pad in the foreground.

This work was done by Howard Feder and Walter Frasch of Kulicke & Soffa Industries, Inc., for **NASA's Jet Propulsion Laboratory.** *For further information, Circle 60 on the TSP Request Card.*
NPO-15506

Solar-Cell String Conveyor

A conveyor positions cells for bonding into strings.

NASA's Jet Propulsion Laboratory, Pasadena, California

The string-conveyor portion of the solar-array assembly line (see preceding articles) holds silicon solar cells while they are assembled into strings and tested. The cells are transported collector-side-down, while uniform cell spacing and registration are maintained. Positioning fixtures along the string conveyor hold the cells at their edges only, minimizing contact and the possibility of damage to the collector. The positioning fixtures are supported by two narrow belts on opposite edges of the wafers, so that the waferlike cell is accessible from below (see figure).

The belts are driven in synchronism by a pair of sprockets. Each contains small holes at the cell-to-cell spacing. The holes engage sensors that control the advance of the belts. For greater accuracy, the belts are made of metal instead of rubber or fabric. The metal does not stretch or creep because of tension in the belt. Its properties are also less sensitive to temperature variations.

(continued on next page)

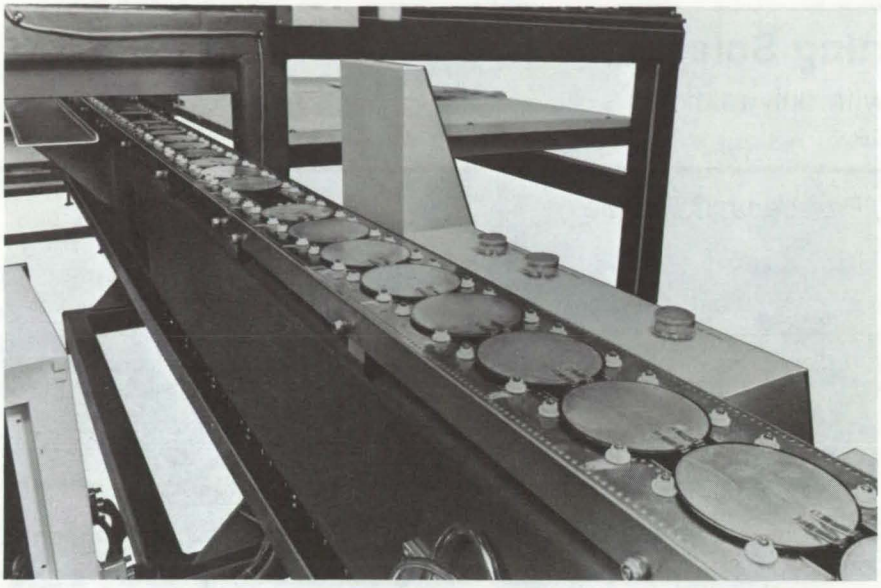

Solar-Cell Wafers Are Indexed along the string conveyor.

The conveyor frame is cantilevered. This construction makes it easy to install new belts for different cell sizes and spacings.

A microprocessor on the machine controls the indexing of the cells. It moves each in turn into the string-bonding machine, which attaches tabs on the cell next in line to the one in position.

The machine attaches any number of cells in a string, according to the instructions given to the microprocessor. It provides three empty cell spaces between strings.

This work was done by Walter Frasch and Sal Ciavola of Kulicke & Soffa Industries, Inc., for **NASA's Jet Propulsion Laboratory.** *For further information, Circle 61 on the TSP Request Card.*
NPO-15508

Bonder for Solar-Cell Strings

Automatic device makes electrical connections for solar-cell strings.

NASA's Jet Propulsion Laboratory, Pasadena, California

The string bonder for solar-cell arrays (see preceding articles) eliminates a tedious manual assembly procedure that could damage the cell face. A vacuum arm picks up a face-down cell from the cell-inverting work station and transfers it to the string conveyor without changing the cell orientation. The arm is activated by a signal from a microprocessor.

The two cell tabs are bonded to the preceding cell on the conveyor. When bonding is completed, the conveyor indexes, moving the newly bonded cell into, the next position under the bonding head (see figure). At the same time, the conveyor moves the tabs of a newly transferred cell under the bonding head.

To make the connections, the bonding head moves down to contact the tabs and the cell. A pulse of heat is applied by the head at a controlled temperature and for a predetermined time. Then the head withdraws, and the conveyor indexes, moving more cells into position. The procedure repeats until the string is complete.

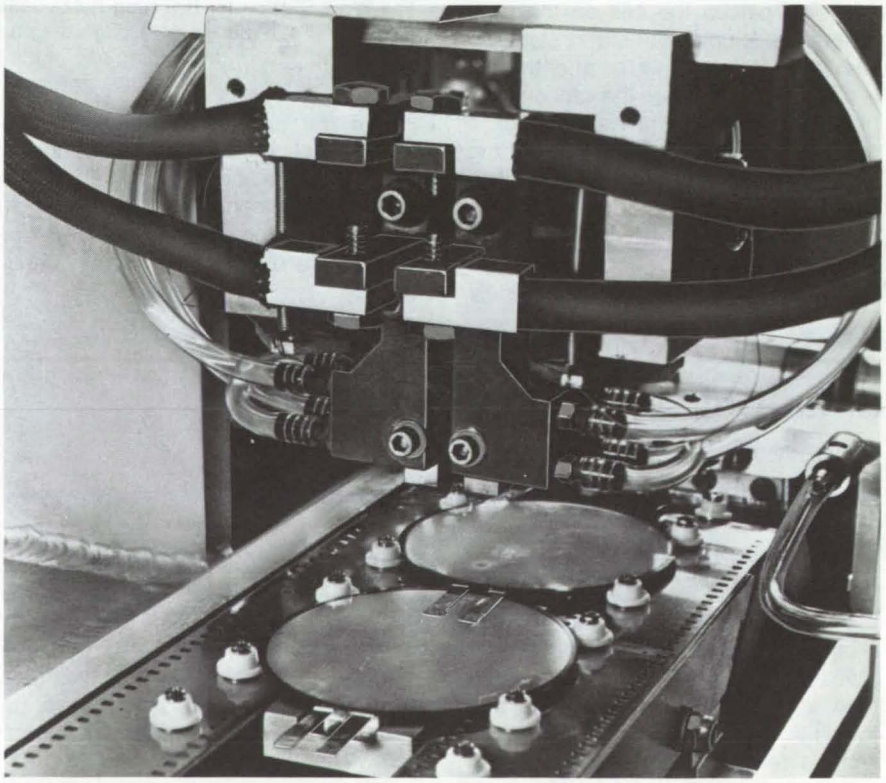

Bonding Head With Two Tools is in the retracted position above the conveyor. The conveyor indexes a solar-cell wafer and the tabs from the following wafer into position under the tools. Then the head lowers and bonds the tabs to the wafer.

The tools on the bonding head are spring-loaded so that they can accommodate minor variations in cell thickness and planarity without significant variations in bonding force. The tools are water-cooled. Their positions are adjustable so that a range of cell sizes and spacings can be handled.

This work was done by George Garwood and Walter Frasch of Kulicke & Soffa Industries, Inc., for **NASA's Jet Propulsion Laboratory.** *For further information, Circle 62 on the TSP Request Card.*
NPO-15507

Transporting Solar-Cell Strings

Vacuum "lance" gently transfers strings from one assembly operation to another.

NASA's Jet Propulsion Laboratory, Pasadena, California

A vacuum "lance" picks up an assembled chain of solar cells from the string conveyor (see preceding articles) without disturbing the cells or their interconnecting tabs. It handles strings of as many as sixteen 3-inch (7.6-cm) cells or as few as two such cells, corresponding to strings from 4 feet to 7 inches (1.2 to 0.18 m) long.

The lance has 2 vacuum pickups per cell, for a total of up to 32 pickups. The positions and number of the pickups can be varied. The lance therefore can be adjusted for a range of cell sizes, shapes, and spacings (see figure).

The string conveyor moves a string under the vacuum lance. A sensor determines when the cells are in position and signals the lance to descend and pick up the string. An operator then moves the lance on a track to the module array, where the cells are gently deposited adjacent to other strings.

Each pickup has its own vacuum supply from a positive-air-pressure venturi valve. Because the cups are independent, the individual cups do not lose vacuum when some of the cell positions are unoccupied.

The lance can rotate in its vacuum frame so that a string can be turned 180°. This allows the strings to be alternated in orientation in an array or to be arranged in virtually any series or parallel grouping.

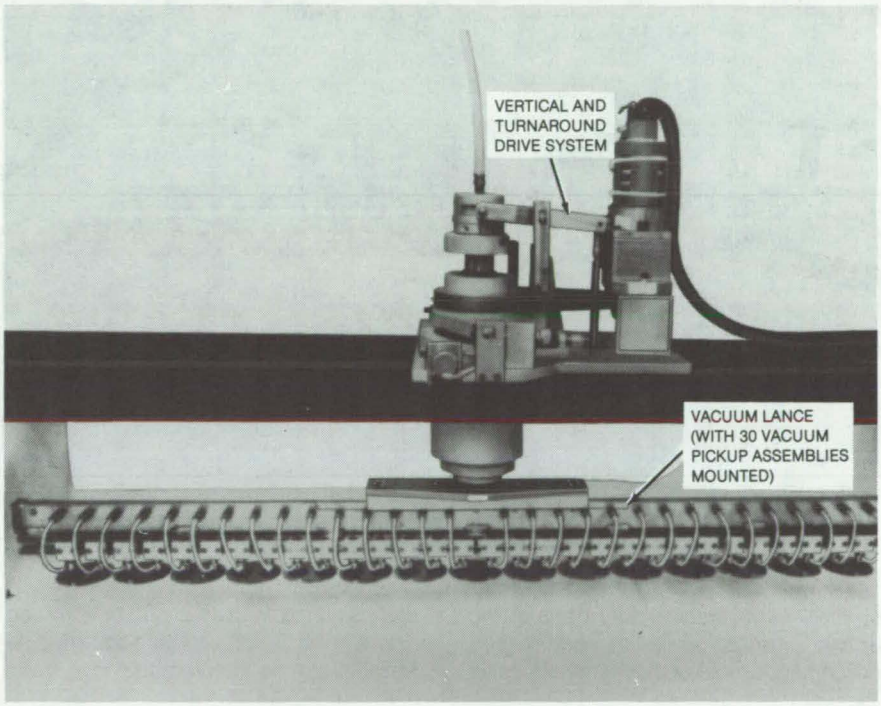

A **String of 15 Solar Cells** is held by a vacuum lance. Two vacuum pickup cups support each cell. The drive mechanism at top center raises and lowers the lance and rotates it if necessary.

This work was done by Max Bycer and Walter Frasch of Kulicke & Soffa Industries, Inc., for **NASA's Jet Propulsion Laboratory.** *For further information, Circle 63 on the TSP Request Card.*
NPO-15502

Articulated Vacuum Chuck

An articulated vacuum chuck holds assemblies together for repairs and handles unusually shaped parts. It conforms to complex surface contours by flexing under vacuum to adjust to the surface, and then bolts are tightened to lock the configuration. Its gripping surface is a polyurethane panel embedded with links of roller chain.
(See page 323.)

Staking Tool for Hard Metals

A simple tool allows small machine shops to stake hard steel without massive presses. The tool forces one part into a recess on another, deforming the receiving part so that it restrains the inserted one. Its use is not limited to hard steel; it can be used as well to assemble parts made of softer materials.
(See page 328.)

High-Speed Wafer Slicer

A high-speed wafer slicer conserves silicon while it speeds up solar-cell production. Two silicon ingots, which are placed in holders on the machine, are sliced simultaneously into wafers by reciprocating wire blades. The wires are impregnated with diamond particles on their lower surfaces.
(See page 324.)

Transfer of Strings to the Module Fixture

Strings of solar cells are positioned accurately in various formats.

NASA's Jet Propulsion Laboratory, Pasadena, California

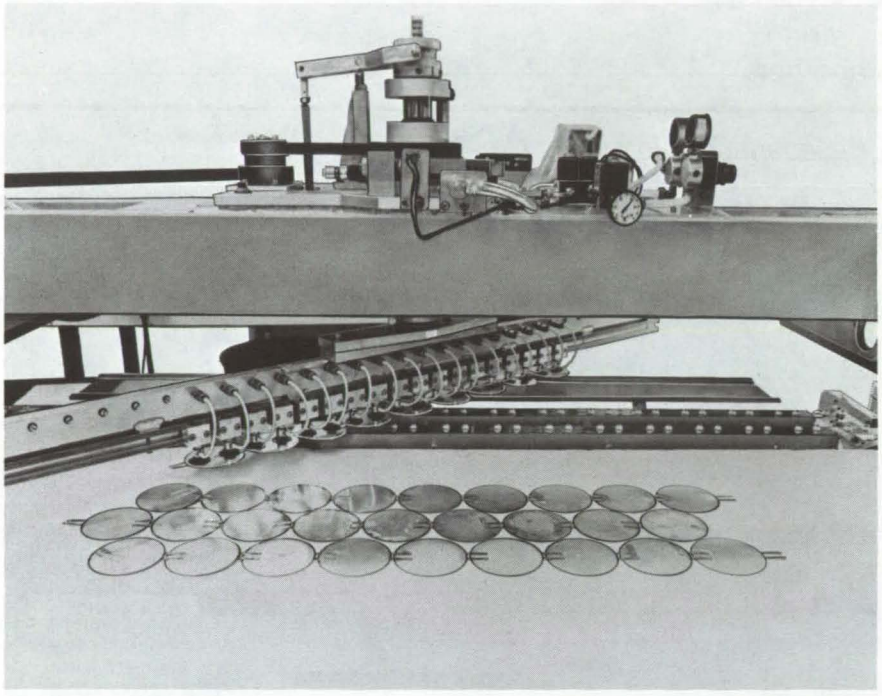

The **Vacuum Transfer Arm** is shown rotating a string of solar cells end for end. It will place the string of cells adjacent to the three strings in the foreground. There are two vacuum cups holding each solar cell in the string being transferred.

The work station for transferring entire strings of solar cells (see preceding articles) places successive strings alined, with an offset, or reversed end for end. Thus, various solar module formats can be accommodated.

The strings of solar cells arrive under the track-mounted vacuum lance described in the preceding article. When a sensor detects the arrival of the end of a string, the lance descends automatically to pick up the cells. The lance then immediately rises so that the next string can arrive underneath it.

In the present version of the system, an operator moves the lance to the correct detented position over the module fixture and actuates the lance cycle to deposit the string in the module fixture. (If the string is known to be defective, the lance is moved instead to a reject station, where the string is deposited.) The operator also controls the motions that are used to reverse strings or to position them with an offset. When the module fixture has been filled, it is removed from the machine for further manufacturing steps, such as wiring interconnects between strings and cleaning.

This work was done by Walter Frasch of Kulicke & Soffa Industries, Inc., for **NASA's Jet Propulsion Laboratory.** *For further information, Circle 64 on the TSP Request Card.*
NPO-15509

Ultrasonic Welding of Graphite/Thermoplastic Composite

Tests show that neither the angular orientation nor vacuum affect weld quality.

Lyndon B. Johnson Space Center, Houston, Texas

Ultrasonic welding of graphite/thermoplastic composite materials eliminates the need for fasteners (which require drilling or punching, add weight, and degrade stiffness) and can be totally automated in beam fabrication and assembly jigs: The feasibility of this technique has been demonstrated in laboratory tests.

The investigation of the effects of gravity and vacuum on the ultrasonic welding process was carried out by instrumenting an off-the-shelf ultrasonic welder to operate in a vacuum chamber at three different angles to the direction of gravity. The test arrangement is shown in the figure. In the first test run, 35 welds were made in air with the welder in a vertical position. The next run of 35 welds were made in vacuum, in the vertical position. Then successive sets of 35 welds were made in air and in vacuum with the welder at 45° and at 90° from vertical. All of the welds were visually inspected, and their strengths were measured by lap-shear and peel tests.

No differences were found between specimens welded in air and those welded in vacuum. Gravity affected welder performance only because the weld horn tended to oscillate laterally during the weld cycle when in the 90° position, thus reducing welding efficiency. (This effect can be corrected by increasing weld pressure or using a stiffer weld

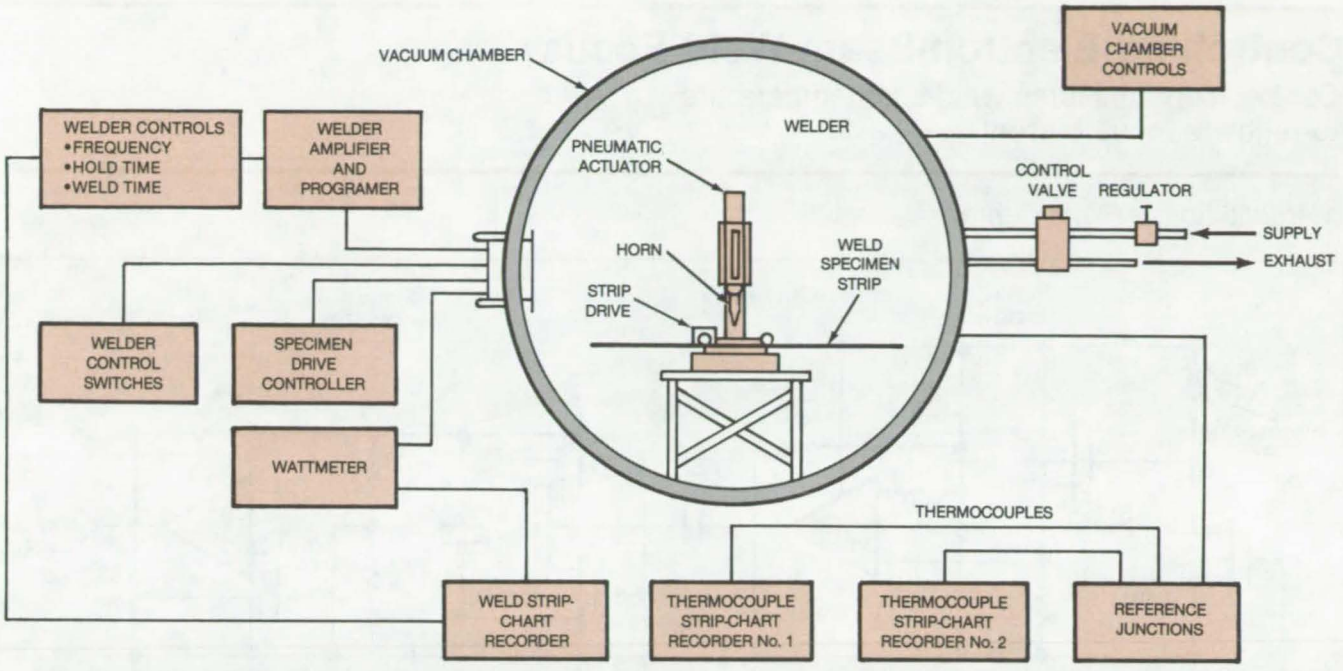

Welder Test Instrumentation and Controls are shown in this diagram. The welder could be rotated to angles of 45° and 90° from vertical in the vacuum chamber to assess the effect of gravity on the welds.

horn; however, it is merely a ground-test consideration and would not affect performance in space.)

The weld power characteristics proved to be a reliable indicator of weld quality. Weaker welds resulting from variations in surface conditions of the strip material were readily detectable by a marked decrease of weld energy. Thus, the tests demonstrated that automatic weld-quality capability can be incorporated into the welding of space structures. Processor control of weld time, hold time, frequency, and weld energy is already used on commercial welders; an added capability for ultrasonic inspection of finished welds would ensure 100 percent verification of weld integrity.

This work was done by Steven S. Hardy and Donald B. Page of General Dynamics Corp. for **Johnson Space Center.** *No further documentation is available.*
MSC-20013

Increasing Metal Fracture Toughness

A brazing technique overcomes the brittleness of high-strength metals at cryogenic temperatures.

Langley Research Center, Hampton, Virginia

Many high-strength metals routinely used at room temperature become brittle and lose fracture toughness (resistance to crack growth) at the low temperatures in the NASA cryogenic tunnels. It has long been recognized that thin sheets of metal have greater fracture toughness than thicker sheets. In a new technique developed at Langley Research Center, several thin sheets are diffusion-brazed together in a vacuum furnace to create a thick piece of metal that retains much of the fracture toughness of its thin components. In preliminary testing, Charpy impact values, indicators of fracture toughness, have been increased by a factor of as much as 5.

This technique is expected to make many of the high-strength stainless steels, not currently suitable, usable at cryogenic temperatures. The concept can also be extended to rods, bars, and other standard shapes that can be constructed from fine wires, rolled foils, and other small metal pieces by diffusion-brazing or other joining processes.

This work was done by Pierce L. Lawing, William H. Wood, and Paul G. Sandefur, Jr., of **Langley Research Center.** *Further information may be found in NASA CR-165745 [N81-30251/NSP], "The Structure and Properties of Diffusion Assisted Bonded Joints in 17-4 PH, Type 347, 15-5 PH and Nitronic 40 Stainless Steels" [$6.50]. A copy may be purchased [prepayment required] from the National Technical Information Service, Springfield, Virginia 22161.*
LAR-12805

Controlling Electron-Beam-Weld Focus

Control loop measures weld-spot temperature to regulate focus current.

Marshall Space Flight Center, Alabama

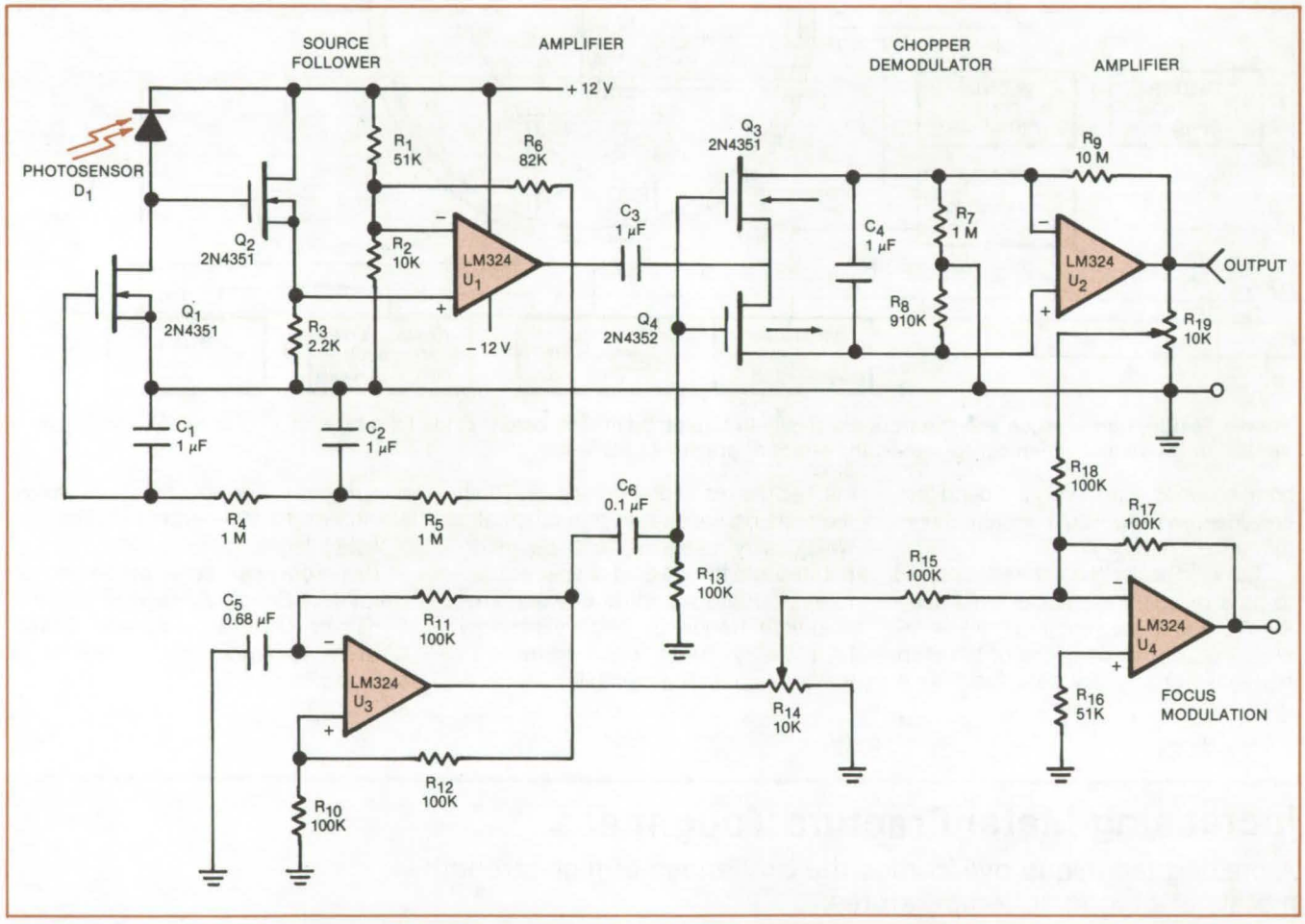

Figure 1. **Feedback Control Circuit** focuses the electron beam in response to the weld temperature sensed by photodiode, D_1.

An electron-beam welder is automatically focused by the feedback circuit shown schematically in Figure 1. A square-wave generator modulates the current in the electron-beam focus coil so that the focal point is varied between points slightly above and below the surface of the weld. A sensor detects the intensity of light emitted by the weld, which is proportional to the fourth power of the temperature at the hottest part of the weld spot. The sensor signal is detected by a chopper demodulator synchronized by the square-wave generator, to determine whether the average position of the focal point is higher than, coincident with, or lower than the optimum point; and the focus coil current is adjusted accordingly.

When the focal point is at the surface of the workpiece, the temperature at the center of the hotspot will be maximum. As the focal point is moved above or below the surface, the electron-beam energy is distributed over a larger area, and peak temperature will decrease. However, if the focal point is controlled so that its average position is at the surface, the power density is approximately constant because the slight degree of defocusing is equal on both sides of the surface. Since power density is then constant, both temperature and light output are also constant. If the beam becomes significantly defocused, however, the light sampled by the sensor will no longer be constant, and the sensor will then produce a difference signal. The difference signal will be detected by a differential amplifier, and a servo circuit will alter the modulating current in the focus coil.

The optics transmit visible light from the weld spot to the sensor while excluding almost all the radiant heat (see Figure 2). An inexpensive glass window admits light to the optics but seals out metal vapors; when the glass becomes

coated with metal, it can be replaced easily. A heat-reflective mirror stops most of the radiant heat and passes visible light. Much of the remaining heat is eliminated by heat-conductive mirrors, which reflect visible light but allow radiant heat to pass through and be lost. A simple lens focuses the visible-light image of the weld spot on the photosensor.

The same principle used to focus the beam can be used to make the beam follow a seam or crack between the parts to be joined. The position of the beam can be alternated between opposite sides of the seam. The temperature in the weld area will be higher on the side of the seam that receives the most power. A servo circuit can center the beam so that it dwells equally on both sides of the seam.

This work was done by F. M. Coate of Rockwell International Corp. for **Marshall Space Flight Center.** *For further information, Circle 65 on the TSP Request Card.*
MFS-19635

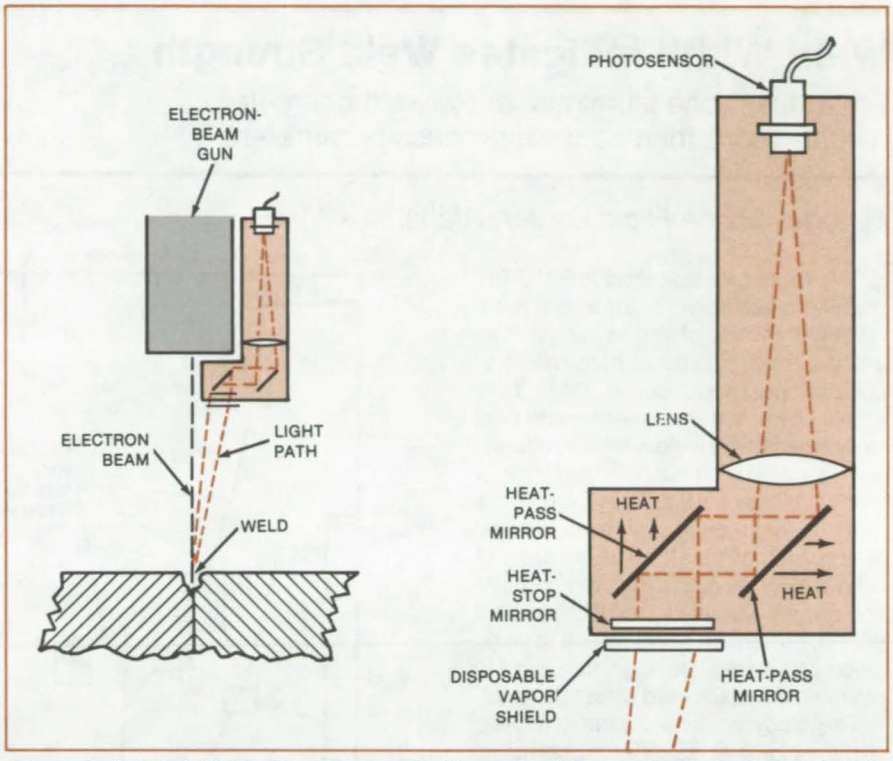

Figure 2. **Visible Light Is Directed to a Photosensor** while heat is eliminated so that it does not damage the sensor, a semiconductor device. An image of the weld spot is thus focused on the sensor. The intensity of the light in the image is a measure of the spot temperature.

Plasma Spray for Difficult-To-Braze Alloys

A sprayed coating of fine nickel powder or powdered braze alloy is an alternative to nickel plating.

Marshall Space Flight Center, Alabama

Nickel plating on the surfaces makes brazing easier for some alloys. Sometimes, however, nickel plating may not be feasible because of the manufacturing sequence, the size of the hardware, or the lack of a suitable source for nickel plating. An alternative surface preparation in such cases is to grit-blast the surface lightly and then plasma-spray 1½ to 2 mils (0.04 to 0.05 mm) of fine nickel powder or braze-alloy material directly on the surface. The powder is sprayed from a plasma gun, using argon as the carrier gas to prevent oxidation of the nickel or braze alloy.

The plasma-spraying technique as a brazing aid to replace nickel plating of braze surfaces can be used for brazing alloys that contain aluminum and titanium, such as A-286, Inconel-718, MAR-M-246, Rene-41, 713, and others. Unlike wet-spray methods, which allow little control and do not work with difficult-to-braze alloys, the plasma-sprayed deposit can withstand handling under manufacturing conditions. Moreover, the sprayed braze alloy does not contaminate furnace atmospheres.

An example of successful use of this technique was the brazing of 1,080 tube-to-hole joints in the aft manifold of a Space Shuttle main-engine flight nozzle. In this case the manifold had been welded to the flight jacket and the braze alloy had been attached to the jacket, prior to the discovery that the nickel plating was peeling off in the manifold holes. The schedule, cost considerations, and lack of nickel-plating facilities all made it mandatory to devise another method for preparing the braze surfaces of the 1,080 holes.

The method used was to plasma-spray Nickel-200 into the entrances and exits of the manifold holes. One constraint on this technique is that alloys containing manganese can be used only if the manganese content is less than 10 percent and special precautions are taken to minimize oxidation of the braze-alloy powder.

This work was done by Alexander Brennan of Rockwell International Corp. for **Marshall Space Flight Center.** *No further documentation is available.*
MFS-19630

Weld Width Indicates Weld Strength

For at least one aluminum alloy, weld geometry reveals more than do weld process parameters.

Marshall Space Flight Center, Alabama

The width of a butt weld in 2219-T87 aluminum has been found to be a more reliable indicator of weld strength than are the more traditional parameters of power input and cooling rate. Yield stress and ultimate tensile strength tend to decrease with weld size (see figure).

This conclusion supports the view of many professional welders who give priority to weld geometry over welding energy or cooling rate as an indicator of weld quality. In fact, it is common practice among welders to adjust weld heat (that is, current) from workpiece to workpiece and even along the same bead to maintain constant weld dimensions.

The study was conducted on specimens welded at 15 different combinations of weld power and heat-removal rate. The specimens were made from plates ¼ inch (6.35 mm) thick, joined with multipass, square-butt, gas/tungsten arc welds.

The elongation at break, yield stress, and ultimate tensile strength were measured for each specimen. Although these properties were clearly functions of both the power input and the cooling rate, the precise relationship could not be discerned. Cooling rate was difficult to determine or even hold constant. Consequently, power input to a weld can be regarded as only a rough determinant of mechanical properties, at best.

The test results agreed generally with predictions based on the soft-interlayer theory of weld strength. According to this theory, weld joints in metals like aluminum may be treated as a soft layer of material between two hard, flat plate ends. If the weld is wider than the thickness of the parent metal plate, the joint yields at about the yield stress of the relatively-soft weld metal. As the weld width decreases, below this value, the joint strength approaches that of the parent metal.

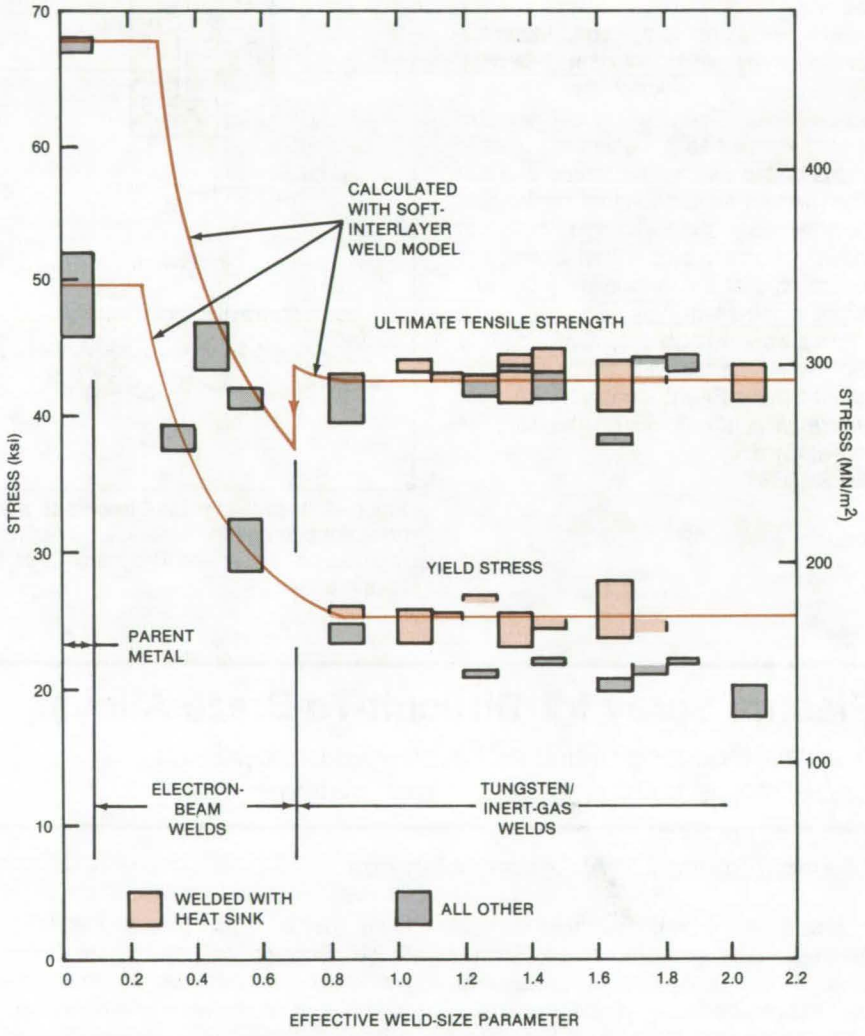

Weld Strength Decreases With Weld Width above a certain value of effective weld size parameter. The parameter is the mean weld width (weld root width plus weld top width divided by 2) divided by plate thickness.

This work was done by A. C. Nunes, Jr., H. L. Novak, and M. C. McIlwain of **Marshall Space Flight Center.** *For further information, Circle 66 on the TSP Request Card.*

MFS-25648

Cleaning Internal-Weld Splatter

Steel balls shaken inside a part remove excess material.

Lyndon B. Johnson Space Center, Houston, Texas

Splattered metal produced by welding can be easily be removed from inaccesible areas by a method resembling ball milling. Hard steel balls are vibrated inside the welded unit so that they "scrub away" excess metal on the interior side of the weld joint.

The method should make it unnecessary to open a joint, to clean it, and to reweld it if splatter occurs. The method also insures that splatter will not loosen later on, causing contamination and failure in fluid systems. It is suitable for parts in which the steel balls can be sealed — such parts as pipes, valves, and tanks.

Balls of stainless steel are placed in the unit to be cleaned. After plugs are inserted in the unit to retain the balls, the unit is inserted in a vibrating-machine fixture. The number of balls and the orientation of the unit that produce fast and thorough cleaning are determined by trial and error. The ball size is selected according to the part internal dimensions and fillets. The unit is shaken along several axes. Finally, the unit is removed, emptied, and inspected.

This work was done by Robert Snodgrass of Parker Hannifin Corp. for **Johnson Space Center.** *No further documentation is available.*
MSC-20068

Eliminating Delamination in Curved Composite Parts

Shims ensure layup of extra material needed to compensate for shrinkage.

Lyndon B. Johnson Space Center, Houston, Texas

A new way of laminating curved graphite/epoxy parts prevents delamination and porosity. Originally developed for a sharply-curved expansion joint frame on the Space Shuttle payload-bay doors, the new method may also be useful in constructing laminated parts for boat hulls or small aircraft. The method employs shims strategically positioned in the layup of graphite/epoxy tape.

Unidirectional tape plies in the channel for the expansion joint frame are continuous around the part. Additional plies are located around cutouts and mounting interfaces for greater strength. The combination of the built-up areas, continuous tape plies, and the tapered closed end of the channel causes problems in the inner flange of the channel: Gaps between side-by-side tapes allow outer plies to bridge to inner ones, pores form, and plies delaminate.

To eliminate these problems, rectangular shims (see figure) are placed in the knee area to accumulate extra tape. The quantity, location, and size of the shims are determined by trial and error and are not necessarily the same for a part of different geometry.

The layup of successive plies proceeds as before, with individual plies being rubbed out by hand. Periodic vacuum-heat debulking compacts the layup. Just before the final bagging and cure, the shims are removed, leaving a gap between the tape and the layup tool at each shim location. The part is then bagged and cured under normal production conditions, resulting in a part that is nonporous and securely laminated in the knee area.

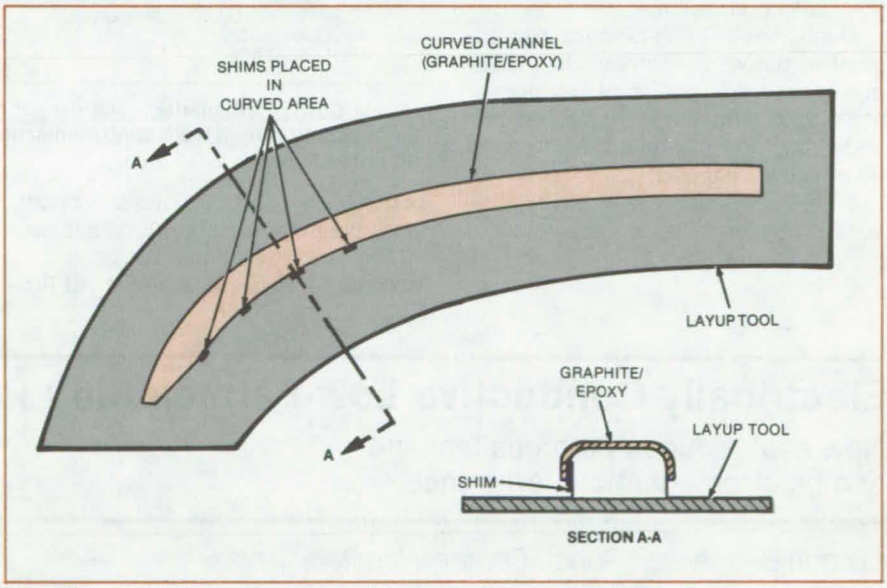

Four Shims Eliminate Porosity and Delamination on the inside knee of a curved channel. The shims allow for extra length in the layup plies. On final cure, the added length compensates for shrinkage that would otherwise have caused delamination.

This work was done by George T. Smith of Rockwell International Corp. for **Johnson Space Center.** *No further documentation is available.*
MSC-20027

Improving Radiometer-Cavity Absorptance

A small tube at the apex of the conical cavity prevents formation of a paint meniscus.

NASA's Jet Propulsion Laboratory, Pasadena, California

In the development of the cavity radiometer sensor shown in the figure, it became apparent to NASA scientists that irregularities in the cavity surface are not the dominant source of error. The principal uncertainty in obtaining a true conical shape is the formation of a paint meniscus at the apex, which truncates the cone and reflects radiation out of the cavity. The size of the meniscus was minimized previously by removing as much of the accumulated paint as possible with a hypodermic syringe, but the properties of the meniscus could not be reproduced or predicted with less than 0.05 percent uncertainty.

To prevent the formation of the meniscus, a small tube is formed at the apex of the cone. One end of the tube, which is bent through a 90° arc, is accessible through a small hole in the thermal conductance.

During the painting process, excess paint is drawn out through the tube, preventing the formation of a meniscus at the apex. After the paint is cured, the end of the tube is crimped shut to form an effective light trap.

With the meniscus-free cavity, the sensor demonstrates an absorptance of 0.999880 ± 0.000020. Equally important, its properties are reproducible.

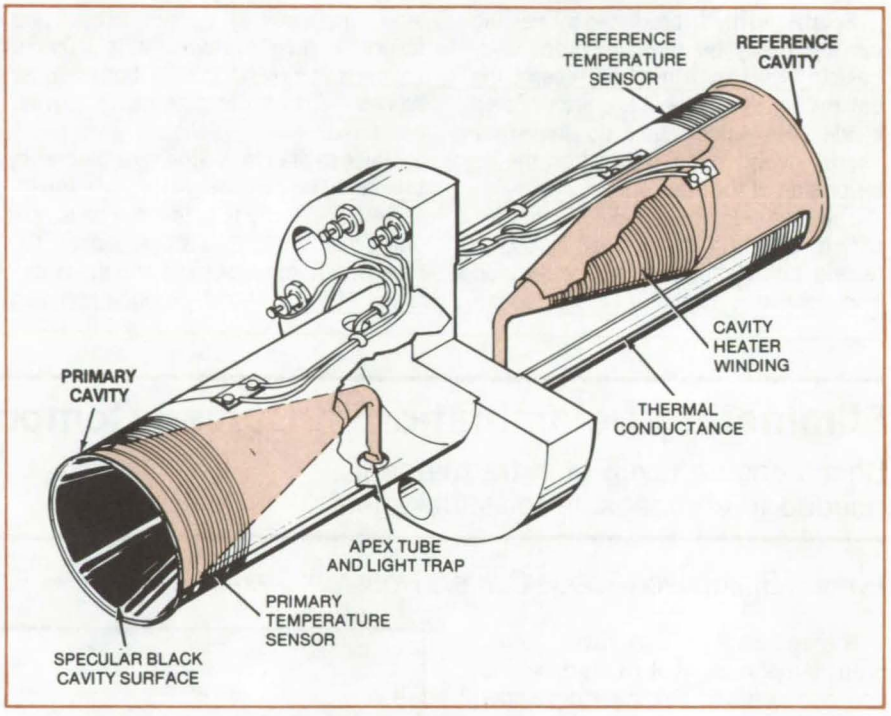

In this **Cavity Radiometer,** each sensor cone ends in a small tube so that the black paint cannot form a truncating meniscus. The inner diameter of the tube is 0.25 mm; its outer diameter is 0.5 mm.

This work was done by Richard C. Willson of Caltech for **NASA's Jet Propulsion Laboratory.** *For further information, Circle 67 on the TSP Request Card.*

NPO-15374

Electrically-Conductive Low-Permeability Pressure Seal

New seal reduces both gas leakage and electromagnetic interference.

Lyndon B. Johnson Space Center, Houston, Texas

A metal-plated butyl rubber seal has been devised for the enclosures of electronic equipment that must be maintained under a dry, inert atmosphere. The seal prevents gas leakage over prolonged periods, while its conductivity suppresses electromagnetic emissions from the sealed equipment.

Simulataneous gas and electromagnetic sealing usually calls for an electromagnetic seal and a separate pressure seal. This, in turn, requires two or more machining operations in each of the sealing flanges and the maintenance of nearly-perfect sealing surfaces. Because precise, near-zero gap alinement has to be maintained, the electromagnetic seal sometimes prevents the proper setting of the pressure seal.

A better approach is to use a conductive elastomer that simultaneously seals against gas and electromagnetic leakage. Heretofore, commercially-available conductive elastomers have been made of silicone rubber impregnated with metallic particles. Silicone, however, has the disadvantage of being permeable to water.

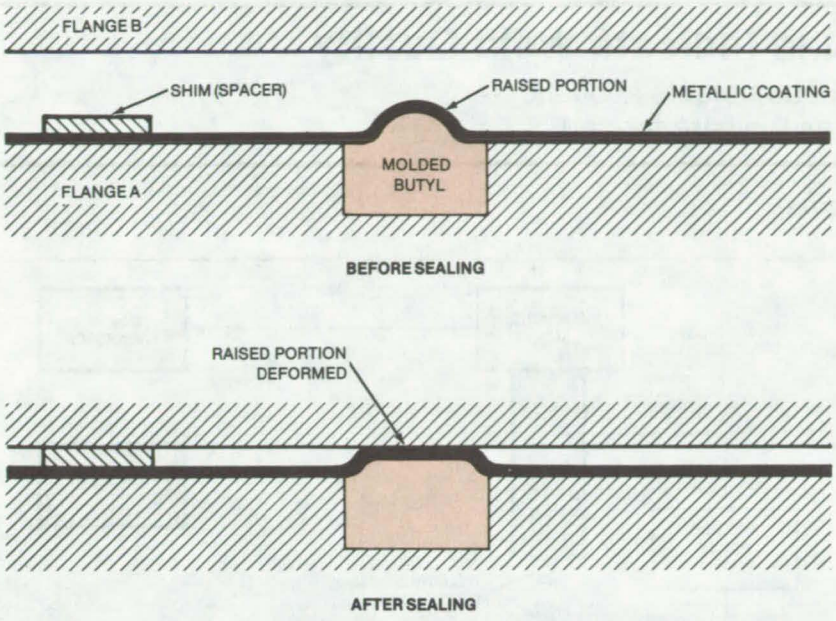

An **Electrically-Conductive Pressure Seal** is formed by depositing aluminum or gold onto the molded-in-place butyl rubber gasket and surrounding areas of flange A. The seal is shown in open (upper) and closed (lower) positions.

In the new system, a thin (up-to-5,000-Å) layer of metal is vacuum vapor-deposited on a molded-in-place butyl rubber gasket and adjacent areas of flange A, as shown in the figure. A small raised portion insures contact with flange B. When sealing pressure is applied, an electrically conductive path is completed between the two flanges, and the butyl rubber deforms to make a pressure seal. The amount of deformation depends on the size and shape of the raised portion and upon the shim thickness. The metal coating is ductile and deforms to fit the shape of the surface of the flange B. An additional advantage is that the metallic coating serves as a redundant gas seal.

Which coating metal is optimum depends upon the flange material. Aluminum is used for pure, uncoated aluminum flanges. If the aluminum flanges are nickel-plated or anodized, then gold is best.

This work was done by Herman C. Krieg of TRW, Inc., for **Johnson Space Center.** *No further documentation is available.*
MSC-20022

Clamp and Gas Nozzle for TIG Welding

Tool holds work while it provides a nonoxidizing atmosphere.

Lyndon B. Johnson Space Center, Houston, Texas

A tool that combines a clamp with a gas nozzle is an aid to tungsten/inert-gas (TIG) welding in hard-to-reach spots. The tool holds the work to be welded while it directs a stream of argon gas at the weld joint, providing an oxygen-free environment for tungsten-arc welding.

The tool consists of a vise, two tubular arms, an adjustable head, and a diffuser (see figure). The two tubes are welded to the vise and serve as extension arms; the lower tube also serves as a channel for the flowing argon. The adjustable head grips the workpiece and holds it securely in place. The diffuser, welded to the lower arm, disperses the argon by passing it through a layer of steel wool and a metal screen. The vise locks the tool members in place.

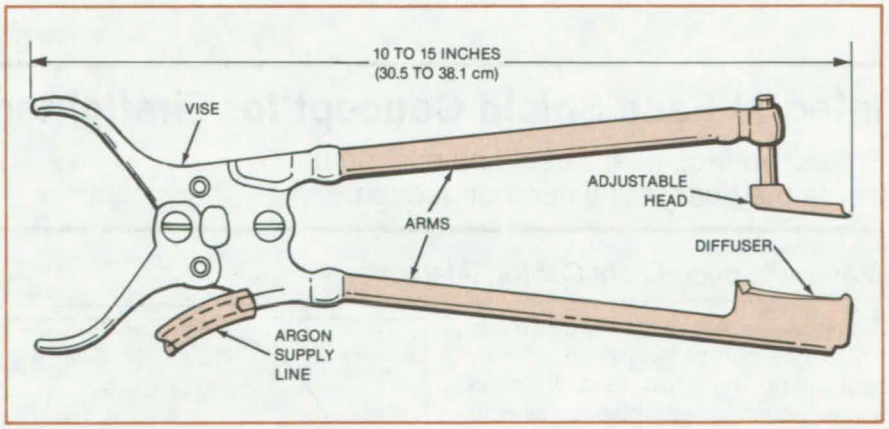

A **Clamp/Gas Nozzle for TIG Welding** holds a workpiece and serves as a conduit for argon or other inert gas. The tool shape is determined by the workpiece geometry.

The tool shape and dimensions are determined by the work piece. The arms can be long or short and straight or curved, according to the contours of the parts to be welded.

This work was done by Galen B. Gue and Herbert L. Goller of AMETEK for **Johnson Space Center.** *No further documentation is available.*
MSC-20108

Acoustic Emissions Could Indicate Weld Quality

A sensor mounted on the welder head detects acoustic emissions emanating from welds as they are formed.

Marshall Space Flight Center, Alabama

Preliminary tests show that the quality of welds can be assessed by an acoustic-emission monitor mounted on the welder. This nondestructive measurement technique allows an operator to determine the uniformity and integrity of the weld as it is being made, to evaluate equipment performance and condition, and to initiate corrective action if quality is not satisfactory.

The acoustic monitoring technique was developed to sense the quality of dual-pulse stitch-wire welds made on the master interconnect boards of the main engine controller for the Space Shuttle. It was incorporated into the stitch-wire welding process to replace a costly 7 pound (31-N) push test to demonstrate weld strength and integrity. However, the concept could readily be applied to the cross-wire and parallel-gap resistance-welding processes that are used in the electronics industry.

The use of the acoustic-emission sensor on the upper electrode of the dual-pulse stitch-wire welder (see figure) has resulted in the successful detection of the acoustic spectrum emanating from the welds as they are produced. A numerical readout and a printout of integrated noise-level count provide the basis for evaluating weld quality. Preliminary test results showed a meaningful correlation between acoustic-emission count and the presence of cold and hot expulsed welds. Electrode surface degradation and the need for redressing have also been detected.

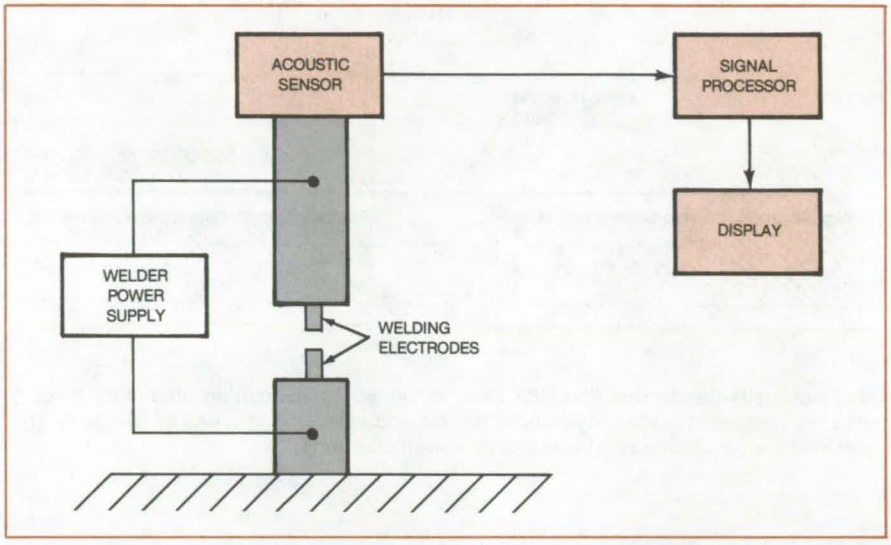

An **Acoustic Sensor** (transducer) mounted on the welder detects emissions from welds as they are being formed. The spectrum of the emissions is read out directly to indicate the quality of the weld and also the condition of the welding apparatus.

This work was done by P. E. Gustafson and F. S. Sutch of Honeywell Inc. for **Marshall Space Flight Center.** *No further documentation is available.*
MFS-25441

Integral Face Shield Concept for Firefighter's Helmet

Protective face guard could be pushed up inside the headgear when not needed.

Marshall Space Flight Center, Alabama

A stowable face shield could be made an integral part of the helmet worn by firefighters. The shield, made from the same tough clear plastic as the removable face shields presently used, would be pivoted at the temples to slide up inside the helmet when not needed (see figure).

A removable face shield may be mislaid and lost when not being used, or it may get scratched or dirty in storage. The stowable face shield, however, being stored in the helmet, is always available, ready for use, and is protected when not being used.

This concept can be applied to other protective headgear too, including hardhats worn in manufacturing and construction work and even some sports helmets such as those worn by jockeys.

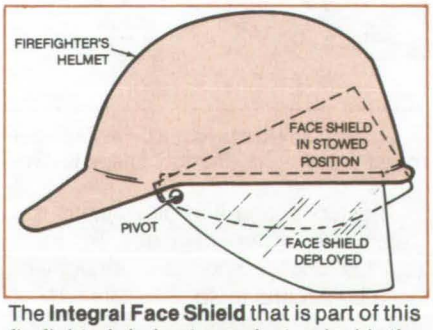

The **Integral Face Shield** that is part of this firefighter's helmet can pivot up inside the headgear for storage and protection when not in use.

This work was done by Fred Abeles, Ernest Hansberry, and Victor Himel of Grumman Aerospace Corp. for **Marshall Space Flight Center.** *No further documentation is available.*
MFS-25493

Radiant Heating of Ampoule Contents

System may heat contents above the softening temperature of the ampoule.

Marshall Space Flight Center, Alabama

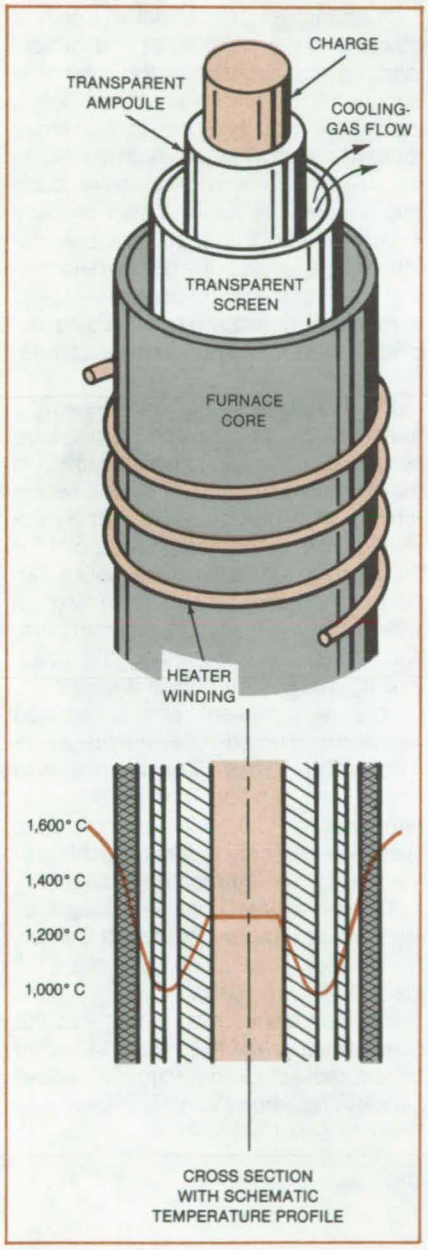

The **Ampoule Charge Heating System** exploits the spectral properties of blackbody radiation and of the ampoule material transparency to heat the charge to a high temperature. The cooling gas prevents softening of the outside wall of the ampoule.

A proposed apparatus would enable the contents of a transparent ampoule (for example, of glass, fused silica, or transparent alumina) to be safely heated above the softening temperature of the ampoule material. Thus the ampoule would not burst, while the ampoule charge would reach the temperature necessary to promote the desired reaction or physical change.

The essential elements of the heating system are shown in the figure. A screen, made of the same material as that of the ampoule, is placed between the ampoule and the furnace lining. A cooling gas or other fluid flows between the screen and the ampoule.

The furnace is raised to a high temperature at which the ampoule material is transparent to much of the blackbody radiation from the furnace lining. The portion of the radiation to which the ampoule is opaque is absorbed by the screen. Most of the radiation that passes through the screen also passes through the ampoule and into the charge, thus heating the charge.

The cooling fluid removes the heat absorbed by the screen and maintains the outside of the ampoule at a temperature below the softening point. The inside of the ampoule in contact with the charge may therefore be above the softening temperature while the outside remains strong enough to keep its shape and to prevent bursting.

Fused silica is essentially transparent to radiation of wavelength shorter than 3.7 microns. At 1,600° C, more than 75 percent of blackbody radiation will pass through. In an ampoule of this material, it should be possible to use the 1,600° C radiation to heat a charge beyond the 1,300° C softening temperature. The outside of the ampoule would be kept rigid by cooling it to 1,000° C. The use of the proposed method may be limited by the tendency of silica (or any other vitreous material) to devitrify on prolonged exposure to temperatures near the softening point.

This work was done by Lawrence R. Holland of Athens State College for **Marshall Space Flight Center.** *No further documentation is available.*

This invention is owned by NASA, and a patent application has been filed. Inquiries concerning nonexclusive or exclusive license for its commercial development should be addressed to the Patent Counsel, Marshall Space Flight Center (see page A5). Refer to MFS-25436.

Blowing Agents for Fabrication of Polyimide Foams

Polyimide resin can be foamed by an agent that is generated within the matrix of the powder precursor. This blowing agent is a mixture of the water and methanol that are byproducts of the condensation/polymerization reaction of the resin. In place of this blowing agent, at least three other blowing agents can be used to attain a more open structure with lower density, which contributes to improved recovery of the foams.

(See page 282.)

Boltless Seal for Electronic Housings

Slip-on clips protect housings for electronic circuitry against electromagnetic interference and dust contamination. A clip is installed by being slipped over the mated flanged edges of a housing box and cover. Because the clip is made of a spring material such as phosphor bronze, it clamps the flanges together tightly but can be removed if it is pulled away from the box.

(See page 248.)

Yielding Torque-Tube System Reduces Crash Injuries

Injury to seat occupants is reduced by a load-limiting system.

Langley Research Center, Hampton, Virginia

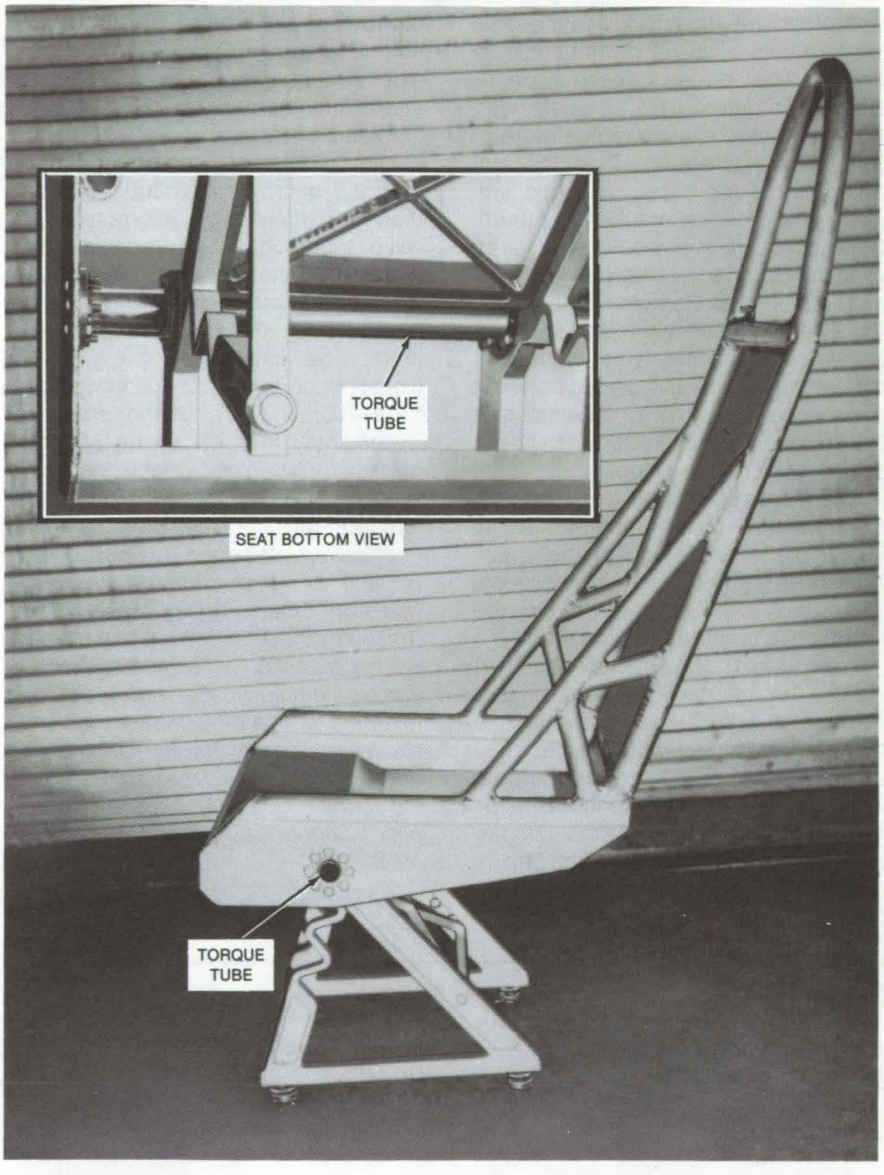

Yielding Torque-Tube System minimizes injuries by limiting the load transferred to the occupant in a crash.

In an aircraft or automotive crash, a combination of longitudinal and vertical loads is transmitted to the seat and occupant. Reaction to these loads causes the seat and occupant to move forward and downward. A new yielding torque-tube system limits these loads and minimizes injuries. When properly integrated into the seat structure, the torque tube yields in the plastic deformation stage of the material and maintains a relatively constant resistance to applied torque for many degrees of rotation.

By properly sizing and selecting material for the yielding torque-tube system, it is possible to limit the loads to the occupant throughout the allowable movement of the seat. By utilizing the yielding torque tube as a pivot point for the legs of the seat, load response can be controlled in a predictable way. A wide variety of seat-support configurations is possible by using this load-limiting design. The design is very compatible with present and anticipated seat-construction techniques, is lightweight, shows smooth response under load, and is not sensitive to temperature. The yielding torque-tube system is expected to find application in the aircraft and automobile industries.

This work was done by Dwight G. McSmith of **Langley Research Center.** *For further information, Circle 68 on the TSP Request Card.*

Inquiries concerning rights for the commercial use of this invention should be addressed to the Patent Counsel, Langley Research Center [see page A5]. *Refer to LAR-12801.*

Monitoring Crystal Growth From Solution

Double-walled cell is used for monitoring the growth of triglycine sulfate.

Marshall Space Flight Center, Alabama

The processing of materials in space will emphasize simple crystal systems. One of these is crystal growth from solution — a simple technique that may be used for many kinds of crystals. The crystals grown from solution in zero-gravity are expected to be more uniform than those grown on Earth, because of the absence of convection currents that would result from the density variations caused by composition gradients associated with growth.

An experimental system for studying the growth of triglycine sulfate (TGS) crystals from solution is shown in the figure. The system consists of an outer cell containing distilled water that is heated and stirred to maintain a constant temperature to within ±0.1° C, an inner (growth) cell containing a supersaturated solution of TGS, and a seed crystal mounted in a plastic-covered stainless-steel sting equipped with a controlled cooling mechanism and temperature sensors.

The dielectric transition temperatures, dielectric properties, and specific heats of growing crystals can be measured with this apparatus. This study is scheduled to be carried out during the SL-3 mission under NASA's program on processing materials in space.

This work was done by R. B. Lal of Alabama Agriculture and Mechanical University for **Marshall Space Flight Center.** *For further information, Circle 69 on the TSP Request Card.*
MFS-25622

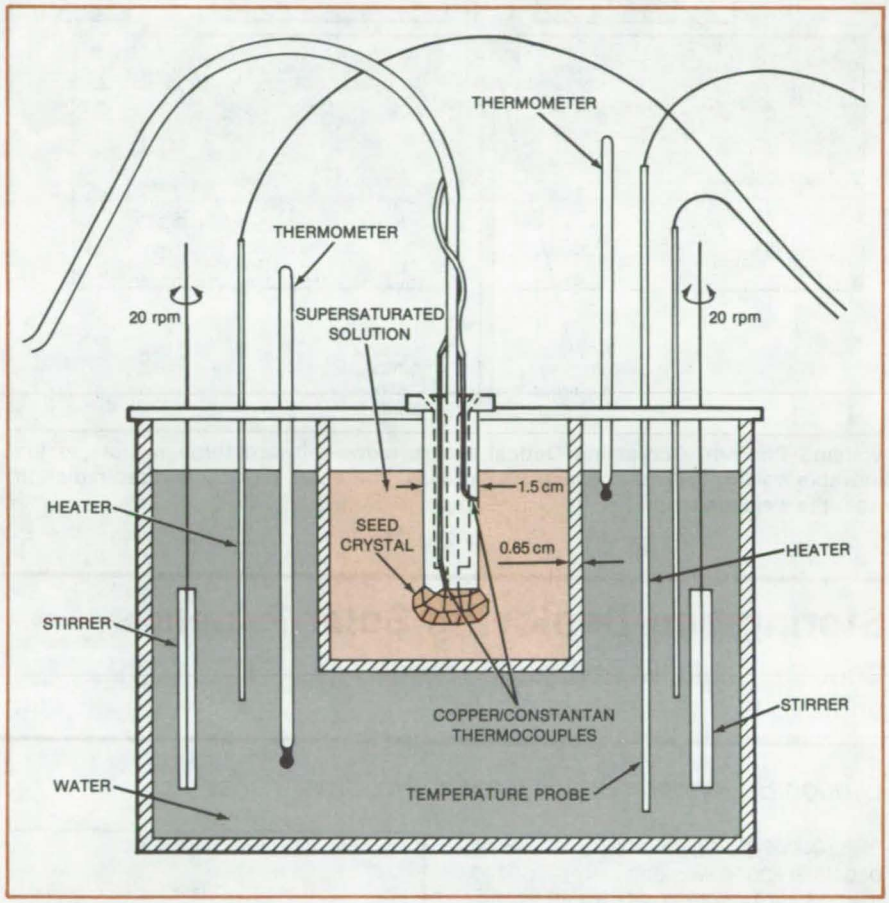

This **Solution Crystal-Growth System** may be used to grow crystals of triglycine sulfate.

Infrared-Controlled Welding of Solar Cells

IR energy carried by optical fibers could help to ensure reliable large-scale arrays.

Marshall Space Flight Center, Alabama

A proposed apparatus for welding large arrays of solar cells to flexible circuit substrates would sense infrared emission from the welding spot. The emission would provide feedback for the control of welding heat.

As shown in the figure, a movable welding platform moves into a solar-array holder against a cell. The holder contains an optical-fiber bundle at its center. The fibers lead to an infrared detector.

The solar cells are placed face down on the holding fixture, and the flexible circuit is positioned over them. The holder is then placed on the welding table with the welding platform in its retracted position.

(continued on next page)

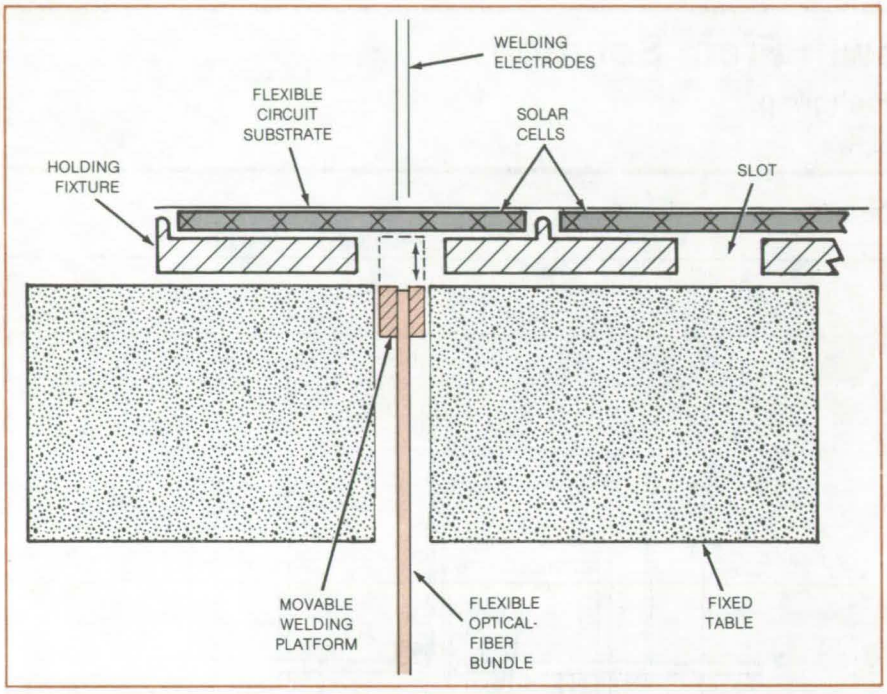

Welding Platform Containing Optical Fibers moves upward through slots in the movable holding fixture to contact solar cells. The fibers pick up infrared radiation from the weld area.

With the first cell in the array over the welding platform, the platform moves into the holder slot until it rests against the surface of the solar cell. The weld is made, controlled by the infrared-sensing circuitry as it monitors the energy passing through the cell into the optical-fiber bundle. The holder can be moved a small distance horizontally if redundant welds are needed.

When the weld is complete, the welding platform is retracted into the table. The control computer moves the holding fixture to the next cell to be welded, and the procedure is repeated.

This work was done by Roy Paulson, Steven E. Finnell, Herman J. Decker, and Jim R. Hodor of Lockheed Missiles & Space Co., Inc., for **Marshall Space Flight Center.** *No further documentation is available.*

Inquiries concerning rights for the commercial use of this invention should be addressed to the Patent Counsel, Marshall Space Flight Center (see page A5). Refer to MFS-25612.

Storing and Deploying Solar Panels

Concept could be applied to mobile photovoltaic generators.

Lyndon B. Johnson Space Center, Houston, Texas

A concept for deploying solar-cell panels in space was originally proposed to allow astronauts to set up a 95.59-meter-square photovoltaic platform without leaving the Space Shuttle orbiter. It may also be adaptable, however, for terrestrial use so that a large-area array of solar cells could be stored compactly, transported easily, and set up quickly for field use.

Working from the orbiter-payload bay, the astronauts erect a square frame and clamp canisters (eight in all) along the base of the frame as the structure is moved through an assembly jig in the bay. The canisters contain rolled-up solar blankets, 11.2 m wide, 0.178 mm thick, and 89 m long, covered with 2- by 4-cm silicon solar cells. The astronauts attach electrical wiring and deployment-cable rigging to the free ends of the rolled blankets as the canisters are attached to the frame (see figure 1).

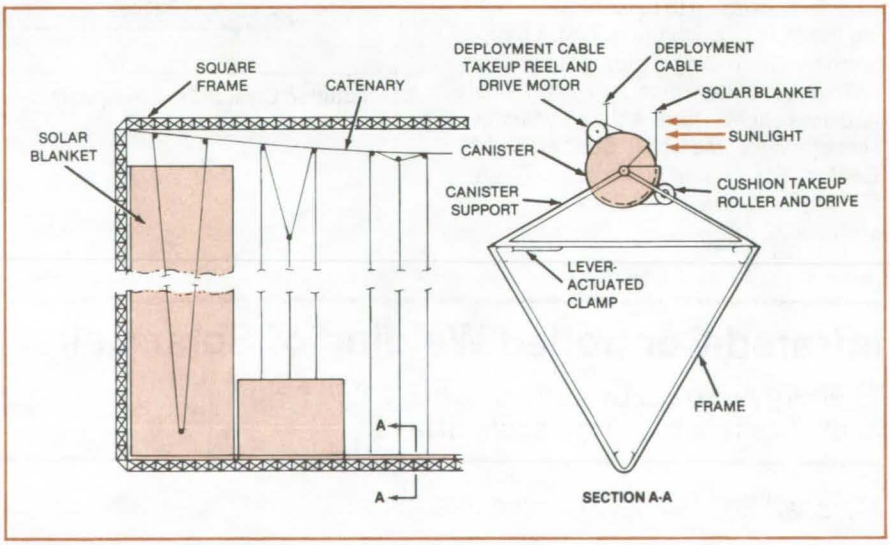

Figure 1. **Like Upward-Drawn Window Shades,** solar blankets are unfurled to a length of 89 m, almost filling the opening in the 95.59-meter-square frame. A catenary wire supports the rigging as deployment cables are taken up by motors on the canisters.

When the frame is completely assembled, the solar blankets are pulled from the canisters, one by one (see Figure 2), by a cable takeup reel driven by an electric motor. A thin cushion sheet is rolled up with each blanket to cushion the solar cells. This sheet is taken up on a roller as the blanket is unfurled. The unrolling proceeds automatically.

The canisters are long, thin cylinders 36 cm in diameter and slightly more than 11 m long. In a terrestrial solar-power version, they could be transported by a truck.

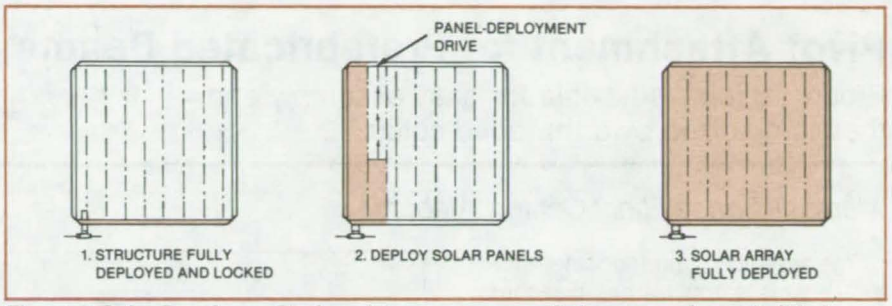

Figure 2. **Solar Panels are Deployed,** in sequence, until the square frame is filled.

This work was done by D. Lee Browning, Hans M. Stocker, and Edward H. Kleidon of General Dynamics Corp. for **Johnson Space Center.** *No further documentation is available.*
MSC-18950

Cutting a Tapered Edge on Padding Material

Felt or rubber is cut while clamped in a deformed condition.

Lyndon B. Johnson Space Center, Houston, Texas

A simple clamping fixture makes it easy to cut a uniform tapered edge on such soft materials as felt or rubber padding. The technique was originally devised for producing a tapered-edge cut on Nomex® (aramid) fiber felt used as a strain-isolation pad under thermal tiles on the Space Shuttle. Cutting at a slant on the dense felt in its free form was extremely difficult and produced rough frayed edges.

As the figure shows, the material to be cut is held in a form block by a plastic insert that is clamped in place. With the material thus held in a slanted position, the edge can be cut straight down; hence the cut depth is minimum. When the material is released from the clamped condition, a straight consistent tapered edge has been formed.

[® Nomex is a registered trademark of E. I. du Pont de Nemours & Co.]

This work was done by Mike J. Mitchell of Rockwell International Corp. for **Johnson Space Center.** *No further documentation is available.*
MSC-20011

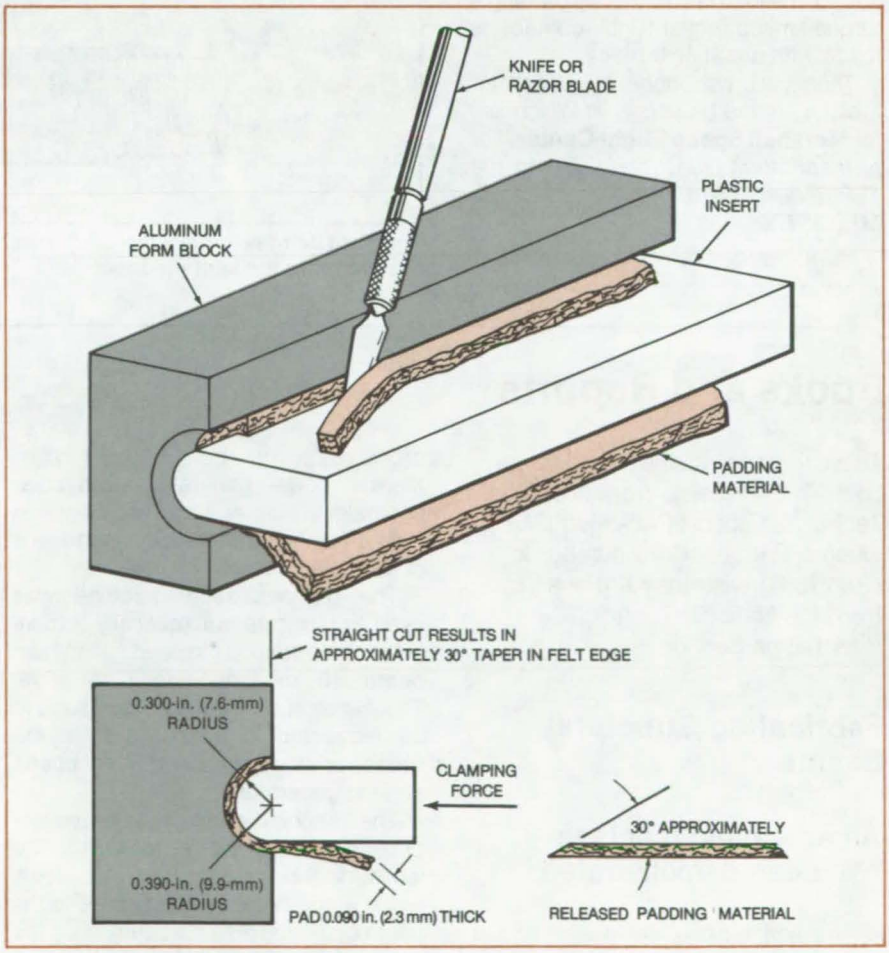

The **Resilience and Flexibility** of felt, rubber, or other padding materials allow them to be clamped in a form block, cut straight down, and then released to produce a straight clean tapered edge.

Pivot Attachment for Prefabricated Beams

Proposed joint is flexible for easy assembly and then is rigidized by a threaded collar.

Marshall Space Flight Center, Alabama

The assembly of prefabricated structural beams for roof trusses, bleachers, or other lightweight structures can be made easier by the use of a flexural pivot at one or both ends. When the pivot is attached, the joint is flexible, thus simplifying alinement; the joint is subsequently rigidized by a threaded collar that completes the attachment.

A proposed flexural pivot attachment is shown in the figure. As can be seen, initial engagement of the joint elements is facilitated by a snap fitting for positive connection via the flexible stiff wire rope. The pivot gives angular freedom for ease of initial assembly. When that alinement freedom is no longer required, the joint is rigidized by rotating a torque-limited collar until contact is made with a mating surface.

This work was done by Henry W. Stoll, Jr., of the University of Wisconsin for **Marshall Space Flight Center.** *For further information, Circle 70 on the TSP Request Card.*
MFS-25476

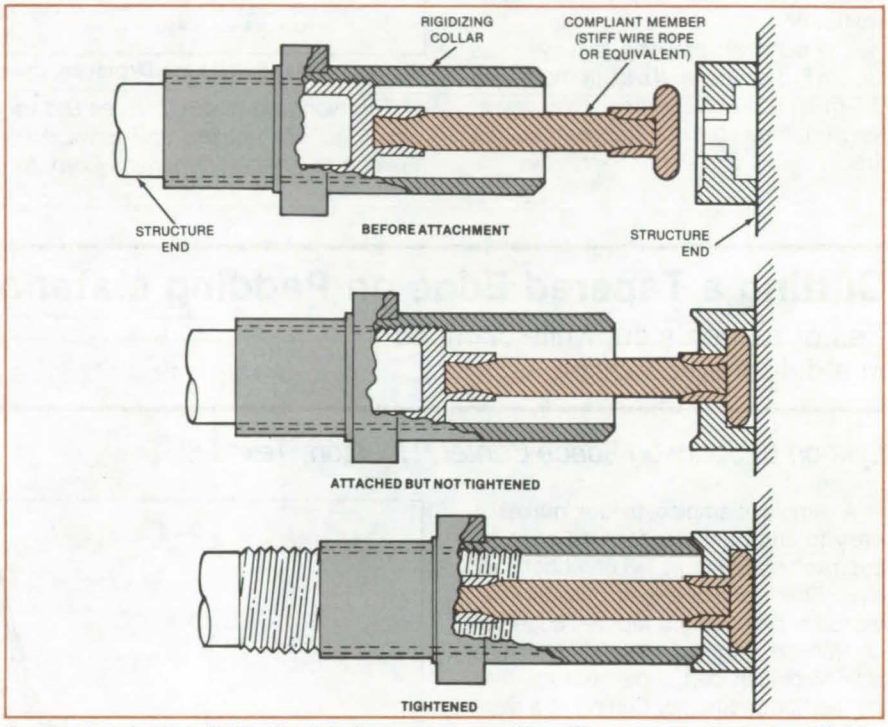

The **Pivot Joint** is initially flexible for easy connection. The screw collar is then tightened to make the joint rigid.

Books and Reports

These reports, studies, and handbooks are available from NASA as Technical Support Packages (TSP's) when a Request Card number is cited; otherwise they are available from the National Technical Information Service.

Fabricating Structural Beams

An automatic machine has been demonstrated.

An automatic machine described in a new report has demonstrated on Earth the feasibility of a machine that could fabricate beams for huge structures in space. Such structures include solar mirrors, radiometer reflectors, microwave power transmitters, solar-thermal power generators, and solar photoelectric generators, ranging in size from a few hundred meters long to tens of kilometers long.

The demonstration machine was used to fabricate automatically a triangular-cross-section trussed aluminum beam 40 m long and 1 m wide. Thousands of such beams would have to be fabricated in space to form the framework for a proposed 5-GW photoelectric generator.

The machine employs three seven-station rolling mills to form the longitudinal beam caps from strip stock, welds prefabricated cross braces to the beam caps, and cuts the beam when the required length has been produced. A computer monitors and controls the operations of rolling the proper length of beam cap to form one beam-bay length (1.5 m), dispensing and welding of cross braces, measuring cumulative beam length, and cutting the beam. Encoders, tachometers, photoelectric sensors, and limit switches provide the monitoring information.

The report provides a structural analysis of the beam and describes the automatic beam builder. It reviews the demonstration and presents data on stress tests of the beam produced in the demonstration.

This work was done by Erich E. Engler, Jim Ehl, Walter Muench, Hank Morfin, John Huber, Ronald Braun, Warren Marx, Al Alberi, Richard Romaneck, Charles Johnson, Ottavio Giannuzzi, and Al Weyhreter of Grumman Aerospace Corp. for **Marshall Space Flight Center.** *To obtain a copy of the report, "Space Fabrication Demonstration System," Circle 71 on the TSP Request Card.*
MFS-25228

Mathematics and Information Sciences

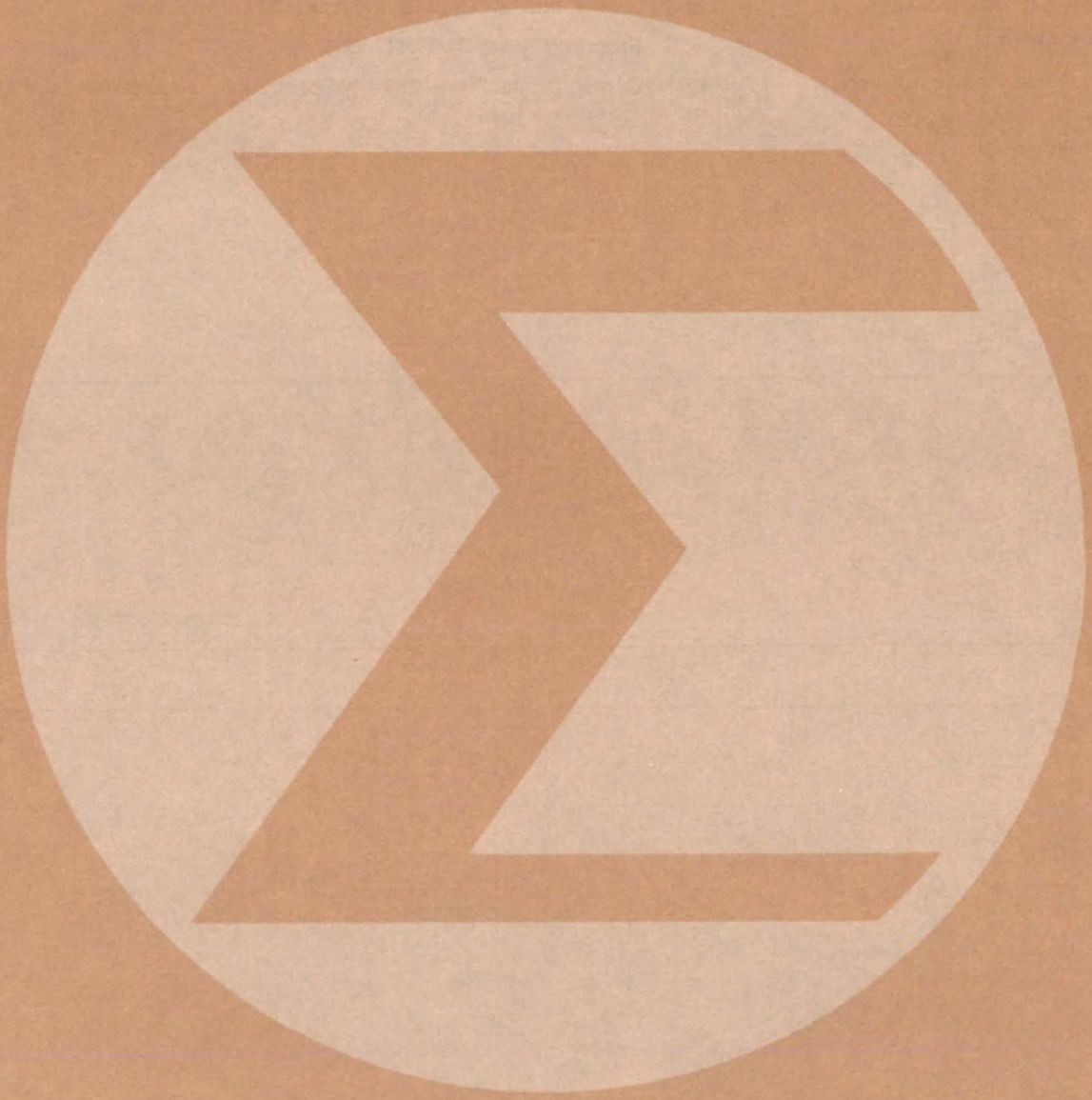

Hardware, Techniques, and Processes

357 Numerical Solution for Navier-Stokes Equations

358 User Documentation for Multiple Software Releases

359 Proposed Reliability/Cost Model

360 Computing the Power-Density Spectrum for an Engineering Model

Numerical Solution for Navier-Stokes Equations

The complete Navier-Stokes problem is formulated for viscous hypersonic flow.

Marshall Space Flight Center, Alabama

A carefully selected blend of computational techniques solves a complete set of equations for viscous, unsteady, hypersonic flow in general curvilinear coordinates. The new algorithm has been tested in the computation of axially directed flow about a blunt body having a shape similar to that of such practical bodies as wide-body aircraft or artillery shells.

The Navier-Stokes equations are differential equations that provide a comprehensive model for compressible, viscous flow in a nonchemically reacting fluid. Conservation equations (for mass, energy, and momentum) and equations of state (relating pressure, temperature, and density) are incorporated, along with relationships giving the specific heats and viscosity parameters of the fluid.

Because of the complexities of applying the equations to hypersonic flow about realistic, blunt bodies, approximate analytical techniques are inadequate, and numerical techniques must be used. A suitably-formulated numerical method should be able to predict the conditions everywhere in the flow field, including the bow-shock region that divides the flow field into regions of supersonic and subsonic flows.

The improved computational method begins with the transformation of the Navier-Stokes equations from Cartesian coordinates to a boundary-fitted curvilinear coordinate system for the prescribed body and boundary shapes. The transformation is performed by the basic relations of tensor analysis. In the case of a two-dimensional flow field, the curvilinear coordinates map onto a rectangular grid in the transformed plane (see figure). Since the body and outer boundary become straight lines in the transformed plane, the statement of boundary conditions is greatly simplified. In addition, this method of generating coordinates easily allows coordinate lines to be concentrated in a dense mesh so as to capture the details of regions of large flow gradients, such as boundary layers and shock waves.

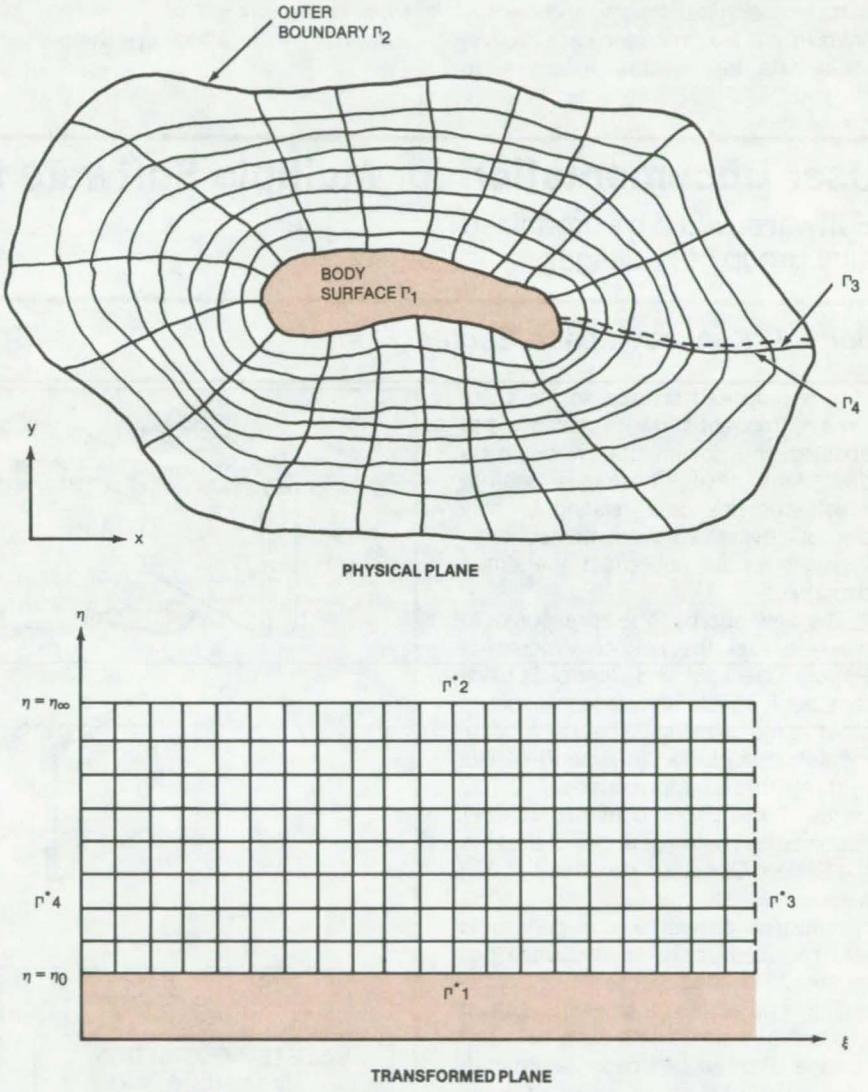

A Curvilinear Coordinate System based on the shape of the body and of the outer boundary is used to simplify the calculations. In the two-dimensional case shown here, the transformed Navier-Stokes equations are expressed in the transformed coordinates ξ,η. The curved physical boundaries Γ become straight lines Γ^* in the transformed coordinates.

The transformed equations retain the conservation-law form of the original equations. The differential equations are replaced by second-order-accurate finite-difference approximations that produce a set of implicit finite-difference equations. The set is solved by the method of successive overrelaxation iteration, which allows for the introduction of an artificial viscosity term to damp numerical (but nonphysical) instabilities. (Numerical instabilities often characterize finite-difference approximations.)

The Navier-Stokes equations are solved for all points in the field; that is, on both sides of the bow shock and within the shock region as well. This is in contrast to previous methods in which

(continued on next page)

the shock has been treated as a sharp boundary across which the solutions for the separated regions had to be fitted via the Rankine-Hugoniot shock relations.

The improved method was applied to axisymmetric flow of a perfect viscous gas about a circular cylinder with hemispherical end caps. Calculations of pressure, temperature, density, and velocity fields for the axisymmetric case provide initial data for eventual extension to three-dimensional flow (e.g., nonzero angle of attack).

The method offers significant computational advantages because of the conservation-law form of the equations and because it reduces the amount of metric data required. A major difficulty was found to lie in choosing an initial guess that would remain stable and converge to a realistic solution. Numerical instabilities persist, although the approach used seems promising. Finally, a more-refined mesh system has been proposed to increase the accuracy of the solution in the shock region.

This work was done by Z. U. A. Warsi, R. A. Weed, and J. F. Thompson of Mississippi State University for **Marshall Space Flight Center.** *For further information, Circle 72 on the TSP Request Card.*
MFS-25617

User Documentation for Multiple Software Releases

Software would be organized as a group of packages.

John F. Kennedy Space Center, Florida

In a proposed solution to the problems of frequent software releases and updates, the documentation would be divided into smaller packages, each of which contains data relating to only one of several software components. Changes would not affect the entire document.

The new approach is in response to the needs of the Launch Processing System Checkout and Control Subsystem, but it should also be applicable to other large systems. The user documentation published in support of this system totals approximately 2,700 pages. These pages comprise 14 user documents. The most active of these is the System Operation document of 800 pages.

Software deliveries are generated and released approximately once per month. "Redlined pages" are subsequently copied, and a small distribution is made coincident with each software release. The redlined pages are generated in lieu of formally published documentation, since the size of existing documents and frequency of software release prohibit the handling of large documentation revisions on a once-per-month production basis.

The problems inherent with copies of redlined pages are as follows:

- Copy quality is poor and difficult to read.
- The distribution of redlined pages creates a storage and maintenance problem, since when redlined data are placed in existing documents, they tend to mask out existing data.

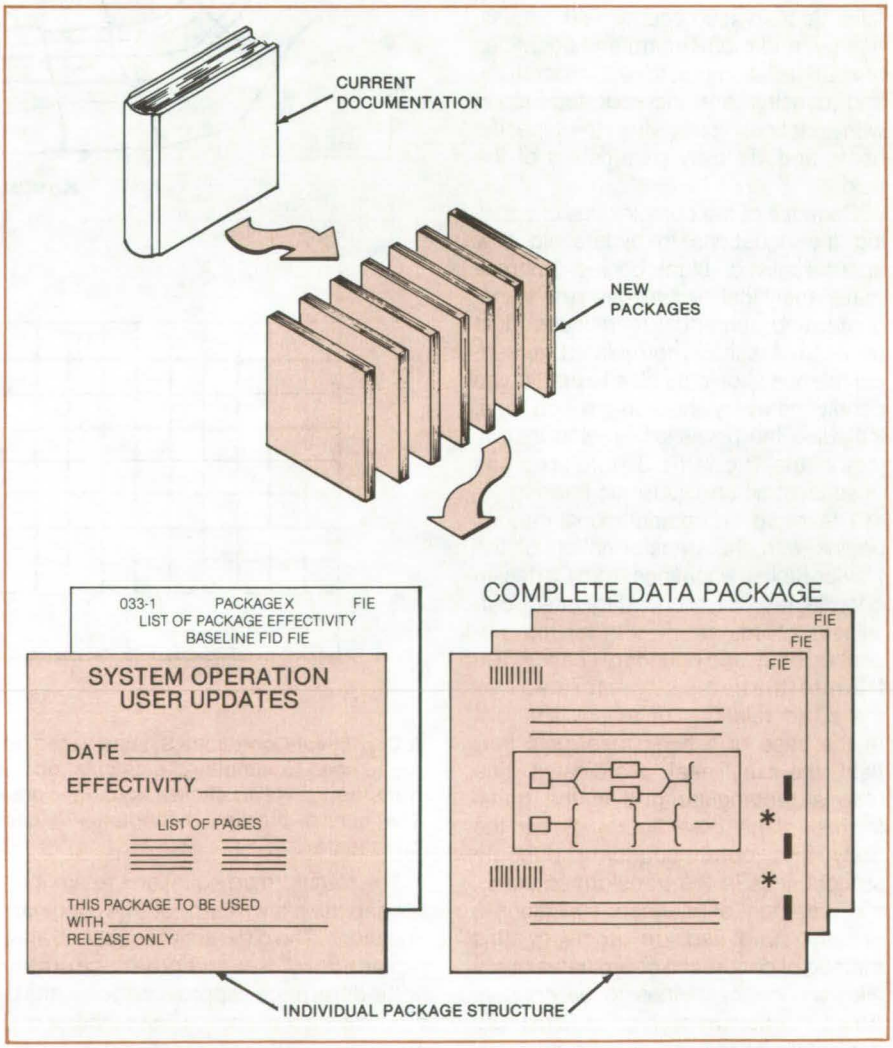

User-Documentation Updates according to the new approach would be released as small packages of formal documentation relating to specific software components.

- Redlined pages create a configuration-management problem since no formal documentation update is made coincident with the release.
- The redlined pages are held in a Pending Publication file until a sufficient quantity (25 percent) of pages has changed to warrant a formal publication of the documentation.

In the new approach, each user package describes only one major user function. Each is marked to permit easy identification of the software release described within the package (see figure). Caution statements are located on the Contents page of the package to advise the potential user of the applicable software release described within the package.

An appropriate packaging configuration is established for each document at the time it is first released. As subsequent software releases occur, new or modified software capabilities are documented by updating the appropriate documentation packages. These packages are produced as formal documentation. Each is printed, distributed, and configuration-controlled as an individual entity. To provide package control, a list of packages is provided that informs the user of the specific effectivity of each package associated with the specific document.

The concept would improve the dissemination of information regarding changes and would improve the quality of the data supporting the packages. It would thus help to insure both timeliness and a more thorough scrutiny of the changes.

This work was done by R. Humphrey of International Business Machines Corp. for **Kennedy Space Center.** *No further documentation is available.*
KSC-11189

Proposed Reliability/Cost Model

An approach is suggested for reliability/cost estimates for complex systems.

Marshall Space Flight Center, Alabama

A new technique estimates the cost of an improvement in reliability for a complex system. The model format/approach is dependent upon the use of subsystem cost-estimating relationships (CER's) in devising a cost-effective policy.

The objectives of a reliability/cost model would normally include the provision of one or more of the following:

- Means to forecast effects on the reliability of the overall system of changes in reliability/cost relationships of the subsystems;
- Means to allocate programed increases or decreases in the cost/reliability function of the whole system among the various subsystems; and
- System methodology to evaluate the cost effectiveness of alternate system configurations or operating plans.

The CER must be established for each subsystem from technical reliability and cost experiences with the subsystem. The example in the figure illustrates typical CER's with relative-cost-versus-reliability plots for the electrical subsystems of two types of spacecraft. The selection of a representative set of subsystem CER's (from the electrical subsystem, mechanical subsystem, and so forth) is up to the decisionmaker, as long as the overall model constraints and requirements are met and as long as the CER's are mathematically well behaved.

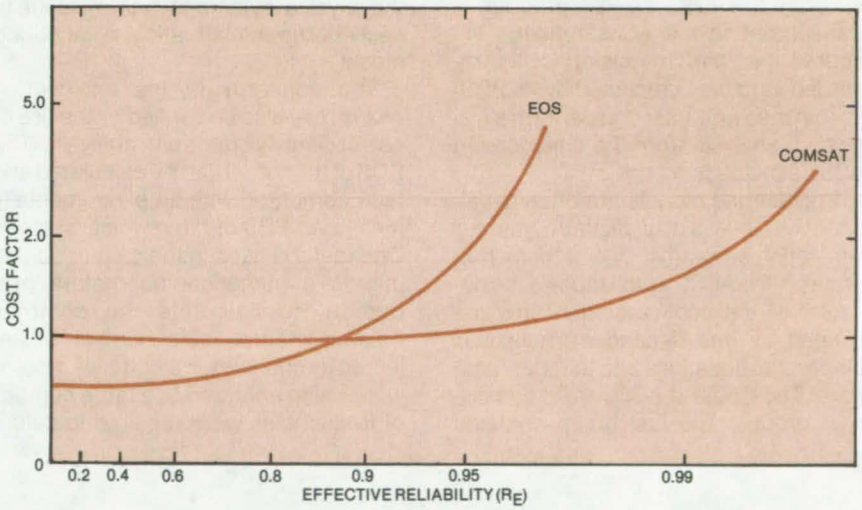

Typical Cost-Versus-Reliability Curves illustrate the concept of subsystem cost-estimating relationships (CER's) essential to the method. These curves are for the electrical subsystems of two types of spacecraft.

The representative set of CER's is used to form a characteristic master cost-versus-reliability function for the whole system. The overall cost figure of merit (a relative measure of total system cost) is taken as a geometric, rather than an arithmetic, sum of subsystem costs. This multiplicative format tends to embed each of the participating variables, minimizing unknown or indeterminate influences and interactions among and within the various subsystems.

The proposed methodology should have application in the broad range of engineering management decisions. By organizing the data requirements and clarifying the assumptions to be made, it can help in the development of cost-effectiveness and reliability relationships. Model users should be able to predict the marginal effect on the reliability of a system from increases or decreases in the resources allocated to reliability.

(continued on next page)

This work was done by Leon M. Delionback of **Marshall Space Flight Center.** *Further information may be found in NASA TMX-64777 [N73-32372/NSP], "Proposed Reliability Cost-Model" [$6.50]. A paper copy may be purchased [prepayment required] from the National Technical Information Service, Springfield, Virginia 22161. The report is also available on microfiche at no charge. To obtain a microfiche copy, Circle 73 on the TSP Request Card.*
MFS-25494

Computing the Power-Density Spectrum for an Engineering Model

A fast-Fourier-transform technique conserves computer resources.

Langley Research Center, Hampton, Virginia

A computer program for calculating of the power-density spectrum (PDS) from a data base generated by an Advanced Continuous Simulation Language (ACSL) uses an algorithm that employs the fast Fourier transform (FFT) to calculate the PDS of the variable. This is accomplished by first estimating the autocovariance function of the variable and then taking the FFT of the smoothed autocovariance function to obtain the PDS. The PDS program is transparent to the ACSL run-time executive (i.e., the time history of the recorded variable is replaced by its PDS) so that the ACSL user can perform a frequency analysis from the time-domain ACSL simulation model.

Engineering models are often developed with the aid of digital computer simulation programs. One of these programs is the ACSL which models the behavior of the continuous systems described by time-dependent, nonlinear differential equations and transfer functions. The inputs to ACSL are in two distinct groups: The first group contains those inputs concerned with defining the model or structure of the system being simulated; the second group contains the sequence of commands that execute this model, such as change parameters, start runs, and plot data. One of the outputs of ACSL can be the time history of specified dynamic variables, sampled at regular intervals and stored on a mass storage device. This record may be compared with the behavior of the physical system to determine the fidelity of the mathematical engineering model.

The accuracy of the engineering model may also be verified by the use of power-density-spectrum analysis. The PDS of the model can be calculated and then compared with an experimentally measured PDS of the physical system. One method used in the past to do this utilizes a numerical quadrature procedure, to calculate the complex Fourier integral, at a number of selected frequencies. If a complex system were being analyzed or a large number of frequencies were required to define the PDS, the numerical quadrature method could use a substantial amount of computer resources.

The new program utilizes a fast-Fourier-transform technique to estimate the PDS of the model. Because of the efficiency of the FFT, the program should require less computer resources than other methods. The program is an extension of the ACSL system so that the PDS analysis can be performed as part of the ACSL sequence of commands that exercise the model.

This work was done by Henry J. Dunn of **Langley Research Center.** *Further information may be found in NASA TM-83120 [N81-25699/NSP]. "A Computer Program for Estimating the Power-Density Spectrum of Advanced Continuous Simulation Language Generated Time Histories" [$6.50]. A copy may be purchased [prepayment required] from the National Technical Information Service, Springfield, Virginia 22161.*
LAR-12918

SUBJECT INDEX

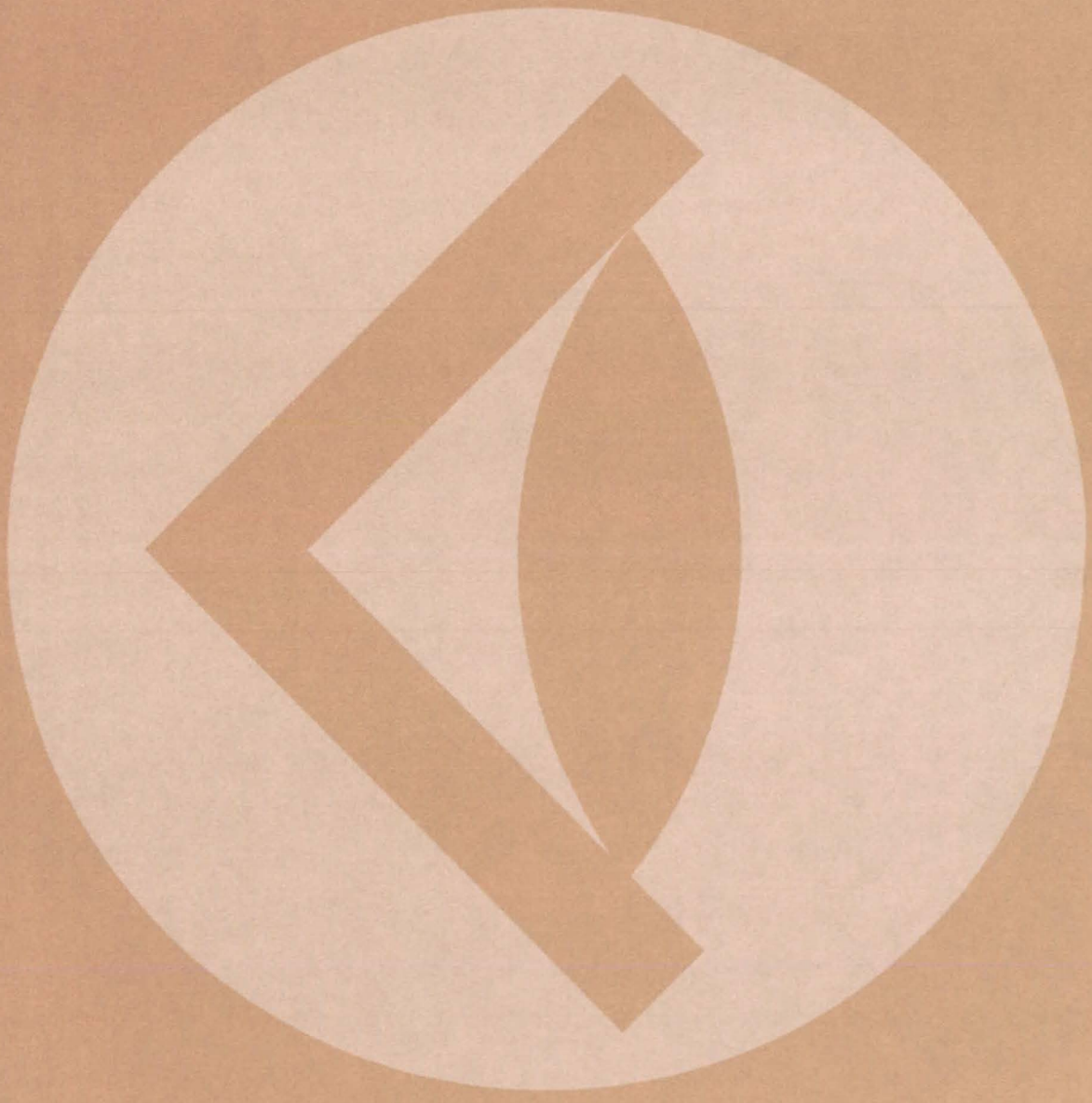

ABSORPTANCE
Improving radiometer-cavity absoptance
page 346 NPO-15374

ACOUSTIC MEASUREMENTS
Acoustic emmissions could indicate weld quality
page 348 MFS-25441

Sound-burst generator for measuring coal properties
page 278 MFS-25438

ACRYLATES
Silicone acrylate copolymers
page 277 NPO-15523

Thermal polymerization of n-butyl acrylate
page 288 NPO-15010

ADHESION TESTS
Double-adhesive tape test reduces waste
page 306 MSC-20047

AIRCRAFT INSTRUMENTS
Improved magnetic-field-component resolvers
page 296 LAR-12638

AIRFOILS
Algorithm for unsteady potential flow about airfoils
page 310 ARC-11378

High-lift separated flow about airfoils
page 315 LAR-12853

AMPLIFIERS
Low-noise band-pass amplifier
page 254 GSC-12567

Wideband amplifier with subpicosecond stability
page 247 GSC-12646

AMPOULES
Radiant heating of ampoule contents
page 349 MFS-25436

ANCHORS (FASTENERS)
Universal assembly for captive bolts
page 322 MSC-18905

ANTENNA ARRAYS
Modular Amplifier/antennna arrays
page 257 MSC-18981

ANTENNA FEEDS
Unequal-split strip-line power divider
page 249 LAR-12797

ARC DISCHARGES
Arc-free high-power dc switch
page 255 MSC-20091

ASSAYING
Electrochemical assay of gold-plating solutions
page 280 MFS-19639

ASSEMBLING
Automated solar-array assembly
page 333 NPO-15501

Bonder for solar-cell strings
page 338 NPO-15507

Orienting and applying flux to solar cells
page 335 NPO-15504

Solar-cell string conveyor
page 337 NPO-15508

Tab interconnect work station
page 336 NPO-15505

Transfer of strings to the module fixture
page 340 NPO-15509

Transporting solar-cell strings
page 339 NPO-15502

Vacuum pickup for solar cells
page 334 NPO-15500

Walking-beam solar-cell conveyor
page 334 NPO-15503

Work station for inverting solar cells
page 337 NPO-15506

ATTITUDE INDICATORS
A simple tiltmeter
page 319 ARC-11344

AUTOMATIC PILOTS
Simple magnetometer for autopilots
page 297 LAR-12832

BAILOUT
Explosively actuated opening for rapid egress
page 312 LAR-12624

BALANCING
Flywheels would compensate for rotor imbalance
page 323 GSC-12550

BALL BEARINGS
Tests of 38 ball-bearing greases
page 330 MFS-25624

BANDPASS FILTERS
Low-noise band-pass amplifier
page 254 GSC-12567

BEAM SWITCHING
Rotating the plane of parallel light beams
page 267 ARC-11311

BEAMS (SUPPORTS)
Fabricating structural beams
page 354 MFS-25228

BENDING
Precise restraightening of bent studs
page 321 MFS-19632

BIOINSTRUMENTATION
Cuff for blood-vessel pressure measurements
page 291 ARC-11264

BLOOD PRESSURE
Cuff for blood-vessel pressure measurements
page 291 ARC-11264

BOLTS
Safety bolt doubles as a bushing-removal tool
page 326 MSC-20032

Universal assembly for captive bolts
page 322 MSC-18905

BORON REINFORCED MATERIALS
Predicting tensile strengths of boron/aluminum composites
page 305 LEW-13745

BOUNDARY LAYER SEPARATION
High-lift separated flow about airfoils
page 315 LAR-12853

BRAKES (FOR ARRESTING MOTION)
Torque simulator for rotating systems
page 311 LAR-12751

BRAZING
Low-gold-content brazing alloys
page 280 MFS-19629

Plasma spray for difficult-to-braze alloys
page 343 MFS-19630

BROADBAND AMPLIFIERS
Wideband amplifier with subpicosecond stability
page 247 GSC-12646

BUBBLES
Gas diffusion in fluids containing bubbles
page 286 NPO-15060

BUCKLING
Structural design with stress and buckling constraints
page 314 MFS-25234

BUSHINGS
Safety bolt doubles as a bushing-removal tool
page 326 MSC-20032

CARBON
Coal as a substitute for carbon black
page 277 NPO-15461

CATALYSTS
Catalyzing the combustion of coal
page 279 NPO-15456

CHECKOUT
One way of testing a distributed processor
page 263 KSC-11123

Processing PCM data in real time
page 263 KSC-11131

CHEMICAL ANALYSIS
Electrochemical assay of gold-plating solutions
page 280 MFS-19639

CLAMPS
Clamp and gas nozzle for TIG welding
page 347 MSC-20108

CLEANING
Brushless cleaning of solar panels and windows
page 325 NPO-14922

Cleaning internal-weld splatter
page 345 MSC-20068

CLEANLINESS
Detecting contamination with photoelectron emission
page 307 MFS-25619

CLIPS
Boltless seal for electronic housings
page 248 NPO-14818

COAL
Catalyzing the combustion of coal
page 279 NPO-15456

Sound-burst generator for measuring coal properties
page 278 MFS-25438

COAL UTILIZATION
Coal as a substitute for carbon black
page 277 NPO-15461

COATINGS
Binders for thermal-control coatings
page 287 MFS-25620

COMBUSTION EFFICIENCY
Catalyzing the combustion of coal
page 279 NPO-15456

COMPARATORS
Precise phase comparator for nearly equal frequencies
page 252 GSC-12645

COMPOSITE MATERIALS
Eliminating delamination in curved composite parts
page 345 MSC-20027

Graphite-fiber-reinforced glass-matrix composite
page 286 LAR-12764

Predicting tensile strengths of boron/aluminum composites
page 305 LEW-13745

Predicting the strengths of angle-plied laminates
page 304 LEW-13733

Small fixture strains composites for environmental tests
page 298 NPO-15062

Ultrasonic instrument for evaluation of composites
page 298 LEW-13716

Ultrasonic welding of graphite/thermoplastic composite
page 340 MSC-20013

COMPRESSION TESTS
New configuration for compression-test fixture
page 301 MSC-18723

CONTAMINATION
Detecting contamination with photoelectron emission
page 307 MFS-25619

CONTROL EQUIPMENT
Hybrid position/force control of robot manipulators
page 320 NPO-14997

COPOLYMERS
Silicone acrylate copolymers
page 277 NPO-15523

COST ANALYSIS
The economics of solar heating
page 274 MFS-25391

COST EFFECTIVENESS
Proposed reliability cost model
page 359 MFS-25494

COUPLINGS
Pivot attachment for prefabricated beams
page 354 MFS-25476

CRYOGENIC FLUID STORAGE
Improved nozzle would reduce cryogenic boiloff
page 327 MFS-25589

CRYSTAL GROWTH
Monitoring crystal growth from solution
page 351 MFS-25622

CRYSTAL STRUCTURE
XPS study of SiO_2 and the Si/SiO_2 interface
page 281 NPO-14968

CUFFS
Cuff for blood-vessel pressure measurements
page 291 ARC-11264

CUTTING
Cutting a tapered edge on padding material
page 353 MSC-20011

High-speed wafer slicer
page 324 NPO-15463

DATA PROCESSING EQUIPMENT
Programable interface handles many peripherals
page 262 KSC-11132

DATA SAMPLING
Analyzing multirate-sampled systems
page 264 MFS-25541

DEFLECTION
Plastic and large-deflection analysis of nonlinear structures
page 314 LAR-12816

DEGRADATION
Mass-loss buttons monitor material degradation
page 302 MSC-18903

DELAMINATING
Eliminating delamination in curved composite parts
page 345 MSC-20027

DESCALING
Cleaning internal-weld splatter
page 345 MSC-20068

DIFFUSION THEORY
Gas diffusion in fluids containing bubbles
page 286 NPO-15060

DIMENSIONAL MEASUREMENT
Tile-gap measurement tool
page 300 MSC-20057

DOCUMENTATION
User documentation for multiple software releases
page 358 KSC-11189

DOPPLER EFFECT
Method for canceling ionospheric Doppler effect
page 261 MFS-25589

DYNAMIC STABILITY
Analyzing multirate-sampled systems
page 264 MFS-25541

EGRESS
Explosively actuated opening for rapid egress
page 312 LAR-12624

ELASTIC DEFORMATION
Plastic and large-deflection analysis of nonlinear structures
page 314 LAR-12816

ELASTIC WAVES
Elastic surface wrinkling
page 313 NPO-15091

ELECTRIC POTENTIAL
Line-replaceable-unit analysis
page 257 MSC-20183

ELECTROMAGNETIC SHIELDING
Electrically-conductive low-permeability pressure seal
page 347 MSC-20022

ELECTRON BEAM WELDING
Controlling electron-beam-weld focus
page 342 MFS-19635

ELECTRONIC CONTROL
Infrared-controlled welding of solar cells
page 351 MFS-25612

ELECTRONIC EQUIPMENT TESTS
High-density terminal box for testing wire harness
page 250 NPO-15147

ELECTROPLATING
Electrochemical assay of gold-plating solutions
page 280 MFS-19639

ENERGY ABSORPTION
Yielding torque-tube system reduces crash injuries
page 350 LAR-12801

ENGINE MONITORING INSTRUMENTS
Modular engine instrumentation system
page 309 LEW-13729

ENVIRONMENTAL CONTROL
Environmental-analysis routine library
page 292 MSC-18925

ENVIRONMENTAL TESTS
Small fixture strains composites for environmental tests
page 298 NPO-15062

EPOXY COMPOUNDS
Neutralizing amine-cured epoxy surfaces
page 284 GSC-12686

ESCAPE SYSTEMS
Explosively actuated opening for rapid egress
page 312 LAR-12624

EXPLOSIVE DEVICES
Explosively actuated opening for rapid egress
page 312 LAR-12624

EYE PROTECTION
Integral face shield for concept firefighter's helmet
page 248 MFS-25493

FASTENERS
Pivot attachment for prefabricated beams
page 354 MFS-25476

Universal assembly for captive bolts
page 322 MSC-18905

FINITE ELEMENT METHOD
Vibration analysis with finite dynamic elements
page 313 NPO-15087

FIRE FIGHTING
Integral face shield concept for firefighter's helmet
page 248 MFS-25493

FIXTURES
New configuration for compression-test fixture
page 301 MSC-18723

Small fixture strains composites for environmental tests
page 298 NPO-I5062

FLASH LAMPS
Flashlamp driver for quasi-CW laser pumping
page 253 GSC-12566

FLATNESS
Gage for surface waviness
page 301 MSC-20055

FLOW DISTRIBUTION
High-lift separated flow about airfoils
page 315 LAR-12853

FLOW MEASUREMENT
Hot film static-pressure probe for flow-field surveys
page 303 LAR-12799

FLUID FLOW
Algorithm for unsteady potential flow about airfoils
page 310 ARC-11378

Hot film static-pressure probe for flow-field surveys
page 303 LAR-12799

Numerical solution for Navier-Stokes equations
page 357 MFS-25617

FLYWHEELS
Flywheels would compensate for rotor imbalance
page 323 GSC-12550

FOAMS
Blowing agents for fabrication of polyimide foams
page 282 MSC-18993

FOCUSING
Controlling electron-beam-weld focus
page 342 MFS-19635

FOLDING STRUCTURES
Storing and deploying solar panels
page 352 MSC-18950

FRACTURE STRENGTH
Increasing metal fracture toughness
page 341 LAR-12805

GAS DETECTORS
Vapor detector
page 282 MSC-18989

GASEOUS DIFFUSION
Gas diffusion in fluids containing bubbles
page 286 NPO-15060

GASKETS
Electrically-conductive low-permeability pressure seal
page 347 MSC-20022

GLASS
Gas diffusion in fluids containing bubbles
page 286 NPO-15060

Graphite-fiber-reinforced glass-matrix composite
page 286 LAR-12764

Using Nomarski interference to detect microcracks in glass
page 310 GSC-12649

GOLD
Electrochemical assay of gold-plating solutions
page 280 MFS-19639

Low-Gold-Content Brazing Alloys
page 280 MFS-19629

GRAPHITE
Graphite-fiber-reinforced glass-matrix composite
page 286 LAR-12764

GREASES
Tests of 38 ball-bearing greases
page 330 MFS-25624

GRIFFITH CRACKS
Using Nomarski interference to detect microcracks in glass
page 310 GSC-12649

GYROSCOPES
Flywheels would compensate for rotor imbalance
page 323 GSC-12550

HEAT TRANSFER
Heat-exchange fluids for sulfuric acid vaporizers
page 285 NPO-15015

HEATING EQUIPMENT
Evaluation of a line-concentrating solar collector
page 271 MFS-25778

Hot water for motor inn — Garland, Texas
page 273 MFS-25726

Manifold insulation for solar collectors
page 271 MFS-25779

Radiant heating of ampoule contents
page 349 MFS-25436

Solar heater in a West Virginia college
page 272 MFS-25706

Solar heating in an elementary school
page 272 MFS-25747

Solar heating system at a racquetball club
page 272 MFS-25720

Solar space heating for workhouse — Kansas City, Kansas
page 273 MFS-25712

Solar-heated hotel in the Virgin Islands
page 273 MFS-25776

The economics of solar heating
page 274 MFS-25391

HELMETS
Integral face shield concept for firefighter's helmet
page 248 MFS-25493

HOLDERS
Articulated vacuum chuck
page 329 MSC-18933

HOT-WIRE FLOWMETERS
Hot film static-pressure probe for flow-field surveys
page 303 LAR-12799

HYDRAULIC CONTROL
Fast-acting electrohydraulic servo
page 295 LEW-13730

HYDRAZINES
Vapor detector
page 282 MSC-18989

IMAGING TECHNIQUES
Test-bed aircraft scanner
page 270 LAR-12796

INFRARED RADIATION
Infrared-controlled welding of solar cells
page 351 MFS-25612

INFRARED RADIATION
Test-bed aircraft scanner
page 270 LAR-12796

INSPECTION
Detecting contamination with photoelectron emission
page 307 MFS-25619

Gage for surface waviness
page 301 MSC-20055

Tile-gap measurement tool
page 300 MSC-20057

Using Nomarski interference to detect microcracks in glass
page 310 GSC-12649

INTERFACES
Programable interface handles many peripherals
page 262 KSC-11132

INTERNAL COMBUSTION ENGINES
Modular engine instrumentation system
page 309 LEW-13729

ION EXCHANGE RESINS
Regenerating water-sterilizing resins
page 283 MSC-20001

IONOSPHERE
Method for canceling ionospheric Doppler effect
page 261 MFS-25599

JETTISON SYSTEMS
Explosively actuated opening for rapid egress
page 312 LAR-12624

JOINTS (JUNCTIONS)
New apparatus tests pressure-suit joints
page 308 ARC-11314

Pivot attachment for prefabricated beams
page 354 MFS-25476

LAMINATES
Predicting the strengths of angle-plied laminates
page 304 LEW-13733

LASERS
Flashlamp driver for quasi-CW laser pumping
page 253 GSC-12566

LEVEL (HORIZONTAL)
A simple tiltmeter
page 319 ARC-11344

LIQUID METALS
Solar-driven liquid-metal MHD generator
page 268 LAR-12495

LUBRICANTS
Tests of 38 ball-bearing greases
page 330 MFS-25624

MAGNETOHYDRODYNAMIC GENERATORS
Solar-driven liquid-metal MHD generator
page 268 LAR-12495

MAGNETOMETERS
Improved magnetic-field-component resolvers
page 296 LAR-12638

MECHANICAL MEASUREMENT
New apparatus tests pressure-suit joints
page 308 ARC-11314

MECHANICAL PROPERTIES
Predicting tensile strengths of boron/aluminum composites
page 305 LEW-13745

Predicting the strengths of angle-plied laminates
page 304 LEW-13733

Ultrasonic instrument for evaluation of composites
page 298 LEW-13716

METAL FATIGUE
Increasing metal fracture toughness
page 341 LAR-12805

METAL WORKING
Staking tool for hard metals
page 328 MSC-20009

MICROCRACKS
Using Nomasski interference to detect microcracks in glass
page 310 GSC-12649

MICROWAVE AMPLIFIERS
Modular Amplifier/antenna arrays
page 257 MSC-18981

MULTISPECTRAL PHOTOGRAPY
Test-bed aircraft scanner
page 270 LAR-12796

NAVIER-STOKES EQUATION
Numerical solution for Navier-Stokes equations
page 357 MFS-25617

NAVIGATION INSTRUMENTS
Improved magnetic-field-component resolvers
page 296 LAR-12638

NEUTRALIZERS
Neutralizing amine-cured epoxy surfaces
page 284 GSC-12686

NITROGEN TETROXIDE
Vapor detector
page 282 MSC-18989

NOISE REDUCTION
Low-Noise band-pass amplifier
page 254 GSC-12567

NONDESTRUCTIVE TESTS
Acoustic emmissions could indicate weld quality
page 348 MFS-25441

Improved tensile test for ceramics
page 304 MSC-20105

NOZZLES
Improved nozzle would reduce cryogenic boiloff
page 327 MFS-25589

NUMERICAL CONTROL
"Teaching" an industrial robot to spray
page 320 MFS-25523

OPTICAL EQUIPMENT
Rotating the plane of parallel light beams
page 267 ARC-11311

OPTICAL PUMPING
Flashlamp driver for quasi-CW laser pumping
page 253 GSC-12566

PAINTS
Wide-temperature-range torque-stripe paint
page 284 MFS-19644

PARALLEL PROCESSING (COMPUTERS)
One way of testing a distributed processor
page 263 KSC-11123

PCM TELEMETERY
Processing PCM data in real time
page 263 KSC-11131

PEELING
Double-adhesive tape test reduces waste
page 306 MSC-20047

PHASE DETECTORS
Precise phase comparator for nearly equal frequencies
page 252 GSC-12645

PHOTOELECTRONS
Detecting contamination with photoelectron emission
page 307 MFS-25619

PIGMENTS
Coal as a substitute for carbon black
page 277 NPO-15461

PIVOTS
Pivot attachment for prefabricated beams
page 354 MFS-25476

PLASMA SPRAYING
Plasma spray for difficult-to-braze alloys
page 343 MFS-19630

PLASTIC DEFORMATION
Plastic and large-deflection analysis of nonlinear structures
page 314 LAR-12816

POLYIMIDES
Blowing agents for fabrication of polyimide foams
page 282 MSC-18993

POLYMERIZATION
Thermal polymerization of n-butyl acrylate
page 288 NPO-15010

POSITIONING DEVICES (MACHINERY)
Hybrid position/force control of robot manipulators
page 320 NPO-14997

POTENTIAL FLOW
Algorithm for unsteady potential flow about airfoils
page 310 ARC-11378

POWER CONDITIONING
Failure detector for power-factor controller
page 251 MFS-25607

Power-MOSFET voltage regulator
page 256 MSC-20059

POWER SPECTRA
Computing the power-density spectrum for an engineering model
page 360 LAR-12918

PRESSURE SENSORS
Cuff for blood-vessel pressure measurements
page 291 ARC-11264

Hot film static-pressure probe for flow-field surveys
page 303 LAR-12799

PRESSURE SUITS
New apparatus tests pressure-suit joints
page 308 ARC-11314

PRISMS
Rotating the plane of parallel light beams
page 267 ARC-11311

PROTECTIVE CLOTHING
Integral face shield concept for firefighter's helmet
page 248 MFS-25493

PROTECTIVE COATINGS
Silicone acrylate copolymers
page 277 NPO-15523

Thermal polymerization of n-butyl acrylate
page 288 NPO-15010

PUMPS
Damping vibration at an impeller
page 329 MFS-19645

QUALITY CONTROL
Acoustic emissions could indicate weld quality
page 348 MFS-25441

Double-adhesive tape test reduces waste
page 306 MSC-20047

RADIANT HEATING
Radiant heating of ampoule contents
page 349 MFS-25436

RADIATION DETECTORS
Improved Lixiscope
page 269 GSC-12587

RADIOMETERS
Improving radiometer-cavity absorptance
page 346 NPO-15374

REAL TIME OPERATION
Processing PCM data in real time
page 263 KSC-11131

RELIABILITY ANALYSIS
Proposed reliability cost model
page 359 MFS-25494

RELIEF VALVES
Force augmentation for relief valve
page 329 MSC-20065

RESOLVERS
Improved magnetic-field-component resolvers
page 296 LAR-12638

ROBOTS
"Teaching" an industrial robot to spray
page 320 MFS-25523

Hybrid position/force control of robot manipulators
page 320 NPO-14997

ROTATING BODIES
Flywheels would compensate for rotor imbalance
page 323 GSC-12550

Rotating the plane of parallel light beams
page 267 ARC-11311

RUBBER
Coal as a substitute for carbon black
page 277 NPO-15461

SAFETY DEVICES
Integral face shield concept for firefighter's helmet
page 248 MFS-25493

Yielding torque-tube system reduces crash injuries
page 350 LAR-12801

SAMPLING
Mass-loss buttons monitor material degradation
page 302 MSC-18903

SCREWS
Universal assembly for captive bolts
page 322 MSC-18905

SEALING
Boltless seal for electronic housings
page 248 NPO-14818

Electrically-conductive low-permeability pressure seal
page 347 MSC-20022

SEATS
Yielding torque-tube system reduces crash injuries
page 350 LAR-12801

SEPARATED FLOW
High-lift separated flow about airfoils
page 315 LAR-12853

SERVOCONTROL
Fast-acting electrohydraulic servo
page 295 LEW-13730

SHOCK ABSORBERS
Yielding torque-tube system reduces crash injuries
page 350 LAR-12801

SILICON COATINGS
Binders for thermal-control coatings
page 287 MFS-25620

SILICON COMPOUNDS
XPS study of SiO_2 and the Si/SiO_2 interface
page 281 NPO-14968

SILICONES
Silicone acrylate copolymers
page 277 NPO-15523

SIMULATORS
Line-replaceable-unit analysis
page 257 MSC-20183

Solar simulator at Marshall Space Flight Center
page 271 MFS-25742

Torque simulator for rotating systems
page 311 LAR-12751

SLICING
Cutting a tapered edge on padding material
page 353 MSC-20011

High-speed wafer slicer
page 324 NPO-15463

SOLAR ARRAYS
Automated solar-array assembly
page 333 NPO-15501

Bonder for solar-cell strings
page 338 NPO-15507

Brushless cleaning of solar panels and windows
page 325 NPO-14922

Modular Amplifier/antenna arrays
page 257 MSC-18981

Orienting and applying flux to solar cells
page 335 NPO-15504

Solar-cell string conveyor
page 337 NPO-15508

Storing and deploying solar panels
page 352 MSC-18950

Tab interconnect work station
page 336 NPO-15505

Transfer of strings to the module fixture
page 340 NPO-15509

Transporting solar-cell strings
page 339 NPO-15502

Vacuum pickup for solar cells
page 334 NPO-15500

Walking-beam solar-cell conveyor
page 334 NPO-15503

Work station for inverting solar cells
page 337 NPO-15506

SOLAR CELLS
Silicone acrylate copolymers
page 277 NPO-15523

Thermal polymerization of n-butyl acrylate
page 288 NPO-15010

SOLAR ENERGY
Evaluation of a line-concentrating solar collector
page 271 MFS-25778

Hot water for motor inn — Garland, Texas
page 273 MFS-25726

Manifold insulation for solar collectors
page 271 MFS-25779

Solar heater in a West Virginia college
page 272 MFS-25706

Solar heating in an elementary school
page 272 MFS-25747

Solar heating system at a racquetball club
page 272 MFS-25720

Solar simulator at Marshall Space Flight Center
page 271 MFS-25742

Solar space heating for workhouse — Kansas City, Kansas
page 273 MFS-25712

Solar-driven liquid-metal MHD generator
page 268 LAR-12495

Solar-heated hotel in the Virgin Islands
page 273 MFS-25776

The economics of solar heating
page 274 MFS-25391

SOUND GENERATORS
Sound-burst generator for measuring coal properties
page 278 MFS-25438

SPRAYED COATINGS
Plasma spray for difficult-to-braze alloys
page 343 MFS-19630

SPRAYING
"Teaching" an industrial robot to spray
page 320 MFS-25523

STORAGE TANKS
Improved nozzle would reduce cryogenic boiloff
page 327 MFS-25589

STRESSES
Structural design with stress and buckling constraints
page 314 MFS-25234

STRIP TRANSMISSION LINES
Unequal-split strip-line power divider
page 249 LAR-12797

STRUCTURAL ANALYSIS
Plastic and large-deflection analysis of nonlinear structures
page 314 LAR-12816

Structural design with stress and buckling constraints
page 314 MFS-25234

STRUCTURAL MEMBERS
Fabricating structural beams
page 354 MFS-25228

Pivot attachment for prefabricated beams
page 354 MFS-25476

STRUCTURAL VIBRATION
Solution accounts for structural damping
page 299 LAR-12863

Vibration analysis with finite dynamic elements
page 313 NPO-15087

STUDS
Precise restraightening of bent studs
page 321 MFS-19632

SULFURIC ACID
Heat-exchange fluids for sulfuric acid vaporizers
page 285 NPO-15015

SURFACE DISTORTION
Gage for surface waviness
page 301 MSC-20055

SURFACE PROPERTIES
Detecting contamination with photoelectron emission
page 307 MFS-25619

SURFACE WAVES
Elastic surface wrinkling
page 313 NPO-15091

SWITCHING CIRCUITS
Arc-free high-power dc switch
page 255 MSC-20091

TEMPERATUE CONTROL

Evaluation of a line-concentrating solar collector
page 271 MFS-25778

Hot water for motor inn — Garland, Texas
page 273 MFS-25726

Manifold insulation for solar collectors
page 271 MFS-25779

Monitoring crystal growth from solution
page 351 MFS-25622

Solar heater in a West Virginia college
page 272 MFS-25706

Solar heating in an elementary school
page 272 MFS-25747

Solar heating system at a racquetball club
page 272 MFS-25720

Solar space heating for workhouse — Kansas City, Kansas
page 273 MFS-25712

Solar-heated hotel in the Virgin Islands
page 273 MFS-25776

TENSILE STRENGTH
Predicting tensile strengths of boron/aluminum composites
page 305 LEW-13745

TENSILE TESTS
Improved tensile test for ceramics
page 304 MSC-20105

THERMAL CONTROL COATINGS
Binders for thermal-control coatings
page 287 MFS-25620

TOOLS
Articulated vacuum chuck
page 329 MSC-18933

Gage for surface waviness
page 301 MSC-20055

Precise restraightening of bent studs
page 321 MFS-19632

Safety bolt doubles as a bushing-removal tool
page 326 MSC-20032

Staking tool for hard metals
page 328 MSC-20009

Tile-gap measurement tool
page 300 MSC-20057

TORQUE
Yielding torque-tube system reduces crash injuries
page 350 LAR-12801

TORQUEMETERS
Wide-temperature-range torque-stripe paint
page 284 MFS-19644

TORQUERS
Torque simulator for rotating systems
page 311 LAR-12751

TOUGHNESS
Increasing metal fracture toughness
page 341 LAR-12805

TRANSMISSION LINES
Unequal-split strip-line power divider
page 249 LAR-12797

TRANSPONDERS
Method for canceling ionospheric Doppler effect
page 261 MFS-25589

ULTRASONIC TESTS
Ultrasonic instrument for evaluation of composites
page 298 LEW-13716

ULTRASONIC WELDING
Ultrasonic welding of graphite/thermoplastic composite
page 340 MSC-20013

UNSTEADY FLOW
Algorithm for unsteady potential flow about airfoils
page 310 ARC-11378

USER MANUALS (COMPUTER PROGRAMS)
User documentation for multiple software releases
page 358 KSC-11189

VALVES
Force augmentation for relief valve
page 329 MSC-20065

VAPORS
Vapor detector
page 282 MSC-18989

VIBRATION DAMPING
Damping vibration at an impeller
page 329 MFS-19645

Solution accounts for structural damping
page 299 LAR-12863

VOLTAGE REGULATORS
Power-MOSFET voltage regulator
page 256 MSC-20059

WAFERS
High-speed wafer slicer
page 324 NPO-15463

WATER TREATMENT
Regenerating water-sterilizing resins
page 283 MSC-20001

WELD TESTS
Acoustic emissions could indicate weld quality
page 348 MFS-25441

WELDING
Cleaning internal-weld splatter
page 345 MSC-20068

Infrared-controlled welding of solar cells
page 351 MFS-25612

Ultrasonic welding of graphite/thermoplastic composite
page 340 MSC-20013

Weld width indicates weld strength
page 344 MFS-25648

WELDING MACHINES
Clamp and gas nozzle for TIG welding
page 347 MSC-20108

Controlling electron-beam-weld focus
page 342 MFS-19635

WIRING
High-density terminal box for testing wire harness
page 250 NPO-15147

WRINKLING
Elastic surface wrinkling
page 313 NPO-15091

X-RAYS
Improved Lixiscope
page 269 GSC-12587

XPS study of SiO_2 and the Si/SiO_2 interface
page 281 NPO-14968

National Aeronautics and
Space Administration

Washington, D.C.
20546

THIRD-CLASS BULK

NASA

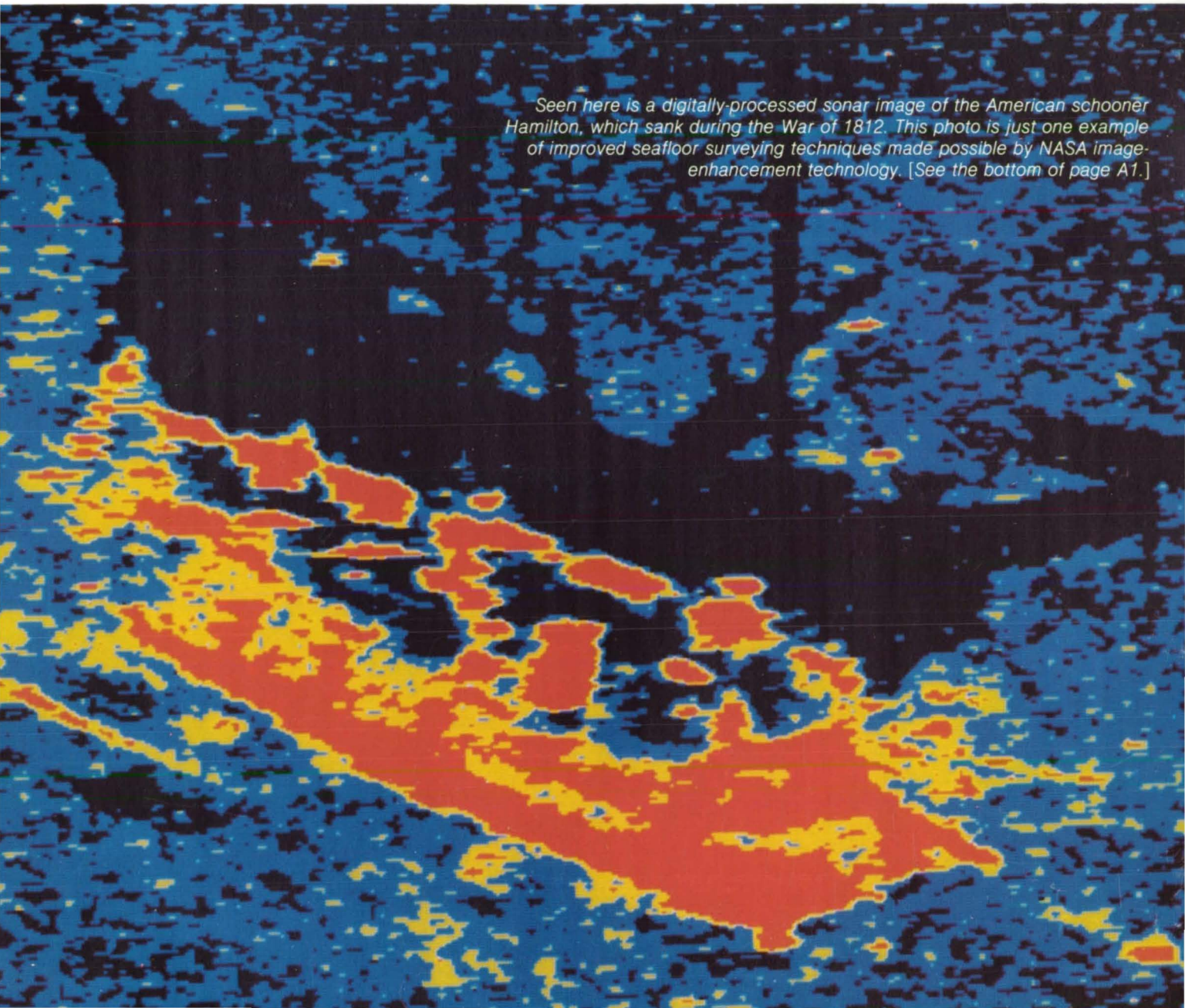

Seen here is a digitally-processed sonar image of the American schooner Hamilton, which sank during the War of 1812. This photo is just one example of improved seafloor surveying techniques made possible by NASA image-enhancement technology. *[See the bottom of page A1.]*